A fluid power application of alternative robust control strategies

Pannett, Richard

Award date:
2010

Awarding institution:
University of Bath

A Fluid Power Application of Alternative Robust Control Strategies

Richard Frank Pannett

A thesis submitted for the degree of Doctor of Philosophy

University of Bath

Department of Mechanical Engineering

March 2010

COPYRIGHT

Summary

This thesis presents alternative methods for designing a speed controller for a hydrostatic power transmission system. Recognising that such a system, comprising a valve controlled motor supplied by the laboratory ring main and driving a hydraulic pump as a load, contains significant non-linearities, the thesis shows that robust 'modern control' approaches may be applied to produce viable controllers without recourse to the use of a detailed model of the system. In its introduction, it considers why similar approaches to the design of fluid power systems have not been applied hitherto. It then sets out the design and test, in simulation and on a physical rig, of two alternative linear controllers using H_∞ based methods and a 'self organising fuzzy logic' controller (SOFLC). In the linear approaches, differences between the characteristics of the system and the simple models of it are accommodated in the controller design route as 'perturbations' or 'uncertainties'. The H_∞ based optimisation methods allow these to be recognised in the design. "Mixed sensitivity" and "Loop shaping" methods are each applied to design controllers which are tested successfully on the laboratory rig. The SOFLC in operation does not rely on a model, but instead allows fuzzy control rules to evolve. In the practical tests, the system is subjected to a range of disturbances in the form of supply pressure fluctuations and load torque changes. Also presented are test results for proportional and proportional plus integral (PI) controllers, to provide a reference. It is demonstrated qualitatively that performance using the linear controllers is superior to that using proportional and PI controllers. An increased range of stable operation is achieved by the controller designed using "loop shaping" – performance is enhanced by the use of two controllers selected automatically according to the operating speed, using a "bumpless" transfer routine. The SOFLC proved difficult to tune. However, stable operation was achieved.

Acknowledgements

I am pleased to acknowledge with grateful thanks the assistance of the following, without whom my progress to date, albeit limited, would not have been possible:

My early stage supervisors Dr P K Chawdhry and Prof C R Burrows for their advice and support and for setting the general direction for this project; my late stage supervisors, Prof P S Keogh and Dr D G Tilley for supporting me in bringing the project to a conclusion;

In the early stages:

Prof K A Edge for providing certain reference material; Dr P S Keogh for advice on H_∞ principles, and access to lecture notes introducing them; Dr I A Njabeleke for detailed advice on advanced state space methods and digital emulation; Mr V Rajput and Mr S J Gould (Instrumentation Section) for advice and support with, respectively, measurement systems and control, data logging and interface software; Dr D G Tilley and Mr A M Monaghan for access to and advice on the motor performance test rig; Mr A Galloway for practical support and mechanical assistance on the test rig; many postgraduate colleagues for general advice on a range of software application issues, and for useful discussion.

Completion would not have been achieved without the strong encouragement and support of my wife, Jacqui.

TABLE OF CONTENTS

NOMENCLATURE

Table of Contents

Nomenclature

In general, **bold** face type is used to denote vector or matrix variables, and plain type scalars.

a_i	coefficients of a polynomial (i=1,…n).
$\boldsymbol{A}$, $\boldsymbol{B}$, $\boldsymbol{C}$, $\boldsymbol{D}$	state matrices.
A_1,A_2	fuzzy controller input fuzzy sets.
$b_{P,C}$	stability margin of closed loop $\boldsymbol{P}$,$\boldsymbol{C}$.
$B(j\omega)$ or $\boldsymbol{B}(j\omega)$	frequency domain performance bound.
$c(nT)$	quantised and scaled discrete time error rate.
$\boldsymbol{C}$	a compensator.
$d(s)$ or $\boldsymbol{d}(s)$	disturbance.
$e(nT)$	quantised and scaled discrete time error.
$e(s)$ or $\boldsymbol{e}(s)$	error input to compensator.
f, f_i	gains in anti-windup/bumpless transfer schemes (i=1,2).
$\boldsymbol{F}$(s)	a stabilising controller.
$\mathbf{F}(.)$	linear fractional transformation.
$\mathbf{F}_l(.)$	lower linear fractional transformation.
$G(s)$ or $\boldsymbol{G}(s)$	plant transfer function.
$G_c(s)$	PID control law.
GC	fuzzy controller control error gain.
GE	fuzzy controller control error rate gain.
GI	fuzzy controller input scaling factors.
GO	fuzzy controller output scaling factors.
GU	fuzzy controller control action gain.
$\boldsymbol{G_o}(s)$	plant transfer function – nominal plant.
i,j,k,m,n	integer indices.
$\mathbf{I}$	identity matrix.
j	$\sqrt{-1}$ (or, in context, an integer index).
k_c	proportional gain in PID control law.
k_{crit}	proportional gain at which stablitiy is lost.
K_i	a gain (i=1, 2,…).

$K(s)$ or $\boldsymbol{K}(s)$	compensator or controller transfer function.
$\boldsymbol{K_{inf}}$	a robust stabilising controller (loop shaping).
$L(s)$ or $\boldsymbol{L}(s)$	open-loop transfer function.
$m(s)$ or $\boldsymbol{m}(s)$	measurement noise.
M	derivation of deterministic control action.
$\boldsymbol{M},\boldsymbol{N}$	left coprime factors of $\boldsymbol{G}$.
$p(nT)$	performance measure.
$P(s)$ or $\boldsymbol{P}(s)$	a prefilter or other transfer function.
$\boldsymbol{P}$	controllability Gramian.
$\boldsymbol{P}_{ij}$	partitions of $\boldsymbol{P}$ (i=1,2;j=1,2).
$\boldsymbol{P},\boldsymbol{P}_1,\boldsymbol{P}_2$	three alternative plants.
Q	quantisation process.
$\boldsymbol{Q}$	observability Gramian.
$\boldsymbol{Q}_{ij}$	partitions of $\boldsymbol{Q}$ (i=1,2; j=1,2).
$\boldsymbol{Q}(s)$	a matrix transfer function; Youla parameter.
r	ratio ω/ω_n.
$r(nT)$	performance reward.
$r(s)$ or $\boldsymbol{r}(s)$	reference signal.
s	complex variable.
$S(s)$ or $\boldsymbol{S}(s)$	sensitivity.
t	time.
T	sample interval.
T_d	time constant of differential gain in PID law.
T_i	time constant of integral gain in PID law.
T_{r1}	rise time.
T_s	settling time.
$T(s)$ or $\boldsymbol{T}(s)$	complementary sensitivity.
$\boldsymbol{T}_{y_1u_1}$	transfer function from $\boldsymbol{u}_1$ to $\boldsymbol{y}_1$.
u_c	controller output.
u_{max}, u_{min}	saturation limits on control effort.
$u(nT)$	deterministic control action.
$u(s)$ or $\boldsymbol{u}(s)$	control effort or plant input.
$\boldsymbol{u}$, $\boldsymbol{v}$, $\boldsymbol{w}$, $\boldsymbol{x}$, $\boldsymbol{y}$, $\boldsymbol{z}$	signal vectors as defined in context.

U	fuzzy controller output fuzzy set.
$U(nT)$	fuzzy control action.
$W_i(s)$ or $\boldsymbol{W}_i(s)$	a weighting function (i=1,2,3).
$y(s)$ or $\boldsymbol{y}(s)$	output.
z	complex operator in z-domain.
γ	a weighting factor; an H_∞ norm.
δ	complex operator in δ-domain.
$\delta_v(.)$	gap metric.
$\boldsymbol{\Delta_a}(s)$	additive perturbation transfer function matrix.
$\boldsymbol{\Delta_i}(s)$	input multiplicative perturbation transfer function matrix.
$\boldsymbol{\Delta_m}(s)$, $\boldsymbol{\Delta_o}(s)$	output multiplicative perturbation transfer function matrices.
$\boldsymbol{\Delta_M}$, $\boldsymbol{\Delta_N}$	uncertainties in coprime factors $\boldsymbol{M}$,$\boldsymbol{N}$.
ε	stability margin.
$\lambda_i(.)$	ith eigenvalue.
ξ	damping ratio.
$\boldsymbol{\varphi}(t)$	state transition matrix.
φ	coprime factor equation error.
$\rho(.)$	spectral radius.
σ	a complex variable.
$\sigma(.)$	principal gain or singular value.
$\sigma_i(.)$	ith Hankel singular value.
ω	circular frequency.
ω_b	bandwidth.
ω_c	gain crossover frequency.
ω_n	natural frequency.
ω_s	sampling frequency.
$\|\boldsymbol{x}\|$	a norm of vector $\boldsymbol{x}$, as defined in context.
$\|\boldsymbol{G}\|$	a norm of matrix $\boldsymbol{G}$, as defined in context.

See APPENDIX 2 and APPENDIX 4 for more details of mathematical notations used.

A Fluid Power Application of Alternative Robust Control Strategies

1 Introduction

1.1 Preamble

This thesis describes research on the design and implementation of robust controllers for non-linear systems, with particular reference to fluid power. An underlying hypothesis of the project is that fluid power systems, which exhibit a high degree of non-linearity, are suitable candidates for the application of (so-called) modern control methods, but that such methods have not been widely applied because the complexity of their theory makes them inaccessible to fluid power system designers. This thesis demonstrates by simulation and practical testing that these methods can be applied successfully to fluid power systems. In doing so, it demonstrates how 'linear' controller design methods can accommodate non-linearities. After a brief introduction, it sets out the motivation for the research. The research area is defined and objectives are set.

The thesis contains in its second chapter a literature review of relevant research, in which an attempt is made to focus on practical applications in the field of fluid power as well as on the theoretical background on which the current work is based. A brief examination of the meaning of the term 'robust' is included. The review found few references to practical applications of 'modern' control to fluid power, developed through to practical application and testing.

The candidate system for study and test is a hydrostatic power transmission system comprising a loaded valve-controlled motor and its speed control loop. This is described in Chapter 3, with further details in Appendix 1. Disturbances and uncertainties are briefly described with reference to this test system. The simulation tools to be used are also introduced. These are Bath*fp*, chosen for its ability to

facilitate fluid power circuit design, and MATLAB, which provides a range of control system design tools.

The applicability of some linear robust and fuzzy logic control techniques to the non-linear system is investigated in simulation and test. For reference, proportional and PID (proportional plus integral plus derivative) control schemes are also applied to the candidate system, as summarised in Chapter 4.

The linear robust control methods examined in depth are H_∞ mixed sensitivity and H_∞ loop shaping, in Chapters 5 and 6 respectively. The backgrounds to these methods and some issues of significance to the fluid power application are discussed. The methods are developed in a fashion consistent with the application in an endeavour to improve their accessibility to fluid power engineers. A design rationale is presented and applied. Controllers are designed using plant models. Where simulation of the closed loop system indicates that the controller is viable, it is rig tested. Appendix 2 contains some of the background mathematics.

Some issues affecting the transport of the controllers to the test rig and the test arrangements are described. The implication of word length in a real-time processor is briefly considered. Issues affecting the choice of sampling frequency are discussed in Chapter 5. Alternative designs in which the same control algorithm is implemented using both *z*- and δ-transforms are also compared in Chapter 5. Test results are presented and compared with each other and with simulation results where appropriate.

Chapter 6 relates to the design, simulation and testing of a controller using H_∞ loop shaping. In an attempt to provide good performance over a wide range of operating conditions, the controller includes a 'bumpless' transfer switch between two control algorithms, one of which is selected at 'low' speed and the other at 'high' speed.

Test results confirm the practicability of the controller designs presented, and show some advantages over PID control.

Fuzzy control strategies are investigated in Chapter 7. The theory of fuzzy control is summarised, and a clear link between basic fuzzy logic theory, including the theory of relations and inference, and its use to implement a controller incorporating expert

rules is developed. More detail is contained in Appendix 4. The theory of the 'self organising fuzzy logic controller' (SOFLC) is summarised in Appendix 5 and an application suitable for the fluid power test system is developed, tested in simulation and applied to the test rig. Particular attention is given to the evolution of the control rules.

Finally, in Chapter 8, the practical issues of implementation for the various controllers are compared and contrasted. Areas for further work are identified. The main conclusion is that the 'modern' control methods described can be successfully applied in a fluid power environment.

1.2 Publications, etc.

The work described in the sequel has resulted in the following publications and conference papers: Njabeleke *et al*. (1997), (1998(1)), (1998(2)), (2000); Pannett *et al*. (1999).

1.3 Motivation

The motivation for pursuing this research area was the author's impression that despite the fact that a range of so-called 'modern control' techniques has been developed, and that some have their origins in analysis undertaken in the 1960s and 70s, the range of industrial applications still remains narrow. There are few reported applications in a fluid power environment. Applications outside aerospace and defence are apparently rare. Is it possible to demonstrate the applicability of these 'modern control' techniques to fluid power systems, and do they offer any benefits with respect to those more commonly used?

Some of the impediments to the wider adoption of 'modern control', along with some remedial actions which might be appropriate, as perceived by the author, are summarised in Figure 1.1.

Williams (1995, (1)) wrote of a gap between theory and application and of a 'knowledge threshold' facing industry which must be overcome before it can achieve the benefits available from the application of advanced control:

"Successful control applications have to be founded on a number of factors:

- appropriate theory
- usable design tools
- computer hardware and software technology
- appropriate practical experience". (Williams, 1995, (2).)

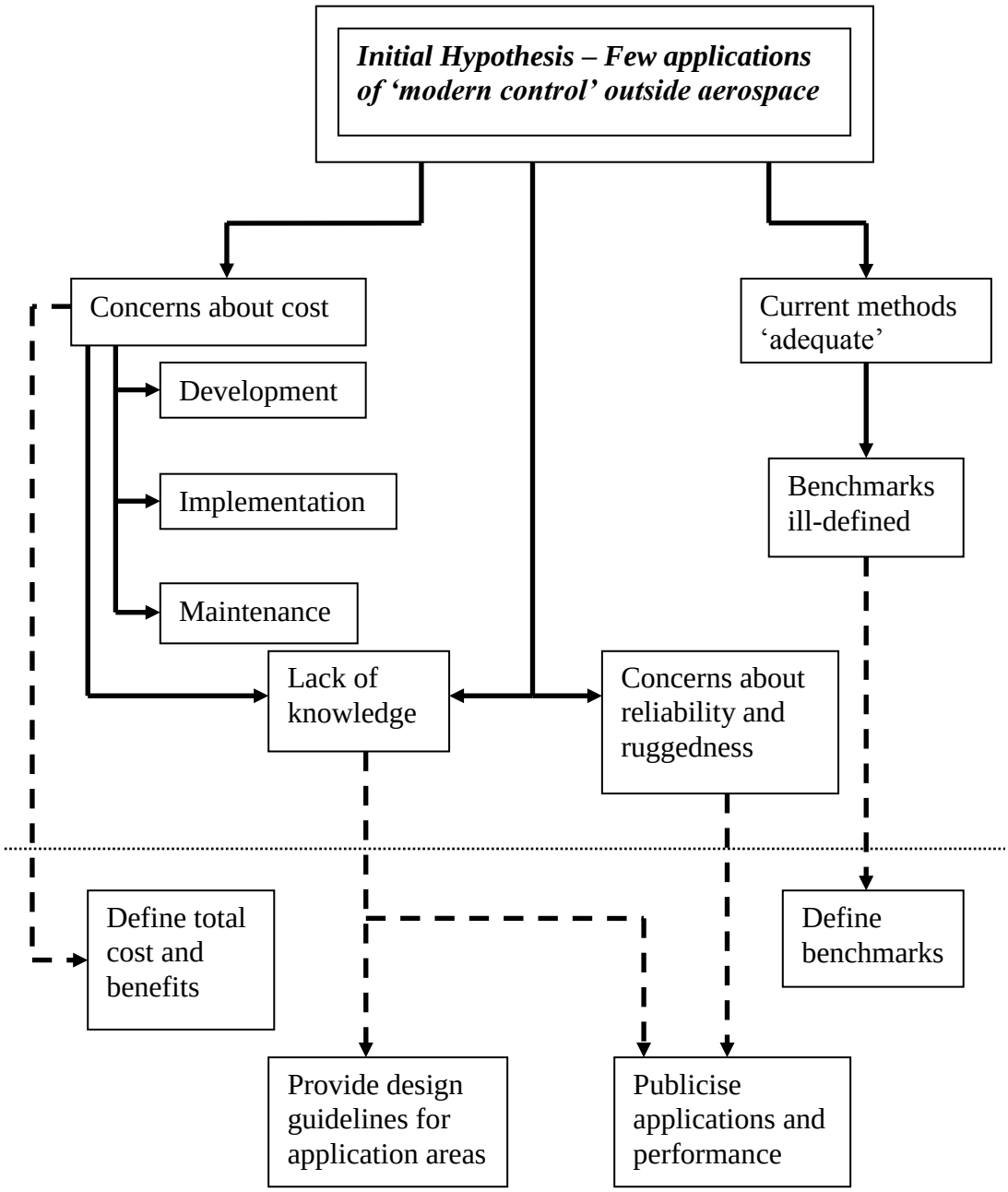

Figure 1.1 Activities needed to stimulate the wider application of 'modern control'

Thus the thrust of the work becomes the investigation and analysis of the theory of a range of modern control techniques and their applicability in a fluid power environment, which is characterised by severe non-linearities. The applications of alternative H_∞ based methods and of a self organising fuzzy logic scheme in simulation and physical implementation are examined.

1.4 Definition of Research Area

Using Williams' terminology, this thesis reports on an investigation into Robust Control as an 'appropriate theory' for application to the domain of fluid power systems based on 'practical experience'. It embraces the development of 'usable control design tools' based on suitable computing platforms, and the acquisition of 'appropriate experience' in their application to industrial problems. There is a considerable literature on 'robust control'; a wide variety of theories has been developed. Much of the theory has been tested in simulation; rather less of it seems to have been applied. Aerospace may be an exception. The sequel has found few applications in the field of fluid power.

1.5 Research Objectives

The objectives of this research, as initially defined, were as follows:

- To compare the merits of alternative robust controllers for non-linear systems, taking account of performance, reliability, cost and complexity of implementation;
- To produce design guidelines, using the results of the above comparison, for controller selection criteria;
- To validate these guidelines by application to physical machinery systems design involving electrical, mechanical and fluid power components.

In the time available to undertake the research which supports this thesis, these objectives have been interpreted by focussing on the application of a range of robust control strategies to a hydrostatic power transmission system: the speed of a valve-controlled fluid power motor supplied from a laboratory ring main and subjected to disturbances both to supply pressure and load torque is controlled.

Emphasis has been placed on practical implementation on a physical test rig. Although the test system clearly contains non-linearities, a fundamental hypothesis of the work is that robust linear control techniques can be applied: the system can usefully be considered to be linear, the non-linearities being treatable as 'perturbations', which a robust controller must accommodate. Thus it is postulated that controllers for this non-linear system can be designed by various 'modern' methods without recourse to a detailed non-linear model of the system: non-linearities can be treated as perturbations to a linear model, so that an H_∞ linear robust controller design method can be used. Alternatively, a fuzzy logic based approach, which requires no plant model, can be used. Consequently, the absence of complex models opens up the possibility of a straightforward route for the generation of controllers for fluid power systems with their inherent non-linearities.

1.6 A Note on 'Modern Control'

Green and Limebeer (1995) consider that the terminology 'Modern Control' has fallen into disuse. It is retained here to identify certain design strategies for controllers which were developed by and subsequent to the work of developers such as Wiener, Hopf and Kalman in the 1950s.

1.7 Controller Design Issues

The controller designer needs to have a specification of the desired performance of the combined system (controller and plant or process). For a mechanical system, this is likely to be defined in terms of its required transient response, ability to reject disturbances, and steady state error (difference between required and actual plant output). For a chemical or manufacturing process, the required response might be expressed in terms of raw material waste avoidance, as well as desired output characteristics such as chemical concentrations or other product parameters.

The control design process requires as inputs:

- information on the dynamic performance of the plant (relationship between its inputs and its outputs);
- information on the variability of this performance with, for example, amplitude or frequency of inputs (due to non-linearities), environmental effects (such as temperature effects on dimensions or material properties e.g. viscosity), wear, and manufacturing tolerance.

In addition, estimates of the shapes of disturbances and extraneous input (noise) signals must be available. Crucially, the controller outputs must lie within a range to which the plant can safely respond.

Additionally, the physical implementation of the controller may be subject to a monetary cost constraint. For both bespoke and mass produced systems, there may be, within an overall system performance specification and monetary cost target (budget), scope for a trade off between controller complexity and plant specification (expressed in terms of manufacturing tolerance, linearity, maximum actuator power, transducer performance, etc). The implication of the application of monetary cost constraints on the selection of components and controller design has not been explored in the current work.

1.8 Units

In general, SI units are used throughout, in accordance with Bureau International des Poids et Mesures "The International System of Units (SI)" 8th edition 2006 (Organisation Intergouvernementale de la Convention du Mètre).

http://www.bipm.org/utils/common/pdf/si_brochure_8_en.pdf
(downloaded 26/06/2009 16:05.)

However, in accordance with standard practice in the fluid power industry, and as permitted by Bureau International des Poids et Mesures, the unit of pressure used is the bar (1 bar = 0.1 MPa). Also, as used in the industry, shaft rotational speeds are generally reported in revolutions per minute using the abbreviation rpm.

2 Literature Review

2.1 Background

To set the work in a historical context, it is informative to look back some 30 years at views held then on the direction that the development of the theory and application of control might take. In his paper, 'The Future of Control', Rosenbrock (1977) identifies the emergence of 'modern control' as occurring in the 1960s. Tools were needed to solve control problems arising in the aerospace industry: in particular, rocket guidance. He associates the term 'modern control' with the formulation of control problems in a style which enables them to be solved algorithmically to synthesise controllers. Rocket guidance problems could be expressed in a closed mathematical form well suited to algorithmic solution routes. However, he suggests that reasons why practising control engineers outside the aerospace industry were slow to adopt 'modern' methods included the difficulty in defining what constituted a desirable response, incomplete knowledge of system constraints, the presence of non-linearities, and the impracticability of producing adequate system models with finite dimensions. Thus, he considered that the importance of the development of 'modern control' lay not with methods, which focussed on the synthesis of controllers, but rather with techniques which enhanced the understanding of the foundations of control and which clarified the definition of the control problem, leading, for example, to an improved understanding of the effects of uncertainty and non-linearity on stability margin. Further, he identified the (then) increasingly ready availability of interactive computing techniques as the means by which designers could apply the sophisticated system analysis techniques which came with 'modern control' developments. Developing graphical user interfaces made the results accessible to the designer and facilitated a high degree of iteration in the design route.

The current work aligns with Rosenbrock's 'prophetic' analysis in that it has made use of advanced interactive software, principally MATLAB and Bath*fp* (see Burrows, *et al.*, 1991, Tomlinson and Tilley, 1993) incorporating powerful and flexible graphical user interfaces. It has endeavoured to apply 'modern control' concepts to a fluid power application.

2.2 Fluid Power Systems

Fluid power systems are commonly used in applications in which their high power to weight ratios and ability to deliver very high forces or torques offer performance, cost or environmental advantages over alternatives (such as systems containing electromagnetic actuators or motors). Backé included a thorough review of the merits of fluid power in his Institution of Mechanical Engineers Thomas Hawksley Memorial Lecture (Backé, 1993). He summarised the key features of fluid power as:

1. Low weight-power ratio
2. Small dimensions
3. Good controllability of pressure and flow
4. Good time response
5. Possibility to transmit power over medium distances
6. Easy transformation of hydraulic to mechanical power of a longitudinal motion (cylinder and piston)
7. Conduction of heat out of components by the pressure fluid.

An unashamed proponent of and enthusiast for fluid power, he nevertheless recognised that developments in competing technologies required that fluid power needs to be constantly improved. This thesis contributes to this improvement by demonstrating how alternative control technologies might be used to improve fluid power system performance or reduce costs by making reduced demands on component manufacturing precision and tolerance. Backé points out that low natural damping and non-linearities constitute disadvantages for fluid power systems which can be mitigated by controller design. He considered that the possible future

developments of fluid power would include an 'intensified application of modern control concepts with adaptation to changes in open-loop properties' (*ibid*. Table 3).

Hydraulic motors and rotary actuators are widely used in industry. Applications include the driving of continuous webs of textiles and paper during manufacture and processing, and in winches and cranes. The latter are found on sea-going ships as well as on land. They are used to drive lead screws in machine tools and in screw forging presses. Pinch rolls in continuous billet casting machines may be driven by hydraulic motors. Other applications include ladle change car drives in converter steel works, manipulators (via rack and pinion drives) for hot steel forming, and theatre stage rotation. Examples of this wide range of applications may be found in, for example, Hunt and Vaughan (1996), Valenti (1997) and Evans-Pughe (2007). The references do not in general give details of the type of control applied to the motors and actuators – there are, of course, many possibilities. Although valve control, as employed in the current work, is not energy efficient (e.g. Backé, 1993), it is straightforward to implement and offers rapid response.

An examination of conference proceedings and journal papers of the late 1960s, 1970s and early 1980s by Edge (1997) revealed a relatively low level of activity with regard to electrohydraulic system control. He found that a wide variety of control schemes had been researched subsequently, most requiring micro-processor implementation. He discusses the strengths and weaknesses of a range of different control strategies, as applied to fluid power and pneumatics, ranging from PID to fuzzy, referring to published research. He concludes that for industry to capitalise on the research, it is important to establish effectively the relative merits of different control schemes for given applications.

Burrows (2000) includes an updated review of the design of controllers for fluid power systems. He acknowledges that if performance specifications are not too arduous, classical PID controllers can be effective despite the non-linear characteristics of valves, pumps and motors. He concludes that 'the evolution of fluid power systems is inextricably linked to advances in control theory. The development of robust control techniques capable of dealing with model uncertainty and parameter variations is of major significance in the design of fluid power systems.'

Fluid power, in particular hydrostatic power transmission systems, continues to be an important and widely used technology. Hydrostatic drives are made attractive by their flexibility and high power density (e.g. Murrenhoff *et al*., 2008).

2.3 'Robustness'

An important concept in controller design is 'robustness'. This is perhaps best considered by examining how it is defined in the literature. Thus, in a selection of control engineering texts, robustness is explained or defined as follows:

- A robust control system exhibits the desired performance despite the presence of significant plant (process) uncertainty (Dorf and Bishop, 1995);
- If the (control system) design performs well for substantial variations in the dynamics of the plant from the design values, we say the design is robust (Franklin, *et al*., 1991);
- The particular property that a control system must possess in order for it to operate properly in realistic situations is called robustness. Mathematically, this means that the controller must perform satisfactorily not just for one plant but for a family (or set) of plants (Stefani *et al*., 1994);
- Robustness can be defined in various ways, but generally the word implies the maintenance of adequate stability margins or other performance levels in spite of model errors or deliberate oversimplifications (Brogan, 1991);
- A control system is robust if it is insensitive to differences between the actual system and the model of the system which was used to design the controller (Skogestad and Postlethwaite, 1997).

An industrialist might define a robust controller as one that is able to withstand physical misuse by installers and operators without suffering irreversible damage.

2.4 Applications of 'Modern' Linear Methods to Fluid Power

The current work has found few applications of 'modern' linear methods to fluid power, carried through from simulation to practical implementation. Piché *et al*. (1991) have reported the application of H_∞ 'mixed sensitivity' to the design of a controller for a hydraulic position servo, with practical test results. They also reported the design of a controller for a similar system using 'structured singular value optimisation' (1992). Simulation, but not practical test, results are reported for the latter. Hampson *et al*. (1996) reported the design of a robust controller for a hydrostatic transmission using H_∞ 'mixed sensitivity'; they included the results of simulations but did not proceed to implement the controllers practically. Sanada and Kitagawa (1996) have provided a limited demonstration of the application of μ-synthesis to the control of the band brake in an automotive automatic transmission. They found that, despite using a detailed model of the system to design their robust controller, the required performance (as measured by shift time) proved to be elusive.

The underlying mathematical theory of modern methods incorporating H_∞ approaches has been developed in depth over the past 30 years or so. Much of the literature is impenetrable to anyone without a strong mathematical background; notations and terminologies in the associated matrix algebra are not always consistent. Francis (1987) provides a detailed mathematical background to H_∞ theory; Macieowski (1989) attempts to provide his readers with enough mathematical background to make the modern multi-variable control theory accessible. Other works such as Skogestad and Postlethwaite (1997) include useful appendices to familiarise the reader with the matrix and other mathematics needed to underpin the control theory presented in the main text. References to particular works appear in the sequel. Some undergraduate textbooks on control engineering (e.g. Stefani *et al*., 1994) now include an introduction to H_∞ theory. The literature demonstrates the effectiveness of H_∞ approaches for the design of multivariable feedback controllers. In the current work, its ability to provide 'guaranteed' robustness and defined performance has been exploited.

The availability of software implementations of complex techniques through MATLAB toolboxes (Chiang and Safanov, 1988 and Balas *et al*., 1994) have facilitated the design of controllers using these techniques. A number of applications in the aerospace industry have been reported. References to these may be found in, for example, Skogestad and Postlethwaite (1997). Morari and Zafirou (1989) show how the techniques may be applied in the process industry, where time delays are significant and the minimisation of wastage, especially during start-up, are important considerations for the control designer.

Zhang *et al*. (2002) sought to apply, *inter alia*, an H_∞ based loop shaping method to the synthesis of a controller for the power train of an earth moving vehicle. They do this using a sophisticated model with 9 measured outputs and 14 states, in contrast with the sequel which seeks to demonstrate that an adequate performance can be achieved without recourse to a complex plant model.

Kim *et al*. (2003) describe the synthesis using an H_∞ optimisation of a controller for a cold rolling strip mill. To use state space methods, they linearise the non-linear system equations at a nominal operating point. They demonstrate in simulation that this controller is superior to controllers designed by other methods. However, there is no report of practical application.

Jayender *et al*. (2005) describe how an H_∞ loop shaping controller design route is applied to a shape memory alloy (SMA) actuator, by selecting an operating point and deriving a linear model for the actuator at that operating point. Although not on a fluid power application, this work is of interest because the SMA actuator, like a fluid power actuator, exhibits severe non-linearities.

Rabbo and Tutunji (2008) have shown how an auto-regressive moving average recursive identification method may be applied to a hydrostatic transmission system to produce third and fifth order transfer functions at selected operating points. The focus of their work is the validation of the models produced, which includes the use of a test rig. They do not report the use of the models to design controllers. Their approach contrasts with that in the sequel: they endeavour to produce accurate models using sophisticated identification methods, rather than rely on simple models for use with robust controllers.

2.5 Fuzzy Logic and Fluid Power

This thesis also examines the application of a 'self organising fuzzy logic controller' to the candidate fluid power system. The application of fuzzy logic has been somewhat contentious in the control community. Thus:

> *'Fuzzy logic is not as good as its strong proponents argue, and not as bad as its detractors say!'*

(Prof Karl Aström at the Institution of Electrical Engineers, London, following his presentation of the Inaugural Tustin Lecture (12 May 1999) entitled 'Digital Control - A Perspective'.)

However,

> *'Fuzzy systems let us guess at the non-linear world and yet do not make us write down a math model of the world'*

(Kosko, 1994)

The seminal work on the application of the principles of fuzzy logic to decision making and control was undertaken by Zadeh at the University of California, Berkeley. His work was largely funded by grants from the US Army and Navy and from NASA. It was Zadeh's contention that techniques employed for the analysis of mechanistic systems were not appropriate for humanistic (or human centred) systems, or, indeed, for systems whose complexity is comparable with that of humanistic systems. 'As the complexity of a system increases, our ability to make precise and yet significant statements about its behaviour diminishes until a threshold is reached beyond which precision and significance (or relevance) become more mutually exclusive characteristics' (Zadeh, 1973).

Building on his earlier work to develop the concept of the fuzzy set, his 'new' approach introduced three main distinguishing features (*ibid.*):

1) The use of so-called linguistic variables in place of or in addition to numerical variables;

2) Characterisation of simple relations between variables by conditional fuzzy statements;

3) Characterisation of complex relations by fuzzy algorithms.

(These features are considered further in the Appendix 4.)

These concepts were introduced in support of decision making and the analysis of complex systems. Typical of early applications employing decision making is the fuzzy logic control of a traffic junction reported by Pappis and Mamdani (1977). In a review of the development of the applications of fuzzy logic, Zadeh (1988) acknowledges that the application of fuzzy logic to process control had not been anticipated when its ground rules had been laid. He credits Mamdani and Assilian (1975) with the first implementation of fuzzy logic based control, for the regulation of a steam engine. He lists a range of control process applications, most in Japan. No fluid power applications are explicitly identified.

King and Mamdani (1977) sought to demonstrate the merits of controlling 'complex' processes by using a heuristic approach incorporating fuzzy control concepts. The 'complex' processes to be controlled are those which are non-linear and time varying, and for which available measurements are poor. The difficulty of modelling such processes made controller design impracticable and resulted in the use of a human operator as controller. A human operator's control strategy is based on intuition and experience, and is considered as a set of 'rules of thumb' ('heuristic rules'). King and Mamdani describe how the theory of fuzzy sets and algorithms developed by Zadeh can be used to model the human operator, thus generating a process controller. The limitation set by available digital computing power resulted in the use of a coarse level of measurement quantisation for error and rate of change of error. Use of quantisation levels of 14 and 13, respectively, together with a set of rules, permits the use of a 182 (= 14 × 13) element pre-computed look-up table to generate the required control action. Implementing the control policy directly at each sampling interval was not considered to be adequately computationally efficient. The use of look-up tables with short word length digital systems and programs to generate suitable tables had been investigated by Rutherford and Bloore (1976). King and Mamdani advise, without explanation, that 'the choice of sampling interval depends on the process to be controlled and should be selected so that at least five significant control actions are made during the process settling time.'

A range of alternative approaches to the implementation of fuzzy control rapidly developed, as reported by Tong (1977) in a review of applications. He found that some used set point error and change in set point error as inputs, while others used set point error and sum of set point error as inputs. Output was either control or change in control. Tong described an application of his own in which the inputs are set point error and change in set point error and the output is control when the error is large and change in control when it is small. He found that a fuzzy controller offered robust closed loop performance, tolerating process parameter changes well, with reasonable noise rejection capability, and even partially insensitive to variation in its own implementation. Tong proposed that further consideration be given to a controller which 'learns' about the process to be controlled. He referred to work by Mamdani and Baaklini (1975) and Procyk (1977) who had already commenced work on 'self organising' fuzzy controllers.

Lee (1990 (1), 1990 (2)) undertook a further review of the theory of fuzzy logic and how it might be applied to controller design. He presents a thorough review of the theory of fuzzy logic, before discussing a range of practical issues related to the implementation of a fuzzy logic controller. In his discussion of the discretisation of the universe of discourse, he refers to the benefit of shortening the controller running time by using a look-up table based on discrete universes. The look-up table defines the controller output for all possible combinations of inputs. On this, Lee refers to the work of Rutherford and Bloore (1976). Lee identifies a wide range of applications of fuzzy logic control, but finds none in the fluid power field. He cites the conception and design of fuzzy systems that have the capability to learn from experience as a direction of then recent exploration.

Recognising that no systematic method for the design and analysis of a fuzzy logic controller had been produced, Zhang and Edmunds (1991) produced one, for stated fuzzy implication, fuzzy inference and defuzzification methods. They showed that the defuzzified output of a 'standard' (proportional plus derivative or proportional plus integral) fuzzy logic controller is arrived at by 'a kind of non-linear interpolation'.

Klein and Backé (1993) provide an *ab initio* introduction to fuzzy logic control, aimed at practitioners of fluid power and pneumatics, and demonstrate the

application of fuzzy logic to the control of a pneumatic system in which the feedback gains in a state space controller were adapted according to fuzzy rules.

In the present work, the focus has been the application of 'self organising fuzzy logic control' (SOFLC) in a fluid power environment; changes in the characteristics of the candidate system (a valve controlled motor) with speed set point and supply pressure suggest that a set of rules in a fuzzy logic controller which is appropriate in one set of conditions might not be appropriate in another, making some form of adaptation necessary.

Procyk and Mamdani (1979) published the first description of a rationale for a 'linguistic self-organising process controller'. They describe a fuzzy logic controller, which is enhanced to include continuous adaptation of the control rules. The adaptation is made in response to the results of performance measurement. A performance measure is set, and adjustments to the control rules are made in an attempt to optimise its value. The designer sets qualitative standards for the performance required; a fuzzy logic approach is used to apply these to the system and modify the current set of rules in the controller. The authors emphasise that the performance measure is not process specific; they retained the same measure in simulation experiments for a range of processes.

In a design study, Daley and Gill (1986) investigated how the attitude of a flexible satellite might be controlled using a self organising fuzzy logic controller. A declared design aim was the production of a controller which would be capable of starting with no initial rules. Discrete universes of discourse and a look-up rules table are used. The rules amendment algorithm described for this complex multi-variable process requires all the current rules in the controller's look-up rules table to be examined in each rule modification cycle. The need for significant computational effort is recognised.

In the current work, described in the sequel, the contents of the rules table, rather than of a look-up table, is updated; only one rule is considered for update in each cycle.

In subsequent work, Daley and Gill (1987) improved the performance of their controller by arranging for the vector of gains on the inputs and outputs of the

controller to be switched between two values according to the satellite's states. They did this in preference to increasing the number of elements in the (quantised) support sets and the number of rules, in order to avoid computation burden, and thus to reduce the achievable computational cycle time.

Linkens and Abbod (1991) investigated the application of SOFLC to two test rigs, one incorporating tank level control and the other belt tension control. Although apparently using a quantised approach and a rules amendment algorithm which involved the update of a look-up table similar to that of Daley and Gill (1986), they found that the processing speed of available personal computers was insufficient to enable the control algorithm for the belt tension control rig to be executed at the required rate (50 Hz). They therefore used parallel processing and 'transputers'. On both test rigs they used a gain switching logic to increase the gains when the systems' outputs were near the set point in order to reduce steady state error whilst maintaining satisfactory transient response. They found that controllers with initially empty look-up rules' tables worked satisfactorily.

Zhang and Edmunds (1991) focus on rule modification algorithms, attempting to devise supervisory rules to determine when rules should be modified and when they are 'good enough'. They do this by reference to phase plane analysis and switching curves (see, for example, Schwarzenbach and Gill (1992)). The credit value for rule modification is determined by the direction of the movement of the process state rather than by the position of the process state. The rule modification algorithm operates on the contents of the look-up table which is applied to the quantised controller inputs. Zhang and Edmunds present a series of simulation results for a series of simple linear process models (first order, second order, and first order with pure time delay). For each simulation, the controller starts with an empty rules' look-up table.

Daley and Newton (1994) explored in simulation the application of both a neural network and self organising fuzzy logic to the control of an electro-hydraulic rotary drive system. They followed the approach of Daley and Gill (1987). Thus the rule modification algorithm operates on the contents of the look-up table; controller inputs are quantised and fuzzy sets are defined on universes of discourse containing 14 elements. They report that they examined continuous set descriptions also, but

record only that similar performance was obtained. Details are not given. They conclude that SOFLC was not as successful as and generated a higher computation burden than a feed forward neural network based controller described in the same reference.

Huang and Huang (2004) describe the design and practical testing of a self organizing fuzzy controller for active vibration suppression of a spring-mass-damper system. The system incorporates two direct current servomotors. They make use of a rules amendment procedure, starting with no initial rules.

Feng (2006) carried out a comprehensive review of the application of fuzzy logic control. He found applications in fields such as electrical power distribution system transient stability control, active queue and asynchronous transfer mode management in telecommunications networks, mechanical/robotic systems, including magnetic bearings, robotic wrists, four bar linkages and autonomous robots, automobiles, including suspension control and anti-lock braking systems, and industrial/chemical processes, with applications including temperature control, heat exchanger control and stirred tank reactor vessel control and tank level control, waste treatment and cement kiln control. However, none of his 349 references appears explicitly to relate to the field of fluid power, in particular to a hydrostatic power transmission system.

2.6 Artificial Neural Networks and Fluid Power

Although not pursued in depth in this thesis, the possible use of artificial neural networks for the control of fluid power systems is recognised here for completeness: such networks are candidates as building blocks for controllers for systems which are not easily and precisely defined by virtue of their non-linearities and uncertainties in the values of key parameters.

The work of Daley and Newton (1994) in which they explored in simulation the application of a neural network to the control of an electro-hydraulic rotary drive system has been referred to in Section 2.5 above. Newton (1993, 1994) details the design and implementation, including training, of various neural network based controllers. He considers that these may have some advantages over ‘robust’ linear design methods, because the latter leads to complexities in the design and analysis of the controller, and may result in a compromise between performance and sensitivity.

Nisiumi and Watton (1996) describe the use of real-time artificial neural network control for a servo valve/motor drive. They disclose favourably a comparison between the performance of the system when controlled using a neural network trained on a simulation of the system with the performance when controlled by a controller designed using a linear model. Wong *et al.* (1998) describe the design of inverse neural network controllers for use with low specification direct current servo drives. They demonstrated by experiment that the performance exceeded that of a PID controller tuned using the Ziegler-Nichols method (e.g. Schwarzenbach and Gill, 1992, p. 218 et seq.). However, stable operation demanded the inclusion of a series gain of less than unity.

Neural networks have been judged unsafe for use in process control industries, such as polymer manufacture. According to Turner *et al.* (2003), neural network process gain predictions can spuriously invert in real time causing valves to open when they should be closed. This unsuitability of neural networks was endorsed by Dr Steve Williams in his IEE Tustin Lecture on Thursday, 5 May 2005.

3 System Description, Simulation Environment and Controller Design Route

The focus of this thesis is the design and testing by simulation and practical investigations of robust controllers in a non-linear system, in particular for the speed control of a hydraulic motor in a hydrostatic transmission system. Particular attention is given to disturbance rejection. Disturbances arise from changes in torque load and supply pressure fluctuations. The former may be cyclical, as, for example, when the motor is driving a reciprocating load. Supply pressure fluctuations can be a consequence of several users sharing a common pressure source. A fluid power transmission system was chosen as candidate because non-linearities and parameter uncertainties can make the design of control arrangements for fluid power challenging (Edge, 1997). However, the characteristics of fluid power systems continue to make them attractive in a wide range of applications (Backé, 1993).

Linear approaches, incorporating H_∞ 'mixed sensitivity' and 'loop shaping', and 'fuzzy logic' are applied to controller design. For the linear approaches, non-linearities are treated as contributions to the uncertainties in linear models of the system. These models are derived from information and specifications contained in the data sheets supplied by the component manufacturers, and from the geometry of the system as measured.

3.1 The Test Rig

The candidate system for study and test is a hydrostatic power transmission system comprising a loaded valve-controlled motor and its speed control loop. The motor is supplied from the laboratory ring main. This and the motor comprise a fluid power transmission system. A second hydraulic system controls the load applied to the

motor. The main components of this second system are a pump discharging into a solenoid actuated proportional pressure relief valve. The pump operates in a closed circuit. In order to prevent overheating of the fluid in this circuit, provision is made to bleed off a proportion of the fluid through an orifice and return it to the reservoir. Fresh fluid from the laboratory ring main is added to the low pressure side of the circuit. To permit bi-directional operation, a series of check valves, mounted in a manifold, is provided. Figure 3.1 shows a simplified schematic of the motor/pump combination.

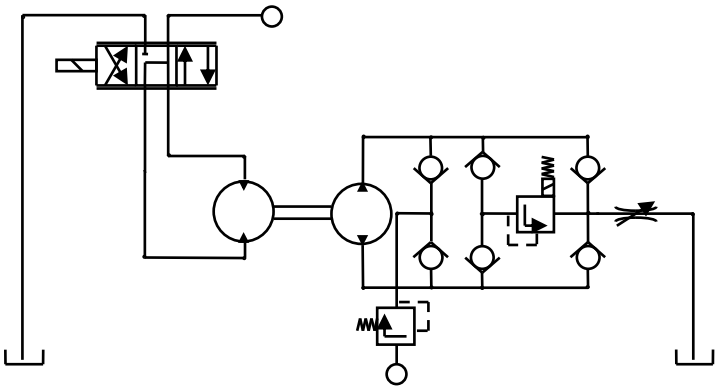

Figure 3.1 Simplified schematic of the test rig

The test rig is a subset of a motor comparator test rig. This was originally created to provide a test bed on which the performances of electric and hydraulic motors could be assessed and compared, and computer simulations of them evaluated and verified. Details of the motor comparator test rig may be found in Monaghan (1998).

Front views of the test rig are shown in Figure 3.2 and Figure 3.3. These show the motor/servovalve combination and the interface unit.

The motor (Figure 3.4) is a Moog-Donzelli Size 2 axial piston motor (39.5 cc/rev displacement) supplied via a Moog model 76M104 servovalve. Its series connected coils are rated at 20 mA.

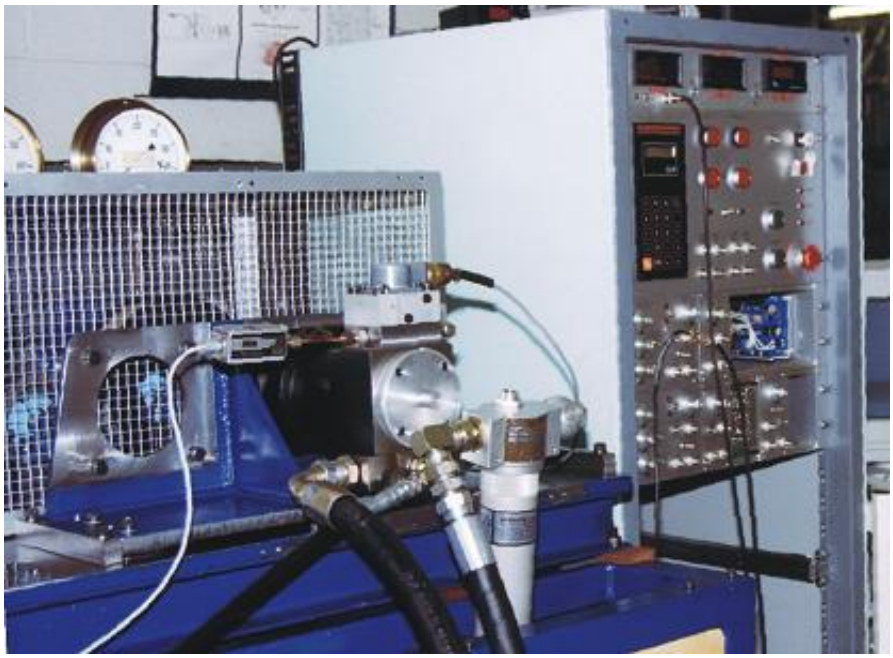

Figure 3.2 Front view of test rig showing hydraulic motor and electronic interface racks

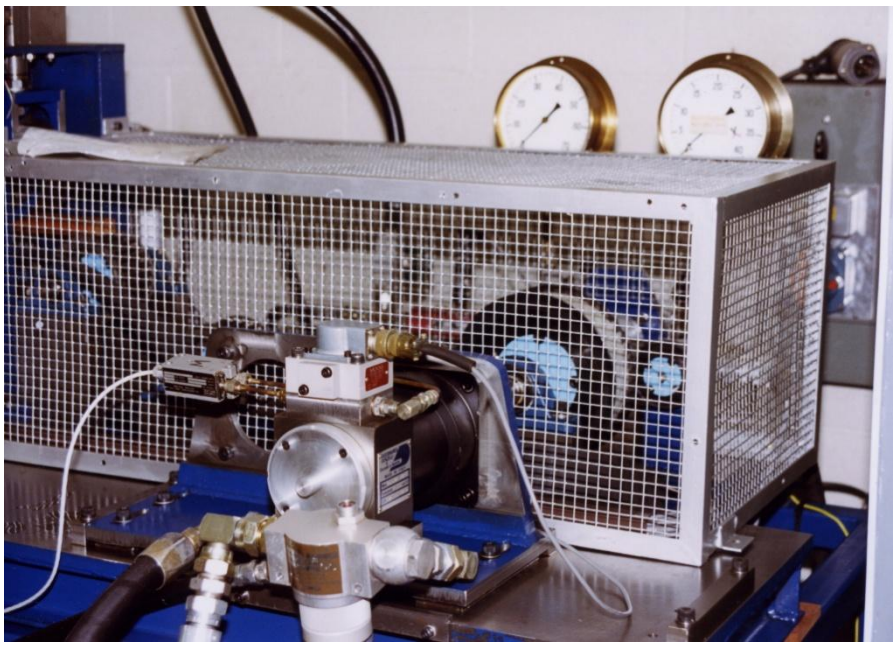

Figure 3.3 Front view of test rig showing hydraulic motor and drive shaft to pump

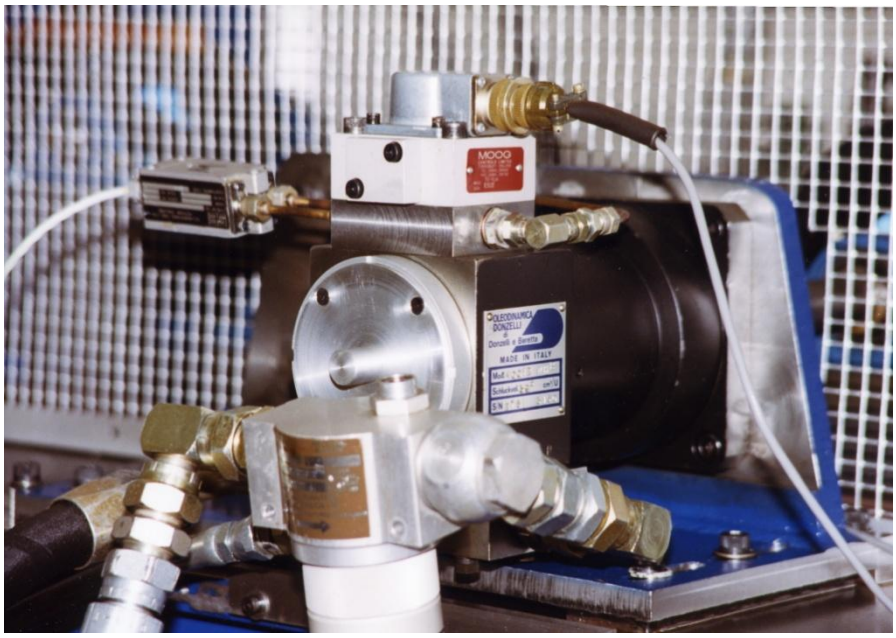

Figure 3.4 Close up of hydraulic motor with servovalve and pressure transducer

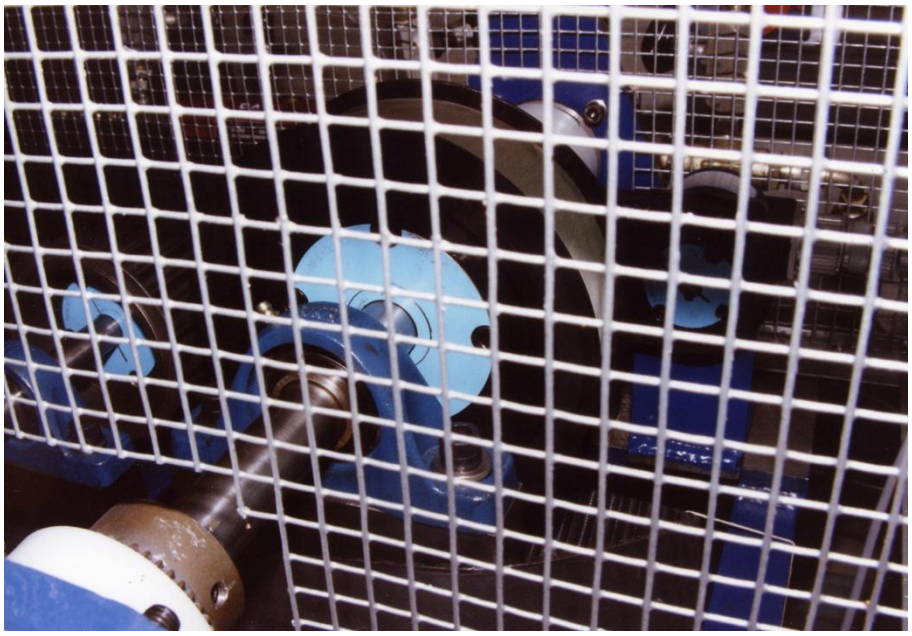

Figure 3.5 View from motor end showing drive shaft, large pulley, and belt drive to optical encoder

The motor is connected via flexible couplings and rigid shaft (Figure 3.5) to a coaxially mounted Sauer Sundstrand gear pump SNM2/19 CO 02 (19.2 cc/rev

displacement) at the rear (Figure 3.6). The shaft drives a BEC734 optical encoder (1250 pulse/rev) through pulleys and a belt. From the output of this encoder is derived electronically a shaft speed signal by an electronic unit which incorporates a Burr-Brown VFC32 voltage-to-frequency and frequency-to-voltage converter chip.

The shaft, couplings and belt driven optical encoder are enclosed within a cage for safety reasons.

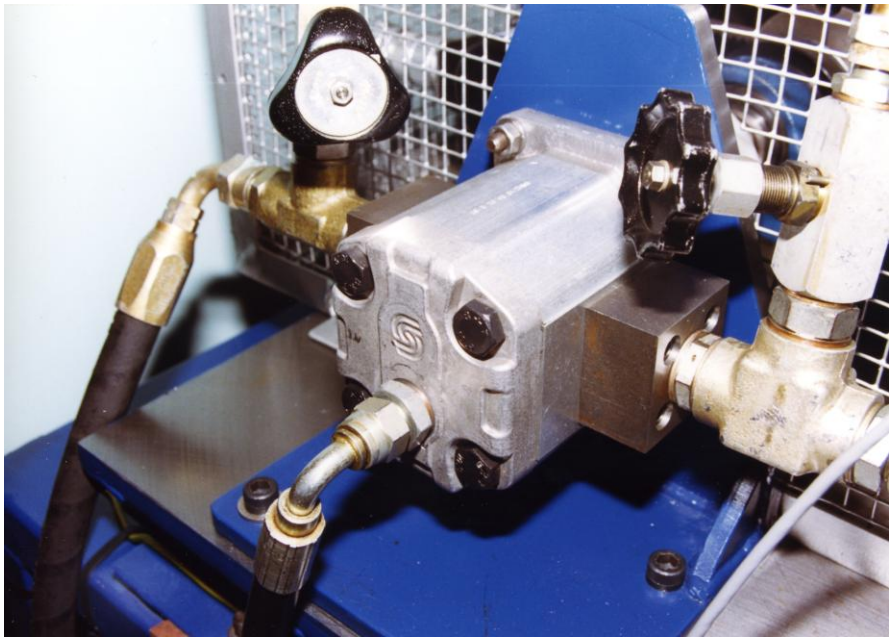

Figure 3.6 View from rear showing gear pump

The pump operates in a closed loop hydraulic circuit built on a purpose designed manifold (Figure 3.7) (see Monaghan, *op. cit.).* This contains a Vickers solenoid actuated proportional pressure relief valve with integral amplifier (KACG-6). The valve may be seen on the manifold at the rear of the photograph (Figure 3.7). The setting of this valve controls pump discharge pressure and thus the motor load torque. Load disturbances are applied by varying the pressure relief valve set point. The load torque is related to the pump discharge pressure by the relationship:

$$shaft\ torque = \frac{pressure\ drop \times pump\ displacement\ per\ revolution}{2\pi}$$

using compatible units (e.g. Cundiff, 2002), ignoring leakage and losses.

Thus, for the Sauer Sundstrand gear pump

$$shaft\ torque\ (Nm) = 0.31\ pressure\ drop\ (bar)$$

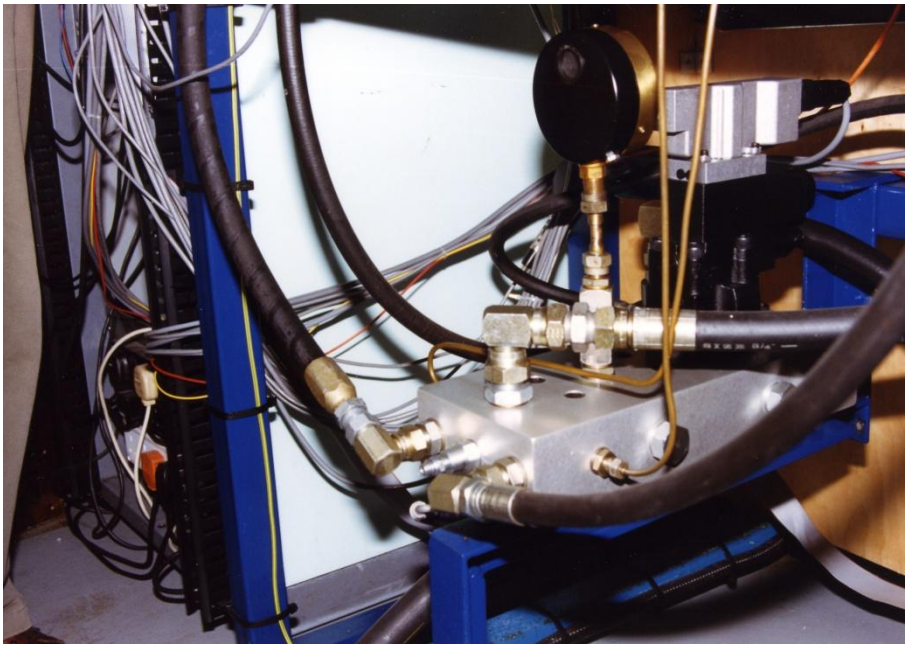

Figure 3.7 Hydraulic loading circuit manifold

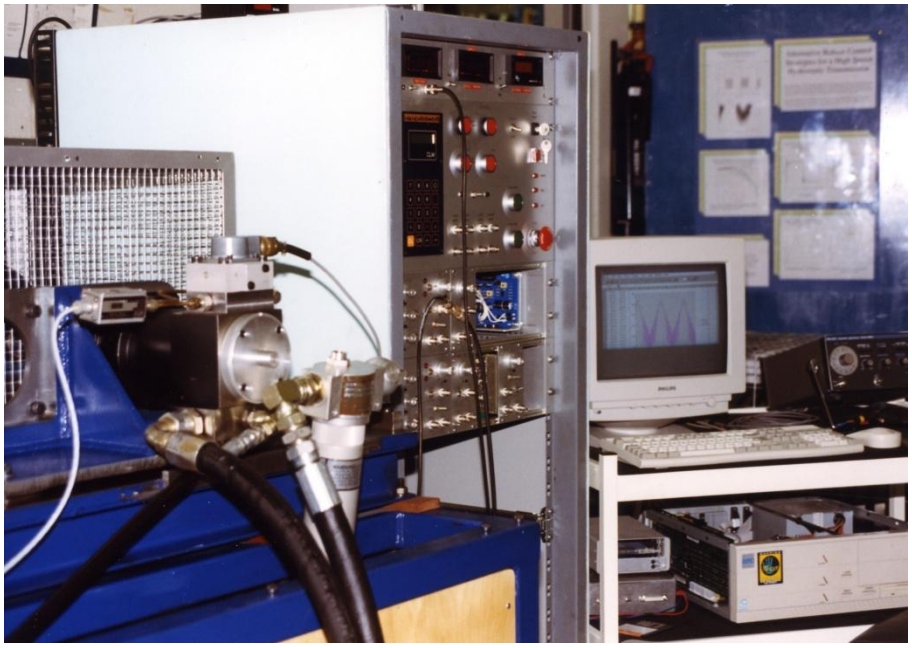

Figure 3.8 Front view of test rig showing electronic interface racks and PC for control and data logging

The manifold also contains a series of cartridge type check valves to allow bidirectional operation of the pump whilst ensuring unidirectional flow in the pressure relief valve.

Other transducers connected to the rig permit the measurement of motor and pump flows, and pump circuit pressure relief valve differential pressure.

An interface unit permits control and data logging to be undertaken using a PC (Figure 3.8). The interface unit includes a current amplifier which delivers 20 mA (maximum) to the servovalve when the control signal derived from the digital to analogue converter driven by the PC is 10 V.

Controllers were implemented digitally using software written in C++. (The interface unit also incorporates an analogue PID controller, used for motor performance testing by Monaghan (1998).)

More information on the test rig, including extracts from component data sheets and key parameters, is contained in Appendix 1.

3.2 Simulation Environment

The simulation tools used for this research are:

- Bath*fp* (Burrows *et al*., 1991) for circuit simulation;
- MATLAB, in particular the Robust Control Toolbox (Chiang and Safanov, 1992) and the μ-Analysis and Synthesis Toolbox (Balas *et al*., 1993)) for the design of linear controllers, and the Fuzzy Systems Toolbox (Wolkenhauer and Edmunds, 1994) for the development of fuzzy logic controllers.

A particularly valuable feature of Bath*fp* is its ability to generate linear models of a system in state space form at user selected operating points. These may be imported into MATLAB to facilitate analysis (e.g. of frequency response) or controller design.

3.3 Controller Design Route

A design methodology for the design of the linear controllers was drawn up as follows, and is illustrated as a flow chart in Figure 3.8.

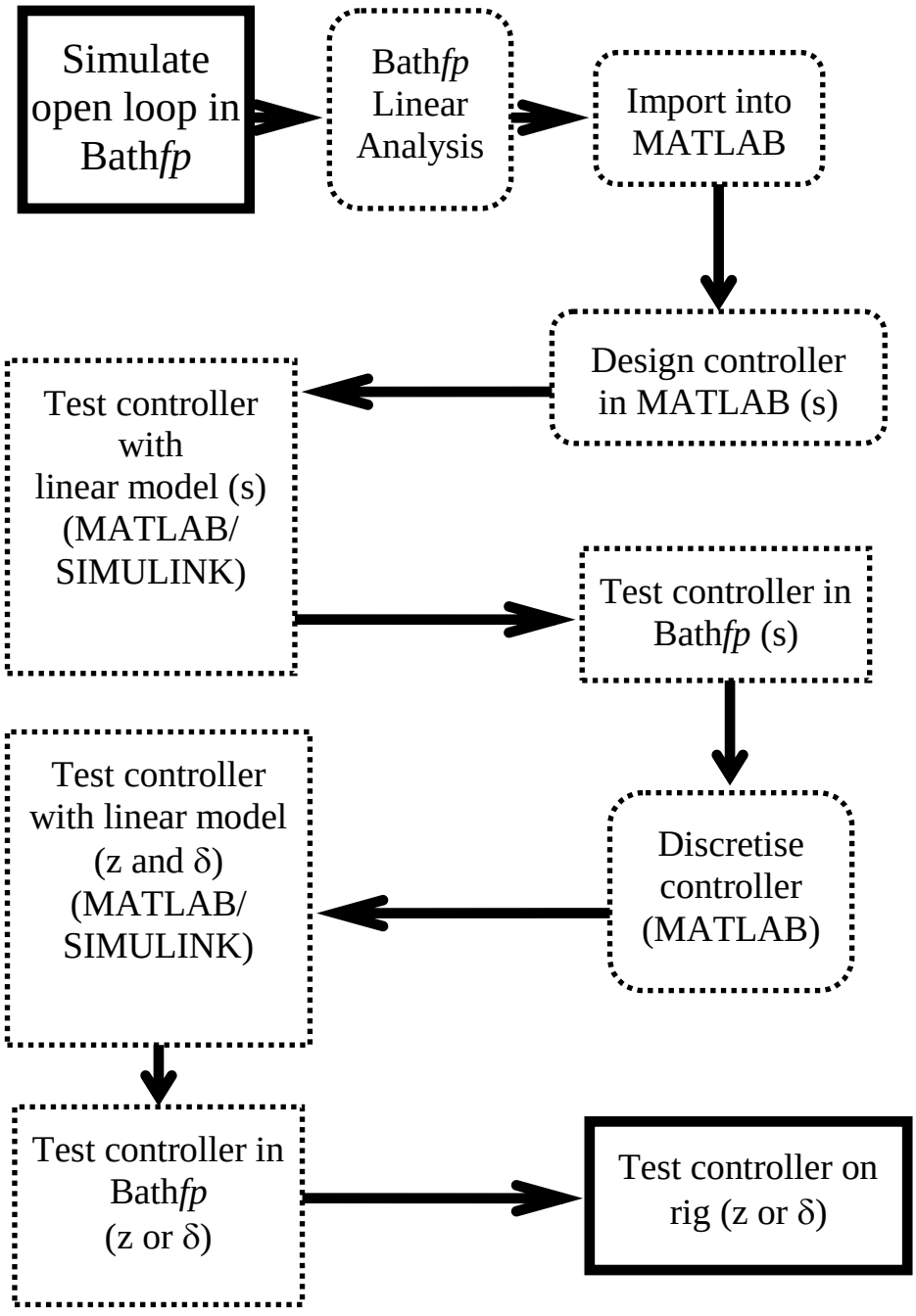

Figure 3.8 Design methodology used in case study

The methodology may be summarised as follows:

1. Simulate the rig in Bath*fp*, creating or modifying component models as necessary and establishing parameters by reference to manufacturers' data sheets and rig dimensions;
2. Use the Bath*fp* Linear Analysis Tool to produce linearised representations of the rig in state space form;
3. Import the linearised representations of the rig into MATLAB and use them to design continuous controllers;
4. Test the continuous controllers using the Bath*fp* rig simulation;
5. Use MATLAB algorithms to discretise the controllers;
6. Test the discretised controllers using (linearised) state space representations of the rig in MATLAB/SIMULINK;
7. Test the discretised controllers using the Bath*fp* rig simulation;
8. Test the discretised controllers using the rig.

Not all of the steps were included in the design of every controller. The exact approach is documented in the appropriate section.

4 Conventional Control

In this chapter is described a short series of experimental tests using P (proportional), PI (proportional plus integral) and PID (proportional plus integral plus derivative) control.

4.1 Performance Using Proportional Control

A series of tests was undertaken using a proportional controller, with unity gain (1 mA/rpm). This was implemented digitally. Similar performance was obtained using sampling rates of 100 Hz and 1000 Hz. The results shown in Figures 4.1 and 4.2 were collected using a sampling rate of 1000 Hz and at a supply pressure of 50 bar.

Tracking test - the proportional controller's tracking capability was examined further by applying a square wave speed reference (demand) signal, as shown by the broken line in Figure 4.1. The control effort is shown in Figure 4.2. Control effort is the voltage signal generated by the PC which runs the control software (see Section 3.1). Its maximum value is 10 volts. This is converted by the interface electronics to provide a current of 20 mA to the servovalve.

In the high speed phase of the demand cycle there is a significant steady state error, as might be expected when proportional control is used. (Note that the controller is not saturated). In the low speed phase of the demand cycle, instability is evident, as shown both in the tracking and control effort plots. This instability results in considerable audible noise, mainly chatter from the couplings between components on the main shaft of the test rig.

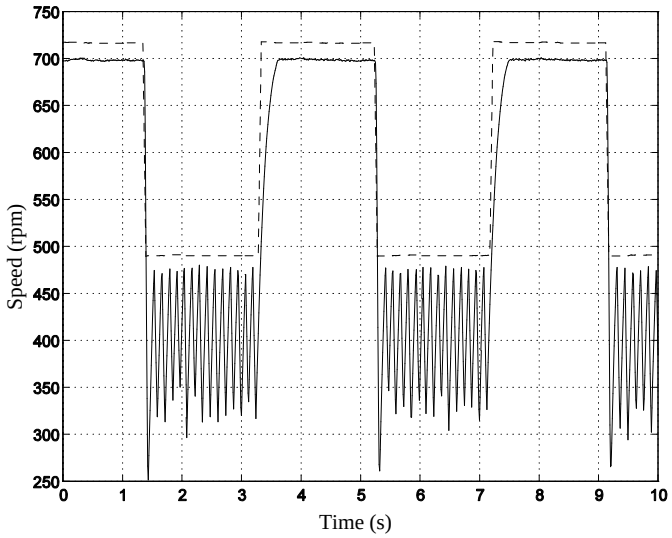

Figure 4.1 Tracking test - proportional control

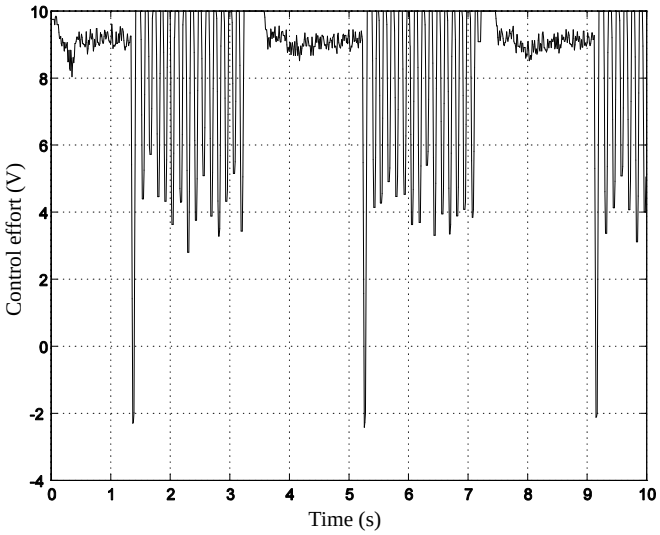

Figure 4.2 Control effort - proportional control

Disturbance rejection test - a cyclical load disturbance was applied by varying the cracking pressure of the Vickers proportional relief valve and hence load torque. The speed regulation, load disturbance (as measured by proportional relief valve cracking pressure) and control effort are plotted respectively in Figures 4.3, 4.4 and 4.5.

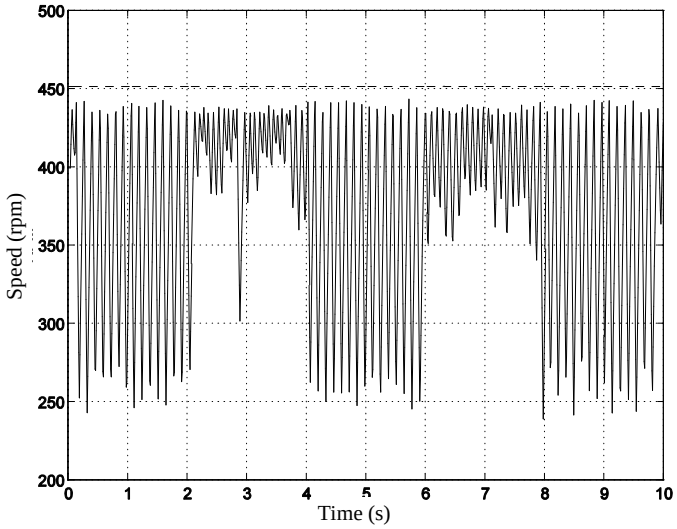

Figure 4.3 Disturbance rejection (proportional control)

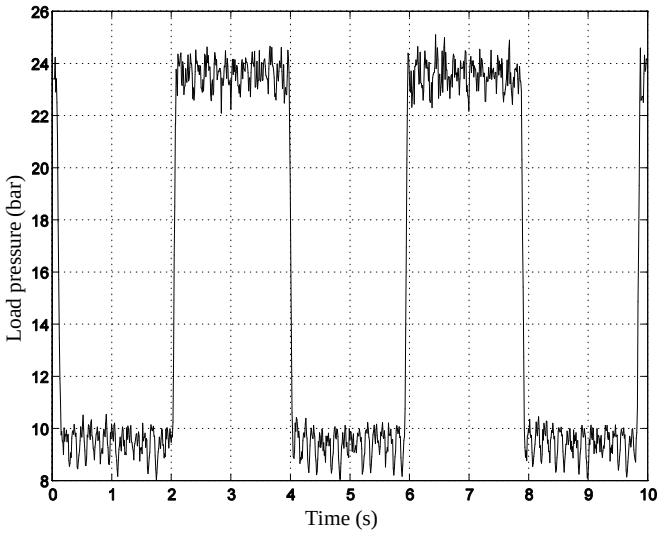

Figure 4.4 Load disturbance (proportional control)

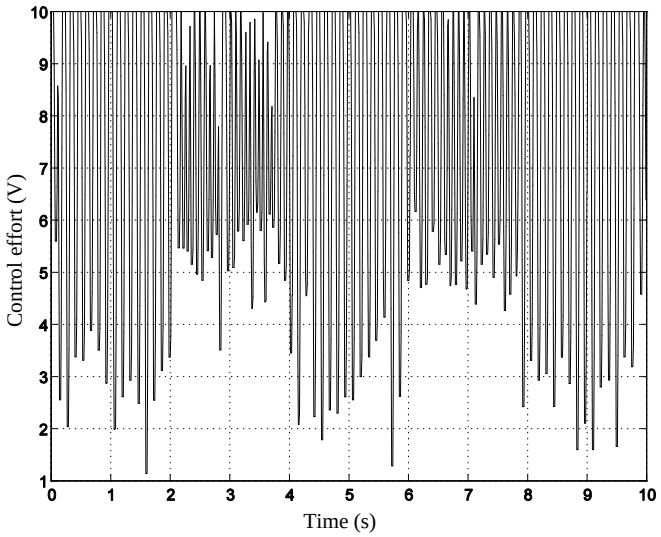

Figure 4.5 Control effort during disturbance rejection (proportional control)

Once again, instability is evident, together with significant mean speed errors.

4.2 PID Control Example

To provide a further reference for the controllers to be designed in the sequel, a PID controller designed according to Ziegler-Nichols (e.g. Schwarzenbach and Gill, 1992, p. 218 *et seq*.) was briefly investigated.

According to this design method, the loop is first closed through a proportional gain controller. The gain is increased progressively until stability is lost, when the gain is k_{crit}. The time period of the resultant oscillation is measured as P_{crit}.

The PID control law is

$$G_c(s) = k_c\left(1 + \frac{1}{T_i s} + T_d s\right) \tag{4.1}$$

Where k_c is the proportional gain and T_i and T_d are the time constants of the integral and differential elements respectively.

The design method provides recommended settings for alternative controllers as shown in Table 4.1.

Table 4.1 Controller designed according to Ziegler-Nichols

	k_c	T_i	T_d
Proportional control	$0.5k_{crit}$		
PI control	$0.45k_{crit}$	$0.83P_{crit}$	
PID control	$0.6k_{crit}$	$0.5P_{crit}$	$0.125P_{crit}$

Operating at 50 bar supply pressure, with a demanded speed of *c.* 700 rpm, the proportional gain at the margin of stability, k_{crit}, was *c.* 1.2 mA/rpm, and the frequency of oscillation was found to be *c.* 35 Hz, giving a value of *c.* 3×10^{-2} s for P_{crit}. However, stable operation of a PID controller having a control law according to the design method above did not prove possible. It is assumed that this was, at least in part, due to the effect of system noise on the 'differential' element of the controller.

Using the method to design a PI controller results in suggested values of 0.54 mA/rpm for k_c and 27.7 s for T_i, corresponding to an integral gain of 12.4 mA/rpm/s.

On the test rig, operation with a proportional gain of 0.5 mA/rpm did not prove practicable with an integral gain greater than *c.* 5 mA/rpm/s. With the two gains set at these values, stable operation was only achievable at higher demanded speeds, as shown in Figure 4.6. The supply pressure for this test was again 50 bar.

The Ziegler-Nichols method requires the system to be operated at or near its stability limit in order to measure k_{crit} and P_{crit}. The non-linearities, which result in gain varying with speed, make this difficult. There is a danger that the rig might be damaged by ensuing oscillations. The gains derived using the method may or may

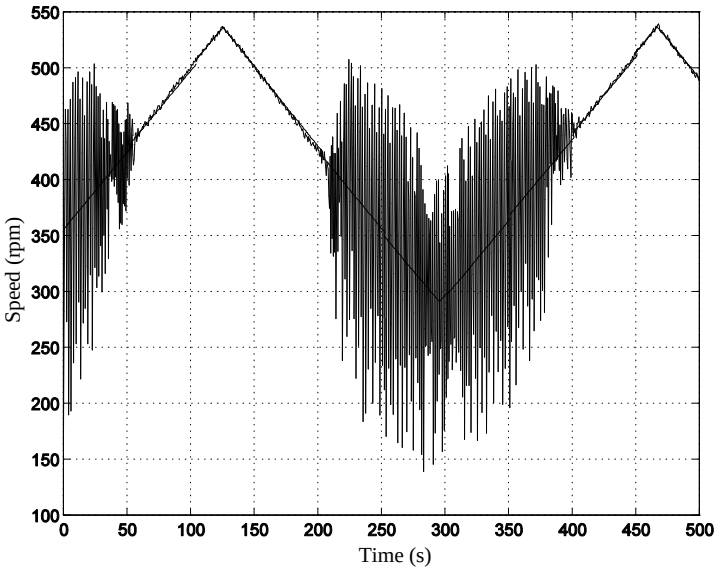

Figure 4.6 Set point tracking performance of a PI controller

not be appropriate for operation under the conditions for which they are calculated. However, moving the set point from zero at start up to the value required for operation requires the system to pass through regions of higher gain (corresponding to lower speeds), making smooth operation impossible.

4.3 Conventional Control – Conclusions

This short series of tests has demonstrated how the non-linearities of the test system lead to control difficulties.

Thus, in the proportional control speed tracking test, a gain which results in stable operation, with steady state error, at 'high' speed leads to instability when the speed is reduced. Reducing the gain to maintain stability at lower speeds would increase the steady state error at higher speeds.

Although in the PID test it was possible to choose control parameters which provided good speed tracking at higher speeds, once again instability occurred when the speed was reduced.

The performance of the unity gain proportional controller and the PID controller will be shown to be inferior to that of the H_∞ designs in the sequel.

5 Linear Robust Control 1

At the commencement of this study, it is taken that the test circuit is non-linear. The presence of the non-linearities and their effects on the performance of the test system are subsequently confirmed and demonstrated. It has been further assumed that the effects of the non-linearities can be treated as if the non-linearities where 'perturbations' to a linear model of the test system. This terminology is developed in the following sections.

5.1 Background to Linear Control Theory

The background analysis in the introductory paragraphs is generally presented with reference to a single input, single output system.

5.1.1 Closed Loop Control - Some Terminology

Variables used in Section 5.1.1:

s	complex variable
$d(s)$	disturbance, in this case at the plant output
$e(s)$	input to compensator
$m(s)$	measurement noise
$r(s)$	reference signal
$u(s)$	control effort
$y(s)$	output
$G(s)$	plant transfer function
$K(s)$	compensator or controller transfer function
$L(s)$	open-loop transfer function
$P(s)$	prefilter transfer function
$S(s)$	sensitivity
$T(s)$	complementary sensitivity

Consider the linear time invariant (LTI) system (following Maciejowski, 1989):

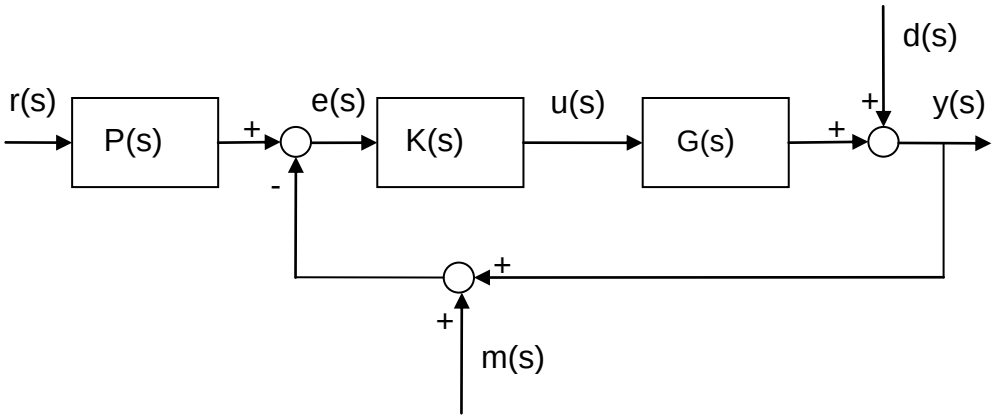

Figure 5.1 General closed loop LTI system

In the following analysis, $r(s)$, $d(s)$, $m(s)$, $y(s)$ are scalars and $P(s)$, $K(s)$, $G(s)$ are rational transfer functions (for the single input, single output (SISO) case). They may be replaced by vectors $\boldsymbol{r}(s)$, $\boldsymbol{d}(s)$, $\boldsymbol{m}(s)$, $\boldsymbol{y}(s)$, and transfer function matrices $\boldsymbol{P}(s)$, $\boldsymbol{K}(s)$, $\boldsymbol{G}(s)$ (multi input, multi output (MIMO) case). The identity matrix $\mathbf{I}$ then replaces unity 1 throughout.

For the system shown in Figure 5.1,

$$e(s) = P(s)r(s) - (y(s) + m(s)) \tag{5.1}$$

$$y(s) = (1 + G(s)K(s))^{-1}d(s) + (1 + G(s)K(s))^{-1}G(s)K(s)P(s)r(s) - (1 + G(s)K(s))^{-1} G(s)K(s)m(s) \tag{5.2}$$

Define sensitivity

$$S(s) = (1 + G(s)K(s))^{-1} \tag{5.3}$$

and complementary sensitivity

$$T(s) = S(s)G(s)K(s) \tag{5.4}$$

then from eq. (5.2)

$$y(s) = S(s)d(s) + T(s)P(s)r(s) - T(s)m(s) \tag{5.5}$$

If $d(s) = m(s) = 0$ and $P(s) = 1$

$$y(s) = T(s)r(s) \tag{5.6}$$

$$e(s) = r(s) - y(s) \tag{5.7}$$

From eq. (5.2)

$$e(s) = r(s) - (1 + G(s)K(s))^{-1}G(s)K(s)r(s) \quad (5.8)$$

$$= S(s)r(s) \quad (5.9)$$

From eq. (5.5), if $r(s) = 0$

$$y(s) = S(s)d(s) - T(s)m(s) \quad (5.10)$$

Also define

$$L(s) = G(s)K(s) \quad (5.11)$$

(open-loop transfer function)

then

$$S(s) = (1 + L(s))^{-1} \quad (5.12)$$

$$T(s) = (1 + L(s))^{-1}L(s) \quad (5.13)$$

Now consider system performance.

For good tracking, $T(s) = 1$ (eq. (5.6)), but for good measurement noise reduction, $T(s)$ should be small (eq. (5.10)), pointing to a conflicting requirement. ($P(s)$ can be used to boost the system response at frequencies where measurement noise dictates that $T(s)$ should be low (see eq. (5.5)).

For low error, $S(s)$ should be low (eq. (5.9)). For good disturbance rejection, $S(s)$ should be low (eq. (5.10)).

However, it is necessary to consider the relationship between $S(s)$ and $T(s)$. From eq. (5.4),

$$S(s) + T(s) = S(s) + S(s)G(s)K(s) \quad (5.14)$$

$$= S(s)\,(1 + G(s)K(s)) \quad (5.15)$$

$$= 1 \quad (5.16)$$

For the MIMO case:

$$\boldsymbol{S}(s) + \boldsymbol{T}(s) = \mathbf{I} \quad (5.17)$$

The above results may be used to specify the performance of the closed loop system.

5.1.2 Specifying the Performance of the Closed Loop

A design approach in which an attempt is made to determine a unique solution in accord with a rigidly defined specification in some optimal way is one of ‘synthesis’

(e.g. Schwarzenbach and Gill, 1992). However, it may be hard to justify the cost of a high order controller, which might result from the design approach, on the grounds of dynamic performance alone. Thus the sensitivity and complementary sensitivity may be specified for the system. The relationship between sensitivity $S(s)$ and complementary sensitivity $T(s)$ (eq. (5.16)) makes it clear that there must be a trade off between them.

The system must also be stable. For stability, *S*, *SG*, *KS* and *KSG* (see Section 5.1.1) must all be stable (e.g. Piché *et al*., 1991, Maciejowski, 1989).

If sensitivity were the only design criterion, then one could derive the required control algorithm from a plant model and a frequency domain specification of the sensitivity. It would be necessary to test the result for stability, as above. If no robustness criterion has been set, even if the stability requirements are met, the system may not be stable if the real plant differs in any way from the plant as modelled.

Closed loop performance specifications may be set as follows by reference to the relationships developed in Section 5.1.1:

(1) Sensitivity: - keep *S* as small as possible (*S* transfers output disturbance to output and reference input to error);

(2) Noise propagation: - keep *T* as small as possible (conflicts with (1)) (*T* transfers measurement noise to output);

(3) Tracking reference signal: - keep $T \approx 1$ (assuming no prefilter *P*, so that design has only one degree of freedom, i.e. *K*) (conflicts with (2) but not (1));

(4) Minimise control effort: - keep *K* as small as possible (may conflict with (1) and (3)).

5.1.3 Using 'Norms' to Specify Performance

To apply the specifications in Section 5.1.2 to SISO systems, the sizes of the transfer functions *S*, *T*, etc., may be defined as their moduli. To apply these specifications to MIMO systems, it is necessary to define a measure of size which recognises that $\boldsymbol{S}$, $\boldsymbol{T}$, etc. are transfer function matrices, i.e. matrices in which each element is the ratio

of a pair of polynomials which represents a transfer function. Size is now measured by the 'norm'.

Matrix norms can be defined in terms of vector norms.

Let $\|\boldsymbol{x}\|$ represent a vector norm.

Let $\|\boldsymbol{G}\|$ represent a matrix norm.

If $\boldsymbol{x}$ is a vector of inputs to matrix $\boldsymbol{G}$, and $\boldsymbol{y}$ is the corresponding vector of outputs, then

$$\boldsymbol{y} = \boldsymbol{G}\boldsymbol{x} \tag{5.18}$$

For a given $\boldsymbol{G}$, the norm (size) of vector $\boldsymbol{y}$, that is $\|\boldsymbol{y}\|$, will clearly vary with the size and direction of vector $\boldsymbol{x}$.

The induced or subordinate norm of $\boldsymbol{G}$ may be defined as the least upper bound (supremum) of the ratio of the norm of the output vector to the input vector, as the size and direction of the latter varies.

$$\|\boldsymbol{G}\| = \sup_{\boldsymbol{x} \neq \boldsymbol{0}} \frac{\|\boldsymbol{y}\|}{\|\boldsymbol{x}\|} \tag{5.19}$$

$$\|\boldsymbol{G}\| = \sup_{\boldsymbol{x} \neq \boldsymbol{0}} \frac{\|\boldsymbol{G}\boldsymbol{x}\|}{\|\boldsymbol{x}\|} \tag{5.20}$$

($\boldsymbol{x} = \boldsymbol{0}$ means that every element of $\boldsymbol{x}$ is identically equal to zero.)

The Euclidean vector norm is defined as follows:

$$\|\boldsymbol{x}\| = \sqrt{\left(\boldsymbol{x}^{\mathrm{H}}\,\boldsymbol{x}\right)} \tag{5.21}$$

where $\boldsymbol{x}^{\mathrm{H}}$ is the transpose of the complex conjugate of $\boldsymbol{x}$.

If the induced or subordinate matrix norm is derived using Euclidean vector norms, then the matrix norm is known as the spectral or Hilbert norm:

$$\|\boldsymbol{G}\|_{\mathrm{S}} = \bar{\sigma} \tag{5.22}$$

where $\bar{\sigma}^2$ is the maximum eigenvalue of $\boldsymbol{G}^{\mathrm{H}}\boldsymbol{G}$ (or of $\boldsymbol{G}\boldsymbol{G}^{\mathrm{H}}$).
Positive square roots of the eigenvalues of $\boldsymbol{G}^{\mathrm{H}}\boldsymbol{G}$ are called singular values of $\boldsymbol{G}$.

If $\boldsymbol{G}$ is transfer function matrix $\boldsymbol{G}(s)$, then the singular values of $\boldsymbol{G}(j\omega)$ are called principal gains, and are functions of the frequency ω. The maximum singular value is the spectral norm at that frequency.

In the SISO case, $G(s)$ is a scalar; it is the transfer function. Following the above analysis results in a single principal gain $\sqrt{\left(G(j\omega)G^*(j\omega)\right)}$, where * indicates a complex conjugate. This is the modulus of $G(j\omega)$, i.e. the Bode gain of $G(j\omega)$.

Specifications for $\boldsymbol{S}$ and $\boldsymbol{T}$ can be stated in terms of $\bar{\sigma}\left(\boldsymbol{S}(j\omega)\right)$ and $\bar{\sigma}\left(\boldsymbol{T}(j\omega)\right)$.

The infinity norm of $\boldsymbol{G}$ is defined as

$$\left\|\boldsymbol{G}\right\|_\infty = \sup_\omega \bar{\sigma}\left(\boldsymbol{G}(j\omega)\right) \qquad (5.23)$$

Thus upper bounds on the maximum singular values (or principal gains) of $\boldsymbol{S}$ and $\boldsymbol{T}$ (which are transfer function matrices) may be defined in terms of "infinity norms".

The infinity norm may be used to specify a frequency dependent bound. Consider first a SISO system. If a scalar transfer function $G(j\omega)$ is required to have a modulus which is less than or equal to a given frequency performance bound $B(j\omega)$, then

$$\left|G(j\omega)\right| \le \left|B(j\omega)\right| \qquad \forall\omega \qquad (5.24)$$

implies that

$$\left|B^{-1}(j\omega)\right|\left|G(j\omega)\right| \le 1 \qquad \forall\omega \qquad (5.25)$$

The literature generally defines bounds in terms of the inverse of a frequency dependent weighting function $W(j\omega)$, i.e.

$$W(j\omega) = B^{-1}(j\omega) \qquad (5.26)$$

Thus

$$\left|W(j\omega)\right|\left|G(j\omega)\right| \le 1 \qquad \forall\omega \qquad (5.27)$$

This implies that

$$\sup_\omega \left(\left|W(j\omega)\right|\left|G(j\omega)\right|\right) \le 1 \qquad (5.28)$$

If $\boldsymbol{G}$ is a transfer function matrix, dimension $m \times n$, representing a multi-input, multi-output system with n inputs and m outputs, then it is necessary to consider how output bounds might be applied to each of its m output channels, by examining all principal gains σ of $\boldsymbol{W}(j\omega)\boldsymbol{G}(j\omega)$. $\boldsymbol{W}(j\omega)$ is now a square diagonal matrix dimensioned to match the number of output channels, that is $m \times m$. Then

$$\sigma\left(\boldsymbol{W}(j\omega)\boldsymbol{G}(j\omega)\right) \le 1 \qquad \forall \omega \tag{5.29}$$

Therefore

$$\bar{\sigma}\left(\boldsymbol{W}(j\omega)\boldsymbol{G}(j\omega)\right) \le 1 \qquad \forall \omega \tag{5.30}$$

$$\sup_{\omega}\left(\bar{\sigma}(\boldsymbol{W}(j\omega)\boldsymbol{G}(j\omega))\right) \le 1 \tag{5.31}$$

That is

$$\left\|\boldsymbol{W}\boldsymbol{G}\right\|_{\infty} \le 1 \tag{5.32}$$

Thus it is, in principle, possible to define frequency dependent bounds on $\boldsymbol{S}$ and $\boldsymbol{T}$, and to define the specification as:

$$\left\|\boldsymbol{W}_1\boldsymbol{S}\right\|_{\infty} \le 1 \tag{5.33}$$

$$\left\|\boldsymbol{W}_3\boldsymbol{T}\right\|_{\infty} \le 1 \tag{5.34}$$

For given specifications, the choice of $\boldsymbol{W}_1$ and $\boldsymbol{W}_3$ is usually not unique, i.e. more than one weighting function can be chosen to embrace a given specification. The order of the controller will, however, depend in part on the order of the weighting function chosen. (For an understanding of choice of subscripts, see Section 5.1.7.)

In addition, as a result of the relationship

$$\boldsymbol{S}(s) + \boldsymbol{T}(s) = \mathbf{I} \tag{5.35}$$

it may be shown (e.g. Doyle *et al*., 1990) that, for the scalar case, that the weights chosen must satisfy the relationship

$$\min\left\{|W_1|, |W_3|\right\} < 1 \qquad \forall \omega \tag{5.36}$$

For a MIMO system, the constraint on the weights can be shown to be

$$\bar{\sigma}\left(\boldsymbol{W}_1^{-1}\right) + \bar{\sigma}\left(\boldsymbol{W}_3^{-1}\right) > 1 \tag{5.37}$$

5.1.4 Robustness and Plant Uncertainty

The meaning of the term 'robustness' was considered in Chapter 2. A robust control system is one which exhibits the desired performance in the presence of significant plant uncertainties (e.g. Dorf and Bishop, 1995). Differences between the actual plant parameters and those included in the model of it used to design a controller may result in instability. Classical design responds to this by introducing concepts such as gain and phase margin. These margins are either chosen arbitrarily, or on the basis of empirical knowledge of the system being designed. The design approach implicitly assumes that the phase lag at the gain cross over frequency might be under-estimated by not more than the phase margin.

The application of the margins in SISO system design is straightforward. The approach does not require the source of the discrepancies between the actual system and its model to be identified. They are known as "unstructured uncertainties". For a MIMO system, interaction between the "loops" leads to additional complexity.

The uncertainty in models of a multivariable plant, which has "true" transfer function matrix $\boldsymbol{G}(s)$, can be represented in three ways. In each case, the nominal plant is represented by a transfer function matrix $\boldsymbol{G_o}(s)$, the nominal transfer matrix, and the uncertainties are represented by a second transfer function matrix $\boldsymbol{\Delta}(s)$ ("perturbations"). The three representations show the uncertainty additively, multiplicatively at the input, and multiplicatively at the output as shown below (Chiang and Safanov, 1988; Maciejowski, 1989):

Additive model:

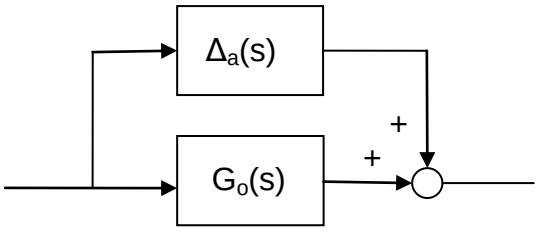

Figure 5.2 Additive perturbation model

$$\boldsymbol{G}(s) = \boldsymbol{G_o}(s) + \boldsymbol{\Delta_a}(s) \qquad (5.38)$$

Input multiplicative model:

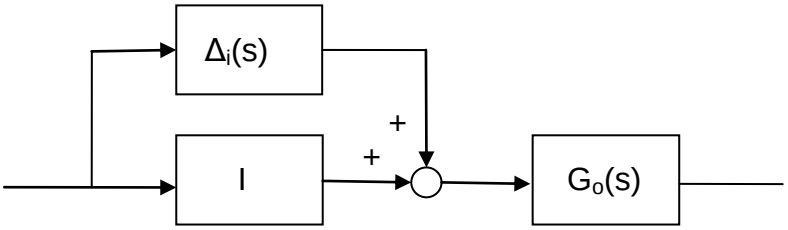

Figure 5.3 Input multiplicative perturbation model

$$\boldsymbol{G}(s) = \boldsymbol{G_o}(s)(\mathbf{I} + \boldsymbol{\Delta_i}(s)) \tag{5.39}$$

Output multiplicative model:

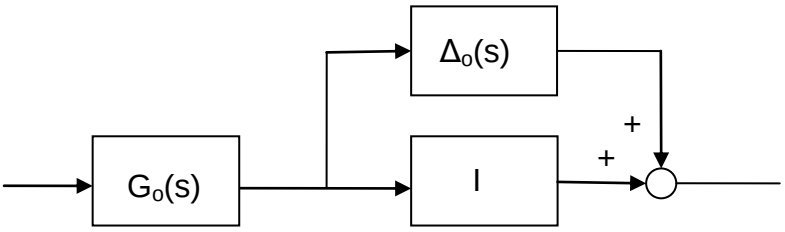

Figure 5.4 Output multiplicative perturbation model

$$\boldsymbol{G}(s) = (\mathbf{I} + \boldsymbol{\Delta_o}(s))\boldsymbol{G_o}(s) \tag{5.40}$$

The sizes of the perturbation matrices can be defined by their norms $\|\boldsymbol{\Delta}\|_\infty$.

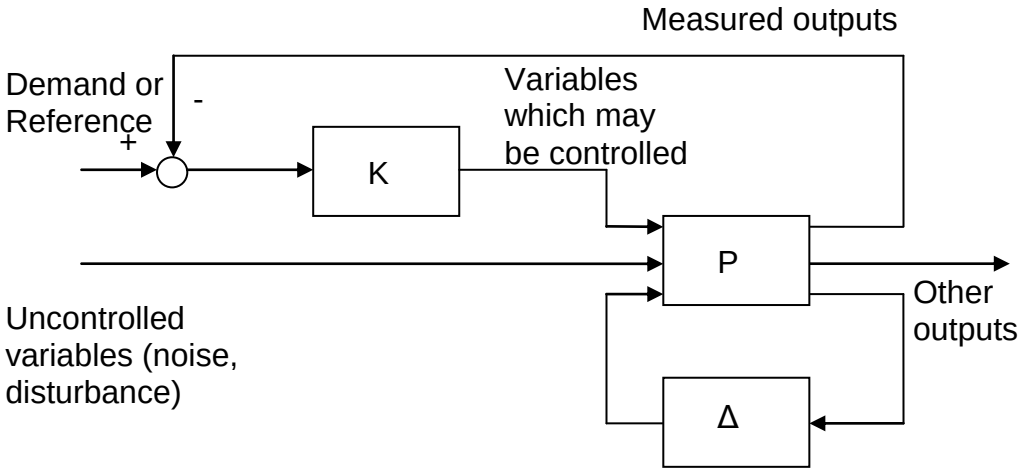

Figure 5.5 Generalised representation of plant and controller

Figure 5.5 is a generalised representation of a compensator/controller ***K***, a reference plant ***P*** and uncertainty ***Δ***. Plant inputs are grouped into those which can be manipulated and those which cannot. The latter include noise signals and disturbances.

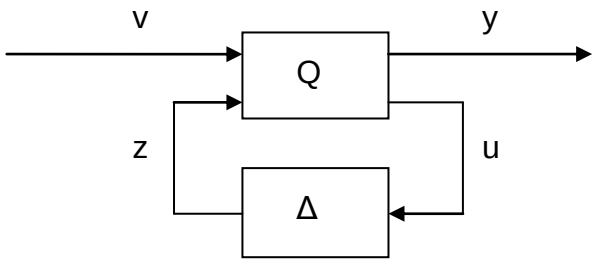

Figure 5.6 Model isolating perturbation

In Figure 5.6, the system model has been redrawn to amalgamate the plant and compensator/controller into a single block ***Q***. For this reduced system, one may write

$$\begin{bmatrix} \boldsymbol{y} \\ \boldsymbol{u} \end{bmatrix} = \begin{bmatrix} \boldsymbol{Q}_{11} & \boldsymbol{Q}_{12} \\ \boldsymbol{Q}_{21} & \boldsymbol{Q}_{22} \end{bmatrix} \begin{bmatrix} \boldsymbol{v} \\ \boldsymbol{z} \end{bmatrix} \qquad (5.41)$$

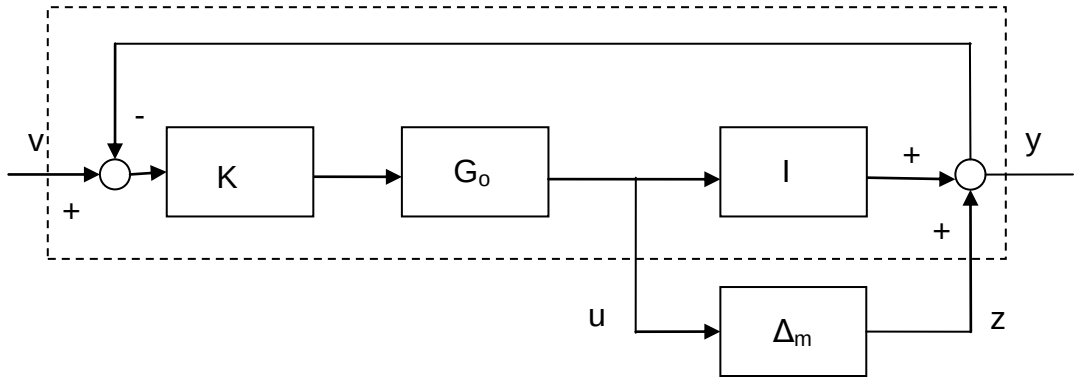

Figure 5.7 Closed loop with output multiplicative uncertainty

By reference to Figure 5.7, which shows an output multiplicative plant uncertainty for a MIMO system, one may write

$$\boldsymbol{y} = \boldsymbol{u} + \boldsymbol{z} \tag{5.42}$$

$$\boldsymbol{u} = \boldsymbol{G}_o\boldsymbol{K}(\boldsymbol{v} - \boldsymbol{y}) \tag{5.43}$$

Substitute for $\boldsymbol{u}$ in eq. (5.42)

$$\boldsymbol{y} = \boldsymbol{G}_o\boldsymbol{K}(\boldsymbol{v} - \boldsymbol{y}) + \boldsymbol{z} \tag{5.44}$$

$$\boldsymbol{y} = (\mathbf{I} + \boldsymbol{G}_o\boldsymbol{K})^{-1}\boldsymbol{G}_o\boldsymbol{K}\boldsymbol{v} + (\mathbf{I} + \boldsymbol{G}_o\boldsymbol{K})^{-1}\boldsymbol{z} \tag{5.45}$$

Substituting for $\boldsymbol{y}$ in eq. (5.43)

$$\boldsymbol{u} = \boldsymbol{G}_o\boldsymbol{K}(\boldsymbol{v} - ((\mathbf{I} + \boldsymbol{G}_o\boldsymbol{K})^{-1}\boldsymbol{G}_o\boldsymbol{K}\boldsymbol{v} + (\mathbf{I} + \boldsymbol{G}_o\boldsymbol{K})^{-1}\boldsymbol{z})) \tag{5.46}$$

$$= \boldsymbol{G}_o\boldsymbol{K}(\mathbf{I} + \boldsymbol{G}_o\boldsymbol{K})^{-1}\boldsymbol{v} - \boldsymbol{G}_o\boldsymbol{K}(\mathbf{I} + \boldsymbol{G}_o\boldsymbol{K})^{-1}\boldsymbol{z} \tag{5.47}$$

Thus, comparing coefficients, from eq. (5.45)

$$\boldsymbol{Q}_{11} = (\mathbf{I} + \boldsymbol{G}_o\boldsymbol{K})^{-1}\boldsymbol{G}_o\boldsymbol{K} \tag{5.48}$$

$$\boldsymbol{Q}_{12} = (\mathbf{I} + \boldsymbol{G}_o\boldsymbol{K})^{-1} \tag{5.49}$$

and from eq. (5.47)

$$\boldsymbol{Q}_{21} = \boldsymbol{G}_o\boldsymbol{K}(\mathbf{I} + \boldsymbol{G}_o\boldsymbol{K})^{-1} \tag{5.50}$$

$$\boldsymbol{Q}_{22} = -\boldsymbol{G}_o\boldsymbol{K}(\mathbf{I} + \boldsymbol{G}_o\boldsymbol{K})^{-1} \tag{5.51}$$

Consider the loop through $\boldsymbol{\Delta_m}$ in Figure 5.7. According to the small gain theorem (e.g. Maciejowski, 1989), for stability, assuming the unperturbed system is stable,

$$\left\|\boldsymbol{Q}_{22}\boldsymbol{\Delta_m}\right\|_\infty < 1 \tag{5.52}$$

It may be noted that $\boldsymbol{Q}_{22}$ derived above is equal to the complementary sensitivity function $\boldsymbol{T}$ (Section 5.1.1). Thus, for stability,

$$\left\|\boldsymbol{T}\boldsymbol{\Delta_m}\right\|_\infty < 1 \tag{5.53}$$

Consider a stable weighting function $\boldsymbol{W}_3$. Then, for stability,

$$\left\|\boldsymbol{T}\boldsymbol{W}_3\boldsymbol{W}_3^{-1}\boldsymbol{\Delta_m}\right\|_\infty < 1 \tag{5.54}$$

But, using the rules of norm algebra,

$$\left\|\boldsymbol{T}\boldsymbol{W}_3\boldsymbol{W}_3^{-1}\boldsymbol{\Delta_m}\right\|_\infty \le \left\|\boldsymbol{T}\boldsymbol{W}_3\right\|_\infty \left\|\boldsymbol{W}_3^{-1}\boldsymbol{\Delta_m}\right\|_\infty \tag{5.55}$$

If

$$\left\|\boldsymbol{W}_3^{-1}\boldsymbol{\Delta_m}\right\|_\infty < 1 \tag{5.56}$$

Then

$$\left\|\boldsymbol{T}\boldsymbol{\Delta_m}\right\|_\infty \le \left\|\boldsymbol{T}\boldsymbol{W}_3\right\|_\infty \tag{5.57}$$

Thus the perturbation will not result in instability of the closed loop if $\boldsymbol{W_3}$ is an upper bound on $\boldsymbol{\Delta_m}$ and

$$\left\|\boldsymbol{T}\boldsymbol{W}_3\right\|_\infty < 1 \tag{5.58}$$

5.1.5 Transfer Function Matrices and Partitions

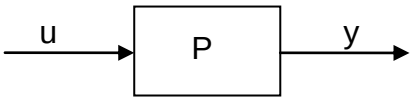

Figure 5.8 To illustrate partitioning

Consider a transfer function matrix $\boldsymbol{P}$ as in Figure 5.8:

$$\boldsymbol{y} = \boldsymbol{P}\boldsymbol{u} \tag{5.59}$$

Partition $\boldsymbol{P}$ as:

$$\boldsymbol{y} = \begin{bmatrix} \boldsymbol{P}_{11} & \boldsymbol{P}_{12} \\ \boldsymbol{P}_{21} & \boldsymbol{P}_{22} \end{bmatrix} \boldsymbol{u} \tag{5.60}$$

Expand

$$\boldsymbol{y}_1 = \boldsymbol{P}_{11}\boldsymbol{u}_1 + \boldsymbol{P}_{12}\boldsymbol{u}_2 \tag{5.61}$$

$$\boldsymbol{y}_2 = \boldsymbol{P}_{21}\boldsymbol{u}_1 + \boldsymbol{P}_{22}\boldsymbol{u}_2 \tag{5.62}$$

Now consider a state space realisation of $\boldsymbol{P}$

$$\boldsymbol{y} = \begin{bmatrix} \boldsymbol{A} & \boldsymbol{B} \\ \boldsymbol{C} & \boldsymbol{D} \end{bmatrix} \boldsymbol{u} \tag{5.63}$$

Thus, where $\boldsymbol{x}$ is a state vector, taking Laplace transforms and expanding eq. (5.63),

$$s\boldsymbol{x} = \boldsymbol{A}\boldsymbol{x} + \boldsymbol{B}\boldsymbol{u} \tag{5.64}$$

$$\boldsymbol{y} = \boldsymbol{C}\boldsymbol{x} + \boldsymbol{D}\boldsymbol{u} \tag{5.65}$$

$$\boldsymbol{y} = [\boldsymbol{C}(s\mathbf{I} - \boldsymbol{A})^{-1}\boldsymbol{B} + \boldsymbol{D}]\boldsymbol{u} \tag{5.66}$$

The state space realisation may be partitioned as

$$\boldsymbol{y} = \begin{bmatrix} \boldsymbol{A} & \boldsymbol{B}_1 & \boldsymbol{B}_2 \\ \boldsymbol{C}_1 & \boldsymbol{D}_{11} & \boldsymbol{D}_{12} \\ \boldsymbol{C}_2 & \boldsymbol{D}_{21} & \boldsymbol{D}_{22} \end{bmatrix} \boldsymbol{u} \tag{5.67}$$

Note: $\boldsymbol{A}$ is the system matrix, and is not partitioned.

Expanding the above partitioned state space realisation eq. (5.67) yields:

$$s\boldsymbol{x} = \boldsymbol{A}\boldsymbol{x} + \boldsymbol{B}_1\boldsymbol{u}_1 + \boldsymbol{B}_2\boldsymbol{u}_2 \tag{5.68}$$

$$\boldsymbol{x} = (s\mathbf{I} - \boldsymbol{A})^{-1}[\boldsymbol{B}_1\boldsymbol{u}_1 + \boldsymbol{B}_2\boldsymbol{u}_2] \tag{5.69}$$

$$\boldsymbol{y}_1 = \boldsymbol{C}_1\boldsymbol{x} + \boldsymbol{D}_{11}\boldsymbol{u}_1 + \boldsymbol{D}_{12}\boldsymbol{u}_2 \tag{5.70}$$

$$\boldsymbol{y}_2 = \boldsymbol{C}_2\boldsymbol{x} + \boldsymbol{D}_{21}\boldsymbol{u}_1 + \boldsymbol{D}_{22}\boldsymbol{u}_2 \tag{5.71}$$

Thus, using eq. (5.69) to eliminate the state vector $\boldsymbol{x}$ from eq. (5.70) and eq. (5.71), yields

$$\boldsymbol{y}_1 = [\boldsymbol{C}_1(s\mathbf{I} - \boldsymbol{A})^{-1}\boldsymbol{B}_1 + \boldsymbol{D}_{11}]\boldsymbol{u}_1 + [\boldsymbol{C}_1(s\mathbf{I} - \boldsymbol{A})^{-1}\boldsymbol{B}_2 + \boldsymbol{D}_{12}]\boldsymbol{u}_2 \tag{5.72}$$

$$\boldsymbol{y}_2 = [\boldsymbol{C}_2(s\mathbf{I} - \boldsymbol{A})^{-1}\boldsymbol{B}_1 + \boldsymbol{D}_{21}]\boldsymbol{u}_1 + [\boldsymbol{C}_2(s\mathbf{I} - \boldsymbol{A})^{-1}\boldsymbol{B}_2 + \boldsymbol{D}_{22}]\boldsymbol{u}_2 \tag{5.73}$$

Then, comparing coefficients of eq. (5.61) with eq. (5.72) and eq. (5.62) with eq. (5.73) yields:

$$\boldsymbol{P}_{11} = \left[\boldsymbol{C}_1(s\mathbf{I} - \boldsymbol{A})^{-1}\boldsymbol{B}_1 + \boldsymbol{D}_{11}\right] \tag{5.74}$$

$$\boldsymbol{P}_{12} = \left[\boldsymbol{C}_1(s\mathbf{I} - \boldsymbol{A})^{-1}\boldsymbol{B}_2 + \boldsymbol{D}_{12}\right] \tag{5.75}$$

$$\boldsymbol{P}_{21} = \left[\boldsymbol{C}_2(s\mathbf{I} - \boldsymbol{A})^{-1}\boldsymbol{B}_1 + \boldsymbol{D}_{21}\right] \tag{5.76}$$

$$\boldsymbol{P}_{22} = \left[\boldsymbol{C}_2(s\mathbf{I} - \boldsymbol{A})^{-1}\boldsymbol{B}_2 + \boldsymbol{D}_{22}\right] \tag{5.77}$$

5.1.6 The Linear Fractional Transformation

The Linear Fractional Transformation provides a route to presenting a controller design problem in a standard form for solution using an H_∞ approach.

If the plant is represented by a transfer function matrix $\boldsymbol{P}(s)$, which is partitioned as follows:

$$\boldsymbol{P}(s) = \begin{bmatrix} \boldsymbol{P}_{11} & \boldsymbol{P}_{12} \\ \boldsymbol{P}_{21} & \boldsymbol{P}_{22} \end{bmatrix} \tag{5.78}$$

Then, if an input vector $[\boldsymbol{w}^{\mathrm{T}}\ \boldsymbol{u}^{\mathrm{T}}]^{\mathrm{T}}$ produces output $[\boldsymbol{z}^{\mathrm{T}}\ \boldsymbol{y}^{\mathrm{T}}]^{\mathrm{T}}$, one may write:

$$\begin{bmatrix} \boldsymbol{z} \\ \boldsymbol{y} \end{bmatrix} = \begin{bmatrix} \boldsymbol{P}_{11} & \boldsymbol{P}_{12} \\ \boldsymbol{P}_{21} & \boldsymbol{P}_{22} \end{bmatrix} \begin{bmatrix} \boldsymbol{w} \\ \boldsymbol{u} \end{bmatrix} \tag{5.79}$$

Here, $\boldsymbol{w}$ is a vector of external inputs which cannot be manipulated by the controller, such as disturbances and noise, $\boldsymbol{u}$ is a vector of inputs derived by the controller, $\boldsymbol{y}$ is a vector of measured outputs which are processed by the controller, and $\boldsymbol{z}$ represents other outputs.

The system of plant $\boldsymbol{P}$ and controller $\boldsymbol{K}$ may be represented as in Figure 5.9.

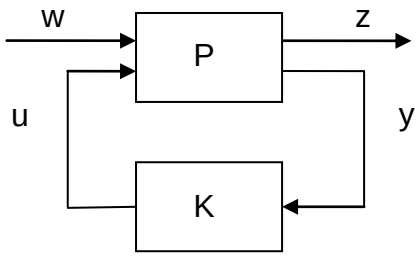

Figure 5.9 To illustrate linear fractional transformation

Expanding eq. (5.79) gives

$$\boldsymbol{z} = \boldsymbol{P}_{11}\boldsymbol{w} + \boldsymbol{P}_{12}\boldsymbol{u} \tag{5.80}$$

$$\boldsymbol{y} = \boldsymbol{P}_{21}\boldsymbol{w} + \boldsymbol{P}_{22}\boldsymbol{u} \tag{5.81}$$

Also, for controller,

$$\boldsymbol{u} = \boldsymbol{K}\boldsymbol{y} \tag{5.82}$$

So, from eq. (5.81)

$$\boldsymbol{y} = \boldsymbol{P}_{21}\boldsymbol{w} + \boldsymbol{P}_{22}\boldsymbol{K}\boldsymbol{y} \tag{5.83}$$

$$\boldsymbol{y} = (\mathbf{I} - \boldsymbol{P}_{22}\boldsymbol{K})^{-1}\boldsymbol{P}_{21}\boldsymbol{w} \tag{5.84}$$

Using eq. (5.82)

$$\boldsymbol{u} = \boldsymbol{K}(\mathbf{I} - \boldsymbol{P}_{22}\boldsymbol{K})^{-1}\boldsymbol{P}_{21}\boldsymbol{w} \tag{5.85}$$

Thus eliminating $\boldsymbol{u}$ and $\boldsymbol{y}$ from eq. (5.79) yields

$$\boldsymbol{z} = [\boldsymbol{P}_{11} + \boldsymbol{P}_{12}\boldsymbol{K}(\mathbf{I} - \boldsymbol{P}_{22}\boldsymbol{K})^{-1}\boldsymbol{P}_{21}]\boldsymbol{w} \tag{5.86}$$

Or

$$\boldsymbol{z} = \mathbf{F}(\boldsymbol{P}, \boldsymbol{K})\boldsymbol{w} \tag{5.87}$$

where $\mathbf{F}(\boldsymbol{P}, \boldsymbol{K})$ is known as the linear fractional transformation of $\boldsymbol{P}$ and $\boldsymbol{K}$. More precisely, as the loop through $\boldsymbol{K}$ links the lower input and output ports of $\boldsymbol{P}$, the function is the lower linear fractional transformation $\mathbf{F}_l$.

A control objective in the above formulation is to choose a structure for $\boldsymbol{K}$ so that the dependence of $\boldsymbol{z}$ on $\boldsymbol{w}$ is minimised. Thus $\left\|\mathbf{F}(\boldsymbol{P}, \boldsymbol{K})\right\|_\infty$ must be minimised.

Minimisation is achieved by searching for a suitable controller $\boldsymbol{K}$. This must be physically realisable, and the resulting closed loop must be stable.

5.1.7 Presenting Design Problems in Standard Form

Section 5.1.3 has shown how a controller design specification can be formulated in terms of H_∞ norms involving frequency dependent weights. In order to solve the design problem using standard algorithms, it is necessary to formulate the problem in 'standard form'.

Sensitivity:

$$\left\|\boldsymbol{W}_1\boldsymbol{S}\right\|_\infty < 1 \tag{5.88}$$

implies that $\boldsymbol{S}$ is 'squeezed' under $\boldsymbol{W}_1^{-1}$ for all frequencies.

Complementary sensitivity:

$$\left\|\boldsymbol{W}_3\boldsymbol{T}\right\|_\infty < 1 \tag{5.89}$$

implies that $\boldsymbol{T}$ is 'squeezed' under $\boldsymbol{W}_3^{-1}$ for all frequencies.

To achieve both objectives, it is necessary to find a controller which stabilises and ensures that the inequality

$$\left\|\begin{matrix}\boldsymbol{W}_1\boldsymbol{S}\\ \boldsymbol{W}_3\boldsymbol{T}\end{matrix}\right\|_\infty < 1 \tag{5.90}$$

is satisfied.

The standard problem is thus defined as finding a stabilising $\boldsymbol{K}$ in F($\boldsymbol{P}$,$\boldsymbol{K}$) such that

$$\left\|\mathbf{F}(\boldsymbol{P},\boldsymbol{K})\right\|_\infty < 1 \tag{5.91}$$

with $\boldsymbol{P}$ defined to encapsulate the inequality of eq. (5.90).

From the definition of $\boldsymbol{S}$, the sensitivity, (Section 5.1.1):

$$\boldsymbol{W}_1\boldsymbol{S} = \boldsymbol{W}_1(\mathbf{I}+\boldsymbol{G}\boldsymbol{K})^{-1} \tag{5.92}$$

$$\boldsymbol{W}_1\boldsymbol{S} = \boldsymbol{W}_1 - \boldsymbol{W}_1\boldsymbol{G}\boldsymbol{K}(\mathbf{I}+\boldsymbol{G}\boldsymbol{K})^{-1} \tag{5.93}$$

Comparing coefficients of eq. (5.93) with those of the lower fractional transformation of eq. (5.86) and eq. (5.87)

$$\mathbf{F}_l(\boldsymbol{P},\boldsymbol{K})\boldsymbol{w} = [\boldsymbol{P}_{11} + \boldsymbol{P}_{12}\boldsymbol{K}(\mathbf{I} - \boldsymbol{P}_{22}\boldsymbol{K})^{-1}\boldsymbol{P}_{21}]\boldsymbol{w} \tag{5.94}$$

gives

$$\boldsymbol{P}_{11} = \boldsymbol{W}_1, \tag{5.95}$$

$$\boldsymbol{P}_{12} = -\boldsymbol{W}_1\boldsymbol{G}, \tag{5.96}$$

$$\boldsymbol{P}_{21} = \mathbf{I}, \tag{5.97}$$

$$\boldsymbol{P}_{22} = -\boldsymbol{G} \tag{5.98}$$

Similarly, consideration of the complementary sensitivity $\boldsymbol{T}$ gives

$$\boldsymbol{W}_3\boldsymbol{T} = \boldsymbol{W}_3(\mathbf{I} - \boldsymbol{S}) \tag{5.99}$$

$$\boldsymbol{W}_3\boldsymbol{T} = \boldsymbol{W}_3 - \boldsymbol{W}_3(\mathbf{I} + \boldsymbol{G}\boldsymbol{K})^{-1} \tag{5.100}$$

$$\boldsymbol{W}_3\boldsymbol{T} = \mathbf{0} + \boldsymbol{W}_3\boldsymbol{G}\boldsymbol{K}(\mathbf{I} + \boldsymbol{G}\boldsymbol{K})^{-1} \tag{5.101}$$

Comparing coefficients of eq. (5.101) with those of the lower fractional transformation of eq. (5.86) and eq. (5.87)

$$\mathbf{F}_l(\boldsymbol{P},\boldsymbol{K}) = \boldsymbol{P}_{11} + \boldsymbol{P}_{12}\boldsymbol{K}(\mathbf{I} - \boldsymbol{P}_{22}\boldsymbol{K})^{-1}\boldsymbol{P}_{21} \tag{5.102}$$

gives

$$\boldsymbol{P}_{11} = \mathbf{0}, \tag{5.103}$$

$$\boldsymbol{P}_{12} = \boldsymbol{W}_3\boldsymbol{G}, \tag{5.104}$$

$$\boldsymbol{P}_{21} = \mathbf{I}, \tag{5.105}$$

$$\boldsymbol{P}_{22} = -\boldsymbol{G} \tag{5.106}$$

Thus to meet both criteria, the partitions of $\boldsymbol{P}$ must be defined as follows

$$\boldsymbol{P}_{11} = \begin{bmatrix} \boldsymbol{W}_1 \\ \mathbf{0} \end{bmatrix}, \tag{5.107}$$

$$\boldsymbol{P}_{12} = \begin{bmatrix} -\boldsymbol{W}_1\boldsymbol{G} \\ \boldsymbol{W}_3\boldsymbol{G} \end{bmatrix}, \tag{5.108}$$

$$\boldsymbol{P}_{21} = \mathbf{I}, \tag{5.109}$$

$$\boldsymbol{P}_{22} = -\boldsymbol{G} \tag{5.110}$$

It may on occasions be necessary or desirable to constrain control effort, i.e. the signal from the controller into the plant. Additionally, constraints imposed by the solution algorithm on system matrix rank may require the introduction of a non-active constraint on control effort (see for example Stefani *et al*., 1994, Chiang and Safanov, 1988). Referring to Section 5.1.1 and Figure 5.1, control effort $\boldsymbol{u}$ (signal from the controller to the plant actuators) is $\boldsymbol{Ke}$. Control effort may be shaped using a weight $\boldsymbol{W}_2$ via the relationship $\|\boldsymbol{W}_2\boldsymbol{KS}\|_\infty < 1$

$$\boldsymbol{W}_2\boldsymbol{KS} = \boldsymbol{W}_2\boldsymbol{K}(\mathbf{I} + \boldsymbol{GK})^{-1} \tag{5.111}$$

$$= \mathbf{0} + \boldsymbol{W}_2\boldsymbol{K}(\mathbf{I} + \boldsymbol{GK})^{-1} \tag{5.112}$$

Comparing coefficients of eq. (5.112) with those of eq. (5.102) gives

$$\boldsymbol{P}_{11} = \mathbf{0} \tag{5.113}$$

$$\boldsymbol{P}_{12} = \boldsymbol{W}_2 \tag{5.114}$$

$$\boldsymbol{P}_{21} = \mathbf{I} \tag{5.115}$$

$$\boldsymbol{P}_{22} = -\boldsymbol{G} \tag{5.116}$$

Thus to meet all three criteria, the partitions of $\boldsymbol{P}$ must be defined as follows:

$$\boldsymbol{P}_{11} = \begin{bmatrix} \boldsymbol{W}_1 \\ \mathbf{0} \\ \mathbf{0} \end{bmatrix}, \qquad \boldsymbol{P}_{12} = \begin{bmatrix} -\boldsymbol{W}_1\boldsymbol{G} \\ \boldsymbol{W}_2 \\ \boldsymbol{W}_3\boldsymbol{G} \end{bmatrix}, \qquad \boldsymbol{P}_{21} = \mathbf{I}, \qquad \boldsymbol{P}_{22} = -\boldsymbol{G} \tag{5.117}$$

The problem when posed in this form is known as the ‘mixed sensitivity problem’ (see, for example, Stephani, *et al*. (1994)).

5.1.8 Solution of the Standard H_∞ Problem

The general problem of finding a stabilising $\boldsymbol{K}$ which minimises $\|\mathbf{F}_l(\boldsymbol{P},\boldsymbol{K})\|_\infty$ (the ‘optimal problem’) is solved via the ‘standard problem’ of finding a stabilising $\boldsymbol{K}$ which results in $\|\mathbf{F}_l(\boldsymbol{P},\boldsymbol{K})\|_\infty < \gamma$. The optimal problem is solved by iteratively adjusting γ in the standard problem to find its minimum achievable value. The general problem can be shown to be reducible to a ‘general distance problem’ (e.g.

Chu *et al*., 1986). An alternative solution route involves the solution of two algebraic Riccati equations (Glover and Doyle, 1988; Doyle *et al*., 1989). (See Appendix 2). Both routes are summarised by Maciejowski (1989). Stefani *et al*. (1994) provide an overview of the latter method, and includes a summary of the constraints on the formulation of the problem which must be met for a solution to be achievable.

The 'general distance problem' is also known as a best (or Hankel) approximation problem or Nehari problem. Chu *et al*. (1986) summarise the process whereby the general problem is transformed into a distance problem in terms of a series of linear fractional transformations as follows.

(1) Find a stabilising $\boldsymbol{K}$ to minimise $\|\mathbf{F}_l(\boldsymbol{P},\boldsymbol{K})\|_\infty$.

(2) Parameterise - replace $\boldsymbol{K}$ by $\mathbf{F}_l(\boldsymbol{K_o},\boldsymbol{Q})$ where $\boldsymbol{K_o}$ is derived from $\boldsymbol{P}$ by a process known as 'coprime factorisation' and $\boldsymbol{Q}$ is the Youla parameter (see e.g. Maciejowski (1989)).

(3) Transform problem: find $\boldsymbol{Q} \in H_\infty$ to minimise $\|\mathbf{F}_l(\boldsymbol{P},\mathbf{F}_l(\boldsymbol{K_o},\boldsymbol{Q}))\|_\infty$, i.e. find $\boldsymbol{Q} \in H_\infty$ to minimise $\|\mathbf{F}_l(\boldsymbol{T},\boldsymbol{Q})\|_\infty$,

(4) It can be shown that $\boldsymbol{T}_{22} = \mathbf{0}$. Thus $\mathbf{F}_l(\boldsymbol{T},\boldsymbol{Q}) = (\boldsymbol{T}_{11} + \boldsymbol{T}_{12}\boldsymbol{Q}\boldsymbol{T}_{21})$. Thus the problem becomes a 'model matching' problem: find $\boldsymbol{Q} \in H_\infty$ to minimise $\|\boldsymbol{T}_{11} + \boldsymbol{T}_{12}\boldsymbol{Q}\boldsymbol{T}_{21}\|_\infty$, i.e. find $\boldsymbol{T}_{11}$ which 'matches' - $\boldsymbol{T}_{12}\boldsymbol{Q}\boldsymbol{T}_{21}$.

(5) Having found the value of $\boldsymbol{Q}$, $\boldsymbol{Q_{opt}}$, which minimises the norms, the controller $\boldsymbol{K_{opt}}$ is found from $\boldsymbol{K_{opt}} = \mathbf{F}_l(\boldsymbol{K_o},\boldsymbol{Q_{opt}})$.

5.1.9 Solving the Standard H_∞ Problem

In the sequel, the MATLAB functions from the Robust Control Toolbox (Chiang and Safonov, 1989) have been used. These solve the small gain infinity-norm robust control problem to find a stabilising controller $\boldsymbol{F}(s)$ for a system $\boldsymbol{P}(s)$, where $\boldsymbol{P}(s)$ is the plant as augmented by suitable weights $\boldsymbol{W_i}(s)$, i=1,2,3. (See Figure 5.10.)

$\boldsymbol{P}(s)$ is partitioned as below.

$$\boldsymbol{P}(s) = \begin{bmatrix} \boldsymbol{A} & \boldsymbol{B}_1 & \boldsymbol{B}_2 \\ \boldsymbol{C}_1 & \boldsymbol{D}_{11} & \boldsymbol{D}_{12} \\ \boldsymbol{C}_2 & \boldsymbol{D}_{21} & \boldsymbol{D}_{22} \end{bmatrix} \tag{5.118}$$

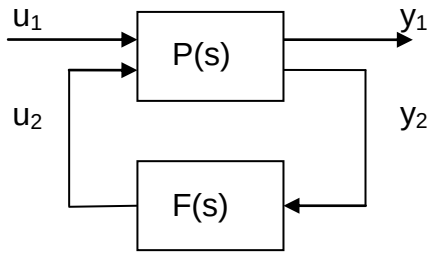

Figure 5.10 Closed loop representation for MATLAB Robust Control Toolbox functions

Controller $\boldsymbol{F}(s)$ is computed to provide a closed loop transfer function (or cost function) $\boldsymbol{T}_{y_1 u_1}$ which satisfies the infinity norm inequality:

$$\left\| \boldsymbol{T}_{y_1 u_1} \right\|_\infty < 1 \qquad (5.119)$$

It is clear that $\boldsymbol{T}_{y_1 u_1}$ is the lower linear fractional transformation of $\boldsymbol{P}$ and $\boldsymbol{F}$, shown in Figure 5.10, so that the MATLAB functions are solving the standard H_∞ problem discussed in the preceding sections.

The MATLAB functions use the loop shifting two Riccati formulae derived from the work of Glover and Doyle (1988) and Doyle *et al*. (1989), as developed by Safanov *et al*. (1989).

The MATLAB functions also undertake a so-called "γ iteration" to compute the "optimal" H_∞ controller. (See, for example, Safanov and Chiang (1988).) A weighting factor γ is applied to one or more output channels of $\boldsymbol{T}_{y_1 u_1}$. The limiting value of γ for which

$$\left\| \gamma \, \boldsymbol{T}_{y_1 u_1} \right\|_\infty < 1 \qquad (5.120)$$

is satisfied is computed iteratively.

5.2 Application of the H_∞ Mixed Sensitivity Method

This section describes the application of the H_∞ Mixed Sensitivity Method (see paragraph 5.1.7) to the design of a robust speed controller. The underlying principles of the method have been described above; the design route set out in Section 3.3 was applied as follows.

5.2.1 Rig Simulation in Bath*fp*

The Bath*fp* circuit, shown in Figure 5.11, was used to simulate the rig. Linearised models were produced using Bath*fp*'s Linear Analysis Tool. This generates linear models in state space form at selected steady state operating points in the state space.

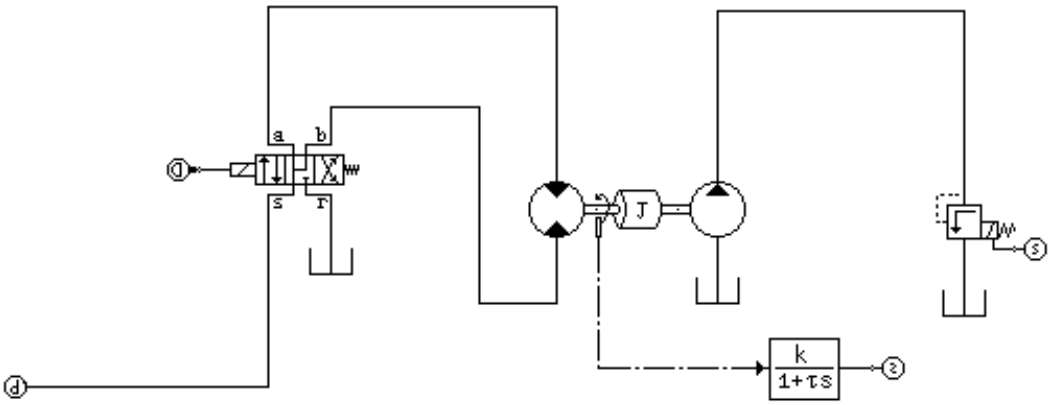

Figure 5.11 Open-loop circuit as represented in Bath*fp*

The circuit shown includes a 'lag' block to permit representation of the (short) delay inherent in the processing of the shaft speed. The Bath*fp* standard component models used and the values of the principal parameters are listed in Appendix 1.

SISO state space representations of the rig, in which the motor control valve solenoid current is the 'input' and the shaft speed transducer signal is the 'output', were produced. These were imported into MATLAB. A Bode plot of the rig transfer function linearised at a steady state shaft speed of 1000 rpm and with a supply pressure of 100 bar is shown in Figure 5.12. The relief valve cracking pressure in the load circuit is set at 40 bar. The rig transfer function is given in below.

$$\frac{4.366e\text{-}011\,s^4 + 2.861e\text{-}006\,s^3 + 2.395e009\,s^2 + 1.36e014\,s + 8.855e017}{s^5 + 8.592e004\,s^4 + 2.028e009\,s^3 + 1.095e013\,s^2 + 1.171e015\,s + 9.629e015} \quad (5.121)$$

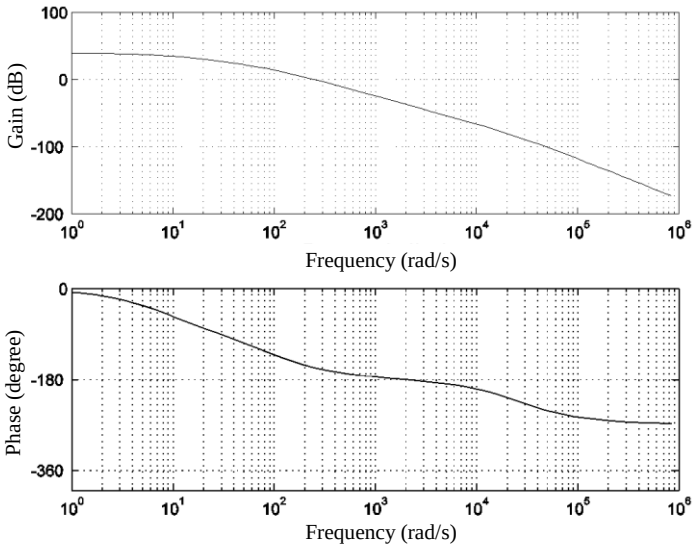

Figure 5.12 Bode plot of rig transfer function

5.2.2 Design of H_∞ Mixed Sensitivity Controllers

Tools in the MATLAB Robust Control Toolbox (Chiang and Safanov, 1988) were used to design 'H_∞' controllers for the SISO using the mixed sensitivity linear fractional transformation method. More details on this method are contained in Section 5.1. The sensitivity transfer function *S* (which relates the output of the closed loop system to a disturbance at the output) and the complementary sensitivity function or closed loop transfer function *T* (which relates the output of the closed loop to the demand) are each shaped in the frequency domain by frequency dependent weighting functions.

5.2.2.1 Choice of Weighting Functions

The weighting function selected to shape the sensitivity transfer function is chosen to attenuate low frequency disturbances. Thus transfer function $W_1(s)$ is selected to have a 'high' gain at low frequency. To avoid synthesis of a controller with an unduly high order, $W_1(s)$ is chosen to have a low order. The transfer function used is

$$W_1(s) = (0.1s+35)/s \qquad (5.122)$$

This function has a gain crossover frequency of about 35 rad/s. Thus disturbances below this frequency will be substantially attenuated. Shaft speed variations induced by load torque fluctuations whose frequency is below this frequency will be attenuated. Fundamental cyclically varying load torques should be substantially

attenuated at speeds of up to about 330 rpm. However, the test rig is not designed to allow such loads to be imposed. The choice of 35 rad/s is compatible with a test regime in which cyclic load disturbances with a fundamental frequency of a few Hz are imposed.

The Bode plot of the inverse of the weighting function, to which the sensitivity transfer function is shaped, is shown in Figure 5.13.

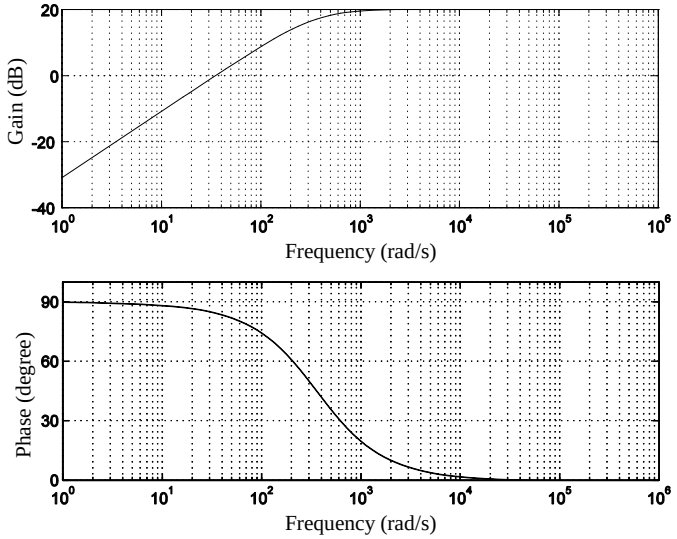

Figure 5.13 Bode plot of inverse of W_1(s)

Similarly, a low order transfer function is required to shape the complementary sensitivity transfer function *T*. A design requirement is that the effect of model uncertainties, and model variations attributable to non-linearities, intuitively assumed to increase in magnitude at high frequencies, are rejected to provide robustness. Again, a simple, low order transfer function is appropriate to minimise controller order.

$$W_3(s) = s^2/250000 \qquad (5.123)$$

This function has a gain crossover frequency of 500 rad/s. This selection prevents the dynamics of any model uncertainties, including unmodelled features, whose gain is significant above this frequency, leading to instability. The Bode plot of $W_3^{-1}(s)$, to which the complementary sensitivity transfer function is shaped, is shown in Figure 5.14.

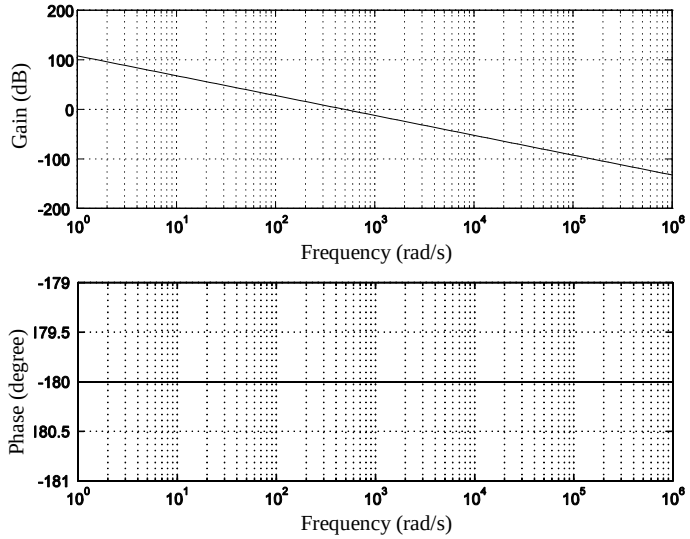

Figure 5.14 Bode plot of inverse of W_3(s)

The functions chosen for W_1 and W_3 satisfy the algebraic constraint on robust performance (Doyle *et al.*, 1990):

$$\min\{|W_1(j\omega)|,|W_3(j\omega)|\} < 1 \qquad \forall\,\omega \qquad (5.124)$$

The solution of the 'H_∞ problem' requires that certain conditions are satisfied by the structure of the 'augmented plant' (see Section 5.1.7). In order to formulate the current problem to satisfy these conditions, a proper transfer function which 'penalises' control effort must be selected. Since the maximum control effort is 20 mA, a constant weight W_2 was chosen as

$$W_2 = 0.02 \qquad (5.125)$$

Thus the constraint on control effort will not be active.

5.2.2.2 Generation of Controller

Using the gamma iteration method (Sections 5.1.8 and 5.1.9) to find an optimal controller, and applying the gamma weighting to output channel 1 (i.e. the weighted sensitivity) yields a controller whose transfer function is represented by the Bode plot shown in Figure 5.15. Its transfer function is given in eq. (5.126).

$$\frac{5.171e005\,s^5 + 4.443e010\,s^4 + 1.048e015\,s^3 + 5.663e018\,s^2 + 6.057e020\,s + 4.979e021}{s^6 + 5.508e005\,s^5 + 3.525e010\,s^4 + 5.754e014\,s^3 + 2.839e018\,s^2 + 2.072e021\,s + 9.233e010} \qquad (5.126)$$

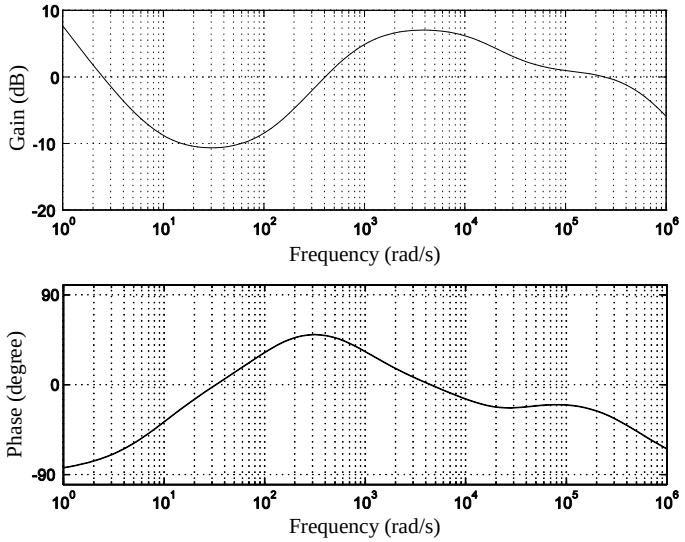

Figure 5.15 Bode plot of optimal controller

It can be seen from the Figure 5.15 that the controller introduces phase advance at mid frequencies, to increase the phase margin and thus improve stability robustness. DC and very low frequency gains are increased to eliminate steady state error; low frequency gain is reduced to meet the disturbance rejection criterion.

The corresponding open-loop transfer function of the compensated system has the Bode plot shown in Figure 5.16.

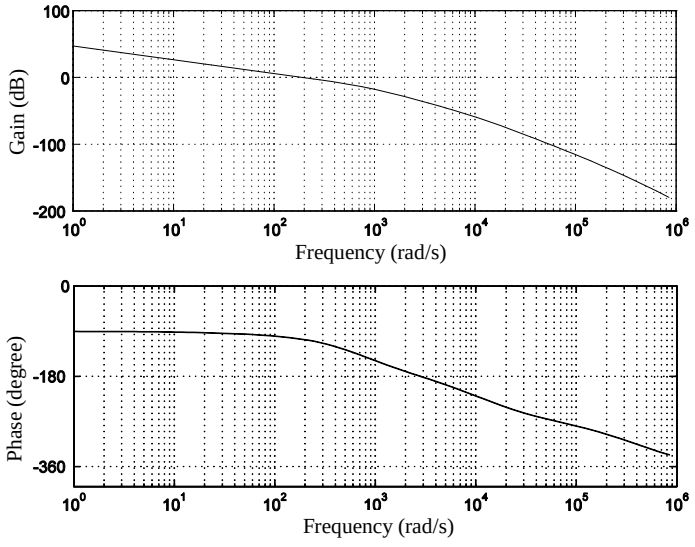

Figure 5.16 Bode plot of open-loop including optimal controller

The singular value frequency plot for the cost function $\boldsymbol{T}_{y_1 u_1}$ which results without gamma iteration is shown in Figure 5.17. Clearly, the criterion $\left\| \boldsymbol{T}_{y_1 u_1} \right\|_\infty < 1$ is met.

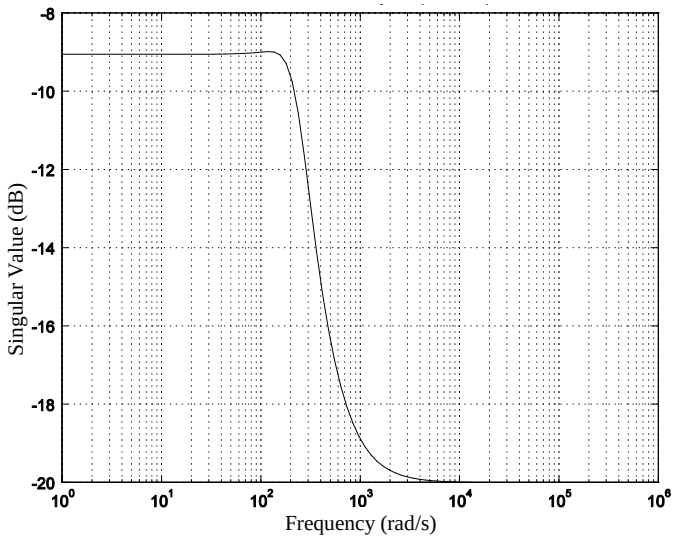

Figure 5.17 Singular value plot for cost function $T_{y_1 u_1}$ (without gamma iteration)

The singular values of the sensitivity function and complementary sensitivity function are respectively compared with $W_1^{-1}(s)$ and $W_3^{-1}(s)$ in Figures 5.18 and 5.19.

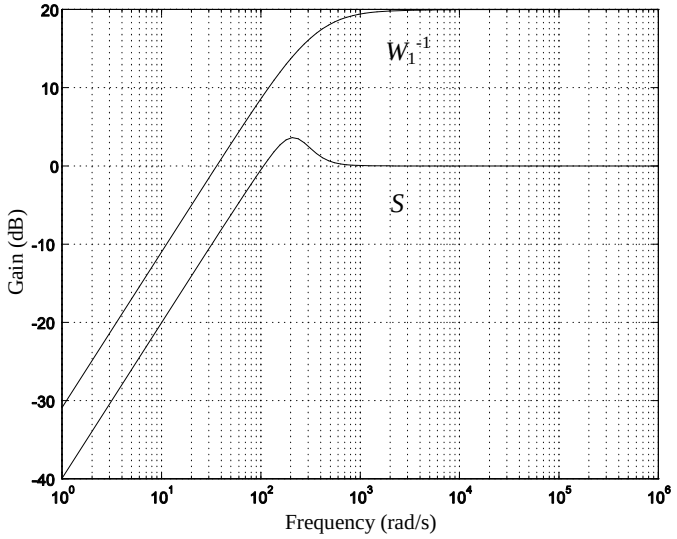

Figure 5.18 Sensitivity function and $W_1^{-1}(s)$

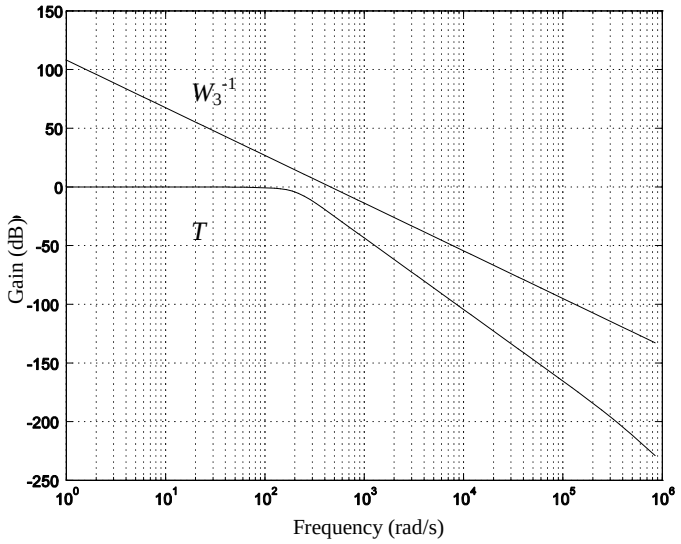

Figure 5.19 Complementary sensitivity function and W_3^{-1}(s)

Clearly, given that the sum of the sensitivity and complementary sensitivity at each frequency must be unity (Section 5.1.1, eq.(5.16)), whereas the sum of the inverses of the weights is not unity at all frequencies, perfect fits are not possible. Indeed, the form of the weights $W_1^{-1}(j\omega)$ and $W_3^{-1}(j\omega)$ is such that they can never sum to unity at any real value of frequency ω.

With gamma iteration, the singular value frequency plot for the cost function $\boldsymbol{T}_{y_1u_1}$ which results is shown in Figure 5.20. This demonstrates the 'all pass' characteristic of the optimal solution $\left\| \boldsymbol{T}_{y_1u_1} \right\|_\infty < 1$.

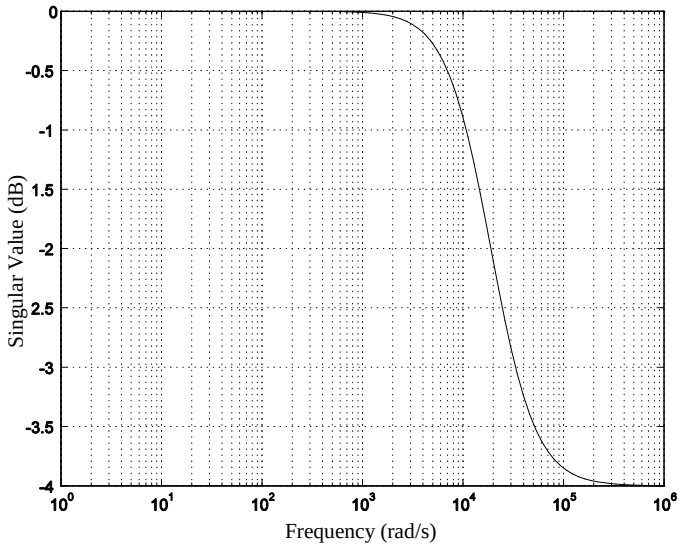

Figure 5.20 Singular value plot for cost function $T_{y_1u_1}$ (with gamma iteration)

In Figure 5.21 the singular value of the sensitivity transfer function which results with gamma iteration is compared with $W_1^{-1}(s)$. The corresponding complementary sensitivity transfer function is compared with $W_3^{-1}(s)$ in Figure 5.22. The optimum controller has shaped the system to meet the design criteria more closely. The gamma weight has been applied to the sensitivity channel. The fit is therefore biased towards matching S to W_1^{-1} at low frequencies.

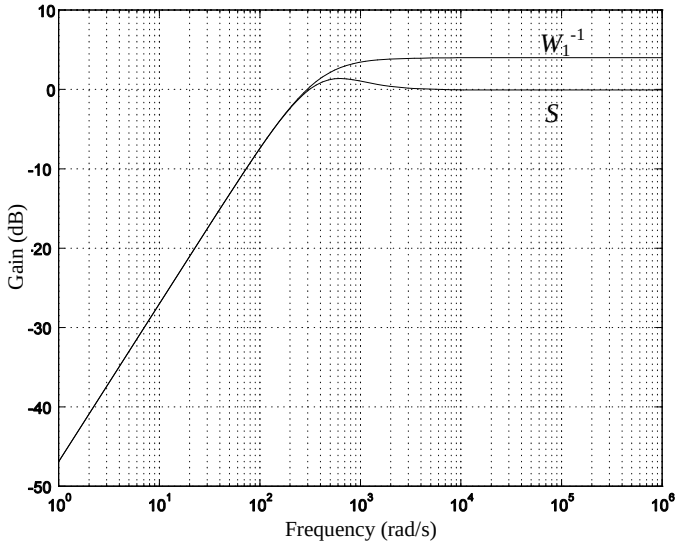

Figure 5.21 Sensitivity function and $W_1^{-1}(s)$

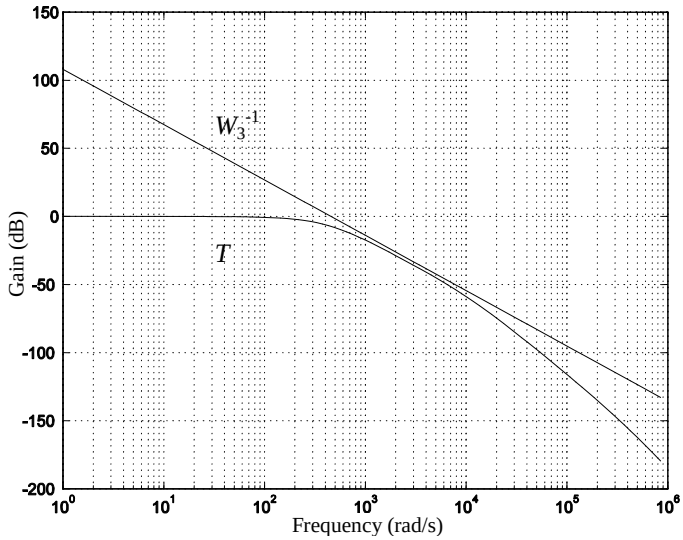

Figure 5.22 Complementary sensitivity function and W_3^{-1}(s)

The superiority of the controller produced by gamma iteration over that produced without gamma iteration is shown by their respective gain and phase margins:

	Gain margin	Phase margin
Without gamma iteration	12.8 dB at 306 rad/s	62.97 degree at 98.65 rad/s
With gamma iteration	35.9 dB at 3368 rad/s	75.28 degree at 214.6 rad/s

The gains of the open-loop transfer functions which result using controllers synthesised with (Plot 2) and without (Plot 1) gamma iteration are compared with each other and with gains of $W_1(s)$ (Plot 4) and $W_3^{-1}(s)$ (Plot 3) in Figure 5.23.

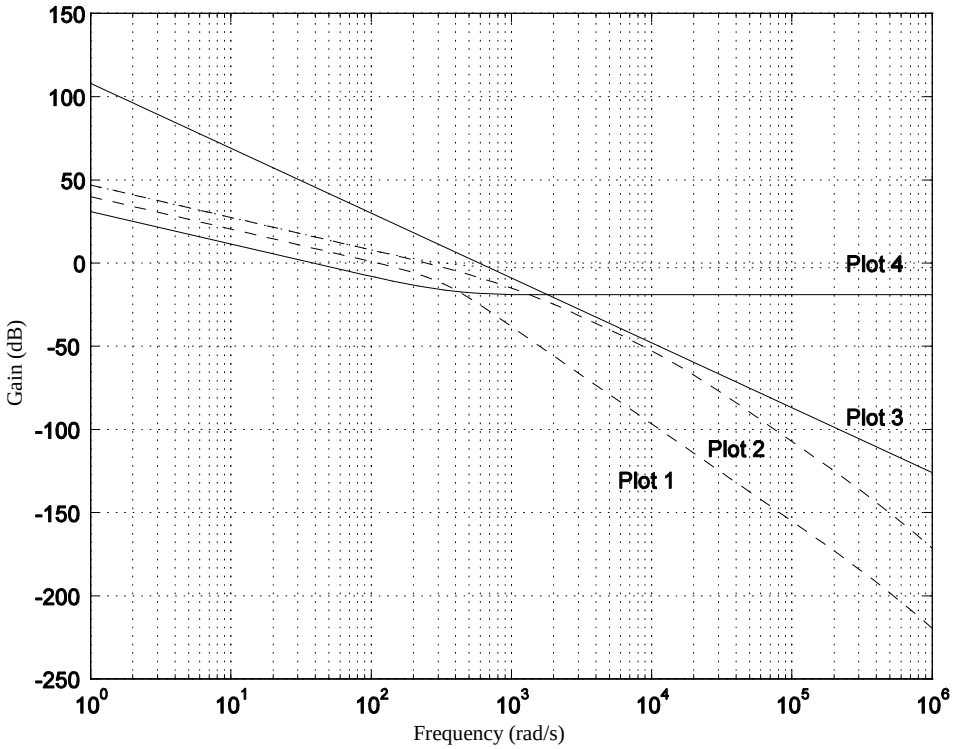

Figure 5.23 Comparison between open-loop transfer functions and weighting functions $W_1(s)$ and $W_3^{-1}(s)$

Figure 5.23 may be interpreted as follows.

Taking L as the open-loop transfer function, (that is GK in the terminology of Section 5.1.1),

then, since $|W_1S| < 1,$ (5.127)

$|S^{-1}| > |W_1|$ (5.128)

But (see Section 5.1.1) $S^{-1} = 1 + L$ (5.129)

so $|1 + L| > |W_1|$ (5.130)

At frequencies where $|L| >> 1$,

$|L| > |W_1|$ (5.131)

Similarly, $|W_3T| < 1,$ (5.132)

$|T| < |W_3|^{-1}$ (5.133)

But (see Section 5.1.1) $T = (1 + L)^{-1}L$ (5.134)

At frequencies where $|L| << 1$,

$$T = L \quad (5.135)$$

$$|L| < |W_3|^{-1} \quad (5.136)$$

Figure 5.23 shows how the open-loop transfer function L is shaped between weighting functions $W_1(s)$ and $W_3^{-1}(s)$ in accordance with the relationships given by eq. (5.131) and eq. (5.136).

The performances of the two controllers in the time domain are compared through the unit step responses of the closed loop systems shown in Figure 5.24. The step speed response of the 'optimal' controller (1) is shown to be superior to that of the suboptimal controller (2) in terms of speed of response and reduced overshoot.

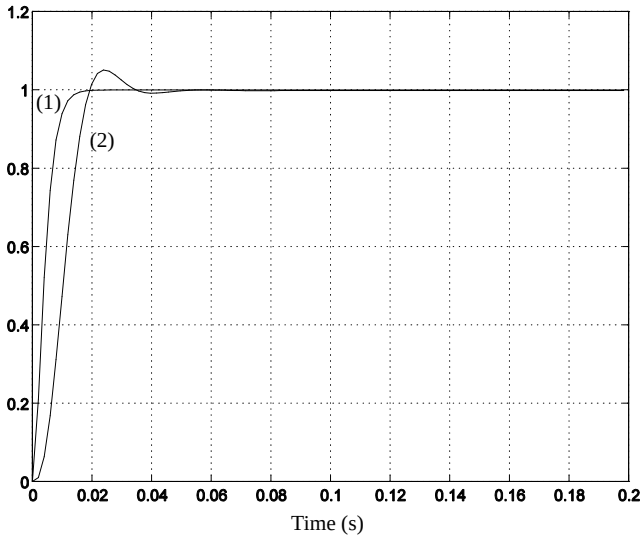

Figure 5.24 Step speed responses of closed loop systems

5.2.3 Emulation of the Controller in Digital Form

5.2.3.1 Sampling Rate Selection

It is necessary to emulate the controller in digital form in order to carry out rig testing.

Forsythe and Goodall (1991) comment that the chosen route in which the controller is designed in the *s*-domain and transformed into the *z*-domain can be expected to give a satisfactory result when the sampling rate is 'high', i.e. the algorithmic error

introduced by the emulation method reduces with increasing sampling rate (p.96); too low a sampling rate can result in stability problems. They also identify as a 'rule of thumb' the choice of a sampling frequency of ten times the system bandwidth (p.95).

A sampling frequency of 1000 Hz was chosen. This was the maximum sampling rate achievable on the test rig with the available software and just captures the system dynamics, as represented by the bandwidth of the complementary sensitivity function (closed loop transfer function) (Figure 5.22) when the above 'rule of thumb' is applied. Tustin's method was used to produce a digital filter (z-domain) to represent the gamma optimised controller, as shown in eq. (5.137). Numerical problems were encountered when attempts were made to use the same method to derive an emulation at a lower sampling frequency.

$$\frac{1.595\,z^6 + 2.354\,z^5 - 2.046\,z^4 - 4.238\,z^3 - 0.2062\,z^2 + 1.892\,z + 0.6649}{z^6 + 1.841\,z^5 - 0.2379\,z^4 - 2.087\,z^3 - 0.9144\,z^2 + 0.2455\,z + 0.1525} \qquad (5.137)$$

A fuller discussion of sampling rate selection is included in Appendix 3 for completeness. The chosen sampling rate is consistent with this discussion.

5.2.3.2 The Discrete Time Filter

The frequency response of the discrete filter (z-domain) is compared with that of the continuous time filter in Figure 5.25 for the gamma optimised controller.

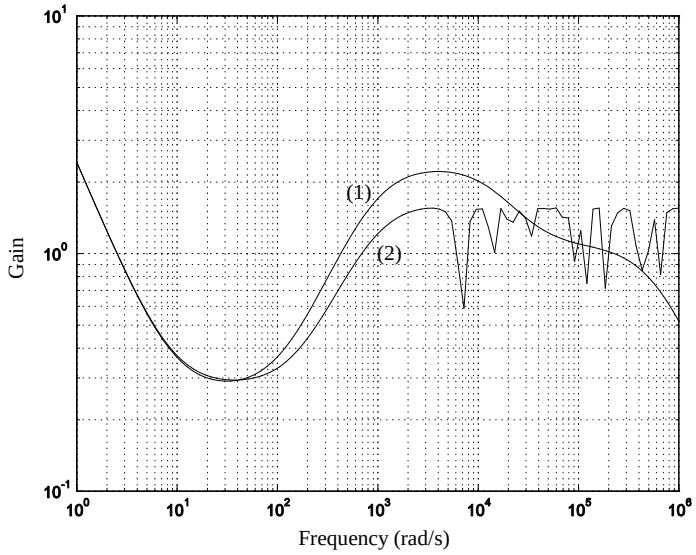

Figure 5.25 Amplitude frequency responses: discrete and continuous time filters

The gain of the digital emulation (2) in Figure 5.25 tracks the gain of the continuous filter (1) shown in the same Figure at low frequencies; the gain of the digital emulation falls in relation to that of the continuous filter as the Nyquist frequency of $10^3\pi$ rad/s is approached.

5.2.4 Simulation Tests on Controller

The performance of the digital controller was checked in the non-linear Bath*fp* environment using the circuit shown in Figure 5.26. More information on the circuit is provided in paragraph 5.2.1 and Appendix 1. The simulation included a model of a digital controller capable of incorporating a *z*-domain digital filter with up to 9 degrees of freedom.

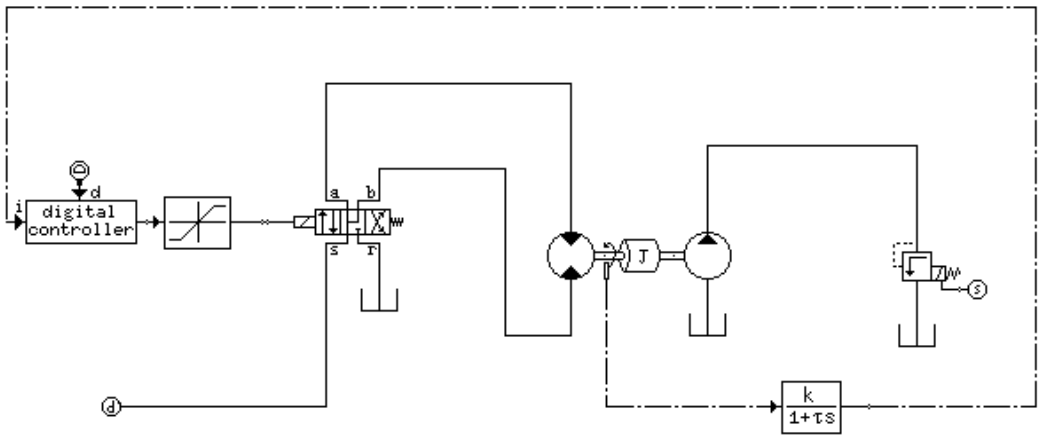

Figure 5.26 Closed loop representation in Bath*fp*

5.2.4.1 Simulation Results – Discretisation Using z-Transforms

The results of a simulation in which a shaft speed demand transient is applied are shown graphically in this paragraph.

Actual and demanded shaft speeds for a transient are compared in Figure 5.27.

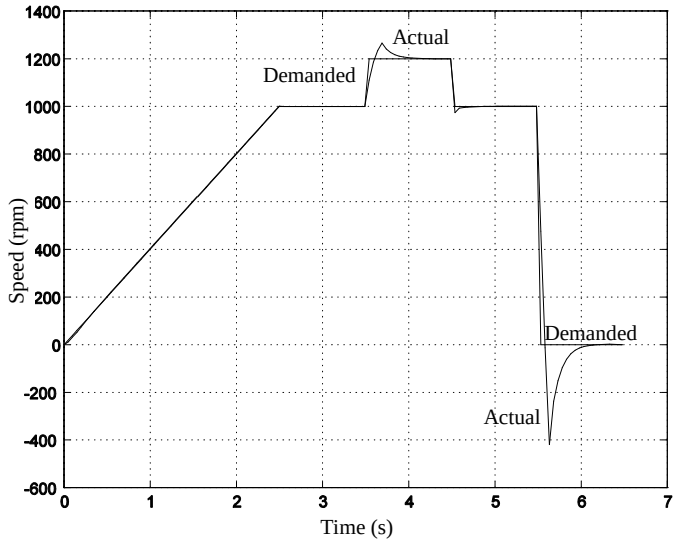

Figure 5.27 Comparison between actual and demanded shaft speeds (simulation using *z*-based emulation)

The associated transient of the valve spool position is as shown in Figure 5.28.

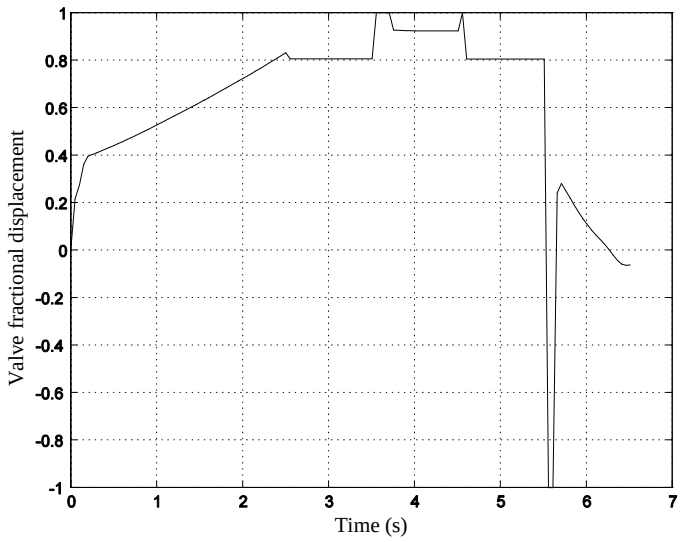

Figure 5.28 Valve spool position (simulation using *z*-based emulation)

The tracking performance is good except when saturation occurs, as indicated by valve fractional displacement reaching +1.0 or -1.0. There is evidence of 'wind-up' at time 3.5 s. This controller was subsequently transported to the rig for further testing.

5.2.5 Emulation of the Controller in δ-Form

5.2.5.1 Coefficient Sensitivity

When the controller described in the preceding sections was rig tested (see Section 5.3 below), 'coefficient sensitivity' was initially identified as a cause of impaired performance. For high order polynomials, small changes in their coefficients may result in large changes in their singular values. Thus, for a controller embodying a high order transfer function, poles and zeros may migrate, leading to performance degradation or even loss of stability, if coefficient precision is lost during the process of implementing the controller. The problem was successfully tackled by amending the control software to extend the widths of the fields into which the coefficients of the filter polynomials were entered. Subsequently, the general problem of coefficient sensitivity (see for example Goodall, 1990; Hu and Edge, 1993) was researched. The continuous time controller was emulated in δ form.

*5.2.5.2 Simulation of δ-Emulation Controller in Bath*fp

The δ-emulation controller was tested in Bath*fp*, using a controller model in δ operator form, created from the continuous filter using MATLAB, and again using a sampling frequency of 1000 Hz. The resulting transfer function is:

$$\frac{1183\,\delta^5 + 3.721\text{e}006\,\delta^4 + 4.067\text{e}009\,\delta^3 + 1.705\text{e}012\,\delta^2 + 1.768\text{e}014\,\delta + 1.403\text{e}015}{\delta^6 + 4584\delta^5 + 8.335\text{e}006\,\delta^4 + 7.503\text{e}009\,\delta^3 + 3.336\text{e}012\,\delta^2 + 5.84\text{e}014\,\delta + 2.6\text{e}004} \tag{5.138}$$

The response to a speed demand transient, in terms of actual and demanded speed is shown in Figure 5.29; control valve spool position is shown in Figure 5.30. They are similar to those obtained using the *z*-based emulation, confirming the efficacy of the emulations.

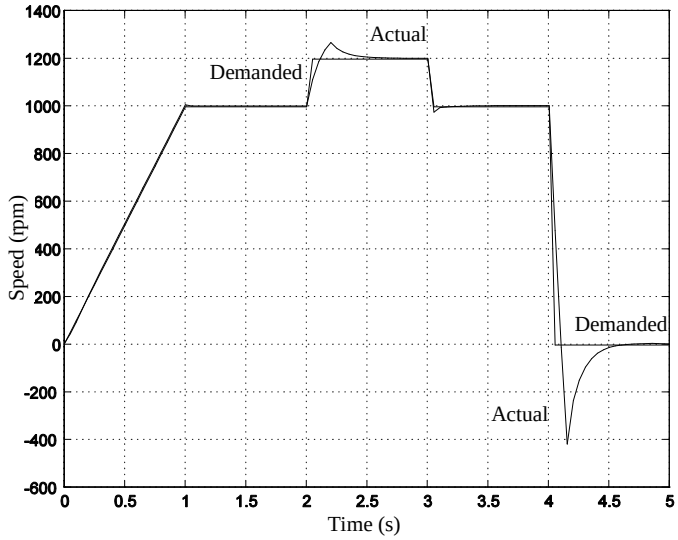

Figure 5.29 Comparison between actual and demanded shaft speeds (simulation using δ-based emulation)

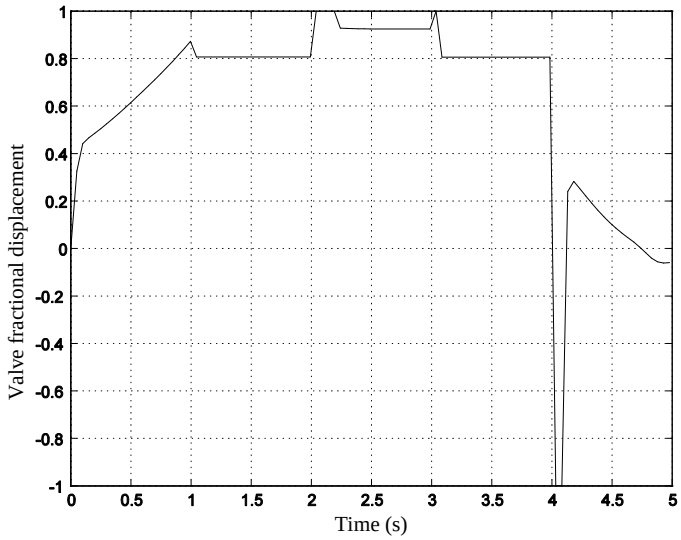

Figure 5.30 Valve spool position (simulation using δ-based emulation)

5.3 Practical Investigation of Mixed Sensitivity Controller Performance

5.3.1 Introduction

A range of tests was devised and implemented to enable the performance of controllers designed using the H_∞ mixed sensitivity method to be investigated

practically. The tests were designed to enable tracking ability and disturbance rejection to be explored. Disturbance rejection was examined by varying the motor load torque. This variation was achieved by disturbing the setting of the solenoid operated throttle valve connected in the load pump circuit. Digital implementations using both *z*- and δ- transforms were tested. Tests were carried out at various supply pressures, in order to investigate robustness (system gain varies with supply pressure). A selection of test results is presented and discussed. Controller sampling frequency is 1000 Hz. A data sampling frequency of 100 Hz is used. Prior to plotting, data were smoothed by computing a moving average over 5 samples.

5.3.2 Implementation Using *z*-Transforms

In the first series of tests, the coefficients of the numerator and denominator polynomials in *z* calculated from the controller designed in the *s*-plane (see eq. (5.137) in Section 5.2.3.1) were rounded to 6 decimal places for input to the controller algorithm. The tracking capability of the controller was investigated by applying a triangular shape speed demand function. This is shown in Figure 5.31 together with the measured speed. Figure 5.32 shows the control effort (controller output). The control effort here is measured in volts. A control effort of 10 V provides the maximum rated current of 20 mA to the servovalve (see Chapter 3). Tracking is good and saturation does not occur. The test was carried out at a supply pressure of 35 bar.

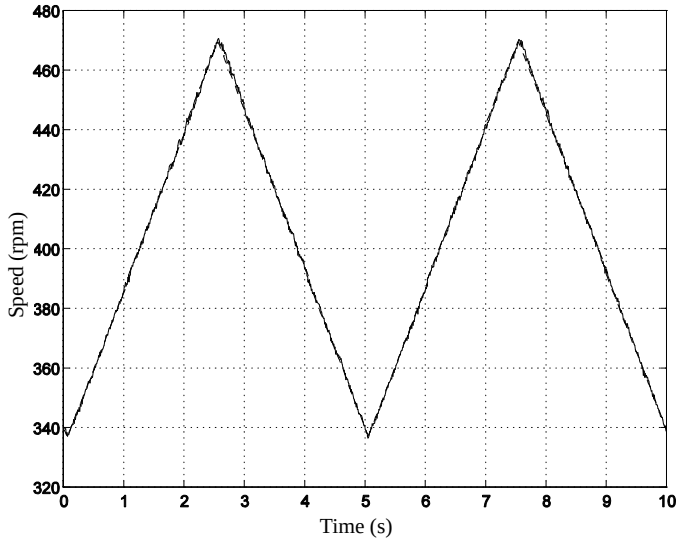

Figure 5.31 Tracking test (*z*-emulation) – actual and demanded shaft speeds

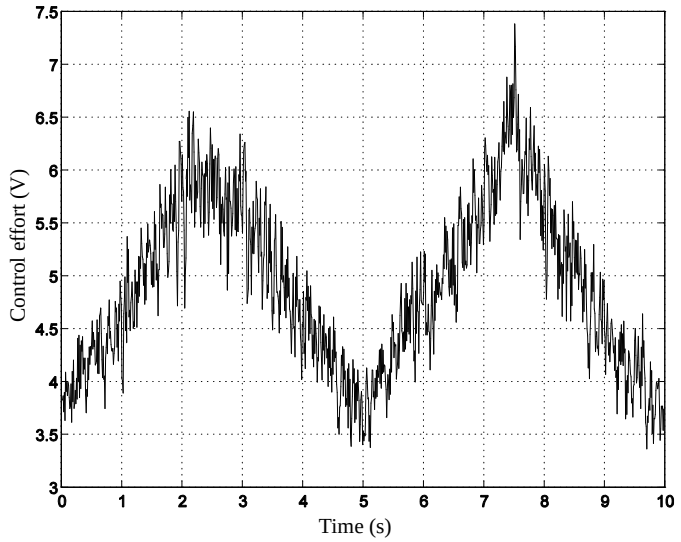

Figure 5.32 Control effort in tracking test (*z*-emulation)

The same controller's disturbance rejection capability was examined by applying a square wave signal to the solenoid controlled throttle valve in the load pump circuit (see Section 3.1). A constant speed demand (693 rpm) was imposed on the system. The disturbance rejection capability is demonstrated by the comparison between the actual and demanded (constant) speed shown in Figure 5.33 when the load disturbance shown in Figure 5.34 is applied.

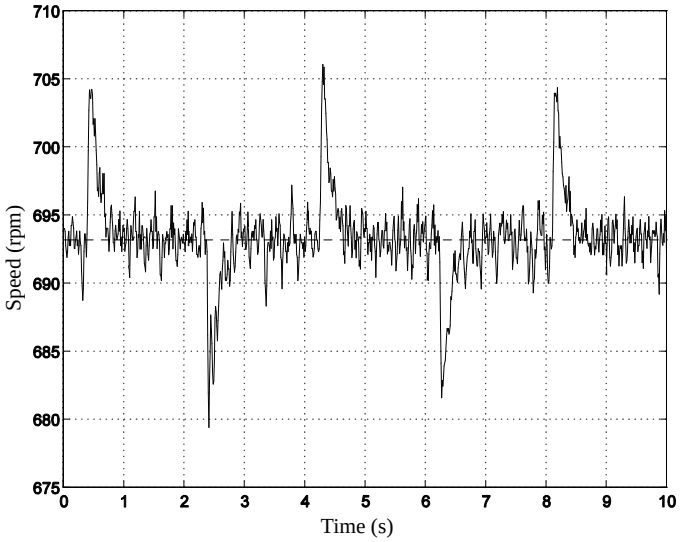

Figure 5.33 Disturbance rejection (*z*-emulation) - actual and demanded shaft speeds

The 'load pressure', i.e. the pressure drop across the throttle valve (which is effectively proportional to shaft torque – see Section 3.1) is plotted in Figure 5.34.

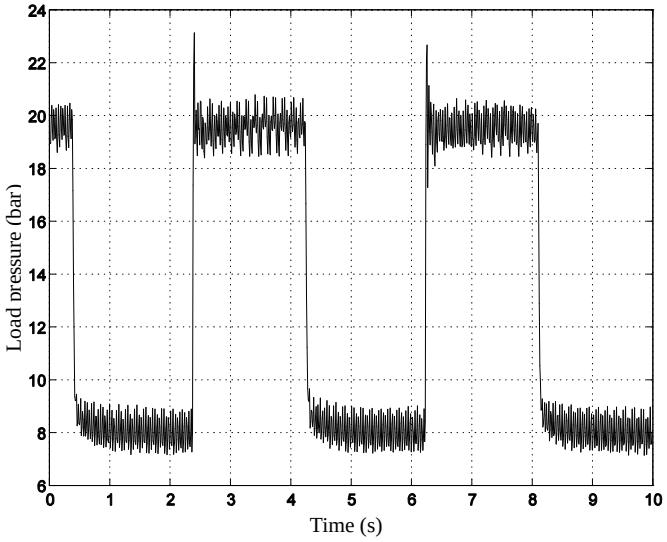

Figure 5.34 Load disturbance (*z*-emulation)

Saturation just occurs when the load torque is 'high', as shown in Figure 5.35. The control effort then reaches its maximum value of 10 V, corresponding to the maximum rated current for the valve of 20 mA. However, the 'steady state' speed error is very low.

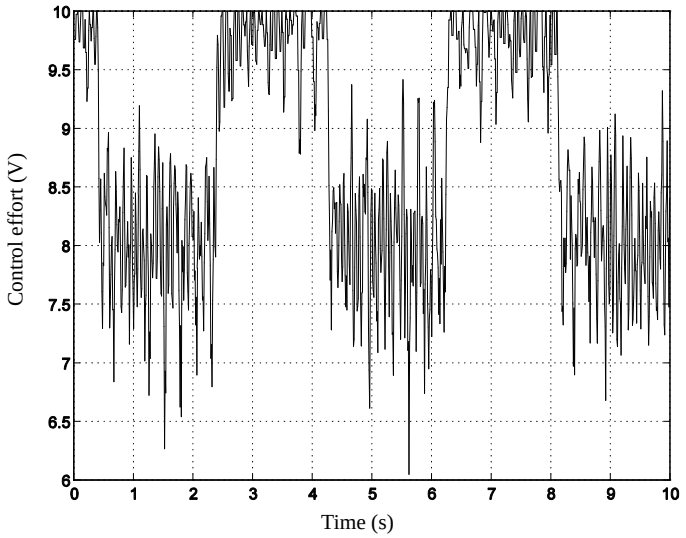

Figure 5.35 Control effort during disturbance rejection (*z*-emulation)

The above rig tests were carried out at a supply pressure of 50 bar.

5.3.3 Implementation Using δ-Transforms

In the next series of rig tests, the same controller designed in the *s*-plane was discretised in δ form (see eq. (5.138) in section 5.2.5.2). The numerator and denominator polynomials were rounded to 4 significant figures for input to the controller algorithm. The tracking capability of the controller was investigated by applying an arbitrary speed demand profile. This is shown by the broken line in Figure 5.36 together with the measured speed. Figure 5.37 shows the control effort.

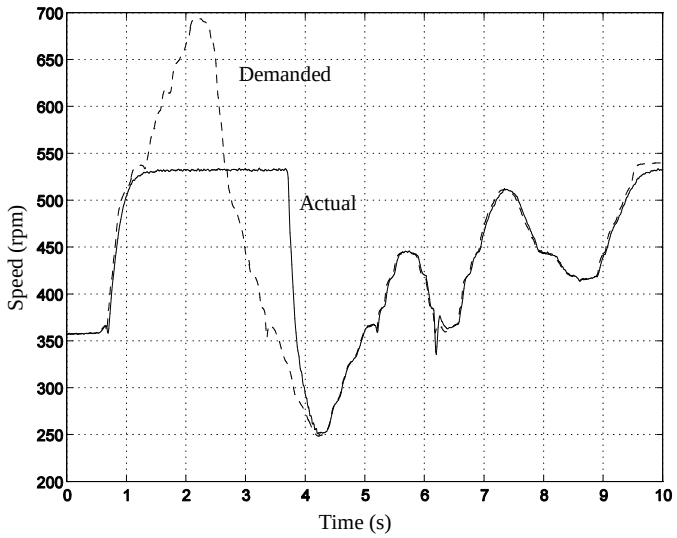

Figure 5.36 Tracking test δ-emulation – actual and demanded shaft speeds

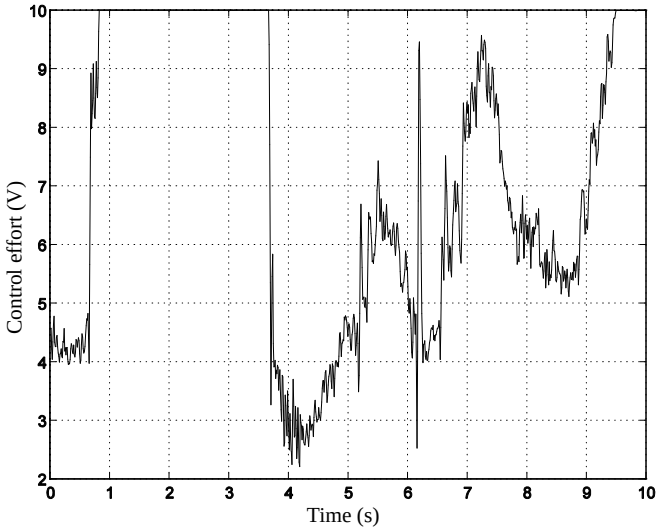

Figure 5.37 Control effort in tracking test δ-emulation

Tracking is good when saturation does not occur. However, it can be seen that once saturation occurs, after about 0.8 s, the controller 'winds up'. Thus, when the demand falls back within the range to within which the system is capable of responding, after about 2.7 s, effective tracking is not immediately resumed. Wind up is an inherent problem of δ controllers. This is because the operation implied by δ^1 is one of accumulation (Forsythe and Goodall, 1991). Rectification of the 'wind up' problem has not been pursued at this stage. It is considered further in Chapter 6. The test was carried out at a supply pressure of 35 bar.

The same controller's tracking capability was examined further by applying a square wave speed reference (demand) signal. Figures 5.38 and 5.39 show tracking and control effort for this test, conducted at 50 bar. Once again, some 'wind up' is evident. In the higher speed phases of the demand cycle, saturation and wind up result in an overshoot before demanded speed is attained.

The negative demand transients are responded to rapidly by the controller, as shown by the control effort in Figure 5.39. The relatively sluggish response of the system, which takes about 0.7 s to reach the 'steady state' at 'low' speed, suggests that the system bandwidth is in fact rather narrower than that modelled in Section 5.2. This needs further consideration, but probably results from inadequately modelled valve dynamics.

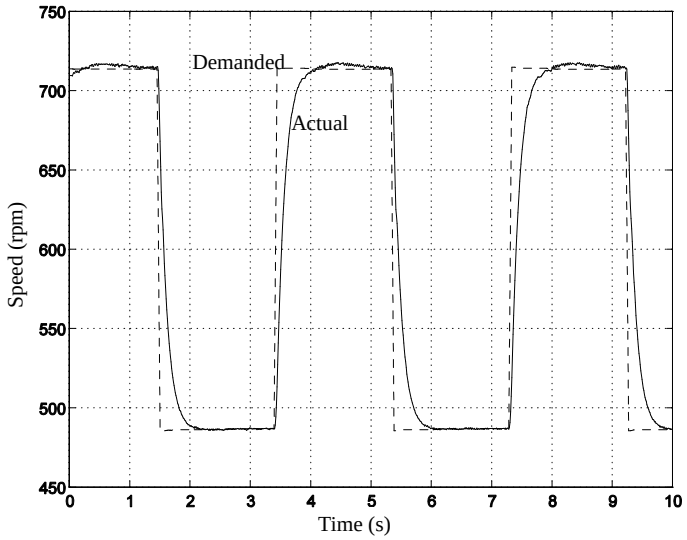

Figure 5.38 Second tracking test δ-emulation– actual and demanded shaft speed

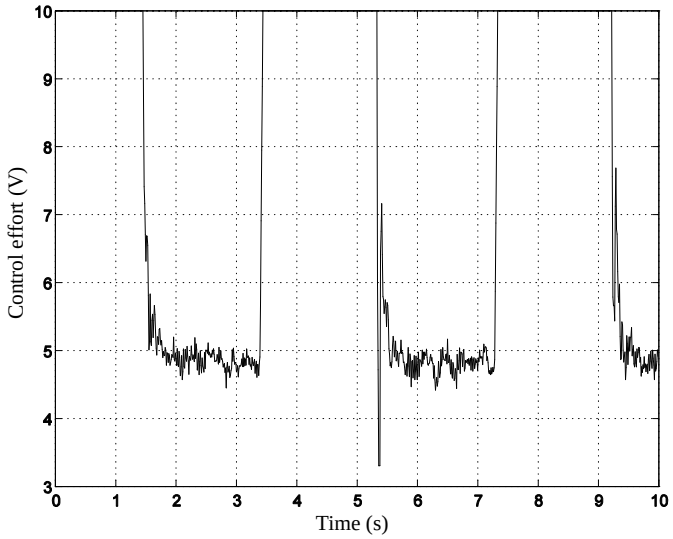

Figure 5.39 Control effort in second tracking test δ-emulation

The same controller's disturbance rejection capability was examined by applying a square wave signal to the solenoid controlled throttle valve in the load pump circuit. A constant speed demand (*c.* 451 rpm) was imposed on the system, and is shown by the broken line in Figure 5.40. Figures 5.41 and 5.42, respectively, show the pressure drop across the throttle valve, which, given the small shaft speed variation, is effectively proportional to shaft torque, and the control effort.

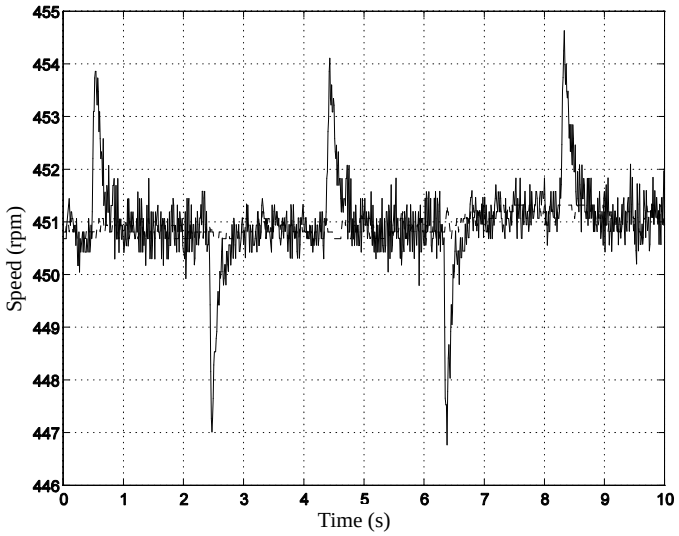

Figure 5.40 Disturbance rejection δ-emulation – actual and demanded shaft speed

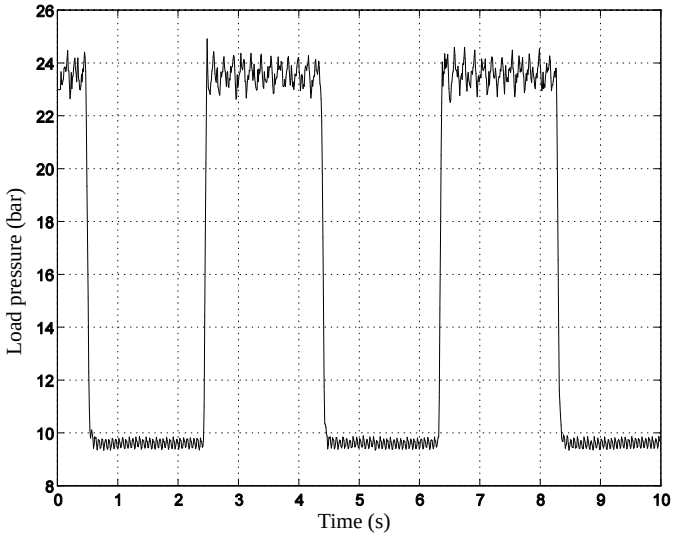

Figure 5.41 Load disturbance δ-emulation

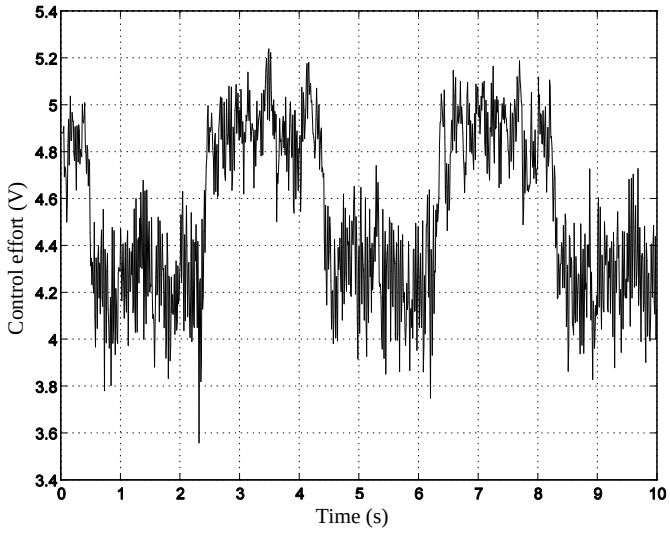

Figure 5.42 Control effort during disturbance rejection δ-emulation

The controller successfully regulates the motor speed. Figure 5.40 indicates a maximum speed excursion of about 4 rpm, with a mean duration for each excursion of about 0.2 s. This corresponds to an angular deviation of about 5^{o}, a very high order of accuracy.

5.3.4 Concluding Remarks

The test results demonstrate that a high order controller, designed in the continuous *s*-domain using an H_∞ mixed sensitivity approach, can be successfully discretised and implemented on a real system. The controller gave good tracking and good disturbance rejection.

Proportional control was unsuccessful on both counts (Chapter 4). The tests do not, however, enable the hypothesis that the observed instability using proportional control might be attributable to discretisation effects rather than closed loop instability to be tested. Simulation does not show instability. Thus another possible cause for it lies in the unmodelled features of the system.

In the load disturbance tests using the high order controllers, the speed error transients are of such magnitude and duration that the angular deviations between the demanded and achieved shaft rotations amount to only a few degrees. This may be significant if the system forms part of a high speed machine in which time domain performance is important.

The non-linear system model used as a basis for controller design was a simplified representation of the real system; values of key parameters were taken from manufacturers' data sheets, and the dimensions and characteristics of pipes were estimated. This was in accord with the design philosophy that, as the controller to be designed would, by virtue of the algorithms used, be robust, effort to define and validate an accurate model was not justified. The test results are a vindication of this approach.

The relatively sluggish response of the system, which takes about 0.7 s to reach the 'steady state' at 'low' speed, as illustrated in the δ emulation tracking tests, suggests that the system bandwidth is in fact rather narrower than that modelled in Section 5.2. This needs further consideration, but probably results from inadequately modelled valve dynamics. Details of the model are included in Appendix 1.

Additionally, conservatism in controller design, in terms of stability margin, results from the use of a model incorporating a higher supply pressure, and thus higher gain, than that used for the tests. Clearly, further work is necessary to refine the controller software to eliminate wind up if the operating regime is such that this may occur.

6 Linear Robust Control 2

6.1 The H_∞ Loop Shaping Method

The controller designed using the H_∞ mixed sensitivity approach showed good load disturbance and tracking characteristics over a limited range of speeds. An alternative approach to controller design was explored with a view to extending the speed range within which operation was possible.

The background analysis contained in the introductory sections of this chapter is expressed in terms of a multi-input multi-output system, to preserve generality and retain consistency with the literature and source material.

6.1.1 Non-linearities in the System

Njabaleke *et al.* (1998) carried out a range of Bath*fp* simulations of the candidate hydrostatic transmission system (Chapter 3), to extract a series of linear models of the plant at a range of operating speeds and supply pressures. Bode gain (or singular value) plots for these are shown in Figure 6.1. They relate to supply pressures ranging from 30 to 100 bar and operating speeds corresponding to valve spool displacements in the range from 5 to 80%.

It is evident from these that non-linearities result in significant changes to the plant's dynamics as the operating point changes. A 'robust' controller is required which will deliver good tracking and disturbance (supply pressure and load) over a wide range of speeds, whilst of course retaining stability.

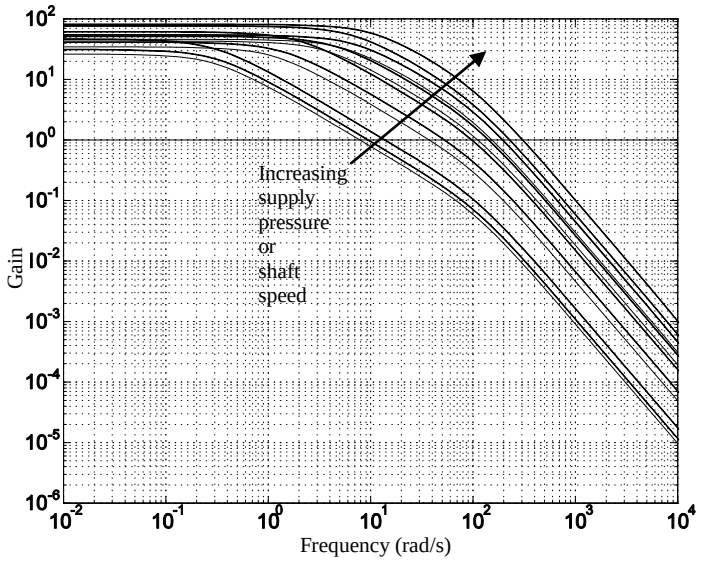

Figure 6.1 Open-loop gains for the candidate system

6.1.2 Quantifying the Effects of Non-Linearities

The deviation between plants has been characterised by the 'gap metric' – this is derived and its history is reviewed by Georgiou and Smith (1990); subsequently, Vinnicombe (1993) refined the gap metric, developing what he termed the 'ν-gap'.

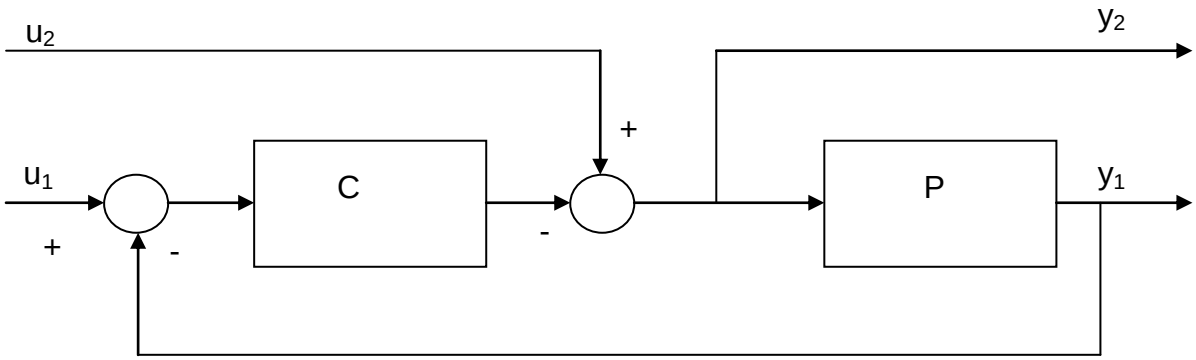

Figure 6.2 Closed loop for a generalised stability margin definition

For the feedback system of Figure 6.2, Vinnicombe defines a generalised stability margin

$$b_{P,C} = \left\| \begin{bmatrix} \boldsymbol{P} \\ \mathbf{I} \end{bmatrix} (\mathbf{I} - \boldsymbol{CP})^{-1} [-\boldsymbol{C} \quad \mathbf{I}] \right\|_{\infty}^{-1} \tag{6.1}$$

for the stable system where $\boldsymbol{P}$ and $\boldsymbol{C}$ are respectively the plant and compensator. He also defines a gap metric ('ν-gap') $\delta_v(\boldsymbol{P}_1, \boldsymbol{P}_2)$ which is a measure of the distance or

difference between two plants $\boldsymbol{P}_1$ and $\boldsymbol{P}_2$. He shows that if a compensator $\boldsymbol{C}$ and a plant $\boldsymbol{P}$ have stability margin $b_{P,C}$, then, if the plant is replaced by $\boldsymbol{P}_1$ the revised stability margin satisfies the inequality

$$\arcsin b_{P_1,C} \geq \arcsin b_{P,C} - \arcsin \delta_v(\boldsymbol{P}, \boldsymbol{P}_1) \qquad (6.2)$$

Clearly, as the measured gap between the two plants widens, the stability margin for a given compensator is (potentially) reduced.

For the range of linear plants characterised by the changes to supply pressure and speed, analysis shows values of 'ν-gap' between the extremes to be approaching unity. This suggests that the design of a robust controller capable of meeting a specified performance standard for a wide range of operating conditions would be challenging.

Gap analysis of the full range of linear models covering operation with supply pressures from 30 to 100 bar and speeds corresponding to valve spool displacements from 5% to 80% indicates that the design of a single mode robust controller which will deliver performance over the entire operating range is unlikely. Examination of the gaps between characteristics shows that the gaps within a high speed group and within a low speed group may be manageable. Defining the transition from 'low' to 'high' speed as occurring at a valve spool displacement of 20% (corresponding to a valve solenoid current of 4 mA) yielded two sets of characteristics. The gap between characteristics within each group was less than 0.5. A design approach incorporating two controllers (for high and for low speeds) was therefore pursued. This necessitated also the incorporation of a means of switching between controllers without disruption.

6.1.3 Principles of the H_∞ Loop Shaping Method

Each of the controllers was designed using the loop shaping procedure using H_∞ synthesis developed by McFarlane and Glover (1992).

In a 'classical' loop shaping approach, a desired closed loop behaviour, chosen on the basis of judgement or knowledge of disturbances and uncertainties, is achieved by 'manipulation' of the open-loop gain; this is achieved by selecting an appropriate compensator transfer function. Deciding on the desirable shape of the loop gain is, at

least superficially, a straightforward matter. However, there are in practice difficulties in achieving a 'tight' design which has adequate stability margins. These arise from conflicts between, for example, the desirability of achieving a rapid roll off rate (to provide, for example, robustness in the face of unmodelled high frequency plant dynamics) at frequencies where phase margin considerations demand that phase lag be limited. The situation can be exacerbated where time delays and 'right hand plane zeros' add to the phase lag.

In the controller design approach used by McFarlane and Glover (1992), loop shaping compensators are used to achieve desired open-loop and thus closed loop gains in the frequency domain; the loop is then closed through a controller designed to provide robust stability and to have minimum impact on the closed loop gain. This latter controller in effect 'looks after' the phase lag and provides robustness. The controller is robust insofar as it provides stability in the face of plant perturbations. The design approach ensures that the stability margin is maximised.

The closed loop system for the MIMO plant may be represented as in Figure 6.3. Here, the loop is shaped by the pre-compensator $\boldsymbol{W}_1$ and the post-compensator $\boldsymbol{W}_2$. The loop is then closed through the robust stabilising controller $\boldsymbol{K}_{\boldsymbol{inf}}$.

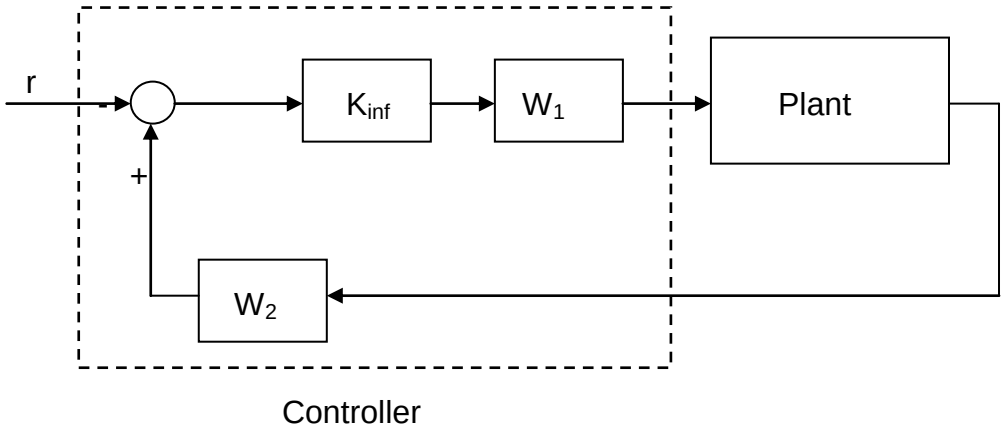

Figure 6.3 Implementation of stabilising loop shaping controller

McFarlane and Glover follow Georgiou and Smith (1990) in the use of a normalised cofactor model of plant perturbations. A plant may be represented by its normalised left coprime factorisation as follows:

$$\boldsymbol{G} = \boldsymbol{M}^{-1}\boldsymbol{N} \tag{6.3}$$

(The 'plant' includes the pre and post compensator weights, that is

$$\boldsymbol{G} = \boldsymbol{W}_2\boldsymbol{P}\boldsymbol{W}_1 \tag{6.4}$$

where $\boldsymbol{P}$ is the system to be controlled.)

A perturbed model of the plant is then written as

$$\boldsymbol{G}_{\boldsymbol{P}} = (\boldsymbol{M} + \boldsymbol{\Delta}_{\boldsymbol{M}})^{-1}(\boldsymbol{N} + \boldsymbol{\Delta}_{\boldsymbol{N}}) \tag{6.5}$$

where the uncertainty in the nominal plant model $\boldsymbol{G}$ is represented by stable unknown transfer functions $\boldsymbol{\Delta}_{\boldsymbol{M}}$ and $\boldsymbol{\Delta}_{\boldsymbol{N}}$ in its coprime factors. The closed loop may then be shown as in Figure 6.4.

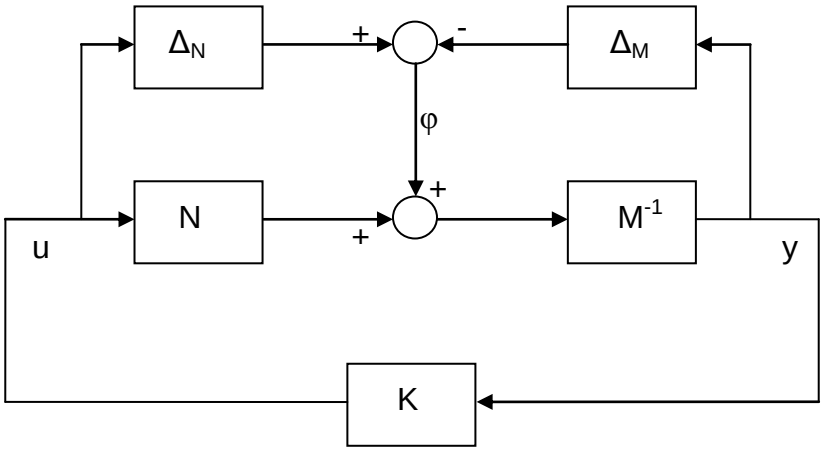

Figure 6.4 Robust stabilisation problem – coprime factorisation

The control objective becomes the design of a robust controller $\boldsymbol{K}$ which stabilises not only the nominal plant but the whole family of perturbed plants $\boldsymbol{G}_P$ defined by

$$\{\boldsymbol{G}_{\boldsymbol{P}} = (\boldsymbol{M} + \boldsymbol{\Delta}_{\boldsymbol{M}})^{-1}(\boldsymbol{N} + \boldsymbol{\Delta}_{\boldsymbol{N}}) : \left\|\boldsymbol{\Delta}_{\boldsymbol{N}}\ \boldsymbol{\Delta}_{\boldsymbol{M}}\right\|_{\infty} < \varepsilon\} \tag{6.6}$$

The transfer function from $\boldsymbol{\varphi}$ to $[\boldsymbol{u}^{\mathrm{T}}\ \boldsymbol{y}^{\mathrm{T}}]^{\mathrm{T}}$ may be written

$$\begin{bmatrix} \boldsymbol{K}(\mathbf{I} - \boldsymbol{G}\boldsymbol{K})^{-1}\boldsymbol{M}^{-1} \\ (\mathbf{I} - \boldsymbol{G}\boldsymbol{K})^{-1}\boldsymbol{M}^{-1} \end{bmatrix} \tag{6.7}$$

Defining the H_∞ norm of this transfer function as follows,

$$\gamma = \left\| \begin{bmatrix} \boldsymbol{K}(\mathbf{I} - \boldsymbol{G}\boldsymbol{K})^{-1}\boldsymbol{M}^{-1} \\ (\mathbf{I} - \boldsymbol{G}\boldsymbol{K})^{-1}\boldsymbol{M}^{-1} \end{bmatrix} \right\|_{\infty} \tag{6.8}$$

then, considering the closed loop in Figure 6.4, in accordance with the small gain theorem, for stability:

$$\gamma\varepsilon \leq 1 \tag{6.9}$$

The lowest achievable value of γ (γ_{min}) and corresponding maximum value of ε (ε_{max}) (stability margin) are given by (Glover and McFarlane, 1989)

$$\gamma_{min} = \varepsilon_{max}^{-1} \tag{6.10}$$

$$= \left(1 - \left\| \begin{bmatrix} \boldsymbol{N} & \boldsymbol{M} \end{bmatrix} \right\|_{\mathrm{H}}^{2}\right)^{-1/2} \tag{6.11}$$

$$= [1 + \rho(\boldsymbol{XZ})]^{1/2} \tag{6.12}$$

In eq.(6.11) $\|.....\|_{\mathrm{H}}$ is the Hankel norm. In eq.(6.12) ρ is the spectral radius (maximum eigenvalue) and $\boldsymbol{X}$ and $\boldsymbol{Z}$ are respectively the solutions to the generalised control algebraic Riccati equation and the generalised filtering algebraic Riccati equations (*ibid*.) as follows:

$$(\boldsymbol{A} - \boldsymbol{BS}^{-1}\boldsymbol{D}^{\mathrm{T}}\boldsymbol{C})^{\mathrm{T}}\boldsymbol{X} + \boldsymbol{X}(\boldsymbol{A} - \boldsymbol{BS}^{-1}\boldsymbol{D}^{\mathrm{T}}\boldsymbol{C}) - \boldsymbol{XBS}^{-1}\boldsymbol{B}^{\mathrm{T}}\boldsymbol{X} + \boldsymbol{C}^{\mathrm{T}}\boldsymbol{R}^{-1}\boldsymbol{C} = 0 \tag{6.13}$$

$$(\boldsymbol{A} - \boldsymbol{BD}^{\mathrm{T}}\boldsymbol{R}^{-1}\boldsymbol{C})\boldsymbol{Z} + \boldsymbol{Z}(\boldsymbol{A} - \boldsymbol{BD}^{\mathrm{T}}\boldsymbol{R}^{-1}\boldsymbol{C})^{\mathrm{T}} - \boldsymbol{ZC}^{\mathrm{T}}\boldsymbol{R}^{-1}\boldsymbol{CZ} + \boldsymbol{BS}^{-1}\boldsymbol{B}^{\mathrm{T}} = 0 \tag{6.14}$$

where (***A***,***B***,***C***,***D***) is a minimal state realisation of the 'plant' and ***R*** and ***S*** are defined as follows:

$$\boldsymbol{R} = (\mathbf{I} + \boldsymbol{DD}^{\mathrm{T}}) \tag{6.15}$$

$$\boldsymbol{S} = (\boldsymbol{I} + \boldsymbol{D}^{\mathrm{T}}\boldsymbol{D}) \tag{6.16}$$

A controller which satisfies

$$\gamma \geq \left\| \begin{bmatrix} \boldsymbol{K}(\mathbf{I} - \boldsymbol{GK})^{-1}\boldsymbol{M}^{-1} \\ (\mathbf{I} - \boldsymbol{GK})^{-1}\boldsymbol{M}^{-1} \end{bmatrix} \right\|_{\infty} \tag{6.17}$$

is given by

$$\boldsymbol{K} = \begin{bmatrix} \boldsymbol{A} + \boldsymbol{BF} + \gamma^{2}(\boldsymbol{L}^{\mathrm{T}})^{-1}\boldsymbol{ZC}^{\mathrm{T}}(\boldsymbol{C} + \boldsymbol{DF}) & \gamma^{2}(\boldsymbol{L}^{\mathrm{T}})^{-1}\boldsymbol{ZC}^{\mathrm{T}} \\ \boldsymbol{B}^{\mathrm{T}}\boldsymbol{X} & -\boldsymbol{D}^{\mathrm{T}} \end{bmatrix} \tag{6.18}$$

where ***F*** and ***L*** in eq. (6.18) are defined as follows:

$$\boldsymbol{F} = -\boldsymbol{S}^{-1}(\boldsymbol{D}^{\mathrm{T}}\boldsymbol{C} + \boldsymbol{B}^{\mathrm{T}}\boldsymbol{X}) \tag{6.19}$$

$$\boldsymbol{L} = (1 - \gamma^{2})\mathbf{I} + \boldsymbol{XZ} \tag{6.20}$$

The controller to be implemented on the real plant is then computed by combining $\boldsymbol{W}_1$, $\boldsymbol{K}$ and $\boldsymbol{W}_2$ in series. For simplicity, $\boldsymbol{W}_2$ was chosen to be unity gain in the present work. Thus the controller to be implemented is $\boldsymbol{W}_1\boldsymbol{K}_{\boldsymbol{inf}}$ (see Figure 6.3).

6.1.4 Controller Order Reduction

The order of the controller produced by the method is high. The implementation of a high order controller may introduce complexity without benefit. Therefore the practicability of reducing the order of the controller is checked and order reduction carried out as appropriate.

Two possible strategies for order reduction are truncation and residualisation. In truncation, the usual strategy is to reduce the model by removing the fastest modes. This may be achieved by describing the model in Jordan form, in which the system dynamic $\boldsymbol{A}$ matrix is diagonalised, with eigenvalues increasing down the leading diagonal. The fast modes are then eliminated by deletion. The poles of the truncated model are therefore a subset of the poles of the full model. The gain of the truncated model is equal to that of the full model only at infinite frequency, since only the $\boldsymbol{D}$ matrix is unmodified by the procedure.

In residualisation, all the dynamics of the states to be discarded are discarded with them. Thus if $\boldsymbol{A}$, $\boldsymbol{B}$, $\boldsymbol{C}$, $\boldsymbol{D}$ is a minimal realisation of $\boldsymbol{G}$, $\boldsymbol{x}_1$ is a vector of states to be retained**,** $\boldsymbol{x}_2$ is a vector of states to be discarded, then

$$\dot{\boldsymbol{x}}_1 = \boldsymbol{A}_{11}\boldsymbol{x}_1 + \boldsymbol{A}_{12}\boldsymbol{x}_2 + \boldsymbol{B}_1\boldsymbol{u} \tag{6.21}$$

$$\dot{\boldsymbol{x}}_2 = \boldsymbol{A}_{21}\boldsymbol{x}_1 + \boldsymbol{A}_{22}\boldsymbol{x}_2 + \boldsymbol{B}_2\boldsymbol{u} \tag{6.22}$$

$$\boldsymbol{y} = \boldsymbol{C}_1\boldsymbol{x}_1 + \boldsymbol{C}_2\boldsymbol{x}_2 + \boldsymbol{D}\boldsymbol{u} \tag{6.23}$$

Setting $\dot{\boldsymbol{x}}_2$ to zero, and eliminating $\boldsymbol{x}_2$ by substitution, gives

$$\boldsymbol{x}_2 = -(\boldsymbol{A}_{22}^{-1}\boldsymbol{A}_{21}\boldsymbol{x}_1 + \boldsymbol{A}_{22}^{-1}\boldsymbol{B}_2\boldsymbol{u}) \tag{6.24}$$

$$\dot{\boldsymbol{x}}_1 = (\boldsymbol{A}_{11} - \boldsymbol{A}_{12}\boldsymbol{A}_{22}^{-1}\boldsymbol{A}_{21})\boldsymbol{x}_1 + (\boldsymbol{B}_1 - \boldsymbol{A}_{12}\boldsymbol{A}_{22}^{-1}\boldsymbol{B}_2)\boldsymbol{u} \tag{6.25}$$

$$\boldsymbol{y} = (\boldsymbol{C}_1 - \boldsymbol{C}_2\boldsymbol{A}_{22}^{-1}\boldsymbol{A}_{21})\boldsymbol{x}_1 + (\boldsymbol{D} - \boldsymbol{C}_2\boldsymbol{A}_{22}^{-1}\boldsymbol{B}_2)\boldsymbol{u} \tag{6.26}$$

Clearly, the steady state gains of the full and reduced models are the same (since all state derivatives are then zero). Thus, the residualised model is accurate at low frequencies.

A rational route to deciding on how many and which states to remove involves first creating a balanced realisation ('an asymptotically stable minimal realisation in which controllability and observability Gramians are equal and diagonal' (Skogestad and Postlethwaite, 1997, p.451).

The controllability and observability Gramians $\boldsymbol{P}$ and $\boldsymbol{Q}$ respectively are defined as

$$\boldsymbol{P} = \int_0^\infty e^{\boldsymbol{A}\tau}\boldsymbol{B}\boldsymbol{B}^{\mathrm{T}}e^{\boldsymbol{A}^{\mathrm{T}}\tau}\mathrm{d}\tau \tag{6.27}$$

$$\boldsymbol{Q} = \int_0^\infty e^{\boldsymbol{A}^{\mathrm{T}}\tau}\boldsymbol{C}^{\mathrm{T}}\boldsymbol{C}e^{\boldsymbol{A}\tau}\mathrm{d}\tau \tag{6.28}$$

For controllability, $\boldsymbol{P}$ must be positive definite (and therefore full rank); for observability, $\boldsymbol{Q}$ must be positive definite (and therefore full rank).

Hankel singular values are defined as

$$\sigma_i = \sqrt{\lambda_i(\boldsymbol{PQ})} \tag{6.29}$$

where $\lambda_i(\boldsymbol{PQ})$ are the eigenvalues of $\boldsymbol{PQ}$.

For a balanced truncation, the states removed are those with the smallest Hankel singular values. In a balanced residualisation, the derivatives of these states are set to zero. The error bounds for balanced truncations and balanced residualisations are the same (see e.g. Skogestad and Postlethwaite, 1997, p.453; Samar *et al*., 1994, 1995).

If $\boldsymbol{G}(s)$ is a stable rational transfer function matrix with Hankel singular values $\sigma_1 > \sigma_2 > \ldots > \sigma_n$ where each σ_i has multiplicity r_i and $\boldsymbol{G_r}(s)$ is obtained by truncating or residualising the balanced realisation of $\boldsymbol{G}(s)$ to the first $(r_1+r_2+\ldots+r_k)$ states, then

$$\left\|\boldsymbol{G}(s)-\boldsymbol{G}_r(s)\right\|_\infty \le 2(\sigma_{k+1}+\sigma_{k+2}+\ldots+\sigma_n) \tag{6.30}$$

(after Skogestad and Postlethwaite, 1997, p.453; Anderson and Liu, 1989, eq. 3.5).

6.1.5 A Design Route for Controller Synthesis

A suitable route for the synthesis of a controller using the H_∞ Loop Shaping Method is as follows:

- Compute the loop shaping H_∞ controller $\boldsymbol{K_{inf}}$;
- Compute and check resulting stability margin;

- Compute the composite controller from the series combination of the weights and the loop shaping controller;
- Compute Hankel singular values for the composite controller to determine the practicability of order reduction;
- By reference to the Hankel singular values, reduce the order of the composite controller as appropriate;
- Check gap between full order and reduced order controllers and compare frequency responses of full and reduced order controllers;
- Discretise reduced order controller for digital implementation.

Where the controller is to be implemented in a digital form, it may be necessary to include a representation of the lag introduced by the sampling process at this stage in the design route.

In the sequel, a MATLAB function from the μ-Analysis and Synthesis Toolbox (Balas *et al*., 1993) is used to find ε_{max} and a loop shaping stabilising controller. Further MATLAB functions are used to form balanced realisations of the composite controller and to calculate its Hankel singular values for inspection prior to reduction of its state dimensions (*ibid*.). The 'gap' between full order and reduced order controllers is then examined. Gap analysis is discussed in 6.1.2 above.

6.1.6 Application of the Design Route to the Test System

6.1.6.1 Shaping the Open-Loop Gains

All of the gain characteristics in Figure 6.1 show 'roll offs' of around 15-30 dB per decade around crossover. Key design targets are the elimination of stead state speed error and the significant improvement of the disturbance rejection capability.

Disturbance transfer function singular values are plotted in Figure 6.5 (supply pressure 30 bar) and Figure 6.6 (supply pressure 100 bar) produced by Bath*fp* simulation by Njabeleke (Njabeleke *et al*., 2000). These portray the disturbance dynamics – the gain linking the disturbance signal to the output (shaft speed).

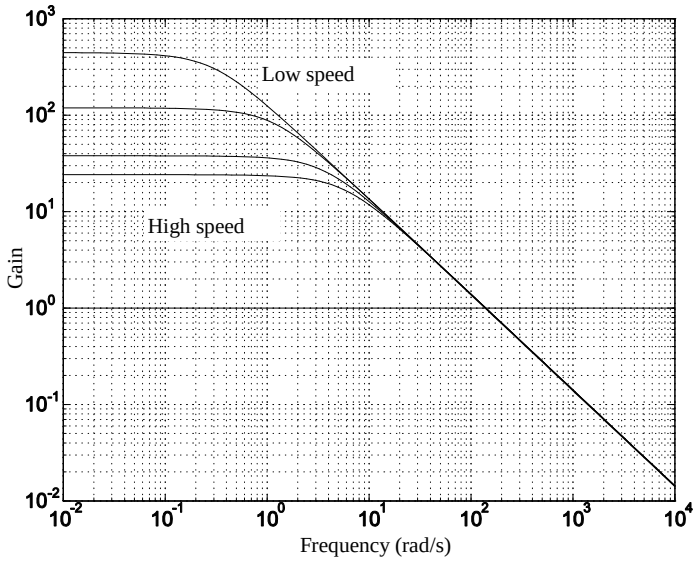

Figure 6.5 Disturbance rejection at 30 bar supply pressure – singular values

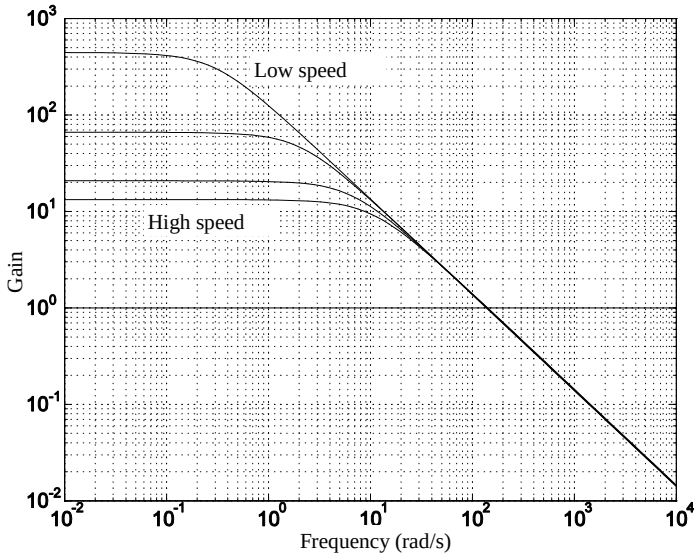

Figure 6.6 Disturbance rejection at 100 bar supply pressure – singular values

To design the two controllers, one for high and one for low speeds (see Section 6.1.2), it was necessary to select two linear models of the plant. The family of gains for a supply pressure of 30 bar and a range of speeds (valve openings) has been extracted from the set in Figure 6.1 and is shown in Figure 6.7.

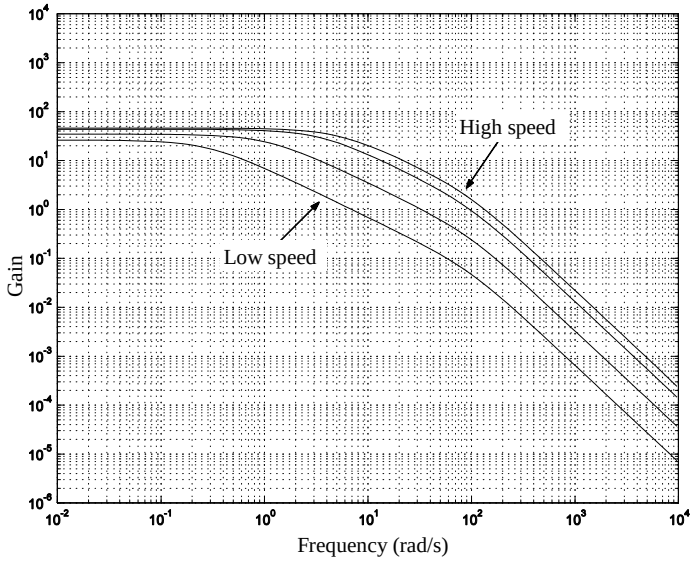

Figure 6.7 Open-loop gains with supply pressure 30 bar

From this set, the 'low' and 'high' speed models were selected and controllers designed as follows.

A PI pre-compensator W_1 of the form $K(s+1)/s$ provides a boost for the low frequency gain, removing any offset error. It also provides some lead around the gain crossover frequency, adding to robustness. For disturbance rejection, by reference to the shape of the disturbance transfer function, it is evident that the sensitivity (which is the gain between a disturbance at the output and the output) should be less than 1, at least at frequencies up to 0.2 rad/s ('low speed') and preferably up to higher frequencies at higher speeds. Again, considering the derivation of the sensitivity function, it is clear that to improve the disturbance rejection in relation to the unshaped plant, the compensator $K(s+1)/s$ must have gain greater than 1 in the frequency range of interest, so that sensitivity is reduced. Choosing $K=0.5$ results in the compensator having gain greater than 1 if

$$\left|0.5\frac{(1+j\omega)}{j\omega}\right| > 1 \tag{6.31}$$

$$\sqrt{(1+\omega^2)} > 2\omega \tag{6.32}$$

$$\omega^2 < \tfrac{1}{3} \tag{6.33}$$

$$\omega < 0.58 \quad \text{rad/s} \tag{6.34}$$

For the low speed controller, the gain K was set at 0.08 due to the much lower roll off rate of the system around crossover.

The open-loop gains of the compensated and uncompensated (shaped and unshaped) plants, high and low speed, are shown respectively in Figures 6.8 and 6.9.

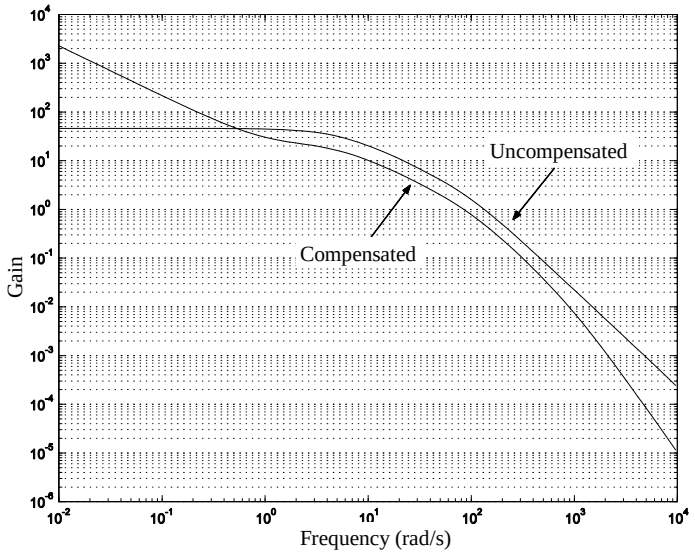

Figure 6.8 Compensated and uncompensated open-loop gains (high speed)

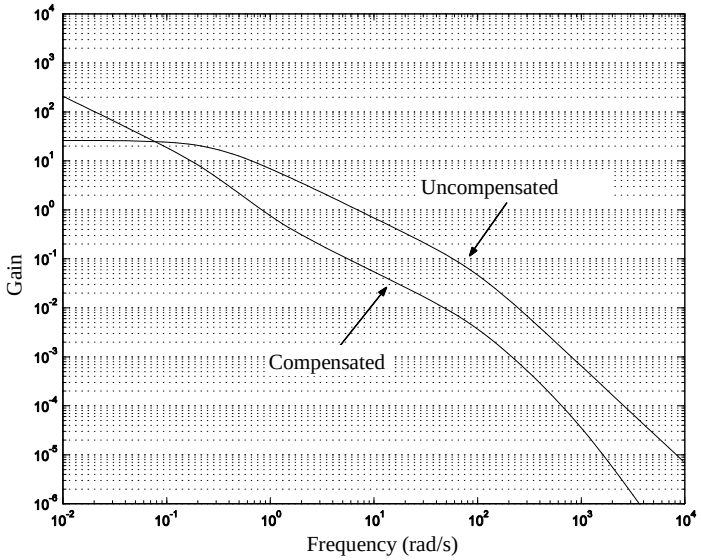

Figure 6.9 Compensated and uncompensated open-loop gains (low speed)

The post compensators W_2 were set to unity for simplicity, and to reduce the order of the controllers generated. In nominal recognition that the controllers would be

implemented digitally, an additional first order lag transfer function was included in series with each precompensator W_1.

Loop shaping H_∞ controllers were computed for the high and low speed compensated plant models; stability margins represented by ε (see Section 6.1.3) were computed as

Low speed	0.601
High speed	0.554

As these comfortably exceed 0.25 (see Skogestad and Postlethwaite, 1997, p.384), the controllers were judged to be acceptable.

The controller transfer functions are:

Low speed:

$$\frac{-7.43s^7 - 1.973e007s^6 - 1.328e013s^5 - 2.463e017s^4 - 1.257e021s^3 - 1.124e024s^2 - 1.006e026s - 4.76e025}{s^8 + 2.655e006s^7 + 1.787e012s^6 + 3.316e016s^5 + 1.694e020s^4 + 1.524e023s^3 + 1.451e025s^2 + 9.463e025s + 7.2e025} \quad (6.35)$$

High speed:

$$\frac{-588.1s^7 - 8.745e007s^6 - 3.898e012s^5 - 5.292e016s^4 - 2.407e020s^3 - 2.129e023s^2 - 2.139e025s - 2.294e025}{s^8 + 1.492e005s^7 + 6.7e009s^6 + 9.317e013s^5 + 4.528e017s^4 + 5.64e020s^3 + 2.345e023s^2 + 3.901e025s + 3.879e025} \quad (6.36)$$

6.1.6.2 Reducing the Order of the Composite Controller

Composite controllers were computed for the series combination of the loop shaping H_∞ controllers of eq. (6.35) and eq. (6.36) with the corresponding precompensator W_1. The composite controllers contained 9 states, as follows:

Low speed:

$$\frac{-0.594s^8 - 1.578e006s^7 - 1.062e012s^6 - 1.971e016s^5 - 1.006e020s^4 - 9.004e022s^3 - 8.136e024s^2 - 1.185e025s - 3.808e024}{s^9 + 2.655e006s^8 + 1.787e012s^7 + 3.316e016s^6 + 1.694e020s^5 + 1.524e023s^4 + 1.451e025s^3 + 9.463e025s^2 + 7.2e025s} \quad (6.37)$$

High speed:

$$\frac{-294.1s^8 - 4.373e007s^7 - 1.949e012s^6 - 2.646e016s^5 - 1.204e020s^4 - 1.066e023s^3 - 1.08e025s^2 - 2.216e025s - 1.147e025}{s^9 + 1.492e005s^8 + 6.7e009s^7 + 9.317e013s^6 + 4.528e017s^5 + 5.64e020s^4 + 2.345e023s^3 + 3.901e025s^2 + 3.879e025s} \quad (6.38)$$

Hankel singular values were computed for each as follows:

Low speed	High speed
0.6737	0.6064
0.0444	0.2440
0.0017	0.1127
(other singular values are of magnitude less than .0001).	0.0004
	(other singular values are of magnitude less than .0001).

Given these values, the two compensators were each reduced to third order by residualisation (after balancing), producing low speed controller:

$$\frac{3.809e-006s^3 - 0.5949s^2 - 0.8779s - 0.283}{s^3 + 6.973s^2 + 5.351s + 1.529e-010} \quad (6.39)$$

and high speed controller:

$$\frac{-0.0007867s^3 - 291.8s^2 - 3.344e004s - 3.59e004}{s^3 + 581.2s^2 + 1.214e005s - 1.365e-006} \quad (6.40)$$

6.1.6.3 Comparison between Full and Reduced Order Controllers

Figures 6.10 and 6.12 show a very close correspondence between the full order and reduced order controller gains. The gaps between them as calculated (see 6.1.2) are zero. The gains of the reduced order controllers exceed those of the full order controllers only at frequencies in excess of around 10^5 rad/s. The contribution of the dynamics of uncertainties at these frequencies is likely to be extremely small for the test system; the effect on stability robustness of order reduction will therefore be very small.

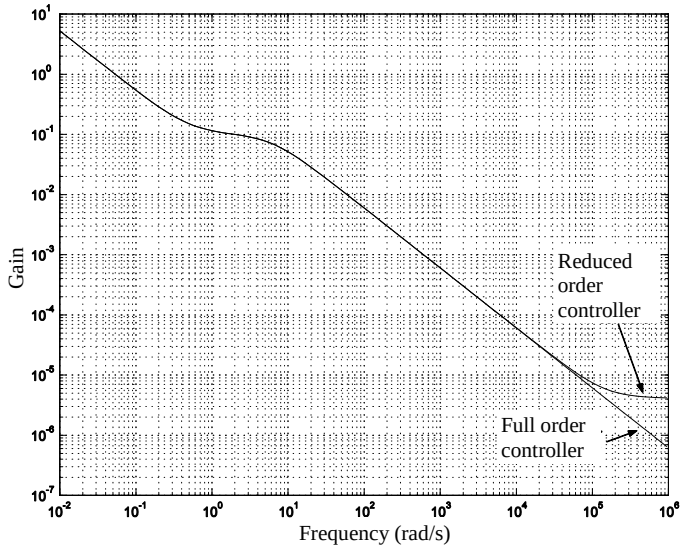

Figure 6.10 Gain of composite controller (low speed)

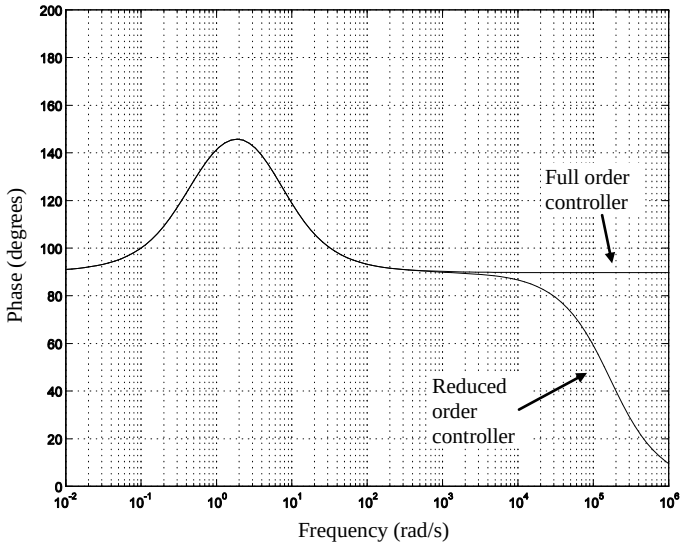

Figure 6.11 Phase of composite controller (low speed)

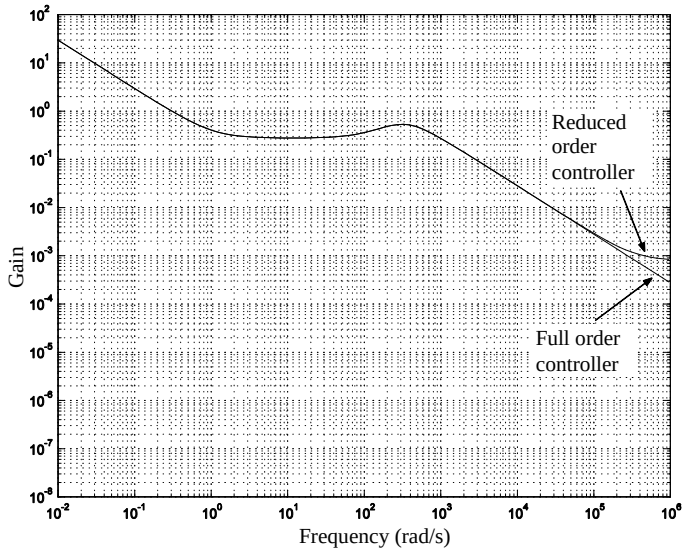

Figure 6.12 Gain of composite controller (high speed)

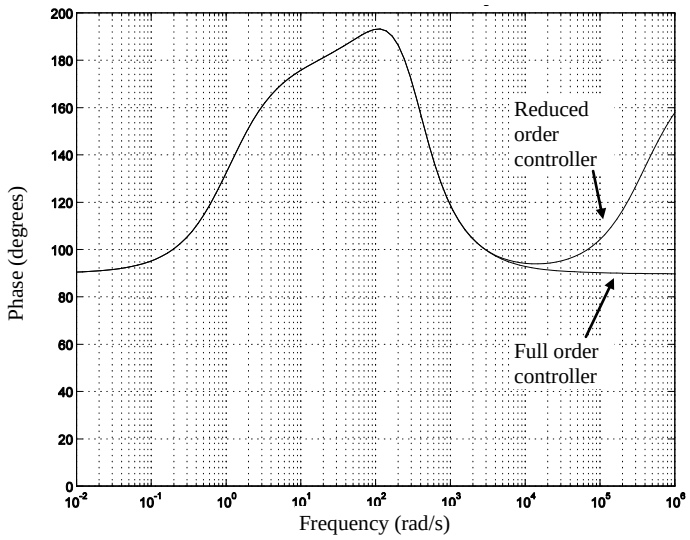

Figure 6.13 Phase of composite controller (high speed)

6.1.7 Implementation Issues

Each of the composite controllers, as derived (eq.(6.37) and eq.(6.38)), includes an integrator to reject low frequency disturbances and eliminate steady state error. The output of the controller to the plant is the electrical current to the solenoid on the valve. The controller must be designed so that the output is limited to 20 mA, corresponding to full opening of the valve, whatever value might be computed by the control algorithm (saturation). In the absence of an 'anti-windup', scheme, such as

that to be described, integrator action could result in the computed value of the control signal, before it is limited, significantly exceeding the saturation limit of 20 mA. If this happens, there will be a delay between the valve starting to close and a reversal in the sign of the speed error: the integrator must initially 'unwind'. The following anti-windup scheme (Green and Limebeer, 1995, p.431) shown in Figure 6.14 prevents windup. This appears to be based on the scheme of Doyle *et al*. (1987) as referenced by Edwards and Postlethwaite (1998).

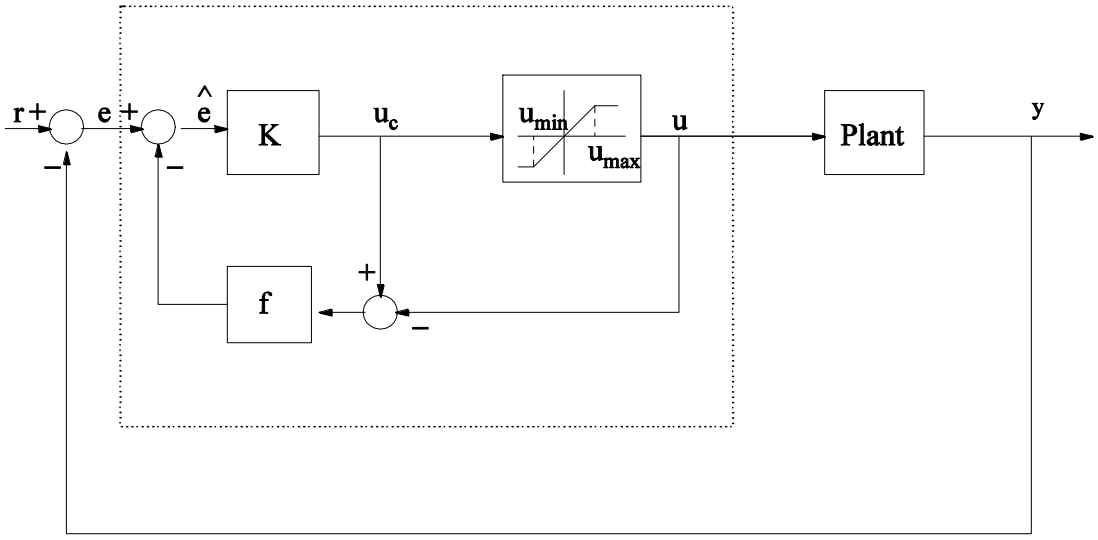

Figure 6.14 Anti-windup scheme

The output of the control algorithm is compared with the limited value; if there is a difference, i.e. the saturating element is active, the error signal supplied to the controller is modified in a sense which limits the magnitude of its output. In the notation of Figure 6.14, the error signal is modified if $u > u_{max}$ or $u < u_{min}$. Otherwise, $u = u_c$ and no modification occurs.

In the former situation, for the case when u is limited to u_{max},

$$u_c = K\left[e - f(u_c - u_{max})\right] \tag{6.41}$$

$$= (1 + Kf)^{-1} K(e + f u_{max}) \tag{6.42}$$

Provided that f is chosen so that $|f| >> 1$ and $|Kf| >> 1$,

$$u_c \approx (Kf)^{-1} K(e + f u_{max}) \tag{6.43}$$

$$u_c \approx u_{max} \tag{6.44}$$

Thus this arrangement ensures that u_c is limited to lie within (or only just outside) the range from u_{min} to u_{max}. Since the additional feedback loop is inactive when control errors and control signal lie in a normal band away from saturation, it has no effect on stability.

Green and Limebeer (1995) show (p.434) how the anti-windup scheme may be extended to provide a 'bumpless' transition between two (or more) controllers. Bumpless transition between two or more controllers has been extensively analysed by, in particular, Hanus *et al.* (1987). They have analysed the impact on stability. In the sequel, the decision on which of two controllers should be active depends on the operating point. When the switch from one to the other is made, it is important to ensure that both are producing control signals of similar magnitude in order to avoid a discontinuity in the signal applied to the plant. A discontinuity could result in electrical overload to an actuator and/or a mechanical shock leading to damage. The two controllers, each with an anti-windup loop, are connected in parallel as shown in Figure 6.15. With the switch in the position as drawn, controller 1 is in service, and anti-windup protection is provided by the feedback loop through f_1.

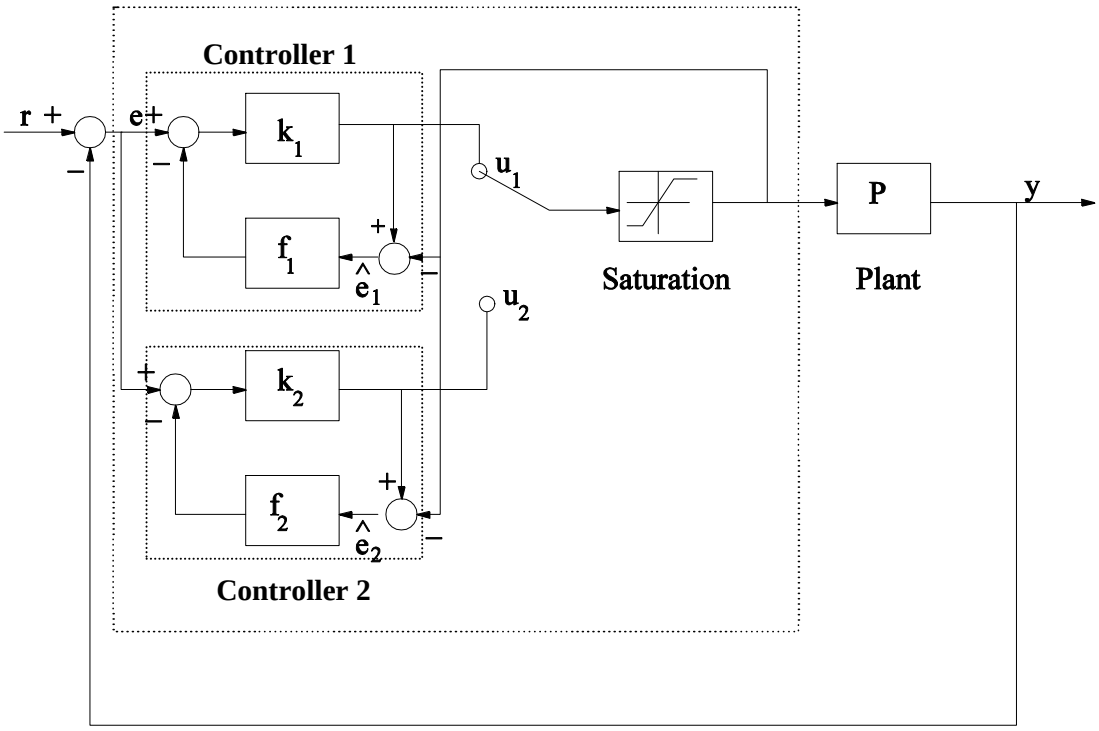

Figure 6.15 Bumpless transfer scheme with anti-windup

In general, for this scheme:

$$u_1 = k_1[e - f_1(u_1 - u)] \tag{6.45}$$

$$= (1 + k_1 f_1)^{-1} k_1 (e + f_1 u) \tag{6.46}$$

$$u_2 = k_2[e - f_2(u_2 - u)] \tag{6.47}$$

$$= (1 + k_2 f_2)^{-1} k_2 (e + f_2 u) \tag{6.48}$$

When controller 1 is in service, and there is no saturation, from eq. (6.45),

$$u = u_1 \tag{6.49}$$

$$u_1 = k_1 e \tag{6.50}$$

From eq. (6.48),

$$u_2 = (1 + k_2 f_2)^{-1} k_2 e + (1 + k_2 f_2)^{-1} k_2 f_2 u \tag{6.51}$$

If $k_2 f_2 >> 1$ then

$$u_2 = \frac{e}{f_2} + u \tag{6.52}$$

so, if $f_2 >> 1$,

$$u_2 = u \tag{6.53}$$

There will therefore be no ‘bump’ if the switch is operated to place controller 2 in control. A similar argument applies for switching from controller 2 to controller 1 if $k_1 f_1 >> 1$ and $f_1 >> 1$. The argument also applies in the presence of saturation.

This bumpless transfer scheme was found to be straightforward to implement (see below). It is rather less complicated than some other schemes, such as Graebe and Ahlen (1996) which requires more than one switch and additional control blocks.

6.2 Rig Testing

6.2.1 Controller Implementation

The high and low speed controllers were discretised using the Tustin method. As the singular values plot (Figure 6.1) shows that the bandwidth at low speeds is an order of magnitude lower than the bandwidth at high speeds, the controllers are designed

with sampling rates of 35 Hz and 350 Hz respectively. (These sampling rates are consistent with the discussion in Section 5.2.3.1 and Appendix 3.)

The transfer functions, derived respectively from the reduced order controller transfer functions of eq. (6.39) and eq. (6.40), are:

Low speed:

$$\frac{-0.007881z^3 + 0.007546z^2 + 0.007892z - 0.007562}{z^3 - 2.815\,z^2 + 2.634z - 0.819} \tag{6.54}$$

High speed:

$$\frac{-0.2339z^3 + 0.1687z^2 + 0.2321z - 0.1674}{z^3 - 1.724z^2 + 0.9249z - 0.2009} \tag{6.55}$$

The control program for the rig PC (written in C++) was amended to incorporate 'bumpless' transfer between controllers, integrator wind-up protection, and sampling rate change at 300 rpm (by Njabaleke); a series of tests was carried out, as illustrated in the following paragraphs.

6.2.1.1 Tracking Tests

The ability of each of the controllers (low and high speed) to follow step changes in speed demand with a wide range of supply pressures is shown in the following group of figures. The threshold between low and high speed is 300 rpm, the switching point between the two controllers. These show speed and demanded speed, and the control signal to the valve. It is not practicable to apply labels to the speed tracking test figures, because of the proximity of the data sets relating to different supply pressures. However, greatest overshoots are associated with the highest supply pressures.

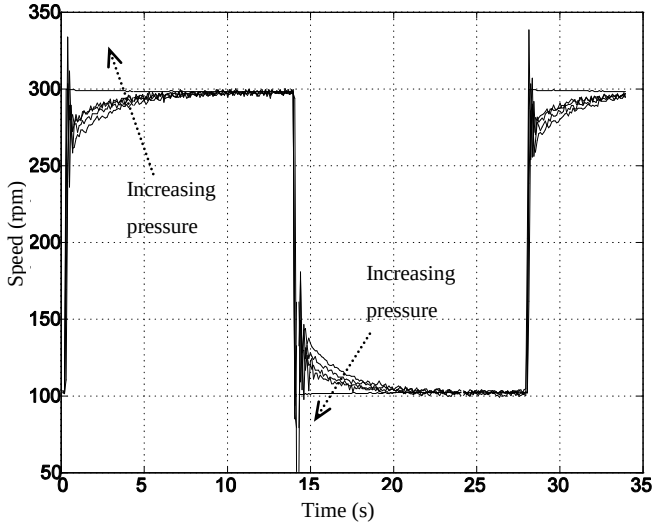

Figure 6.16 Set point tracking at low speeds with supply pressure variation

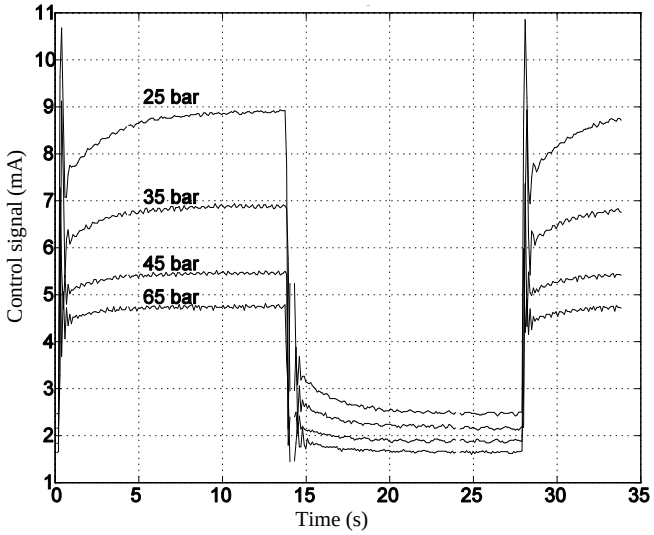

Figure 6.17 Control signals for set point tracking at low speeds

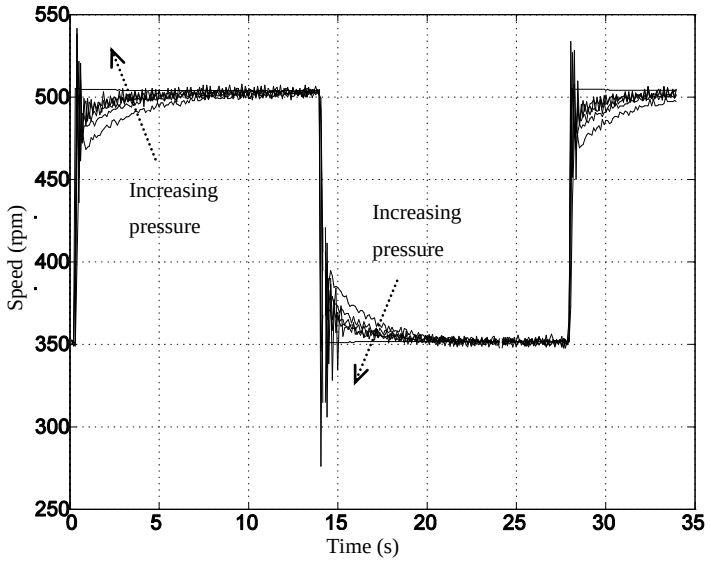

Figure 6.18 Set point tracking at high speeds with supply pressure variation

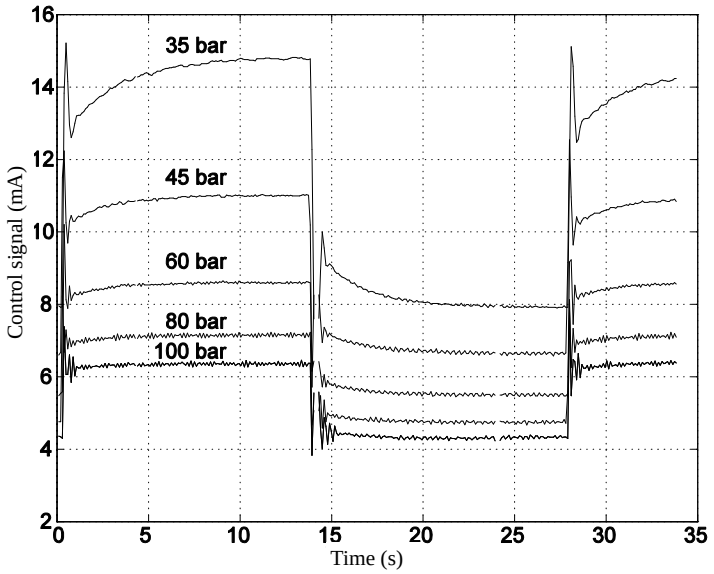

Figure 6.19 Control signals for set point tracking at high speeds

6.2.1.2 Disturbance Rejection Tests

Disturbances in the form of load torque changes are applied in a further series of tests. The motor under test drives a pump as a load. Load torque is altered by a signal applied to a valve in the pump discharge line. Load disturbances are applied at a range of operating speeds and supply pressures. Test results are illustrated in Figures 6.20 to 6.27. At each of a series of supply pressures (35, 45, 60 and 100 bar) are

shown the speed set point, actual speed, and load torque (derived from pump discharge pressure). Control signals (currents to valve solenoid) are plotted separately.

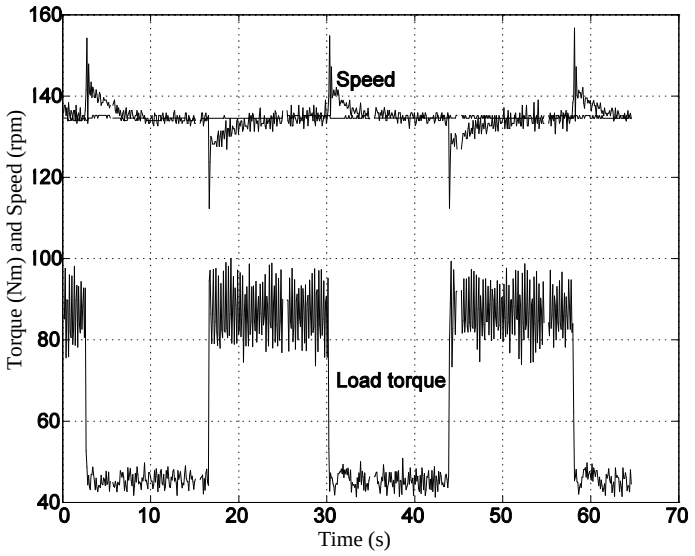

Figure 6.20 Disturbance rejection at 35 bar – speed and load torque

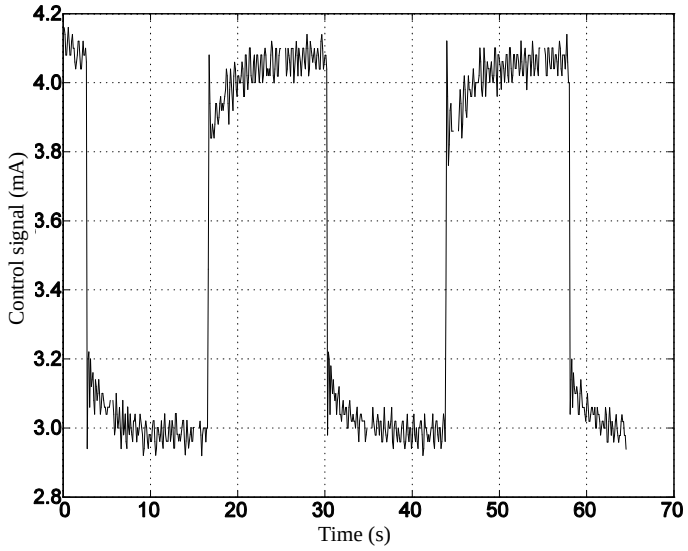

Figure 6.21 Disturbance rejection at 35 bar – control signal

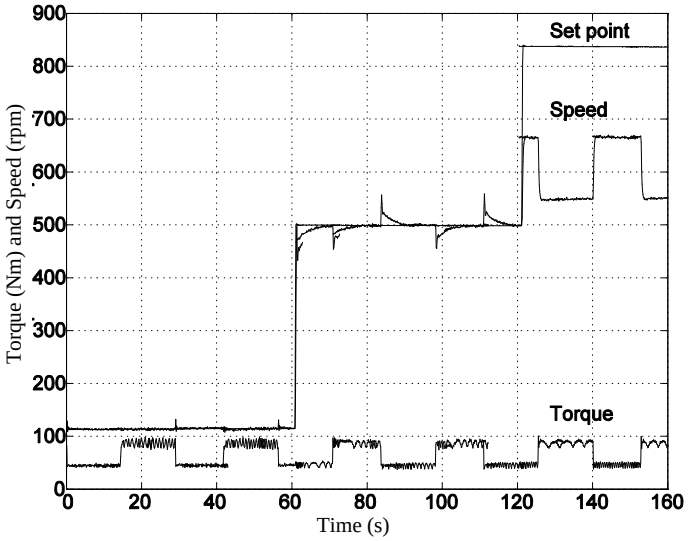

Figure 6.22 Disturbance rejection at 45 bar – speed and load torque

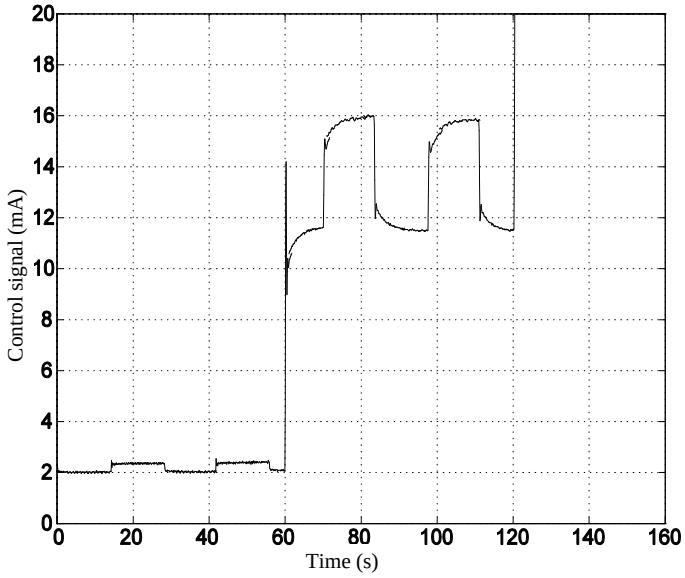

Figure 6.23 Disturbance rejection at 45 bar – control signal

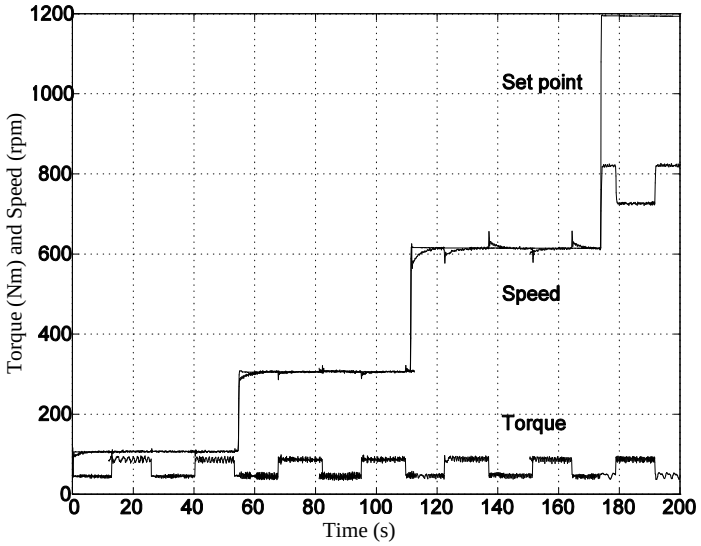

Figure 6.24 Disturbance rejection at 60 bar – speed and load torque

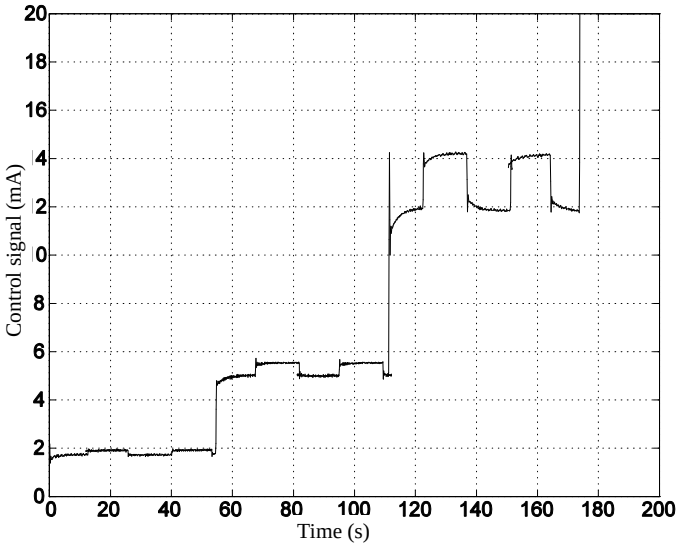

Figure 6.25 Disturbance rejection at 60 bar – control signal

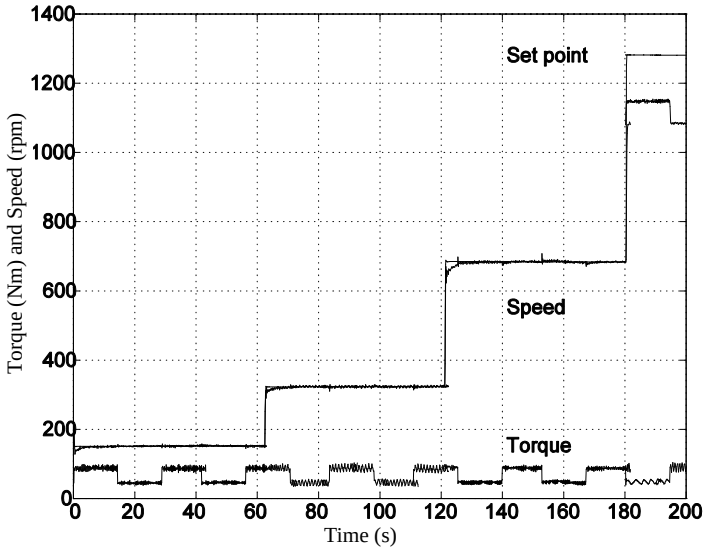

Figure 6.26 Disturbance rejection at 100 bar – speed and load torque

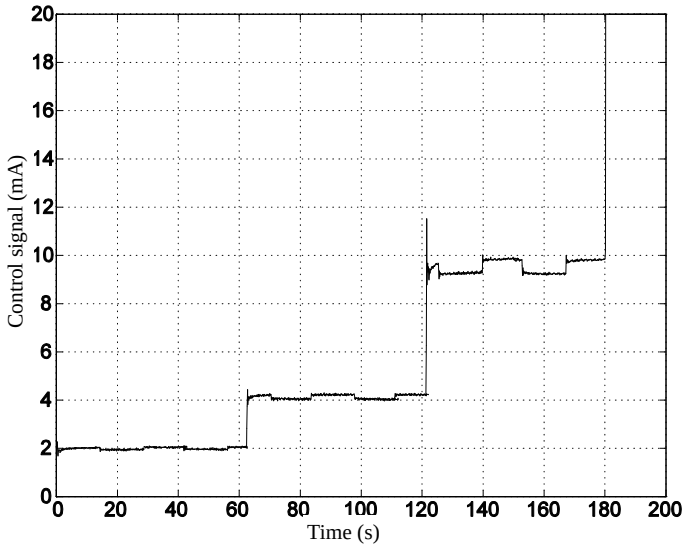

Figure 6.27 Disturbance rejection at 100 bar – control signal

The magnitude of the load disturbances is generally the same for each test (load step changes between 40 and 80 Nm). Disturbance rejection appears to be good to excellent throughout, improving with increasing supply pressure. This is attributable to an increase of forward path gain with pressure. The speed set point ranges through the controller switching threshold (300 rpm) for the tests at 45 bar and above, without readily discernible effect on tracking and regulation. In the tests at 45 bar and above, the controller is taken into saturation (valve current 20 mA) towards the end of the test interval, when speed demands are highest. In these phases of the tests,

the system is unable to reject the disturbances imposed by the fluctuating load torque.

6.2.1.3 Bumpless Transfer and Integrator Wind-Up Protection Scheme

A series of tests to check the performance of the bumpless transfer and integrator wind-up scheme (Green and Limebeer – see Section 6.1.7) was carried out, with results exemplified in this section.

Figure 6.28 and Figure 6.29 show the effect of applying a triangular speed demand to the system, taking the demanded speed through the switching point of 300 rpm in both directions. In these figures the results of tests carried out at 35, 45, 60, 80 and 100 bar supply pressure are superimposed. The effect of the switch between high and low speed controllers is not readily discernible at any supply pressure. Figure 6.29 shows the corresponding control signals. As well as demonstrating the efficacy of the bumpless transfer scheme, this latter figure also illustrates an effect of the non-linearity of system, its gain reducing at higher speeds for all pressures.

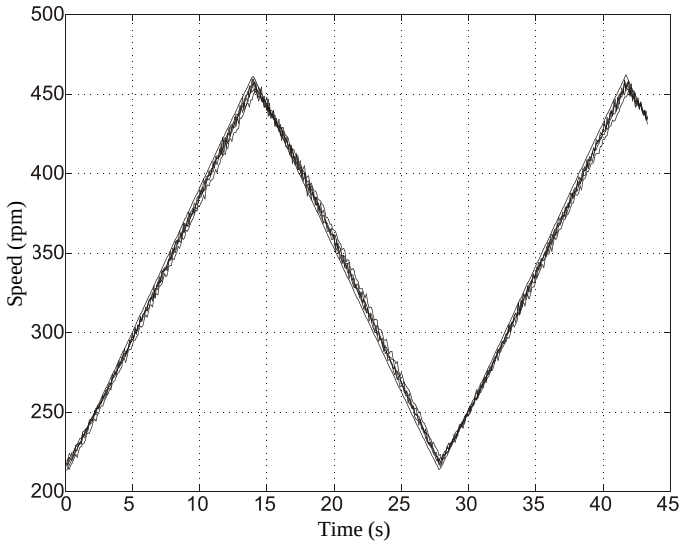

Figure 6.28 Bumpless transfer between high and low speed controllers at a range of supply pressures – set point tracking

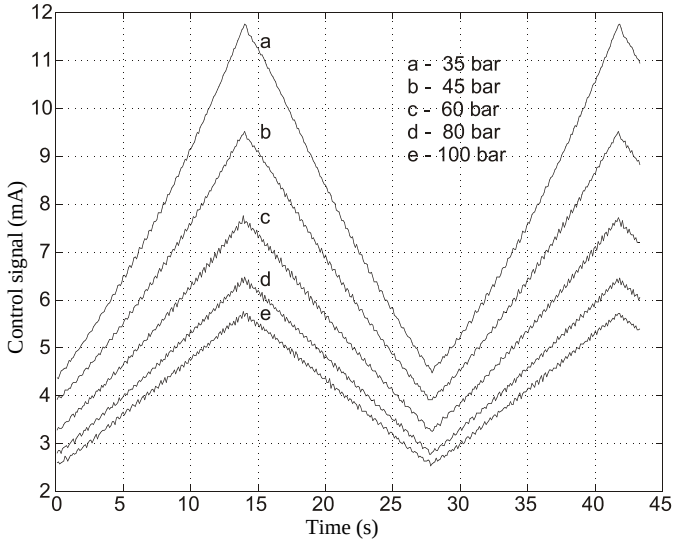

Figure 6.29 Bumpless transfer between high and low speed controllers at a range of supply pressures – control signals

To test the integrator wind-up protection scheme, a speed demand signal, which takes the controller into saturation, is applied.

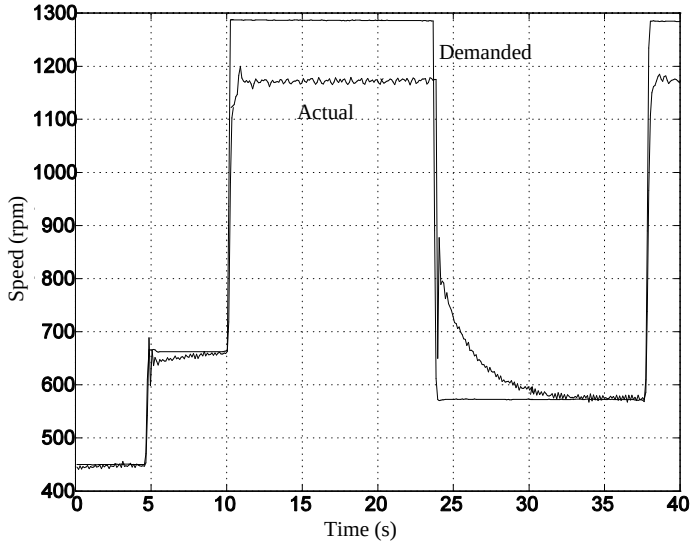

Figure 6.30 Anti-wind-up performance – set point tracking

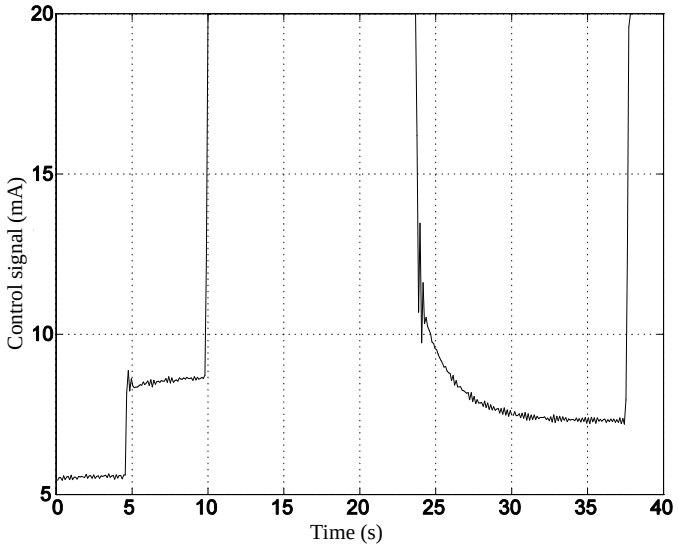

Figure 6.31 Anti-wind-up performance – control signal

The set point is taken from *c.* 650 rpm to *c.* 1290 rpm, and returned to *c.* 570 rpm. Set point tracking and control signals are illustrated in Figures 6.30 and 6.31 respectively. The former shows that, at the supply pressure of 100 bar, with the applied load, the motor cannot reach the demanded speed. The latter shows that when the demanded speed reaches 1290 rpm, the control signal rises to its maximum value of 20 mA. However, when the demand speed is reduced, the control signal reduces immediately, resulting in the new set point being reached within seconds.

6.3 Concluding Remarks

This Chapter has elaborated on the linear method of Chapter 5 by using the results of an examination of how the open-loop gain of the candidate system, as illustrated by its bode gain (or singular value) plots, varies with operating parameters, in particular supply pressure and speed set point. Application of 'gap analysis' to these gain characteristics was found to indicate that the design of a single robust controller to provide specified performance across the full range would be challenging. Therefore, in an alternative approach, two controllers were designed, one for 'high' speed and the other for 'low' speed operation, each using a 'loop shaping' approach. For each of these, the loop was shaped using a PI compensator. The orders of the controllers in combination with the compensators were reduced to facilitate implementation. A suitable bumpless switching scheme was identified. This, with the two reduced order

controllers, was successfully implemented and tested on the rig. The resulting composite controller was found by experiment to have good speed set point tracking and load disturbances rejection properties; the selected bumpless transfer scheme was also found to give integrator wind-up protection. The bumpless transfer and integrator wind-up protection scheme could in principle be used with two PID controllers. However, such a scheme would not provide the robustness afforded by the use of the H_∞ loop shaping controllers: more than two PID controllers may be required to achieve operation over the entire range. The investigation of the applicability of multiple PID controllers with the bumpless transfer and integrator wind-up protection scheme might be the subject of future work.

Future work might also include assessing the benefits or otherwise of implementing a control scheme in which the control algorithm was selected according to supply pressure as well as or in addition to operating speed. However, such a development would require the provision of a suitable supply pressure sensor.

7 Fuzzy Logic Controllers

'Fuzzy logic is not as good as its strong proponents argue, and not as bad as its detractors say!' - Prof. Karl Aström at the Institution of Electrical Engineers, London, following his presentation of the Inaugural Tustin Lecture (12 May 1999) entitled 'Digital Control - A Perspective'.

7.1 Introduction

The hydrostatic power transmission system has been shown to be highly non-linear (Chapter 4); its gain changes significantly when the speed set point or supply pressure is varied. A precise model of the system would be difficult to derive. If such a model were to be used, a supply pressure transducer would be essential; this would add to the initial cost of the controller and, through additional maintenance requirements, to its operating costs. However, it is possible to make general verbal 'intuitive' statements about the relationship between its required input (the electrical signal to the valve) and the difference between the required and actual output (shaft speed).

'Fuzzy systems let us guess at the non-linear world and yet do not make us write down a math model of the world' (Kosko, 1994, p.165)

In this phase of the project, the objective was to develop in simulation 'self organising' fuzzy logic controllers to provide speed control for the test rig, to test the ability of these controllers to track and regulate in the face of load and supply pressure disturbances, and then to implement similar controllers on the test rig itself.

This Chapter summarises work at Bath on the application 'self organising fuzzy logic control' (SOFLC) to the system. The development of controllers and their testing in simulation and on the rig is then described.

7.2 Review of the History of Fuzzy Logic and Its Application to Control and to Fluid Power

This section contains a brief review of the development and application in the field of fluid power of controllers using what in the present work is termed ‘self organising fuzzy logic’, itself an extension of ‘fuzzy logic’. An introduction to those principles of fuzzy logic which are of particular relevance to the current work is contained in the Appendix 4. The principles of fuzzy logic control and SOFLC are set out in Appendix 5.

Some initial investigations within the Department into the application of fuzzy logic to the speed control of a fluid power motor have been reported by Njabeleke (1998). In these the application of a PD fuzzy logic and PD self organising fuzzy logic controller (SOFLC) were explored jointly with the author in simulation. The initial results of this exploration have been summarised and published (Njabeleke *et al*., 1998). Studies of the disturbance rejection capability of the SOFLC have been undertaken by the author and published (Pannett *et al*., 1999). In this work, the inputs to the controller were presented on a discrete universe of discourse; operation was simulated in continuous rather than discrete time. The approach demonstrated the practicability of applying ‘fuzzy’ control to the system. However, in order to implement controllers in test, it was necessary to review the control algorithms and to generate discrete time versions of them. These discrete time versions were tested in simulation; those which performed satisfactorily in simulation were tested practically. This Chapter describes its extension of the initial work to include the development of real time fuzzy and SOFLC controllers and presents their implementation and physical testing.

7.3 Application of the Controller

The SOFLC with structure as set out in Appendix 5 is applied to the speed control of the motor in the hydrostatic power transmission system described in Chapter 3 as follows. Initial work on the design of a SOFLC centred on simulation. The inputs are the motor speed error and rate of change of motor speed error while the output is the valve current in mA.

7.3.1 Key Parameters

The valve rated current is 20mA. The universes of discourse used are:

motor speed error [-1200 1200] rpm;

rate of change of motor speed error [-1200 1200] rpm/s;

controller output [-20 20] mA.

Each of these universes of discourse is discretised into 200 elements.

7.3.2 Membership Functions

The membership functions used are triangular and have 25% overlap for the motor speed error and rate of change of motor speed error and 20% overlap for the valve current. Triangular membership functions were chosen because their encoding is straightforward. The use of triangular membership functions is well supported by the literature, for example Pedrycz (1994). Pedrycz and Vukovich (2002) include a discussion of the significance of overlap. (In the sequel (Section 7.5.5), it is shown that a control deadband can be influenced by the membership function.)

The membership functions are shown graphically in Figure 7.1. They were prepared using MATLAB, in particular the Fuzzy Systems Toolbox from UMIST (Wolkenhauer and Edmunds, 1994).

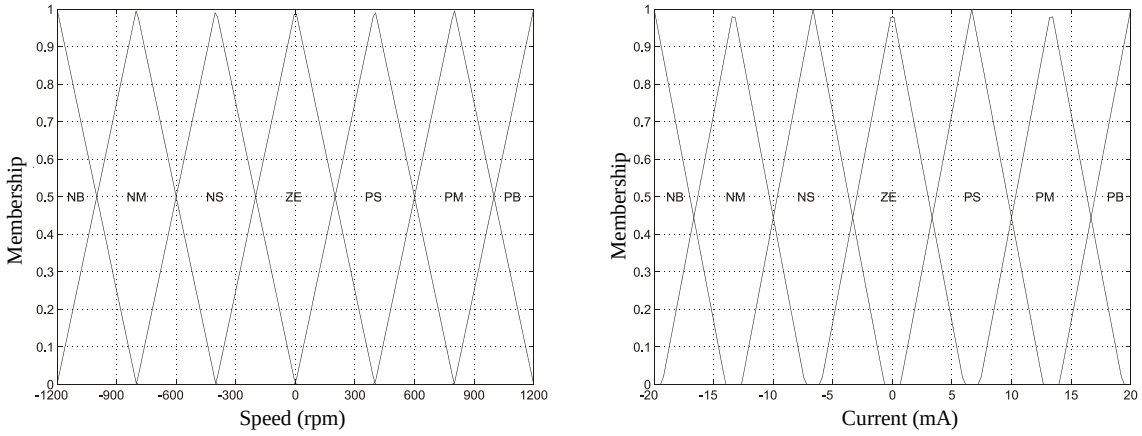

(a) Error (and error rate) **(b) Valve current**

Figure 7.1 Membership functions

7.4 Simulation of SOFLC Closed Loop Controller

This SOFLC was tested in simulation using Bath*fp*.

A schematic of the closed loop system is shown in Figure 7.2.

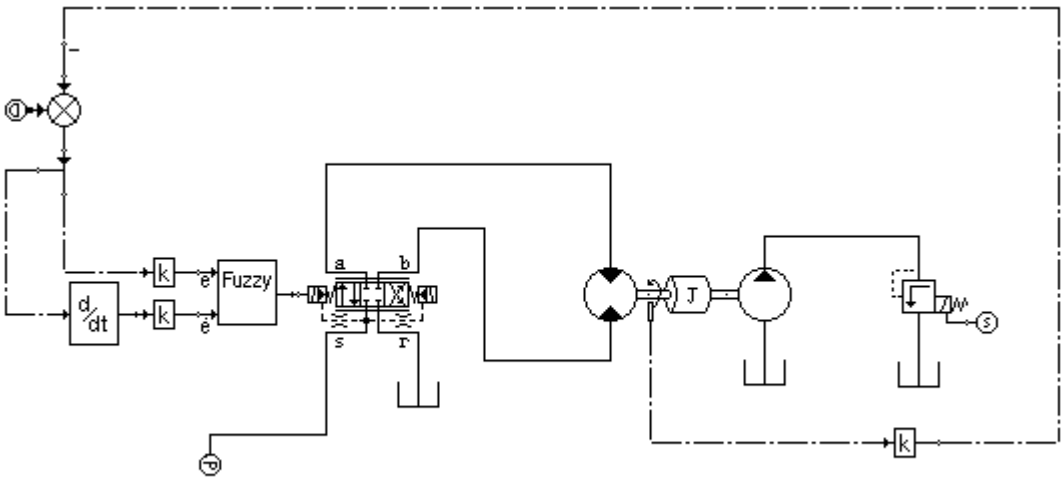

Figure 7.2 Circuit as represented in Bath*fp*

To tune the controller, three parameters must be set. These are the gains for the 'error' and 'error rate' signals and the 'reward delay' time. Gain values for 'error' used lay in the range 5-20 and for 'rate' 0.1-0.5. A selection of the results of simulations is presented in graphical form in Figures 7.3, 7.4 and 7.5. These demonstrate the tracking of a speed demand transient in the presence of supply pressure changes and load changes, imposed by adjusting the cracking pressure of the relief valve in the load circuit. In each, the speed demand transient is shown as a broken line. No initial rules were given for any of these simulations (i.e. FAM empty (all elements zero) at commencement).

Error gain	Rate gain	Reward delay (s)	Figure
10	.1	.01	Figure 7.3
10	.1	.02	Figure 7.4
10	.1	.04	Figure 7.5

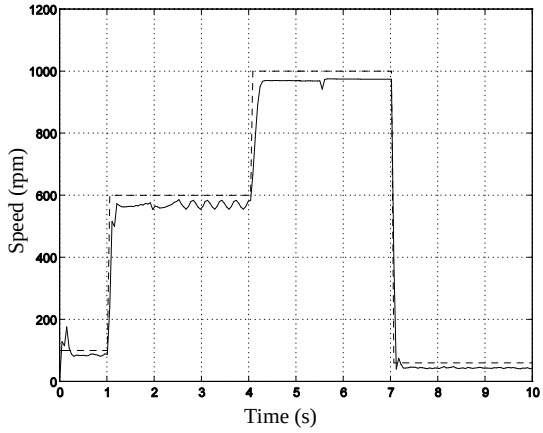

(a) Tracking

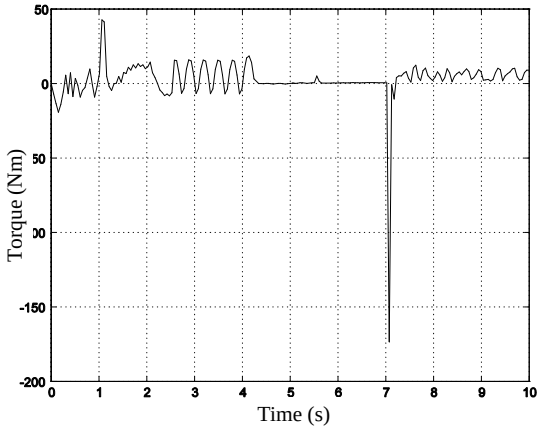

(b) Torque

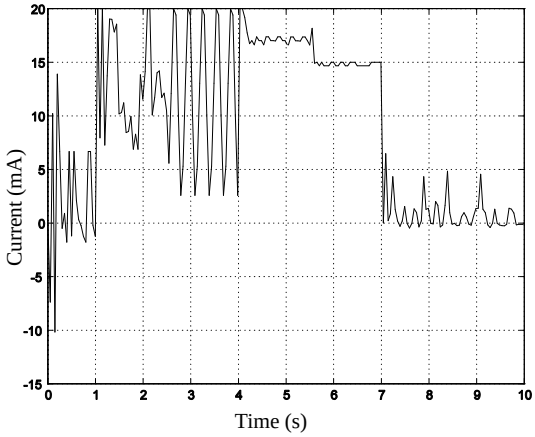

(c) Control signal

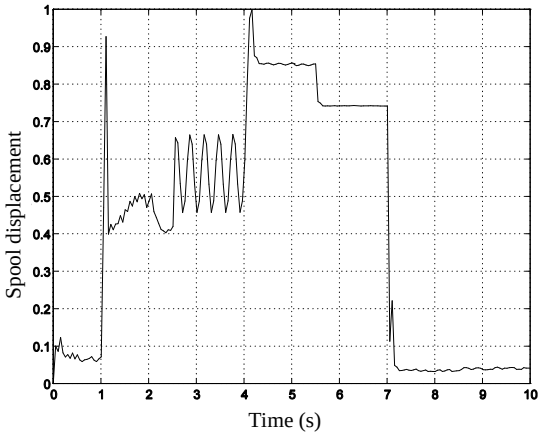

(d) Spool displacement

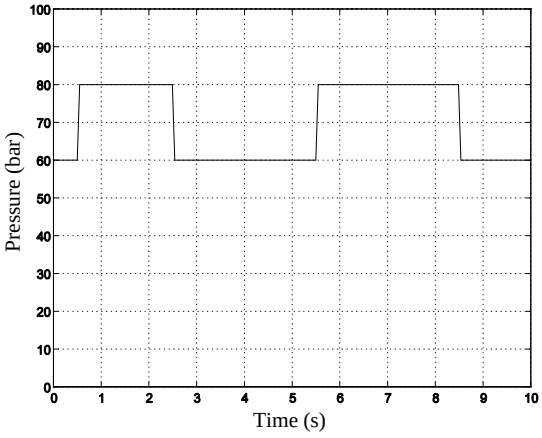

(e) Supply pressure

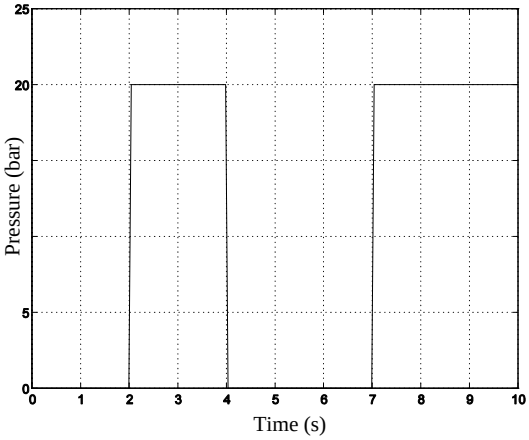

(f) Load circuit pressure

Figure 7.3 SOFLC simulation 1 – reward delay .01 s

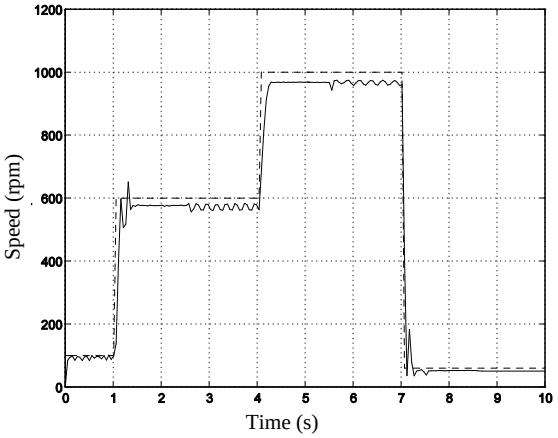

(a) Tracking

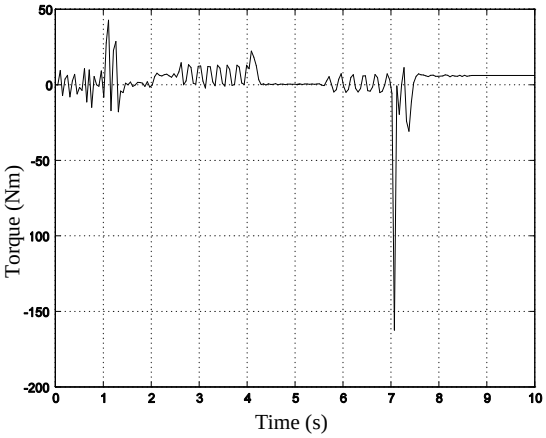

(b) Torque

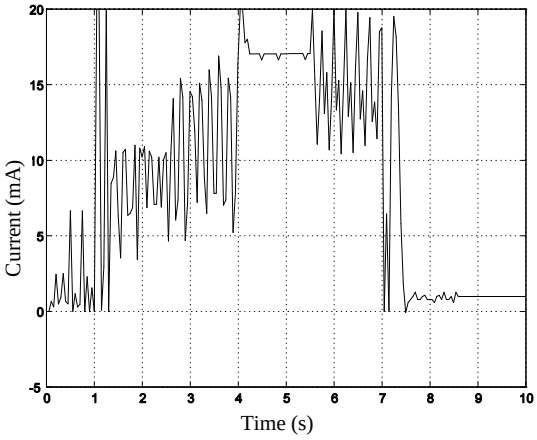

(c) Control signal

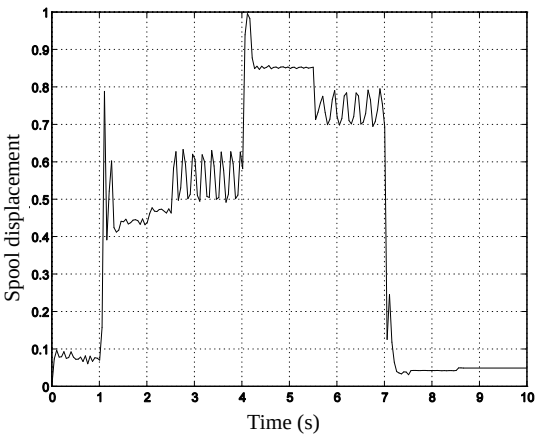

(d) Spool displacement

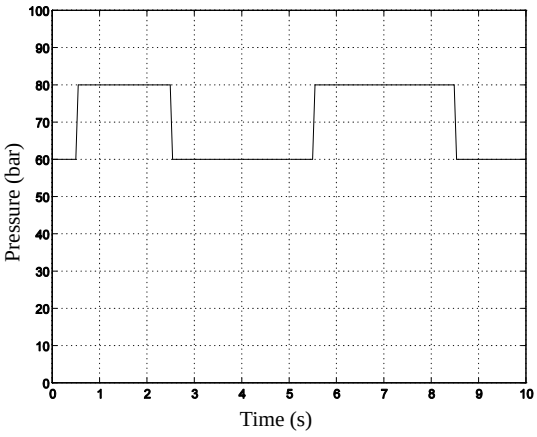

(e) Supply pressure

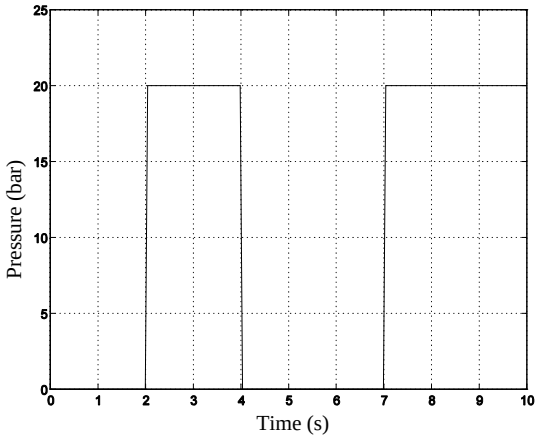

(f) Load circuit pressure

Figure 7.4 SOFLC simulation 2 – reward delay .02 s

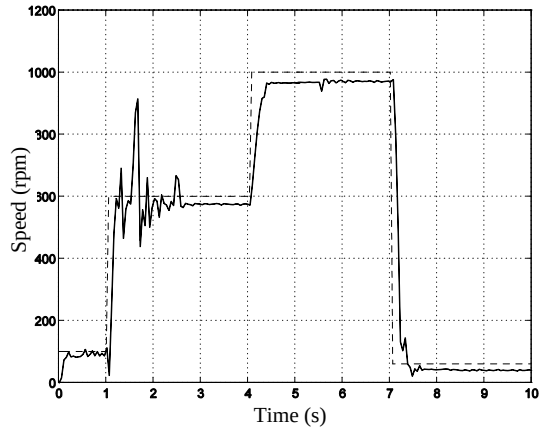

(a) Tracking

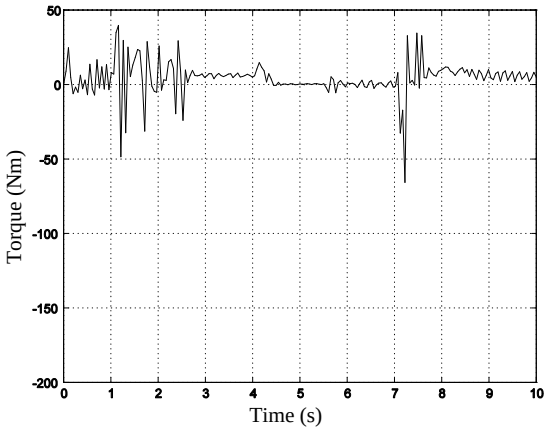

(b) Torque

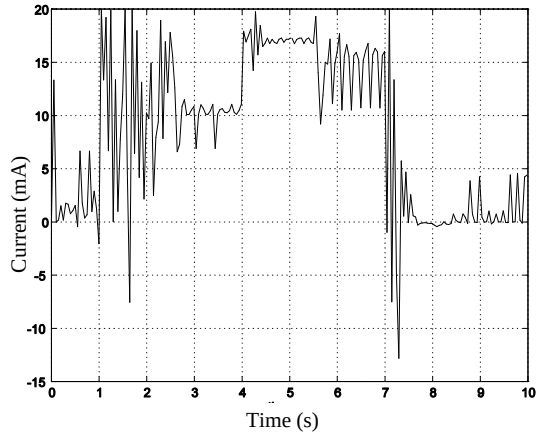

(c) Control signal

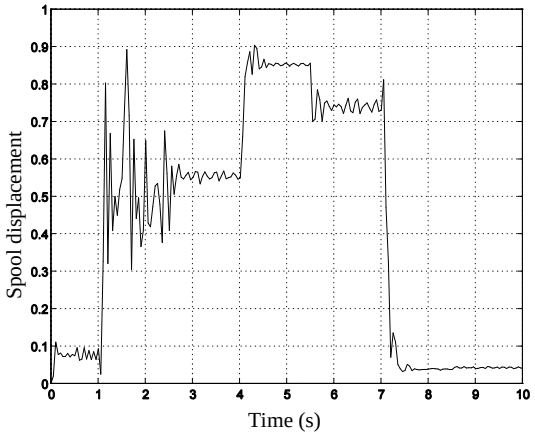

(d) Spool displacement

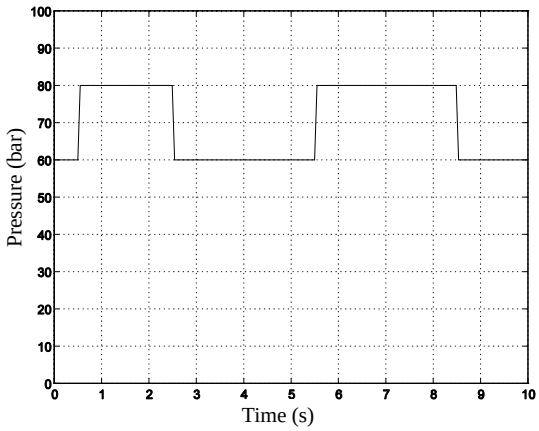

(e) Supply pressure

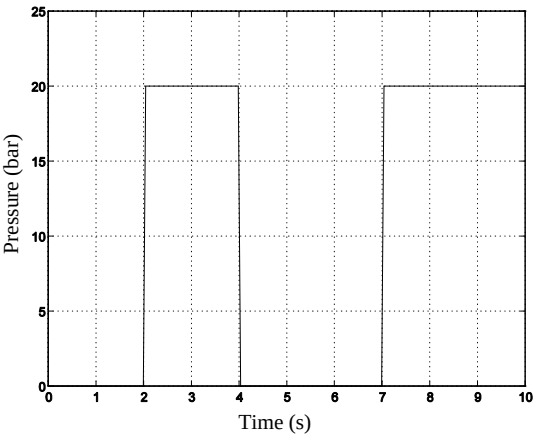

(f) Load circuit pressure

Figure 7.5 SOFLC simulation 3 – reward delay .04 s

7.4.1 Discussion of Simulation Results

The simulation results show a clear variation in performance as the parameters are varied. The values for which tracking of the given speed transient is achieved with least overshoot and shortest settling times appear to be:

error gain	10
rate gain	0.1
reward delay	0.02 s

The speed tracking behaviour at 600 rpm is more oscillatory in response to supply and load circuit pressure disturbances when the reward delay is increased to .04 s. The speed tracking behaviour at 600 rpm shows increased error and more oscillation in response to a supply pressure transient when the reward delay is reduced to .01 s.

All results contain a steady state error; this may appear to be unsurprising given the essentially PD nature of the controller. However, the granularity introduced by the quantisation process, the form of the membership functions and the rules amendment process combine to introduce a deadband; a steady state error is thus probable. Deadbands are considered further in Section 7.5.5.

The results of simulation studies using this control structure with parameters similar to those given above were presented at Control98 (Njabeleke *et al.*, 1998). The ability of the system with SOFLC to reject supply pressure disturbances, such as might occur in a multi-user system, as well as load disturbances, was studied further - simulation results were included in the presentation at ACC99 (Pannett *et al.*, 1999).

7.4.2 Rules Evolution

The evolution of the rules in an FAM table may be presented in the form of a family of three dimensional control surfaces which relate controller output in mA to the controller inputs (error and error rate). A family of figures showing the evolution of the rules as control surfaces, sampled at intervals of 0.4 s, starting from an empty FAM table, is contained in Appendix 6. A selection of control surfaces is shown in Figure 7.6. Their evolution is discussed in Section 7.4.3.

These surfaces relate to simulation 2 where

error gain	10
rate gain	0.1
reward delay	0.02 s

The surfaces have been generated using MATLAB tools from the Fuzzy Systems Toolbox from UMIST (Wolkenhauer and Edmunds, 1994).

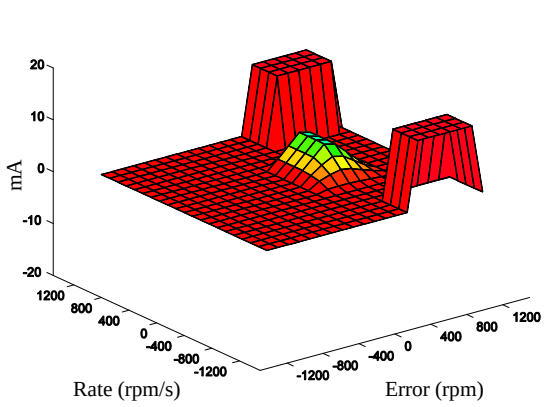

(a) Time = 0.4 s

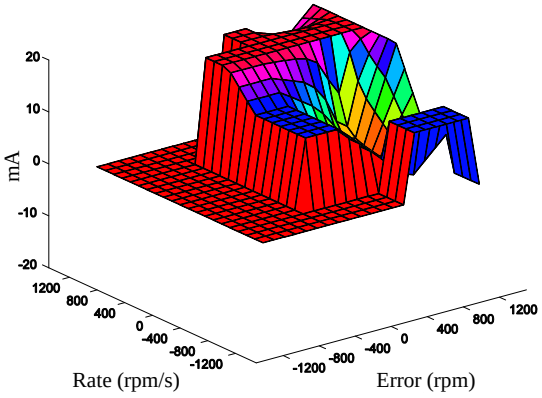

(b) Time = 1.2 s

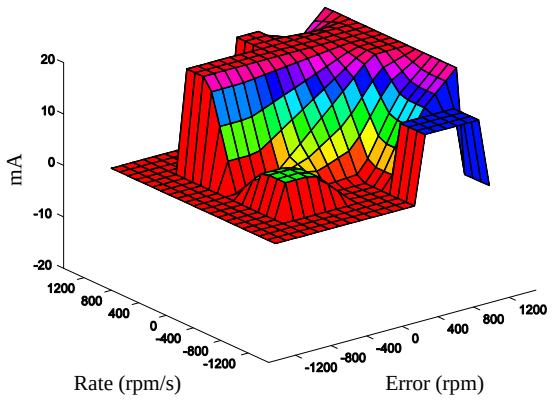

(c) Time = 1.6 s

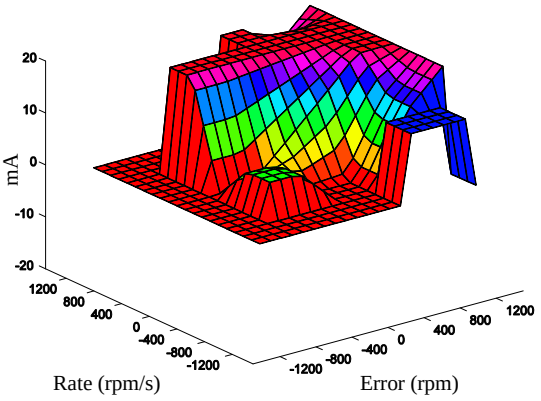

(d) Time = 2.0 s

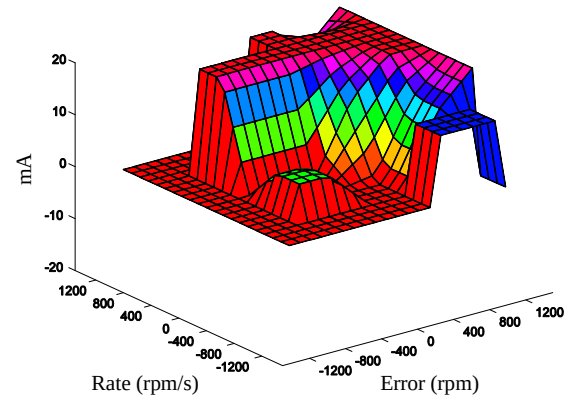

(e) Time = 2.4 s

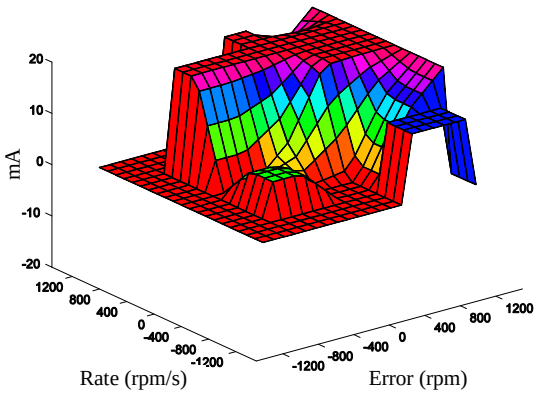

(f) Time = 2.8 s

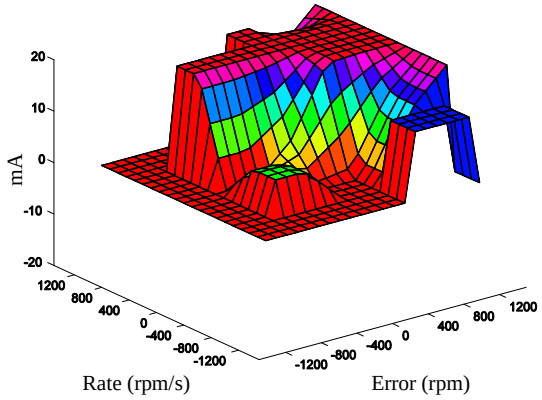

(g) Time = 4.0 s

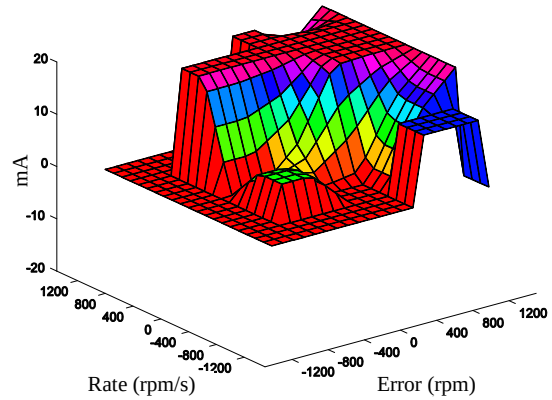

(h) Time = 4.8 s

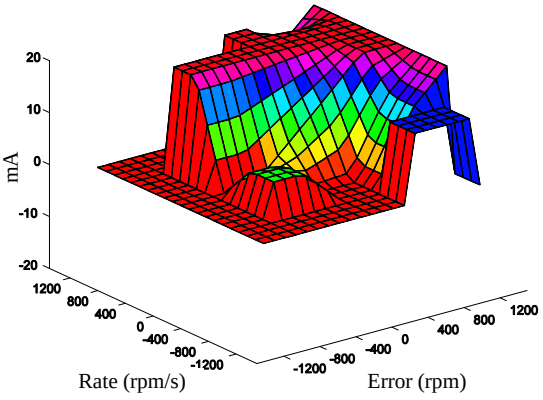

(i) Time = 6.8 s

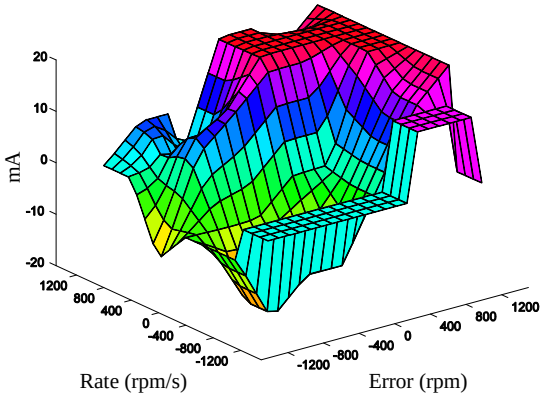

(j) Time = 7.2 s

Figure 7.6 Control surfaces for simulation 2

7.4.3 Discussion of Rules Evolution

The rules are represented graphically in the surfaces shown in Figure 7.6. Since the error gain is set to 10, the initial demand step from 0 to 100 rpm generates rules for errors of about 1000 rpm and PB and NB rates. The former is attributable to the demand transient; the rapid reduction of error which then follows generates the latter. Hence the surface at time = 0.4 s.

The 'experience' gained during the step increase in speed demand at time = 1.0 s is reflected in the surface for time = 1.2 s. The surface for time = 1.6 s shows that rules for a negative error have been developed during the overshoot transient. Following this transient, the controller successfully reduces, but does not eliminate, steady state error (about 20 rpm). The combined effects of discretisation of the universes of discourse and the adaptation algorithm introduce a deadband. This is examined further in Section 7.5.5.

The increased load torque at time = 2.0 s does not result in the generation of any new rules; the step reduction in supply pressure at time = 2.5 s results in an increase in controller gain around the zero error/zero rate point on the control surface (hard to identify in the figures). This gain increase mitigates somewhat the open loop gain reduction which results from the supply pressure reduction. No further rules evolution occurs, although 'hunting' around a steady state error of about 30 rpm takes place.

The step change of reference at time = 4.0 s does not result in further rules changes. Operation is stable with steady state error of about 80 rpm until the supply pressure rises at time = 5.5 s. The increased loop gain once more results in hunting. There is some readjustment of the rules around the zero error/zero rate point before the negative step change in demand occurs at time = 7.0 s. This step change leads to the extension of the control surface to incorporate rules for negative error and negative rate, as shown by the surface for time = 7.2 s. By time = 7.6 s, the transient has died away. Thereafter, no further rules evolution occurs; the system maintains stable low speed operation.

7.5 Rig Testing the Self Organising Fuzzy Logic Controller

7.5.1 Discrete Time SOFLC

To take the work further, in order to investigate the applicability of SOFLC on a test rig rather than in simulation, it was necessary to design discrete time controllers which could be implemented in software on the rig PC. A discrete time SOFLC with a structure and rules amendment rationale similar to that described above was simulated in Bath*fp*. The reward delay was set to be an integer multiple of the sampling interval.

7.5.1.1 Results of Discrete Time Simulation

The results of a typical simulation using a discrete time controller are shown below in Figure 7.7. The same membership functions constructed on discrete universes of discourse are used as in Section 7.3.

The controller parameters used are

sampling interval	0.01 s
error gain	10
rate gain	0.1
reward delay	0.02 s

In the controller model the reward delay is constrained to be an integer multiple of the sampling interval.

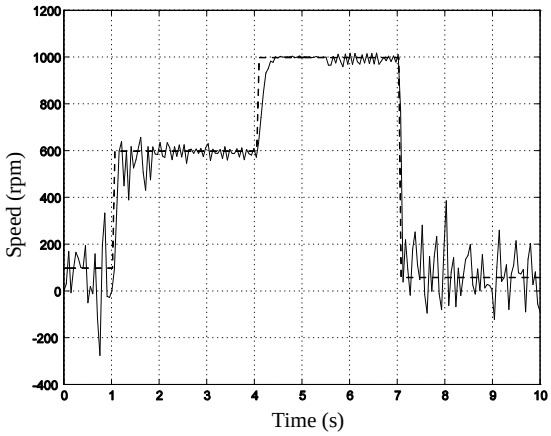

(a) Tracking

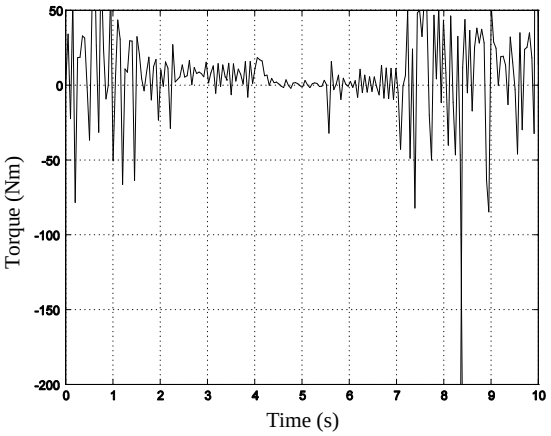

(b) Torque

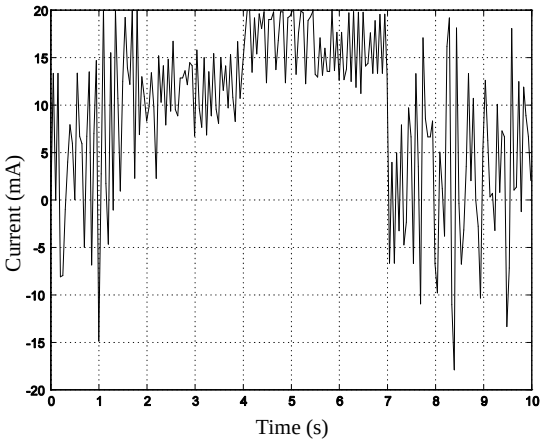

(c) Control signal

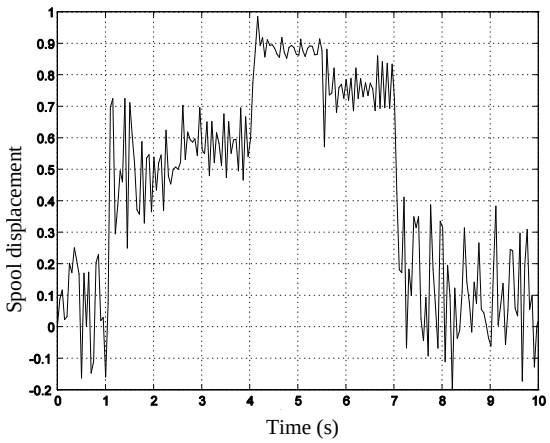

(d) Spool displacement

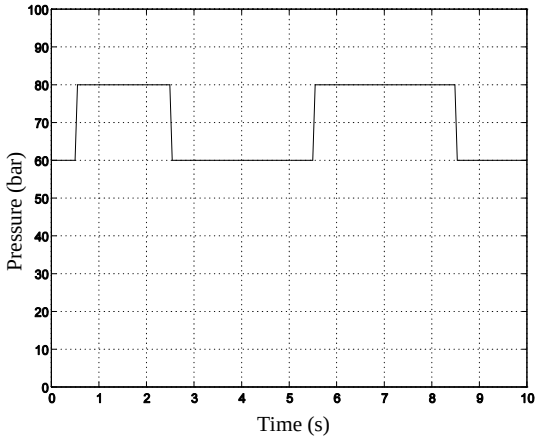

(e) Supply pressure

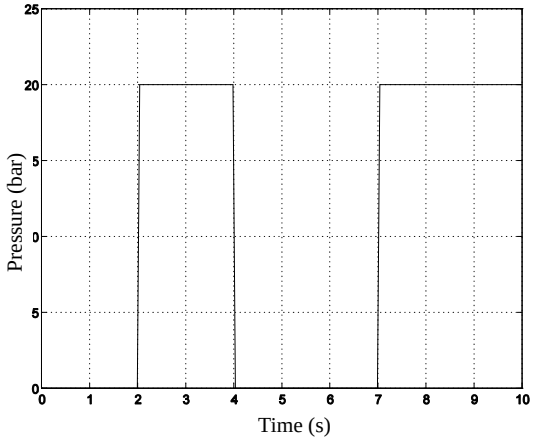

(f) Load circuit pressure

Figure 7.7 SOFLC discrete time simulation

It can be seen that this controller does not perform well at low speed and/or high supply pressure. There is considerably more noise in the data of Figure 7.7 than in those of Figure 7.4.

7.5.1.2 Rig Testing

Nevertheless, rig testing was briefly attempted, but suspended because of the risk of equipment damage. Noise levels were high; there were unpredictable changes in the direction of shaft rotation. These effects are believed to arise from the combined effects of:

the differentiation process used to derive error rate from error;

and

the inability of the rig speed transducer to recognise negative angular velocity.

Thus it did not prove practicable to transport a controller with the current structure to the test rig; stable control could not be achieved. The simulation results were, of course, not encouraging.

7.5.2 Discrete Time SOFLC - Revised Approach

The control strategy was revised to use the output of the inferencing process as a change in the control output to the system, rather than as control effort. The fuzzy sets are formed upon a continuous universe of discourse, the inputs (in this case, as before, error and rate of change of error) are fuzzified, a fuzzy inference is made from the fuzzified inputs and the resulting output is defuzzified into a crisp value which becomes the change in controller output. Each change is accumulated. The action is thus integrating. The accumulated changes are scaled to give the controller output. This revised approach is shown in Figure 7.8, in which Σ represents the summation of the change in output generated with the current value of the output to produce a new output.

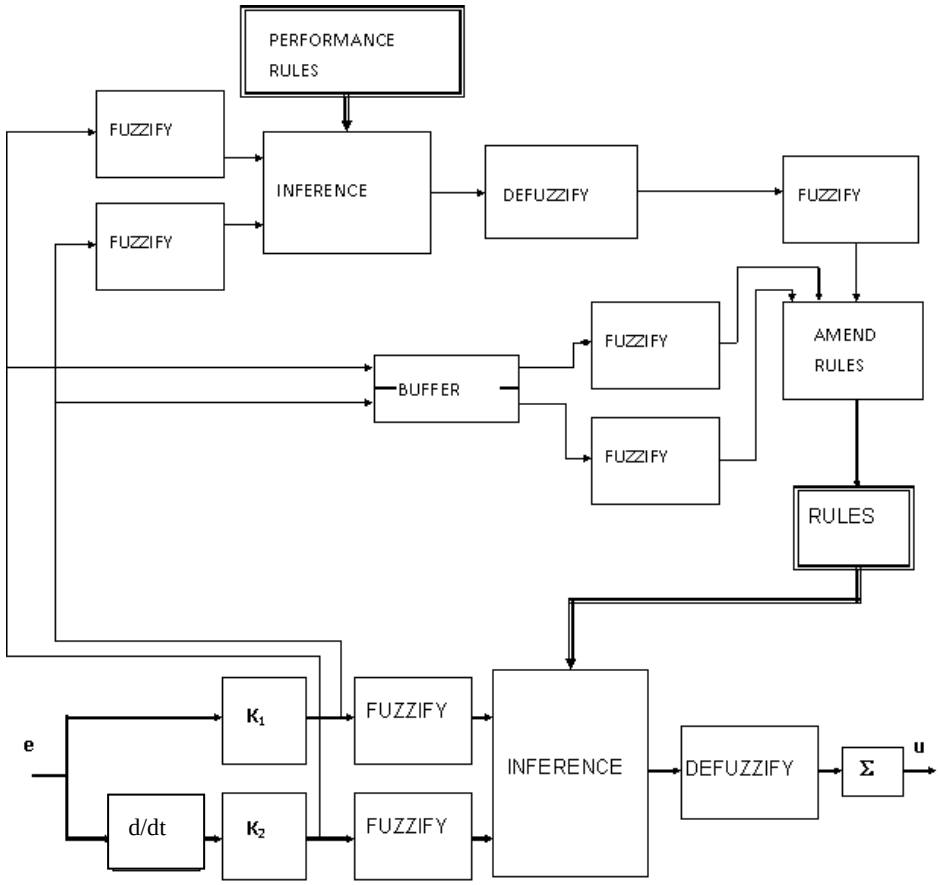

Figure 7.8 SOFLC structure – revised

This revision necessitated a change in the rules amendment procedure, which is considered further below.

To simplify the structure of the controller to be implemented on the rig, similar membership functions (incorporating 25% overlap) were used for both controller inputs and for its output. These are shown in Figure 7.9. These are constructed on continuous, rather than discrete, universes of discourse.

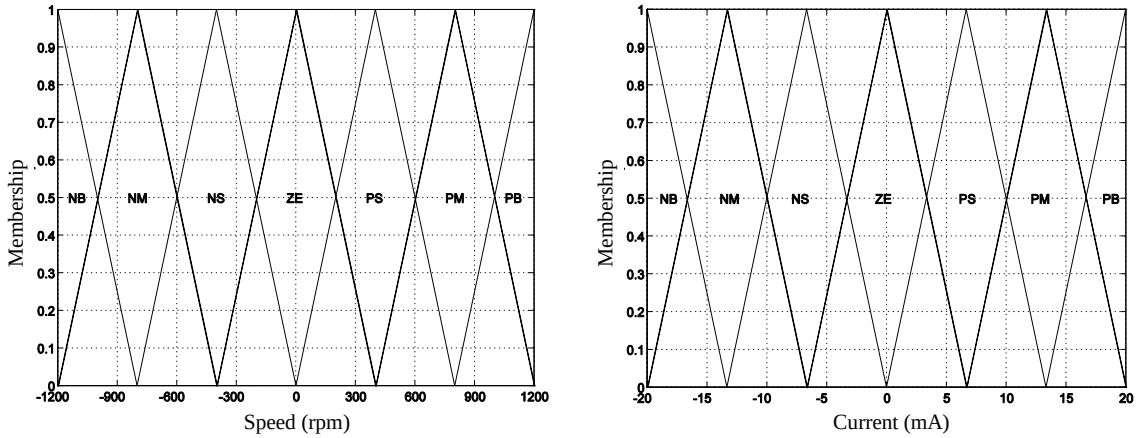

(a) Error (and error rate rpm/s) **(b) Valve current.**

Figure 7.9 Membership functions

A discrete time controller which used this revised rationale was tested in simulation, and, following satisfactory results, was transported to the test rig for further testing. Results of tests in simulation and on the rig, are presented below. The development of the control surface is also illustrated.

7.5.2.1 Revised Rules Amendment Procedure

The revised rationale of the rule modification algorithm is as follows:

Use fuzzy values of current error and current error rate with the performance rules to calculate a 'performance output adjustment'. This is the change in output which would have resulted in improved performance;

Fuzzify the 'performance output adjustment';

Fuzzify the 'delayed error' and 'delayed rate of change of error' (read from the buffer). For improved performance, these should have resulted in the 'performance output adjustment' rather than the change in output which actually obtained;

Find the highest memberships for 'delayed error' and 'delayed rate of change of error';

Use these as cell co-ordinates in the rule table to determine which rule in the FAM table to modify;

Find the fuzzy output set having the highest membership for ‘performance output adjustment’;

Use this fuzzy output set in the new rule;

Update the corresponding cell in the FAM table.

7.5.2.2 Simulation Results

The results of simulation using the following controller parameters are shown in Figure 7.10.

sampling interval	0.01 s
error gain	10
rate gain	0.1
reward delay	0.02 s

The figure demonstrates the ability of the controller to reject transients in both supply pressure and load torque. The high frequency component in the control signal is now absent, so that the valve spool is able to follow closely the input current. The integrating action of the controller results, for example, in an extended rise time for the shaft speed (Figure 7.10(a)) in response to a increase in demanded shaft speed (see time 1.0 s, 4.0 s) in comparison with the response shown in Figure 7.7(a).

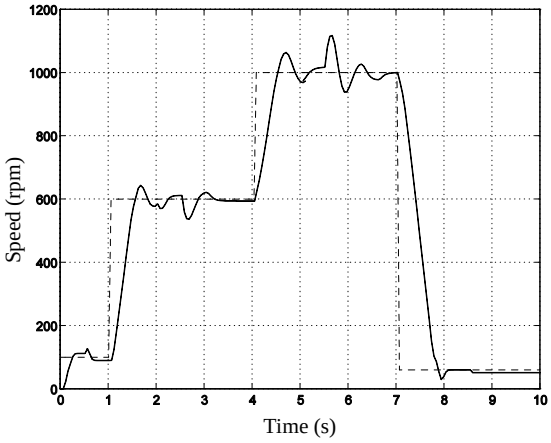

(a) Tracking

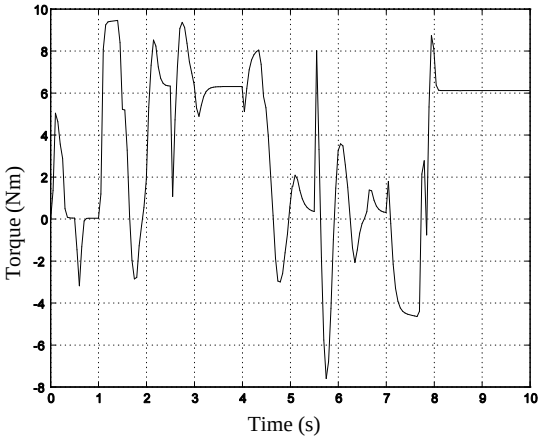

(b) Torque

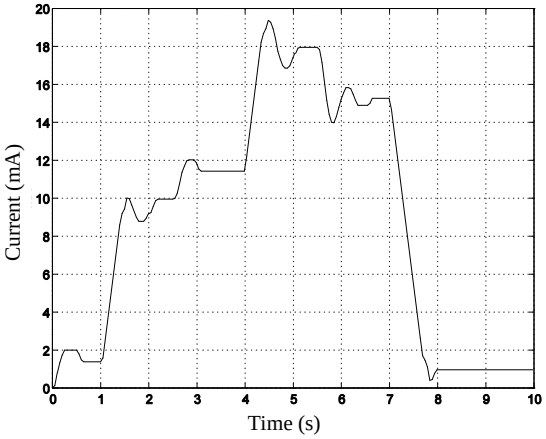

(c) Control signal

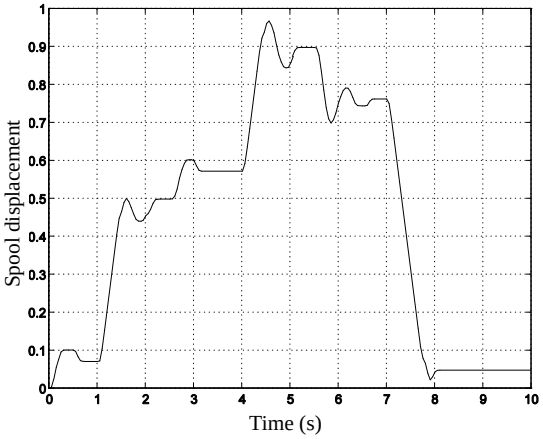

(d) Spool displacement

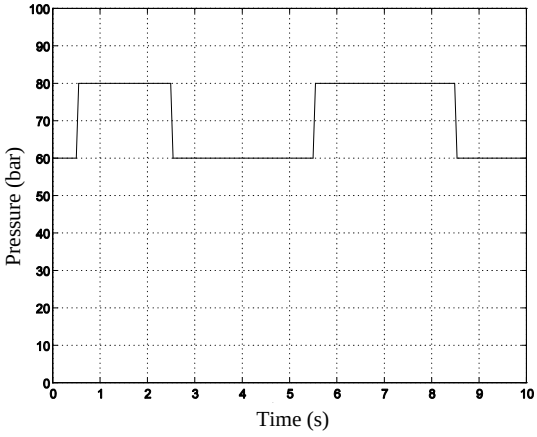

(e) Supply pressure

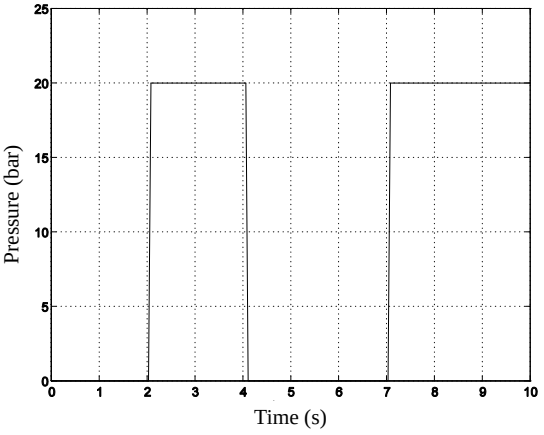

(f) Load circuit pressure

Figure 7.10 SOFLC simulation – revised structure

The development of the control surfaces, stored as before at 0.4 s intervals, is reproduced in Appendix 6; a selection is shown in Figure 7.11.

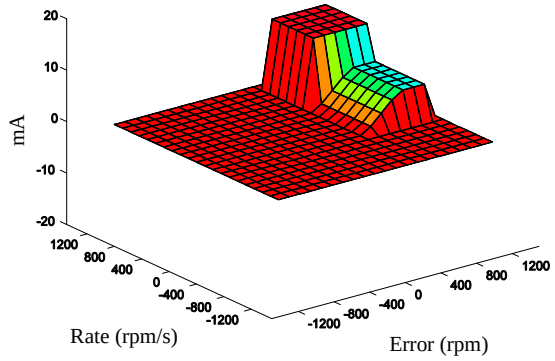

(a) Time = 0.4 s

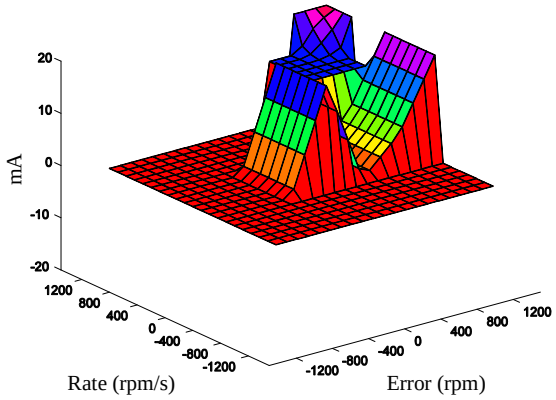

(b) Time = 1.2 s

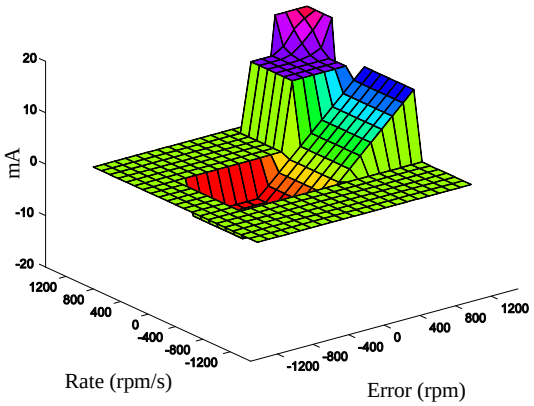

(c) Time = 1.6 s

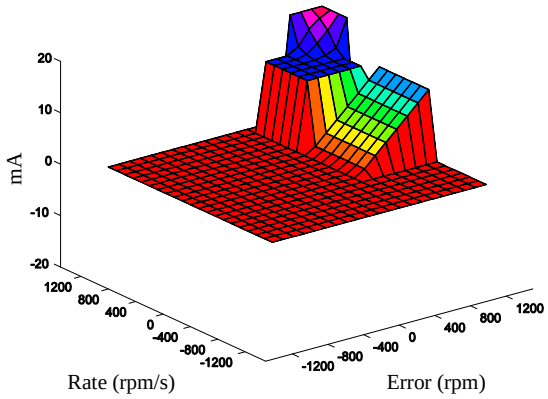

(d) Time = 2.0 s

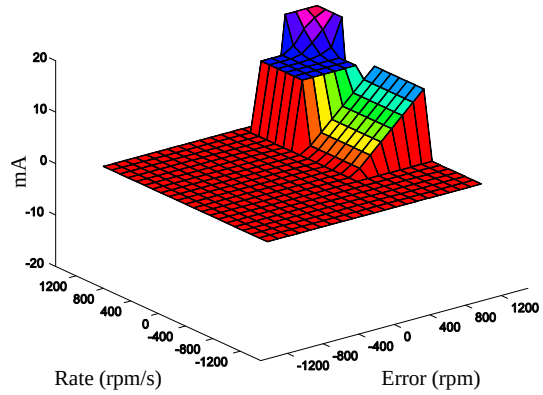

(e) Time = 3.2 s

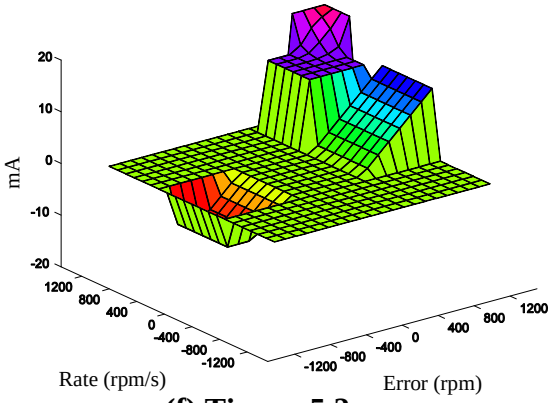

(f) Time = 5.2 s

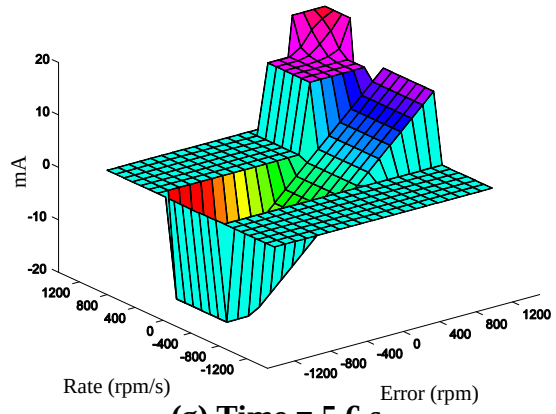

(g) Time = 5.6 s

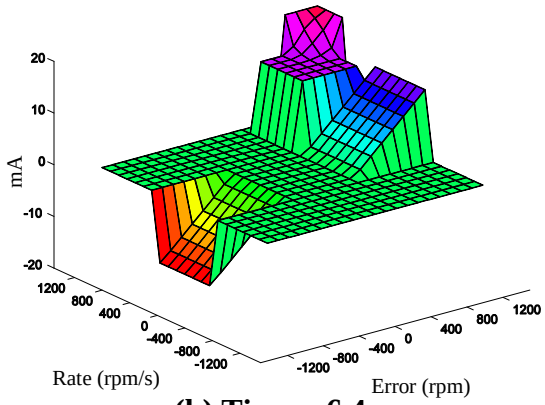

(h) Time = 6.4 s

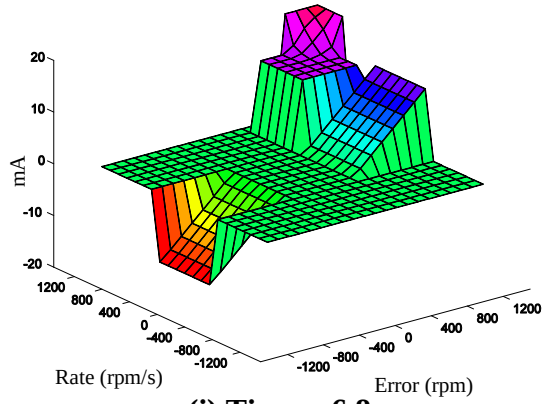

(i) Time = 6.8 s

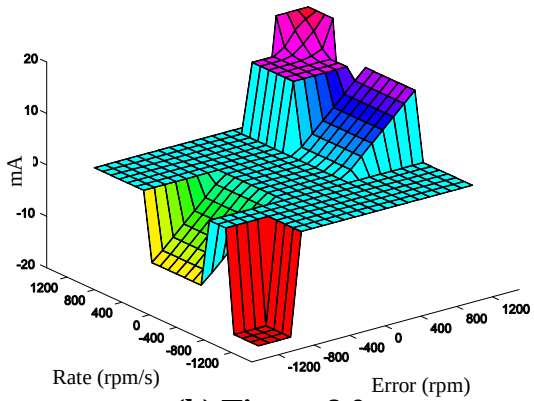

(h) Time = 8.0 s

Figure 7.11 Control surface evolution – revised SOFLC (simulation)

7.5.2.3 Rules Evolution

The integrating action of the controller results in greatly reduced control activity in relation to that of the previous control structure.

The development of the control surfaces is less vigorous than in the previous case; the surface for time = 1.2 s incorporates rule changes in response to the positive step change in demand; that for time = 1.6 s incorporates the effect of responding to the overshoot, when the error is negative. The integrating nature of the controller requires that the control surface should indicate a zero output whenever the system is operating in a steady state with zero error. The surfaces for time = 3.2 s (and time = 3.6 s and 4.0 s) show zero output around the zero error and zero rate point; those for time =6.4 s, time=6.8 s and time =8.0 s exhibit a similar feature.

7.5.3 Rig Testing

A controller with the structure described above was implemented on the test rig, using C++. As a further simplification, similar membership functions incorporating 25% overlap were used for both controller inputs and for its output. These are shown in Figure 7.12.

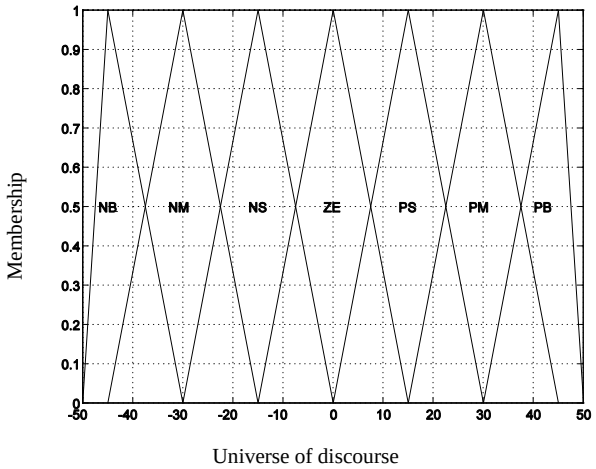

Figure 7.12 Membership function used for revised SOFLC rig testing

These are constructed on continuous universes of discourse. The two inputs to the controller are scaled to lie in the range -50:0:50, and then limited so as not to lie outside the range -45:0:45. Similarly, the output is scaled so that the computed value of output

voltage lies in the range -10:0:10. (An output of 10 V is converted to a 20 mA current to the valve solenoid.)

As a demonstration of the functionality of the controller, the results of three tests are presented and reviewed below. The rules are written to file at a rate which is one hundredth of the data acquisition rate. From the stored rules are derived control surfaces as for the simulations. The control surfaces indicate graphically how the rules evolve. As noted above, in the rig software the same universes of discourse and membership functions have been used for error, rate and output. The axis labelling on the control surfaces therefore corresponds to this single universe of discourse. Thus, for example, an output of 45 units indicates that the inferencing algorithm has generated a fuzzy output which has 100% membership of the PB fuzzy set and zero membership of the other sets. In the controller software and hardware suitable scaling factors are applied to ensure that this output generates a current of 20 mA (i.e. maximum) to the valve.

7.5.4 Rig Test Results

A selection of test results is presented in this section. This selection is intended to demonstrate the effects of changing key parameters on the tracking and disturbance rejection capability of the controller. Key parameters are shown in Table 1.

Table 7.1 Rig tests - key parameters

	Test 1	Test 2	Test 3
Step input speed demand	0-700 rpm	0-440 rpm	0-400 rpm
Supply pressure	Nominally constant: 60 bar	Step changes between 40 and 60 bar	Nominally constant: 60 bar
Load torque	Nominally constant	Nominally constant	Nominally constant
Initial rules	None	None	None
Control frequency	400 Hz	400 Hz	100 Hz
Data acquisition frequency	100 Hz	100 Hz	100 Hz
Error gain	0.1	1.0	1.0
Error rate gain	0.02	0.02	0.02
Reward delay - samples	8	8	8
Reward delay - time	0.02	0.02	0.08

7.5.4.1 Rig Test 1

Step input speed demand from 0 to 700 rpm; supply pressure nominally constant (60 bar); load torque nominally constant; no initial rules.

Control frequency 400 Hz; data acquisition frequency 100 Hz. Error gain 0.1; error rate gain 0.02; reward delay 8 samples (.02 s).

The speed tracking, control signal and supply pressure are shown in Figure 7.13; the control surfaces are shown in Figure 7.14.

Detailed examination of the logged values of actual speed show that it does not increase monotonically. As rate is computed by dividing the difference between successive error samples by the sampling interval, some negative rates of change of error are detected; these are responsible for the appearance of corresponding rules in the FAM table, illustrated in the control surfaces (Figure 7.14) More control surfaces are shown in Appendix 6.

By time = 1 s, the controller has experienced a range of errors and error rates; Figure 7.13(a) shows that the error has fallen to 200 rpm. Allowing for the error gain, it is clear from the membership functions shown in Figure 7.12 that the controller has experienced PB, PM and PS errors. The surface for time = 1 s reflects this.

By time = 6 s, little rules evolution is taking place; the surface continues to exhibit some of the experience gained during the initial training, and, arguably, remains susceptible to the effects of noise.

By time = 10 s, the combined effects of the low gain and the deadband effect discussed in Section 7.5.5 below have resulted in drift, i.e. an error between set point and actual speed.

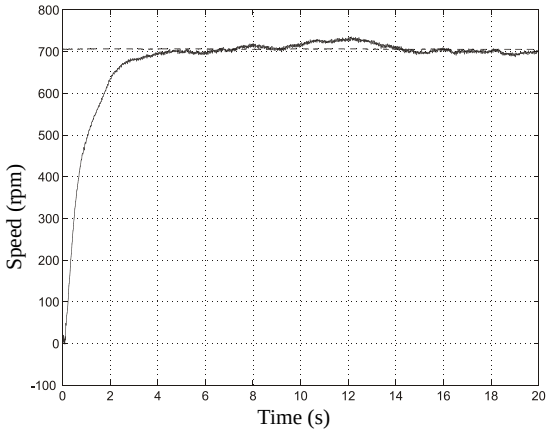

(a) Tracking

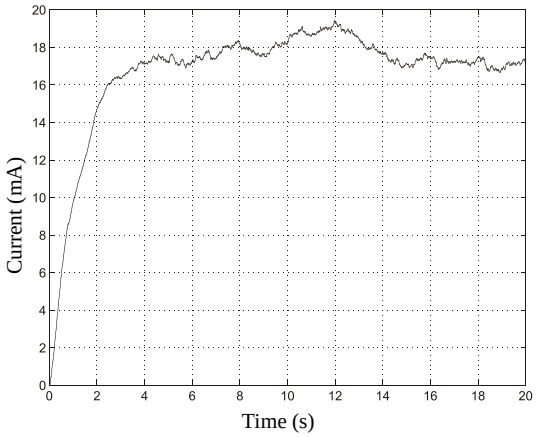

(b) Control signal

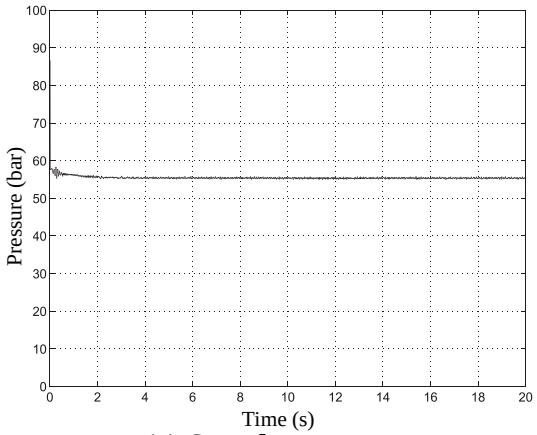

(c) Supply pressure

Figure 7.13 Rig test results – test 1

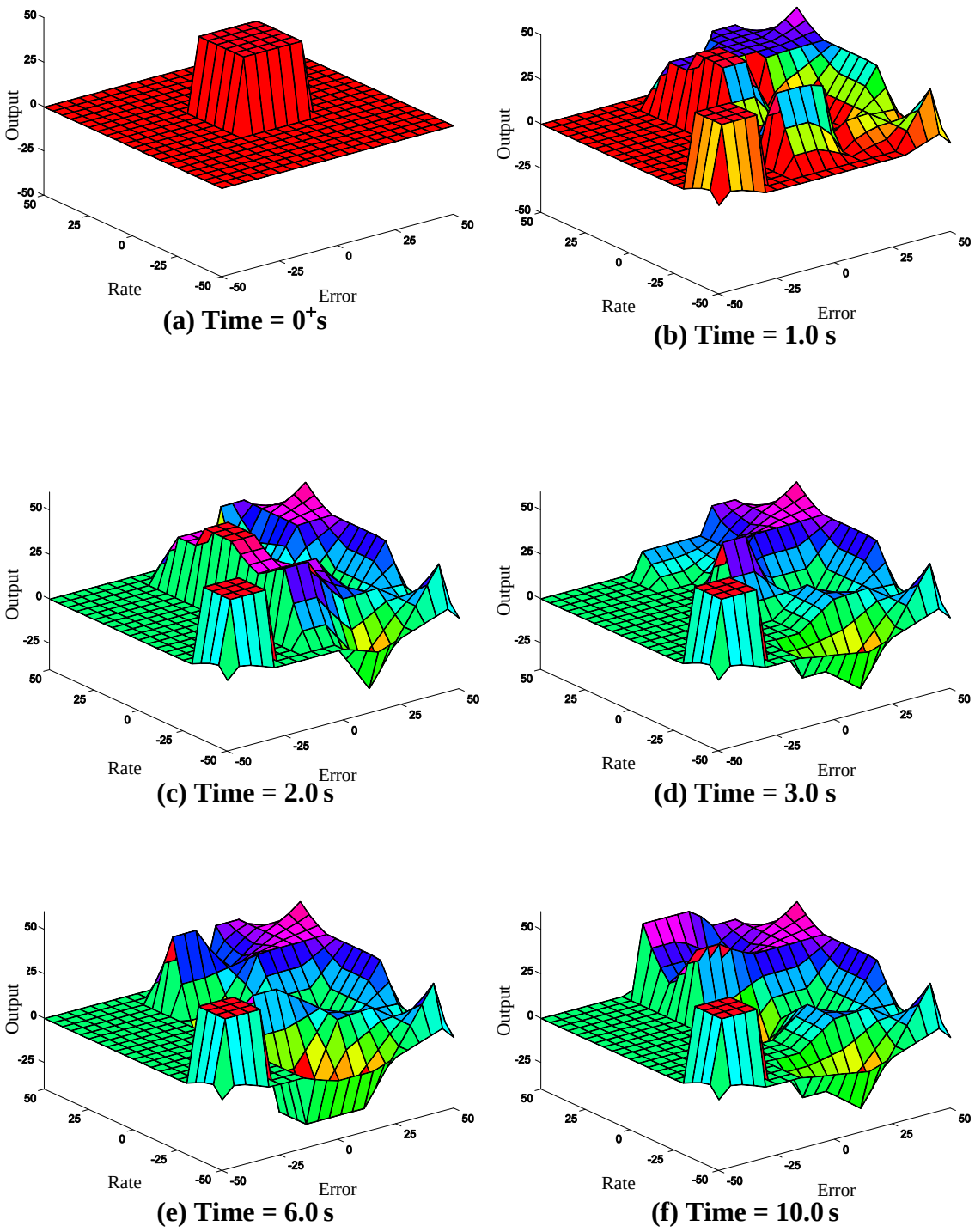

(a) Time = 0^{+}s **(b) Time = 1.0 s**

(c) Time = 2.0 s **(d) Time = 3.0 s**

(e) Time = 6.0 s **(f) Time = 10.0 s**

Figure 7.14 Control surfaces for rig test 1

7.5.4.2 Rig Test 2

Step input speed demand from 0 to 440 rpm; supply pressure subject to step changes in the range 40 bar to 60 bar; load torque nominally constant; no initial rules.

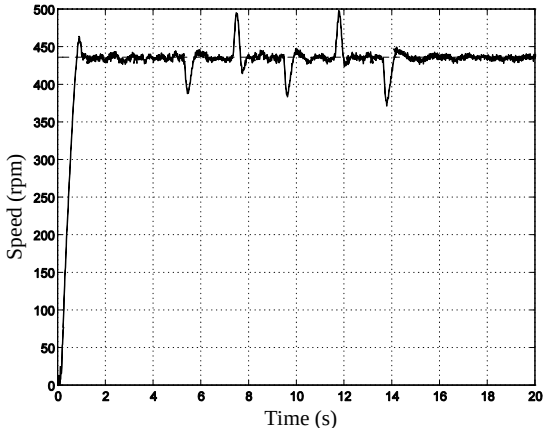

(a) Tracking

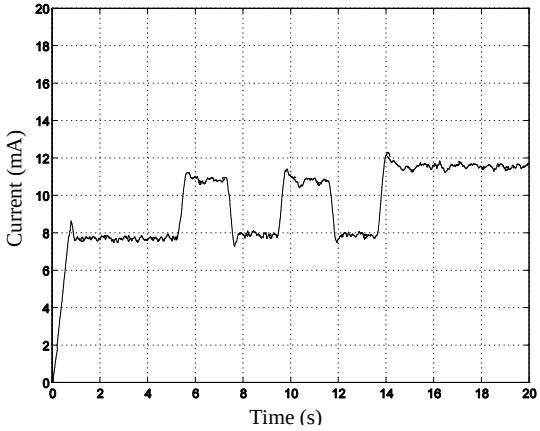

(b) Control Signal

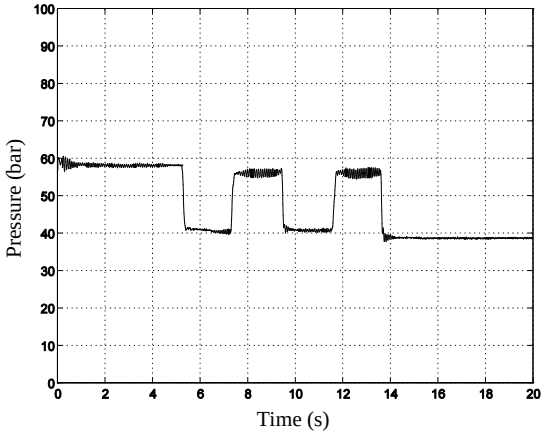

(c) Supply pressure

Figure 7.15 Rig test results – test 2

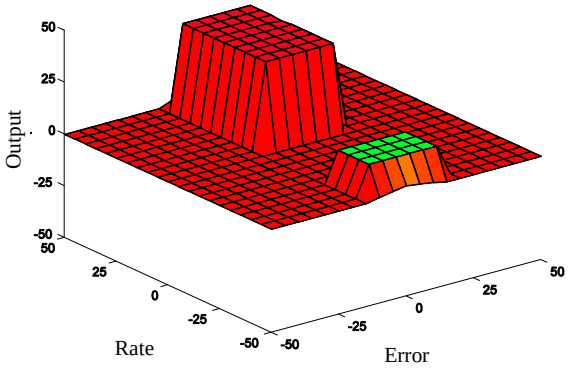

(a) Time = 0^{+}s

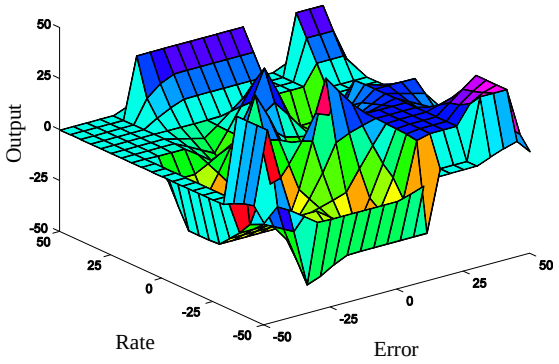

(b) Time = 1.0 s

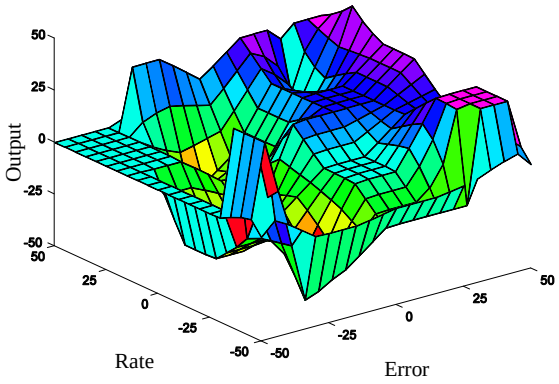

(c) Time = 6.0 s

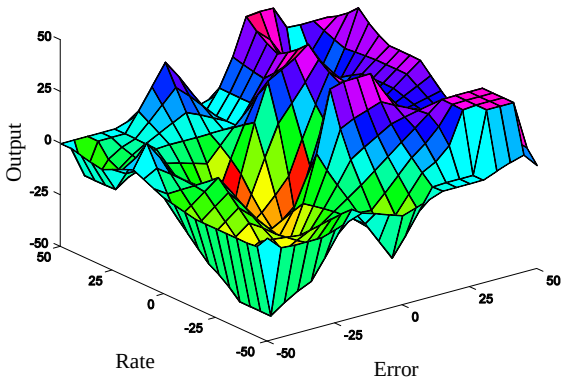

(d) Time = 8.0 s

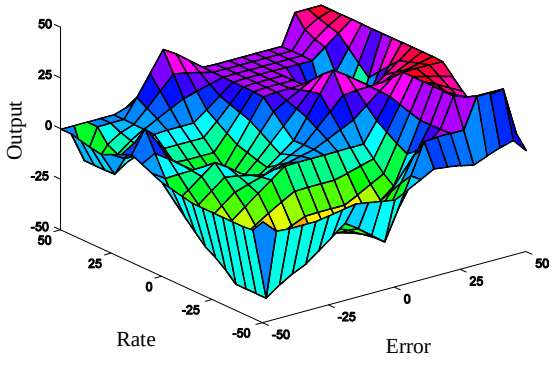

(e) Time = 10.0 s

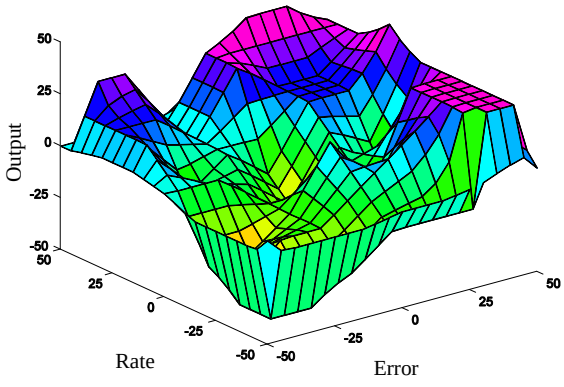

(f) Time = 14.0 s

Figure 7.16 Control surfaces for rig test 2

Test 2 demonstrates the improved tracking and disturbance rejection performance attainable if a higher error gain is used (Figure 7.15; a selection of control surfaces is shown in Figure 7.16; more are shown in Appendix 6).

Close examination of the logged data shows that there is a maximum overshoot of about 30 rpm at time = 0.8 s (Figure 7.15(a)). The overshoot represents a negative error. The incorporation of a response to a negative error in the FAM table is evident from the control surface for time = 1.0 s (Figure 7.16(b)). The effect of the positive step change in supply pressure at about time = 7.2 s is a substantial modification of the rules associated with large negative errors, as shown in the surface for time = 8.0 s (Figure 7.16(d)). The learning which has occurred during the initial step change in speed reference and during the negative and positive step changes in supply pressure at time = 5.2 s and time = 7.2 s generates rules which are appropriate and sufficient for the subsequent supply pressure changes at time = 9.5 s, time = 11.5 s and time = 13.5 s. These pressure changes do not apparently result in major changes to the control surface. Away from the transients, speed tracking is maintained to ±3 rpm.

7.5.4.3 Rig Test 3

Step input speed demand from 0 to 400 rpm; supply pressure nominally constant (60 bar); load torque nominally constant; no initial rules. Control frequency 100 Hz; data acquisition frequency 100 Hz. Error gain 1; error rate gain 0.02; reward delay 8 samples (.08 s).

Test 3 was designed to demonstrate the effect of reducing sampling rate and extending reward delay time. Comparison of the tracking shown in Figure 7.17(a) with that for Test 2 (Figure 7.15 (a)) shows that the times to reach and pass the initial step speed demand are similar, but the overshoot is greater than in Test 2 (c. 40 rpm c.f. c. 15 rpm). The speed 'hunts' in a band of about ± 25 rpm about the set point for about 8 s. Only beyond this time does a zero control plateau in the control surface develop around the zero error axis, consistent with stable steady state operation with low error (Figure 7.18(f)). The tracking error stabilises at about ±3 rpm. The longer sampling interval results in a narrowing of the range of rates of change of error which is sensed; rules tend not to be generated for rates which are NB or PB, as reflected in the control surfaces (Figure 7.18). (More control surfaces are shown in Appendix 6.)

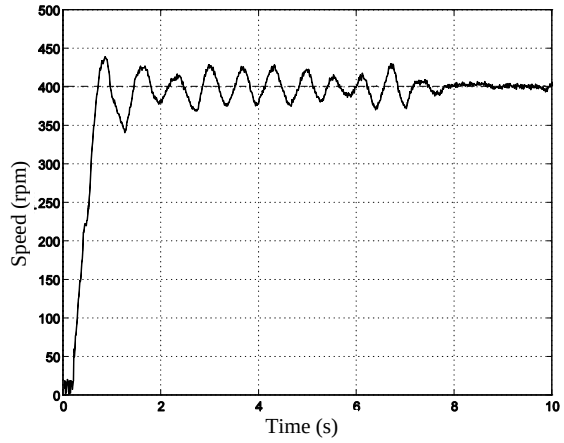

(a) Tracking

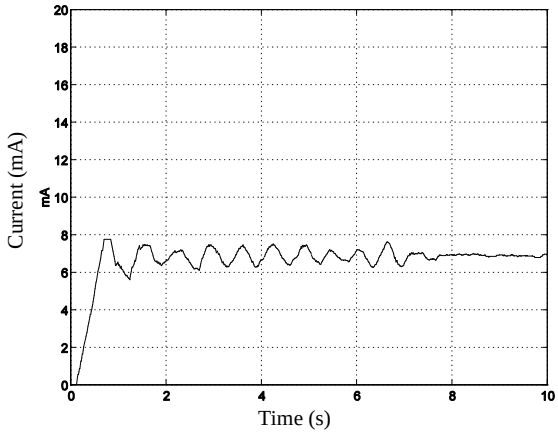

(b) Control signal

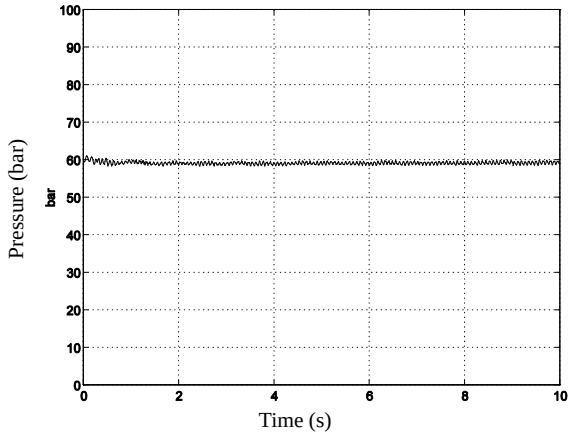

(c) Supply pressure

Figure 7.17 Rig test results – test 3

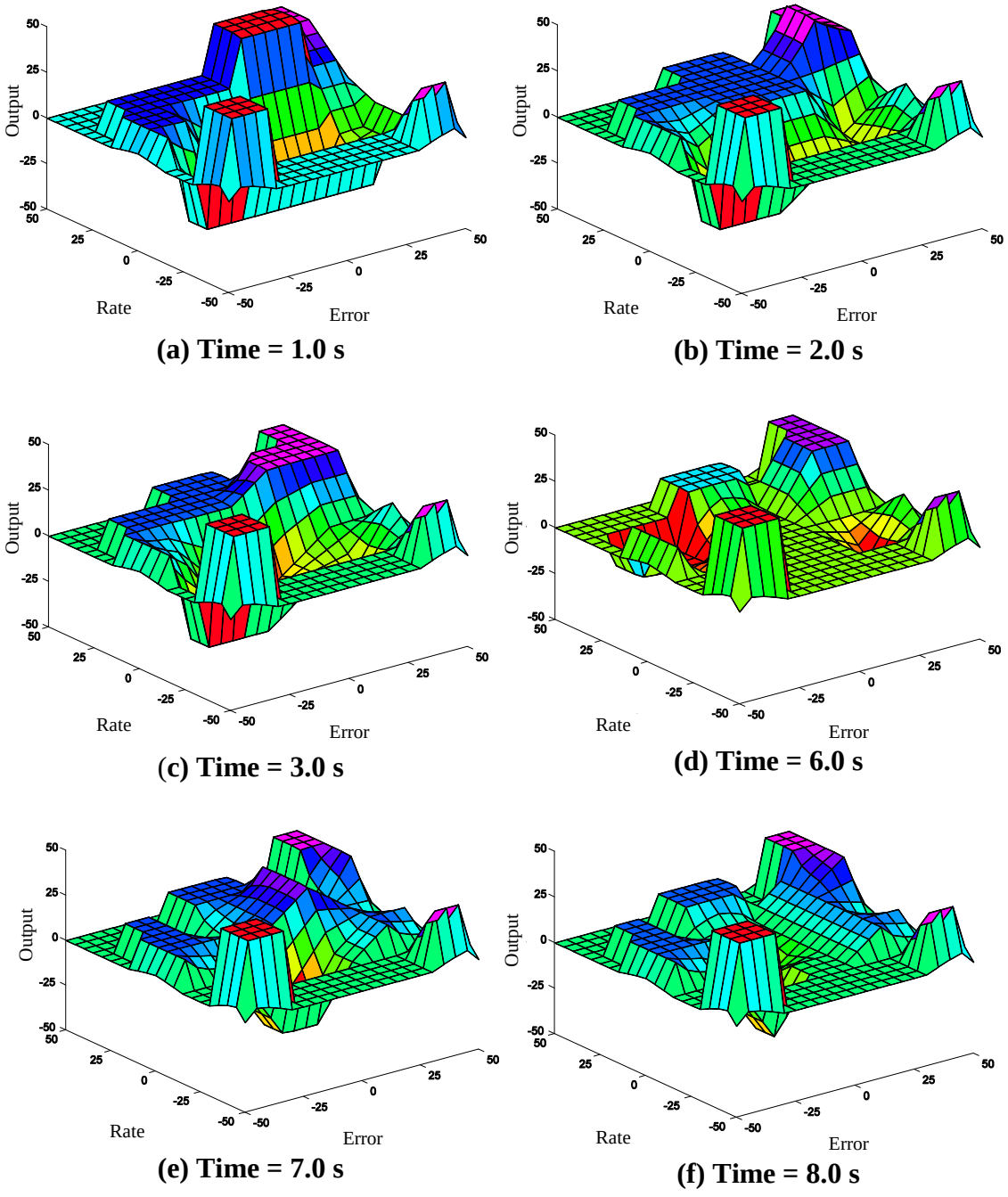

(a) Time = 1.0 s **(b) Time = 2.0 s**

(c) Time = 3.0 s **(d) Time = 6.0 s**

(e) Time = 7.0 s **(f) Time = 8.0 s**

Figure 7.18 Control surfaces for rig test 3

7.5.4.4 Conclusions on Test Results

The tests demonstrate that the SOFLC algorithm described in Section 7.5.2 is capable of implementation on a real system, provided that appropriate values are chosen for gains,

reward delay and sampling interval. A 'low' value of gain for the error signal results in poor tracking, principally because of the existence of a deadband.

7.5.5 Need for Initial Rules - Deadband Effect

It is important to note that the SOFLC algorithm can introduce a deadband. This can be understood as follows:

Consider a situation in which there is a (positive) steady state error. Thus error rate is zero. If the error gain is 10 and the error is less than 20 rpm, then, the error will have maximum membership in the ZE fuzzy set, as will, of course, the error rate. (See membership functions in Figure 7.9.) The output fuzzy set which has maximum membership for the fuzzified performance output adjustment is also ZE. The rules amendment procedure (Appendix 5) will thus ensure the rule in the FAM table which corresponds to 'error is ZE' and 'error rate is ZE' is adjusted to give output ZE.

Example:

$$error = +10 \tag{7.1}$$

$$rate = 0 \tag{7.2}$$

$$error\ gain = 10 \tag{7.3}$$

$$error\ vector = [0,0,0,0.75,0.25,0,0] \tag{7.4}$$

$$rate\ vector = [0,0,0,1.0,0,0,0,] \tag{7.5}$$

Thus the fuzzy performance output adjustment, from the performance table, is given by

$$\text{fuzzy performance output adjustment} = 0.75\times 1.0\times \text{ze} + 0.25\times 1.0\times \text{ps} \tag{7.6}$$

Using the centre of gravity method for defuzzification (Appendix 4):

$$\text{defuzzified performance output adjustment} = \frac{0.75\times 0.0 + 0.25\times 6.67\times 6.67}{0.75\times 6.67 + 0.25\times 6.67} \tag{7.7}$$

The defuzzified performance output adjustment is thus 1.67 mA. This has membership 0.75 in ZE and 0.25 in PS, or [0,0,0,0.75,0.25,0,0] in vector form. It has highest membership in ZE.

In the FAM table, the 'error is ZE' and 'rate is ZE' rule will be updated, if necessary, to yield output ZE in accordance with the rules amendment procedure. If the FAM table currently contains the rule that 'error is PS' and 'rate is ZE' results in output ZE, a

deadband will result This is because application of the above membership vectors to the FAM table will result in a zero change in output even though the error is non-zero.

7.6 Concluding Remarks

This Chapter has introduced the application of fuzzy logic to the candidate system and set out the motivation for using self organising fuzzy logic control (SOFLC), namely the avoidance of an extension to the rules database. The Chapter has also described the successful rig testing of a SOFLC on the candidate system. However, the controller which had been tested successfully in simulation was not successful on the rig.

It was recognised that extending the rules database to recognise that system performance changes with supply pressure and operating speed would have extended the dimensions of the database from two (embracing speed error and rate of change of error) to three or four. This would have added greatly to computational complexity and required the designer to formulate suitable rules. This in turn would have required either a complex non-linear model of the system or an extensive series of system tests. Instead, a two dimensional rules database was retained and strategies whereby the rules would be dynamically amended and implemented using a 'self organising' approach were pursued.

The effect of variation in the three key parameters – speed error gain, speed error rate gain and reward delay (which is the key parameter in the rules amendment procedure) – was explored in simulation. Evolution of the form of the rules database was monitored in simulation during the application of transients in speed set point, supply pressure and load. The simulation results indicated that, with suitable choice of the three key parameters, successful implementation on the rig might be possible. Examination of the evolution of the rules database was undertaken by presenting sampled sets of rules as three dimensional surfaces. Although attempts have been made to interpret and document their evolution, it is the overall performance of the controller as indicated by set point tracking in the face of disturbances which is important. This encouraged the transfer of the controller from the simulation environment on to the test rig. However, the initial simulations were carried out without imposing a sampling routine.

Implementation on the rig in real time requires that the controller should work with sampled data inputs rather than in 'continuous time' Simulation of the sampled data

system resulted in considerably more noise. Nevertheless, rig testing was briefly attempted, but suspended because of high noise levels and the risk of equipment damage. Some of the noise might have been associated with differentiation of error to provide error rate. The rig shaft speed sensor is not able to recognise the direction of shaft rotation. This resulted in unpredictable changes in the direction of rotation. Further work might therefore include the modification of the rig to include a shaft speed sensor which is able to sense the direction as well as the magnitude of the speed of rotation.

As described, a revised strategy, in which the output of the SOFLC is 'change in control effort' (change in signal to servovalve) rather than control effort was devised and implemented. This is essentially an integrating action. This strategy was demonstrated to be successful, provided that appropriate values are chosen for the gains, reward delay and sampling interval. A 'low' value of gain for the error signal results in poor tracking, principally because of the existence of a deadband. The 'deadband effect' is briefly discussed. A deadband can, in some circumstances, result from the rules amendment procedure. The form of the membership functions and the gain values determine the size of this deadband.

Further work is needed to establish a tighter rationale for the selection of the key parameters. The significance of a deadband also requires further examination. However, the application of a SOFLC strategy which benefits from not requiring a system model has been demonstrated. As the strategy is model free, issues associated with non-linearities and/or variations with operating conditions of key system parameters need not be addressed.

This phase of the project has demonstrated the viability of SOFLC schemes which:

use continuous, rather than quantised, universes of discourse;

use a procedure which adjusts the FAM table directly, rather than look-up rules tables.

This SOFLC scheme therefore differs significantly from those in the literature. Its viability has been demonstrated in simulation and by rig testing.

8 Conclusions and Further Work

The objectives of this research, as initially defined, were as follows:

1. To compare the merits of alternative robust controllers for non-linear systems, taking account of performance, reliability, cost and complexity of implementation;
2. To produce design guidelines, using the results of the above comparison, for controller selection criteria;
3. To validate these guidelines by application to physical machinery systems design involving electrical, mechanical and fluid power components.

In the time available to undertake the research which supports this thesis, these objectives have been interpreted by focussing on the application of various robust control strategies to a hydrostatic power transmission system: the speed of a valve-controlled fluid power motor supplied from a laboratory ring main and subjected to disturbances both to supply pressure and load torque is controlled.

Thus the aim of this research has been to explore the applicability of 'modern' linear control and fuzzy logic to the above system. This fluid power system has significant non-linearities, a principal source of which is orifice effects, and is subject to disturbances in the form of supply pressure fluctuations and load torque changes.

In accordance with objective 1 above, the performance of alternative control strategies has been investigated qualitatively. Reliability and cost have not been assessed, and might be the subject of further work. Complexity has not been quantified. However, the detailed descriptions of the derivations of each of the controllers provide a pointer to the degree of complexity of each.

In accordance with objective 2, design guidelines are included with the controller descriptions, in particular on the choice of sampling rates and weights for the different linear robust controllers. For the SOFLC, the significance of the 'reward delay' is indicated, and attention is drawn to the possibility of deadbands.

In accordance with objective 3, the above guidelines have been validated by application, for resource reasons, to the candidate fluid power system only.

A short series of conventional (proportional and PID) control tests (Chapter 4) has demonstrated how the non-linearities of the test system lead to control difficulties. Thus, in a proportional control speed tracking test, a gain which results in stable operation, with steady state error, at 'high' speed leads to instability when the speed is reduced. Reducing the gain to maintain stability at lower speeds would increase the steady state error at higher speeds. Although in a PID test it was possible to choose control parameters which provided good speed tracking at higher speeds, once again instability occurred when the speed was reduced.

The research has demonstrated the practicability of designing viable controllers for a system having non-linearities without recourse to the construction of a detailed non-linear model. It has used 'modern' H_∞ linear control methods in accordance with a straightforward design route which it has introduced and applied. The H_∞ linear control methods facilitate the design of controllers which treat uncertainties and omissions in the system model as perturbations. The design route has used readily available user-friendly software (Bath*fp* and MATLAB) for modelling, controller design and testing in simulation, prior to testing on a physical rig. The rig includes a PC based controller and data logger. Controllers for test have been coded in the C++ programming language, compiled and loaded on to the PC.

The research has confirmed that non-linear systems can be represented as linear systems to permit the design of controllers using H_∞ methods. The mixed sensitivity method has been used in Chapter 5 with a simple linear model of the system to provide a robust controller with specified performance, the robustness accommodating the perturbations to the linear model which are attributable to un-modelled features and non-linearities in the system.

The test results demonstrate that a high order controller, designed in the continuous *s*-domain using an H_∞ mixed sensitivity approach, can be successfully discretised and implemented on a real system. The controller gave good tracking and good disturbance rejection.

Proportional control was unsuccessful on both counts (Chapter 4). The tests do not, however, enable the hypothesis that the observed instability using proportional

control might be attributable to discretisation effects rather than closed loop instability to be tested. Simulation does not show instability. Thus another possible cause for it lies in the unmodelled features of the system.

In the load disturbance tests using the high order controllers, the speed error transients are of such magnitude and duration that the angular deviations between the demanded and achieved shaft rotations amount to only a few degrees. This close tolerance may be significant if the system forms part of a high speed machine in which time domain performance is important.

The non-linear system model used as a basis for controller design was a simplified representation of the real system; values of key parameters were taken from manufacturers' data sheets, and the dimensions and characteristics of pipes were estimated. This was in accord with the design philosophy that, as the controller to be designed would, by virtue of the algorithms used, be robust, effort to define and validate an accurate model was not justified. The test results are a vindication of this approach.

The relatively sluggish response of the system, which takes about 0.7 s to reach the 'steady state' at 'low' speed, as illustrated in the δ-emulation tracking tests, suggests that the system bandwidth is in fact rather narrower than that modelled in Chapter 5. This needs further consideration, but probably results from inadequately modelled valve dynamics.

Additionally, conservatism in controller design, in terms of stability margin, results from the use of a model incorporating a higher supply pressure, and thus higher gain, than that used for the tests. Clearly, further work is necessary to refine the controller software to eliminate wind-up if the operating regime is such that this may occur. Wind-up was considered in the next phase.

Chapter 6 has elaborated on the linear method of Chapter 5 by using the results of an examination of how the open-loop gain of the candidate system, as illustrated by its bode gain (or singular value) plots, varies with operating parameters, in particular supply pressure and speed set point. Application of 'gap analysis' to these gain characteristics was found to indicate that the design of a single robust controller to provide specified performance across the full range would be challenging. Therefore, in an alternative approach, two controllers were designed, one for 'high' speed and

the other for 'low' speed operation, each using a 'loop shaping' approach. For each of these, the loop was shaped using a PI compensator. These controllers were found by analysis to provide adequate in stability margins. The orders of the controllers in combination with the compensators were reduced to facilitate implementation. A suitable bumpless switching scheme was identified. This, with the two reduced order controllers, was successfully implemented and tested on the rig. The resulting composite controller was found by experiment to have good speed set point tracking and load disturbances rejection properties; the selected bumpless transfer scheme was also found to give integrator wind-up protection.

Future work might include assessing the benefits or otherwise of implementing a control scheme in which the control algorithm was selected according to supply pressure as well as or in addition to operating speed. However, such a development would require the provision of a suitable supply pressure sensor.

The mixed sensitivity and loop shaping controllers have been shown to be superior to proportional and proportional integral controllers by practical testing. Use of the latter controllers leads to a more conservative performance. This is because of the need to maintain stability in the face of both uncertainties in system parameter values and of system non-linearities. It is proposed now that, although the controllers which use H_∞ methods are superficially more complex than a PI or PID controller, this added complexity is justified by the provision of robust performance over a wide range of speeds, and the demonstrated absence of the need for other than simple models of the system. It is conjectured that the low and still decreasing cost of electronic hardware means that any cost premium is likely to be small. The work presented here provides a general approach to the design of linear controllers for fluid power systems which are capable of satisfying performance specifications in the presence of model uncertainty, some of which is attributable to non-linearities, and system disturbances.

The research has also demonstrated that a non-model based controller using self organising fuzzy logic (SOFLC) can be applied to the candidate fluid power system. Chapter 7 introduced the application of fuzzy logic to the candidate system and set out the motivation for using self organising fuzzy logic control (SOFLC), namely the avoidance of an extension to the rules database. It was recognised that extending the rules database to recognise that system performance changes with supply pressure

and operating speed would have extended the dimensions of the database from two (embracing speed error and rate of change of error) to three or four. This would have added greatly to computational complexity and required the designer to formulate suitable rules. This in turn would have required either a complex non-linear model of the system or an extensive series of system tests. Instead, a two dimensional rules database was retained and strategies whereby the rules would be dynamically amended and implemented using a 'self organising' approach was pursued.

The effect of variation in the three key parameters - error gain, error rate gain and reward delay (which is the key parameter in the rules amendment procedure) – was explored in simulation. Evolution of the form of the rules database was monitored in simulation during the application of transients in speed set point, supply pressure and load. The simulation results indicated that, with suitable choice of the three key parameters, successful implementation on the rig might be possible. Examination of the evolution if the rules database was undertaken by presenting sampled sets of rules as three dimensional surfaces. Although attempts have been made to interpret and document their evolution, it is the overall performance of the controller as indicated by set point tracking in the face of disturbances which is important. This encouraged the transfer of the controller from the simulation environment on to the test rig. However, the initial simulations reported on in Chapter 7 were carried out without imposing a sampling routine necessary for implementation of the SOFLC in real time.

Chapter 7 went on to describe the successful rig testing of a SOFLC on the candidate system. However, the controller which had been tested successfully in simulation was not successful on the rig. Implementation on the rig in real time requires that the controller should work with sampled data inputs rather than in 'continuous time' as represented in the earlier simulations. Simulation of the sampled data system resulted in considerably more noise. Nevertheless, rig testing was briefly attempted, but suspended because of high noise levels and the risk of equipment damage. Some of the noise might have been associated with differentiation of error to provide error rate. The rig shaft speed sensor is not able to recognise the direction of shaft rotation. This resulted in unpredictable changes in the direction of rotation. Further work might therefore include the modification of the rig to include a shaft speed sensor which is able to sense the direction as well as the magnitude of the speed of rotation.

A revised strategy, in which the output of the SOFLC is 'change in control effort' (change in signal to servovalve) rather than control effort was devised and implemented. This is essentially an integrating action. This strategy has been demonstrated to be successful, provided that appropriate values are chosen for the gains, reward delay and sampling interval. A 'low' value of gain for the error signal results in poor tracking, principally because of the existence of a deadband. The 'deadband effect' has been discussed briefly.

However, the application of a SOFLC strategy which benefits from not requiring a system model has been demonstrated. As the strategy is model free, issues associated with non-linearities and/or variations with operating conditions of key system parameters need not be addressed.

This phase of the project has demonstrated the viability of SOFLC schemes which:

- use continuous, rather than quantised, universes of discourse;
- use a procedure which adjusts the FAM table directly, rather than look-up rules tables.

This SOFLC scheme has been demonstrated in simulation and by rig testing.

However, the rules amendment procedure can, in some circumstances, result in a 'deadband'. The form of the membership functions and the gain values determine the size of this deadband. The significance of the deadband requires further examination.

Further work is recommended to:

- investigate the effect of alternative membership functions, including membership functions with alternative shapes;
- investigate the use of filtering to condition the rate of change of error signal to reduce the susceptibility of the rules amendment algorithm to noise;

The values of certain parameters essential to correct operation have been found to be less easily determined that some advocates of SOFLC might imply. Thus, further work is needed to establish a rational basis for determining how to select 'reward delay', and to investigate alternative choices of performance measure. Other future work might be undertaken to determine whether a more complex rules table might be

beneficial. However, including a more complex table would add to the complexity of the controller program. Similarly, the advantages, if any, of alternative shapes for membership functions need investigation. The introduction of deadbands and their consequences for controller performance has been identified: some initial analysis has been undertaken. However, this, again, needs further investigation. The software needed to implement the SOFLC controller in practice is rather more complex than that needed for the 'linear' methods, which is disadvantageous.

The 'self organising' nature of the controller makes it difficult to diagnose any maloperation, and may militate against the application of SOFLC in safety critical operations, because any post-incident investigation of faults or mal-operation would be hindered by the lack of availability of details on the behaviour of the control algorithm, unless a module to log details of controller operations, including the evolution of the rules, is incorporated. This would, of course, add to the controller software complexity. Nevertheless, a programme of further work might usefully include an investigation into the means of providing such a module. Other non-model based controllers, such as those based on neural networks, might also usefully be investigated.

9 References

ANDERSON, B.D.O., AND LIU, Y., 1989. Controller reduction: concepts and approaches. *IEEE Trans. Autom. Control.*, Volume 34, Number 8. pp.802-812.

ASTROM, K.J. AND WITTENMARK, B., 1990. *Computer controlled systems: theory and design.* (2nd Edition.) Prentice Hall.

BACKÉ,W., 1993. The present and future of fluid power. *Proc. Inst. Mech Eng. Part I J. Syst. Control Eng.*, 207. pp.193-211**.**

BALAS, G.J., DOYLE, J.C., GLOVER, K., PACKARD, A. AND SMITH, R., 1993. *μ-Analysis and synthesis toolbox for use with MATLAB*. The Mathworks Inc.

BEALE, D., LEE, S.W. AND BOGHIU, D., 1998. An analytical study of fuzzy control of a flexible rod mechanism. *J. Sound Vib.*, 210(1). pp.37-52. (on-line)

BITMEAD, R.R., GEVERS, M. AND WERTZ, V., 1990. *Adaptive optimal control : the thinking man's GPC*. Prentice Hall of Australia Pty Ltd.

BROGAN, W.L., 1991. *Modern control theory*. Prentice Hall International Ltd.

BURROWS, C.R., 2000. Fluid power systems—some research issues. *Proc. Inst. Mech. Eng. Part C J. Mech. Eng. Sci.*, 214. pp.203-220.

BURROWS, C.R., TOMLINSON, S.P., AND HOGAN, P.A., 1991. Some modelling aspects of Bath*fp*. In: EDGE, K.A. AND BURROWS, C.R., eds. *Fluid Power Systems Modelling and Control, Proceedings of the Fourth Bath International Fluid Power Workshop*. pp. 201-216. Taunton, Somerset. Research Studies Press Ltd.

CHIANG, R.Y. AND SAFANOV, M.G., 1988. *Robust control toolbox for use with MATLAB - users' guide control theory*. The Mathworks Inc.

CHU, C-C., DOYLE, J.C. AND LEE, E.B., 1986. The general distance problem in H_∞ optimal control theory. *Int. J. Control*, 44(2). pp.565-596.

CUNDIFF, J.S., 2002. *Fluid power circuits and controls – fundamentals and applications*. CRC Press LLC, Florida.

DALEY, S. AND GILL, K.F., 1986. A design study of a self organising fuzzy logic controller. *Proc. Inst. Mech. Eng.*, 200, C1. pp.59-68.

DALEY, S. AND GILL, K.F., 1987. Attitude control of a spacecraft using an extended self organising fuzzy logic controller. *Proc. Inst. Mech. Eng.*, 201, C2. pp.97-106.

DALEY, S. AND NEWTON, D.A., 1994. Intelligent control of an electro-hydraulic rotary drive system. In: *Proceedings of IEE International Conference on Control '94*, (CP389) at Coventry, 21-24 March 1994. pp.699–704.

DORF, R.C. AND BISHOP, R.H., 1995, *Modern control systems.* (7th Edition.) Addison-Wesley Publishing Company.

DOYLE, J.C., FRANCIS, B.A. AND TANNENBAUM, A.R., 1990. *Feedback control theory*. Macmillan Publishing Company.

DOYLE, J.C., GLOVER, K., KHARGONEKAR, P.P. AND FRANCIS, B.A., 1989. State-space solutions to standard H_2 and H_∞ control problems. *IEEE Trans. Autom. Control*, AC-34(8). pp.831-847.

DOYLE, J.C., SMITH, R.S., AND ENNS, D.F., (1987). Control of plants with input saturation non-linearities. In Proceedings of: *American Control Conference, San Diego, Minneapolis.* pp. 2147-2152.

EDGE, K.A., 1997. The control of fluid power systems - responding to the challenges. *Proc. Inst. Mech. Eng. Part I J. Syst. Control Eng.*, 211. pp.91-108.

EDWARDS, C. AND POSTLETHWAITE, I., 1998. Anti-windup and bumpless-transfer Schemes. *Automatica*, 34, No 2. pp.199-210.

EVANS-PUGHE, C., 2007. Hidden engineering (behind the scenes). *Engineering & Technology*, Volume 2, Issue 11. pp.38-41.

FENG, G., 2006. A survey on analysis and design of model-based fuzzy control systems. *IEEE Trans. Fuzzy Syst.,* Vol. 14, No. 5. pp.676-697.

FORSYTHE, W. AND GOODALL, R.M, 1991. *Digital control: fundamentals, theory and practice*. Macmillan Education Ltd.

FRANCIS, B.A., 1987. *A course in H_∞ control theory.* Lecture notes in control and information sciences, Springer-Verlag.

FRANKLIN, G.F. AND POWELL, J.D., 1981. *Digital control of dynamic systems*. Adison-Wesley Publishing Company.

FRANKLIN, G.F., POWELL, J.D., AND EMAMI-NAEINI, A., 1991. *Feedback control of dynamic systems.* (2nd Edition.) Adison-Wesley Publishing Company.

GEORGIOU, T.T. AND SMITH, M.C., 1990. Optimal robustness in the gap metric. *IEEE Trans. Autom. Control*, 35(6). pp.673-686.

GLOVER, K. AND DOYLE, J.C., 1988. State-space formulae for all stabilizing controllers that satisfy an H_∞ -norm bound and relations to risk sensitivity. *Syst. Control Lett.,* 11. pp.167-172.

GLOVER, K. AND MCFARLANE, D., 1989. Robust stabilization of normalized coprime factor plant descriptions with H_∞ bounded uncertainty. *IEEE Trans. Autom. Control*, AC-34(8). pp.821-830.

GOODALL, R.M., 1990. The delay operator z^{-1} - inappropriate for use in recursive digital filters? *Trans. Inst. Meas. Control*, 12(5). pp.246-250.

GRAEBE, S.F. AND AHLEN, A.L.B., 1996. Dynamic transfer among alternative controllers and its relation to antiwindup controller design. *IEEE Trans. Control Syst. Technol.,* Vol 4, No 1. pp.92-99.

GREEN, M. AND LIMEBEER, D.J.N., 1995. *Linear robust control*. Prentice Hall, Englewood Cliffs, NJ.

HAMILTON, A. G., 1978. *Logic for mathematicians*. Cambridge University Press.

HAMPSON, S.P., CHAWDHRY, P.K. AND BURROWS, C.R., 1996. The design of a robust controller for hydrostatic transmissions. In: *Proceedings of International Mechanical Engineering Congress & Exposition: The Fluid Power and Systems Technology Division*, Vol.3. pp.107-112.

HANUS, R., KINNAERT, M. AND HENROTTE, J-L., 1987. Conditioning technique, a general anti-windup and bumpless transfer method. *Automatica*, 23, No 6. pp. 729-739.

HOUPIS, C.H. AND LAMONT, G.B., 1985. *Digital control systems: Theory, Hardware, Software*. McGraw-Hill, New York.

HU, F. AND EDGE, K., 1993. Delta-operator-based adaptive control of a piston pump. In: MAEDA, T., ed. *Fluid Power: Proceedings of the Second JHPS International Symposium on Fluid Power*. pp.373-378. London ; New York: E & F N Spon.

HUANG, S-J. AND HUANG, K-S., 2004. A self-organizing fuzzy controller for an active vibration suppression. *J. Soc. Mech. Eng. Int. J. Ser.C*, Vol. 47, No. 4 Special Issue on Bioengineering. pp.1156-1160.

HUNT, T.M. AND VAUGHAN, N., 1996. *The hydraulic handbook*. (9th Edition.) Elsevier.

JAMSHIDI, M., VADIEE, N. AND ROSS, T.J. (eds), 1993. *Fuzzy logic and control.* Prentice Hall.

JAYENDER, J., PATEL, R.V., NIKUMB, S., AND OSTOJIC, M., 2005. H_∞ Loop shaping controller for shape memory alloy actuators. In Proceedings of: *The 44th IEEE Conference on Decision and Control, and the European Control Conference 2005* at Seville, Spain, December 12-15, 2005. pp. 653-658

KIM, S.S., KIM, J.S., LEE, B.R., AND AHN, K.K., 2003. Design of a strip thickness control system for tandem cold mills using H_∞ control techniques. *Proc. Inst. Mech. Eng. Part I J. Syst. Control Eng.*, 217. pp.319-327.

KING, P.J. AND MAMDANI, E.H., 1977. The application of fuzzy control systems to industrial processes. *Automatica,* 13. pp.235-242.

KLEIN, A. AND BACKE, W., 1992. An intelligent optimisation of a state loop controller with fuzzy set logic. In Circuit, Component and System Design. In: *Proceedings of Fifth Bath International Fluid Power Workshop 1992*. pp. 381-399. Research Studies Press.

KOSKO, B., 1994. *Fuzzy thinking - the new science of fuzzy logic.* Flamingo.

KUO, B.C., 1992. *Digital control systems*. Saunders College Publishing.

LEE, CHUEN CHIEN, 1990. Fuzzy logic in control systems: fuzzy logic controller – Part I. *IEEE Trans. Syst. Man Cybern.,* 20, 2. pp.404-418.

LEE, CHUEN CHIEN, 1990. Fuzzy logic in control systems: fuzzy logic controller - Part II. *IEEE Trans. Syst. Man Cybern.,* 20, 2. pp.419-435.

LINKENS, D.A. AND ABBOD, M.F., 1991. Self organising fuzzy logic control for real time processes. In: Proceedings of: *IEE Control91,* Conf 332. pp.971-975.

MACIEJOWSKI, J.M., 1989. *Multivariable feedback design*. Addison-Wesley Publishers Ltd.

MCFARLANE D.C. AND GLOVER K., 1990. *Robust controller design using normalized coprime factor plant descriptions*. Lecture Notes in Control and Information Sciences, Springer Verlag.

MCFARLANE, D. AND GLOVER, K., 1992. A loop shaping design procedure using H_∞ synthesis. *IEEE Trans. Autom. Control,* AC-37(6). pp.759-769.

MADWED, A., 1953. Numerical analysis by the number series transformation method. In Proceedings of: *Symposium on nonlinear circuit analysis*. Brooklyn, April 1953. pp.320-368.

MAMDANI, E.H., AND ASSILIAN, S., 1975. An experiment in linguistic synthesis with a fuzzy logic controller. *Int. J. Man Mach. Stud.,* Volume 7, Issue 1. pp.1-13.

MAMDANI, E.H., AND BAAKLINI, N., 1975. Prescriptive method for deriving control policy in a fuzzy logic controller. *Electron. Lett.*, Volume 11, Numbers 25/26. pp.625-626.

MONAGHAN, A.M., 1998. *Development of a systematic approach to assist power transmission system design.* Thesis submitted for the Degree of MPhil at the University of Bath.

MORARI, M. AND ZAFIRIOU, E., 1989. *Robust process control*. Prentice Hall International, Inc.

MURRENHOFF, H., PIEPENSTOCK, U. AND KOHMÄSCHER, T., 2008. Analysing losses in hydrostatic drives. In: *Proceedings of the 7th JFPS International Symposium on Fluid Power, TOYAMA September 15-18, 2008*. pp103-108.

NEWTON, D.A., 1993. Design and implementation of an intelligent electro-hydraulic rotary drive system. *IMechE Seminar Machine Actuators and Controls* 1993. pp.25-35.

NEWTON, D.A., 1994. Design and implementation of a neural network controlled electro-hydraulic drive system. *Proc. Inst. Mech. Eng. Part I J. Syst. Control Eng.*, 208. pp 31-42.

NISIUMI, T. AND WATTON, J., 1996. Some practical considerations of real-time artificial neural network control of a servo valve/motor drive**.** In: *Proceedings of the 9th Bath International Fluid Power Workshop, September 1996.*

NJABELEKE I.A., PANNETT R.F., CHAWDRY, P.K., AND BURROWS, C.R., 1997. H_∞-control in fluid power. *IEE Colloquium on Robust Control: Theory, Software and Applications.* Stevenage, England: IEE Digest No: 1997/380. pp.7/1-7/4.

NJABELEKE I.A., 1998. *Fluid power systems – an integrated approach: Control system design - Part II: Some nonlinear control approaches*. Report 02/98, Fluid Power Centre, University of Bath.

NJABELEKE I.A., PANNETT R.F., CHAWDRY, P.K., AND BURROWS, C.R., 1998. Self-organising fuzzy logic control of a hydrostatic transmission. In: *Proceedings of*

Control '98. UKACC International Conference (Conf. Publ. No. 455). 01/10/1998. Vol.1 pp.66-72.

NJABELEKE I.A., PANNETT R.F., CHAWDRY, P.K., AND BURROWS, C.R., 1998. Modeling and control of a high speed hydrostatic transmission. In: *Proceedings of International Mechanical Engineering Congress & Exposition: The Fluid Power and Systems Technology Division*. Anaheim, CA, November 1998. pp.1-10.

NJABELEKE I.A., PANNETT R.F., CHAWDRY, P.K., AND BURROWS, C.R., 2000. Design of H_∞ loop-shaping controllers for fluid power systems. *Proc. Inst. Mech. Eng. Part C J. Mech. Eng. Sci.,* 214. pp.483-500.

PANNETT R.F., CHAWDRY, P.K., AND BURROWS, C.R., 1999. Alternative robust control strategies for disturbance rejection in fluid power system. In: *Proceedings of American Control Conference, San Diego, California.* pp.739-743.

PAPPIS, C.P. AND MAMDANI, E.H., 1977. A fuzzy logic controller for a traffic junction. *IEEE Trans. Syst. Man Cybern.*, SMC-7, 10. pp.707-717.

PEDRYCZ,W., 1994. Why triangular membership functions? *Fuzzy Sets and Systems*. Volume 64, Issue 1. pp.21-30

PEDRYCZ, W., 1996. *Fuzzy control and fuzzy systems.* (2nd Edition.) Research Studies Press Ltd, John Wiley and Sons Inc.

PEDRYCZ,W. AND VUKOVICH, G., 2002. On Elicitation of Membership Functions. *IEEE Trans Syst. Man Cybern., Part A, Systems and Humans*, Volume. 32, Number 6. pp.761-767.

PICHÉ, R. AND POHJOLAINEN, S., 1991. Design of robust controllers for position servos using H_∞ theory. *Proc. Inst. Mech. Eng. Part I J. Syst. Control Eng.*, 205. pp.299-306.

PICHÉ, R., POHJOLAINEN, S. AND VIRVALO, T., 1992. Design of robust two-degree-of-freedom controllers for position servos using H_∞ theory. *Proc. Inst. Mech. Eng. Part I J. Syst. Control Eng.*, 206. pp.135-142

PROCYK, T.J., 1977. A self-organizing controller for single-input single-output systems. Fuzzy Logic Working Group, Research Rep. No. 6, Queen Mary College, London.

PROCYK, T.J. AND MAMDANI, E.H., 1979. A linguistic self organising process controller. *Automatica*, 15. pp.15-30.

RABBO, S.A. AND TUTUNJI, T., 2008. Identification and analysis of hydrostatic transmission system. *Int. J. Adv. Manuf. Technol*., Volume 37, Numbers 3-4. pp.221-229.

ROSENBROCK, H.H., 1977. The future of control. *Automatica,* 13. pp.389-392.

ROSS, T. J., 1995. *Fuzzy logic with engineering implications.* McGraw-Hill Inc.

RUTHERFORD, D.A. AND BLOORE, G.C., 1976. The implementation of fuzzy algorithms for control. *Proceedings of IEEE*, 64, 4. pp.572-573.

SAFANOV, M.G., AND CHIANG, R.Y., 1988. CACSD using the state-space L_∞ theory – a design example. *IEEE Trans. Autom. Control*, AC-33(5). pp.477-479.

SAFANOV, M.G., LIMEBEER, D.J.N., AND CHIANG, R.Y., 1989. Simplifying the H_∞ theory via loop-shifting, matrix-pencil and descriptor concepts. *Int. J. Control*, 50(6). pp.2467-2488.

SAMAR R., POSTLETHWAITE I. AND GU D-W., 1995. Model reduction with balanced realizations. *Int. J. Control*, 62(1). pp.33-64.

SANADA, K. AND KITAGAWA, A., 1996. Robust control of rotating speed in an automatic transmission considering modelling error. In: *Proceedings of 9th Bath International Fluid Power Workshop, September 1996.*

SCHWARZENBACH, J. AND GILL, K.F., 1992. *System modelling and control*. (3rd Edition.) Edward Arnold.

SKOGESTAD, S. AND POSTLETHWAITE, I., 1997. *Multivariable feedback control: analysis and design.* John Wiley & Sons.

STEFANI, R.T., SAVANT, C.J., SHAHIAN, B. AND HOSTETTER, G.H., 1994. *Design of feedback control systems.* (3rd Edition.) Saunders College Publishing.

STOLL, R.R., 1961. *Sets, logic and axiomatic theories.* W H Freeman and Company.

TOMLINSON, S.P. AND TILLEY, D.G., 1993. Computer modelling of aircraft hydraulic systems using BATH*fp*. *Proc. Inst. Mech. Eng. Part G J. Aerosp. Eng.*, 207. pp.139–143.

TONG, R.M., 1977. A control engineering review of fuzzy systems. *Automatica*, 13. pp.559-569.

TSOUKALAS, L.H. AND UHRIG, R.E., 1997. *Fuzzy and neural approaches in engineering.* John Wiley and Sons Inc.

TURNER, P., GUIVER, G., AND LINES, B., 2003. Introducing the state space bounded derivative network for commercial transition control. In: *Proceedings of American Control Conference Denver, Colorado, June 4-6, 2003*. pp.5400-5404.

UNIVERSITY OF BATH, FLUID POWER CENTRE, 1993. Bath*fp* Manual Volume 2: The Bath*fp* Model Reference Guide.

VALENTI, M., 1997. Hydraulics take center stage. *Mechanical Engineering (ASME)*, Volume 119, Issue 4. pp.52-57.

VIBET, C., 1987. Guide to choosing the sampling rate in computerised controllers. *Electron. Lett.*, Volume 23, Issue 19. pp.1002-1004.

VINNICOMBE, G., 1993. Frequency domain uncertainty and the graph topology. *IEEE Trans. Autom. Control*, Volume 38, Number 9. pp.1371-1383.

WILLIAMS, S., 1995. Turning advanced technologies into products and benefits. *IEE Comp. and Cntrl. Jnl.*, February. pp.2.

WILLIAMS, S., 1995. Making advanced control work. *IEE Comp. and Cntrl. Jnl.*,, February. pp.5-10.

WILLIAMS, S., 2005. Industrial process control, modelling and a broader process automation context. *IEE Tustin Lecture on Thursday, 5 May 2005*. http://tv.theiet.org/technology/manu/538.cfm .

WOLKENHAUER, O. AND EDMUNDS, J., 1994. *Fuzzy systems toolbox for use with MATLAB and SIMULINK*. Control Systems Centre, UMIST, UK.

WONG, C.F., SHIPPEN, J., AND JONES, B., (1998). Neural network control strategies for low specification servo actuators. *Int. J. Mach. Tools Manuf.*, 38. pp. 1109–1124.

ZADEH, L.A., 1973. Outline of a new approach to the analysis of complex systems and decision processes. *IEEE Trans. Syst. Man Cybern.*, SMC-3, 1. pp.28-44.

ZADEH, L.A., 1988. Fuzzy Logic. *IEEE Computer*, April. pp.83-93.

ZHANG, B.S. AND EDMUNDS, J.M., 1991. On fuzzy logic controllers. In: *Proceedings of IEE Control91*, Conf 332. pp.961-965.

ZHANG, R, ALLEYNE, A, AND PRASETIAWAN, E., 2002. Modeling and H_2/H_∞ MIMO control of an earthmoving vehicle powertrain. *J. Dyn. Syst. Meas. Contr.*, Volume 124, Issue 4. pp. 625-636.

ZIKIC, A.M., 1989. *Practical digital control*. Ellis Horwood Limited.

APPENDIX 1 System Information

A1.1 Extracts from Moog Data Sheet 841 – Series A084 Servodrives

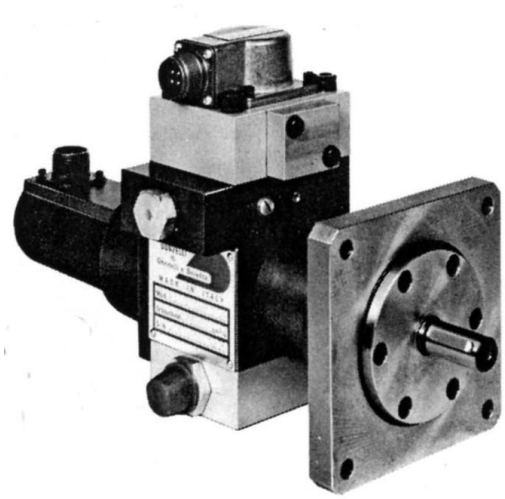

Figure A1.1 Servomotor with servovalve (taken from Data Sheet 841)

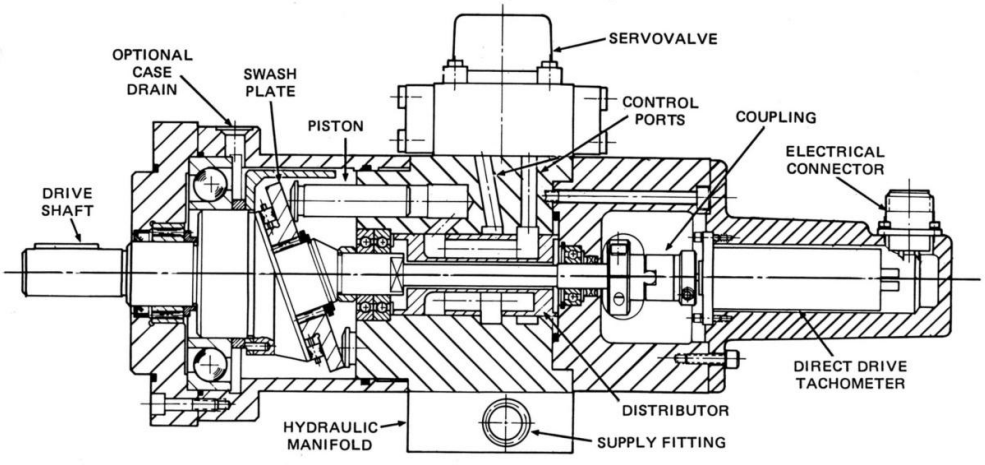

Figure A1.2 Schematic of Moog Donzelli servodrive (Figure 1 of Data Sheet 841)

Table A1.1 Moog Donzelli servomotor parameters (taken from Table 1 of Data Sheet 841)

Motor Size	Motor Displacement Approx.		Stall Torque Factor (in lb/ 100 psi)	Max Speed (rpm)	Max Pressure (psi)	Max Axial Shaft Load (lb)	Max Radial Shaft Load (lb)	Servovalve Type	Motor Inertia (lb sec^2)
	(in^3/ rev)	(in^3/ rad)							
2	2.41	0.383	33.9	2000	2500	180	450	62,73,76	0.0170

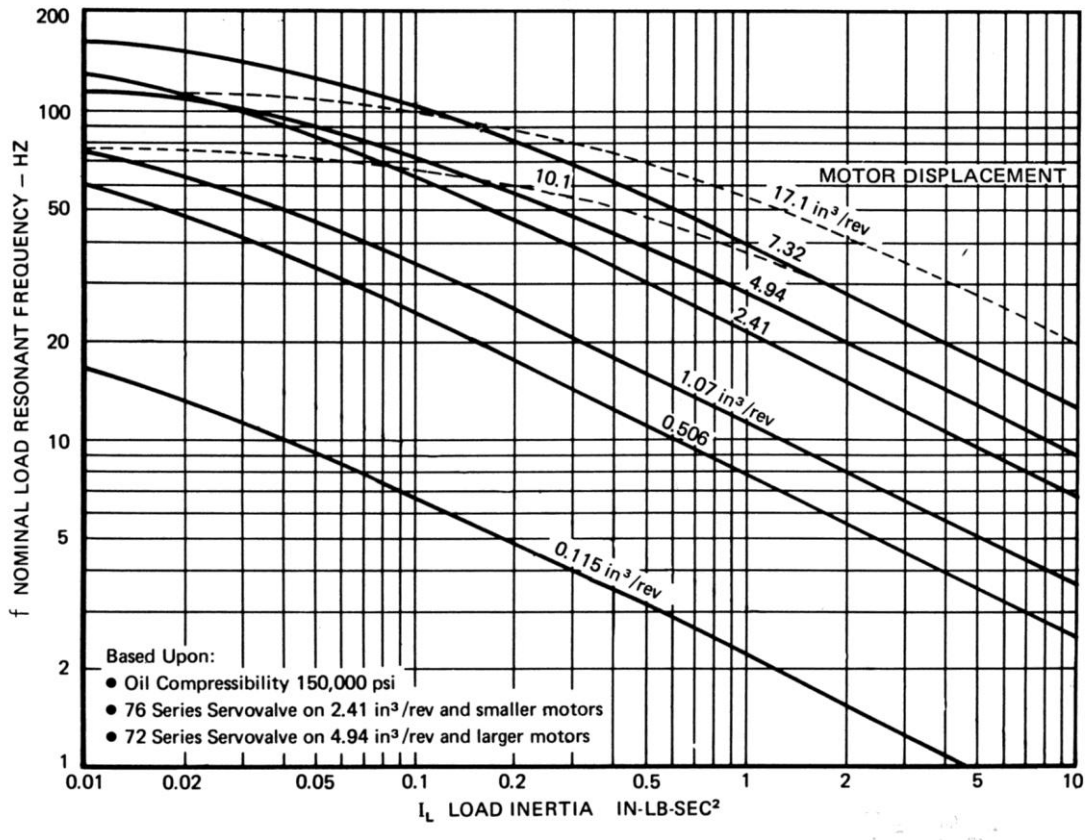

Figure A1.3 Servodrive resonant frequency (taken from Figure 4 of Data Sheet 841)

Table A1.2 Characteristics of servovalves (taken from Figure 4 of Data Sheet 841)

Servovalve Model	Rated Flow @ 1000 psi gpm	Rated Current		Coil Resistance ohms/coil
		Series Coils ma	Parallel or Diff. Coils ma	
62-102	2½	±50	±100	27
62-105	5	±50	±100	27
62-110	10	±50	±100	27
62-115	15	±50	±100	27
62-120	20	±50	±100	27
73M100	1	± 7½	± 15	200
73M101	2½	± 7½	± 15	200
73M102	5	± 7½	± 15	200
73M125	7½	± 7½	± 15	200
73M103	10	± 7½	± 15	200
73M104	15	±20	± 40	80
76M100	1	± 7½	± 15	200
76M101	2½	± 7½	± 15	200
76M102	5	± 7½	± 15	200
76M125	7½	± 7½	± 15	200
76M103	10	± 7½	± 15	200
76M104	15	±20	± 40	80
72M101	25	± 7½	± 15	200
72M102	40	± 7½	± 15	200
72M103	60	±20	± 40	80

A1.2 Principal Parameters used in the Bath*fp* Plant Model

Details of the component models used may be found in Bath*fp* Manual Volume 2 – The Standard Bath*fp* Model Reference Guide.

A1.2.1 Rotating Components

Parameter	Value	Reference
Load Pump Displacement	19.2 cc/rev	Sauer Sundstrand data sheet - gear pump/motor SNM2/19 CO 02
Motor Displacement	39.5 cc/rev ($2.41in^3$/rev)	MOOG Series A084 Servo drives Data Sheet 841
Total Inertia of Rotating Parts	0.075 kgm^2	data sheets + estimates

A1.2.2 Pipes

	Supply	Valve -Motor (2)
Length	10 m	0.01 m
Internal diameter	25.4 mm	25.4 mm
Wall thickness	2.54 mm	2.54 mm
Material	steel/cupro-nickel	steel/cupro-nickel
Pipe model (Bath*fp*)	HP01	HP00

A1.2.3 Valve

Valve type: Moog Donzelli 76M104
Valve flow characteristic: p/q 68 l/min (from data sheet)
Valve model (Bath*fp*):VB04

A1.2.4 Speed transducer

Transducer time constant: .01 sec (estimated)

APPENDIX 2 Mathematical Notations, Sets, Matrices, etc.

A2.1 General

For all: $\forall$

There exists at least one: $\exists$

A implies *B*: $A \Rightarrow B$

B is implied by *A*: $B \Leftarrow A$

D is true if and only if (iff) *A* is true: $D \Leftrightarrow A$

Rational number: expressible as quotient of two integers e.g. 0.5 = 1/2

Irrational number: not a rational number e.g. √(2)

Triangle inequality: $|a| + |b| \geq |a + b|$

A2.2 Sets

a is *an element* of set *A*: $a \in A$

B is *a subset* of *A*: $B \subseteq A$

Elements of set *A*: A = {list of elements in set}

Set *A* consists of elements *a* which have a property *Q*: $A = \{a \mid a \text{ is } Q\}$

Set *A* contains *B* and more (*B* is a proper subset of *A*): $B \subset A$

Set *D* is *union* of sets *A* and *B*: $D = A \cup B$

means $D = \{d \mid d \in A \text{ or } d \in B\}$

(i.e. the set *D* is sets *A* and *B* 'added together')

Set *C* is *intersection* of sets *A* and *B*: $C = A \cap B$

means $D = \{d \mid d \in A \text{ and } d \in B\}$

(i.e. the set C is the 'overlap' of sets A and B)

Empty set: O

Universal set (of all elements relevant to the current problem): U

(so $O \subseteq A \subseteq U$)

Complement of set A (all elements not in set A) is A'

(i.e. $A \cap A' = O$; $A \cup A' = U$)

A2.3 Sets and the Complex Plane

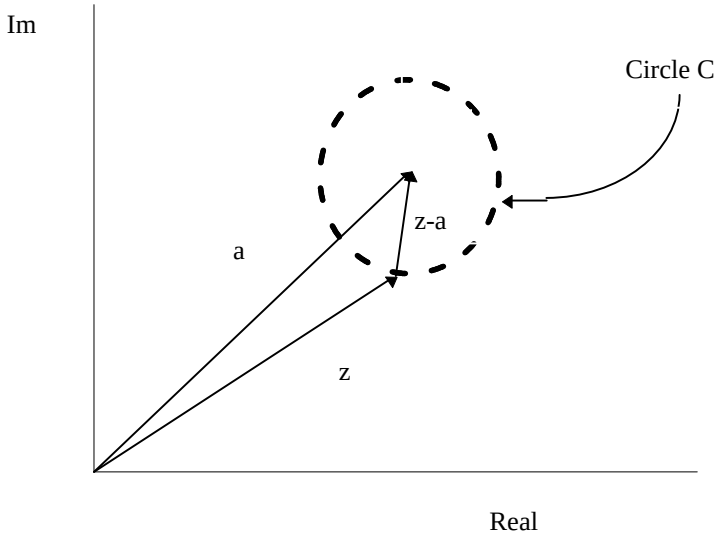

Circle C is defined by $|z - a| = r$ where r is the radius.

The interior of C is defined by $|z - a| < r$. This is an open circular disc. It is a *neighbourhood* of a. There is an infinite number of such neighbourhoods given by all $r > 0$.

The closed circular disc is defined by $|z - a| \leq r$.

A set of points in the complex plane is any collection of points, finite or infinite in number. Examples: solutions of a quadratic equation, points in the interior of a circle.

A set S is *open* if every point in S has a neighbourhood every point of which belongs to S.

The set of points in the interior of a circle form an *open set*; the set of points which lie in the interior of a circle or on it form a *closed set*, because no neighbourhood of a point lying on the circle can lie entirely within it. The *complement* of set S is the set of all points in the complex plane which do not belong to S. A set is *open* if its

complement is closed. A set is *bounded* if a circle can be drawn which encloses all its points. A *connected set S* is one in which any two of its points can be joined by a finite line of finitely many linear segments, all of whose points belong to *S*. An *open connected set* is a *domain*. A point is a *boundary point* of a set if every neighbourhood of that point contains both points inside and outside the set. If a set is open, then no boundary point belongs to the set.

A2.4 Matrices and Determinants

Transpose of $\boldsymbol{A}$: $\boldsymbol{A}^{\mathrm{T}}$ (or $\boldsymbol{A}'$) - rows and columns interchanged

$(\boldsymbol{AB})^{\mathrm{T}} = \boldsymbol{B}^{\mathrm{T}}\boldsymbol{A}^{\mathrm{T}}$

Complex conjugate of $\boldsymbol{A}$: $\overline{\boldsymbol{A}}$ - elements are complex conjugates of elements in A

Identity matrix **I** (all elements on leading diagonal equal to one; other elements zero)

Transpose of complex conjugate of $\boldsymbol{A}$: $\boldsymbol{A}^{\mathrm{H}}$ ($\boldsymbol{A}^{\mathrm{H}} = \overline{\boldsymbol{A}}^{\mathrm{T}}$)

Determinant of $\boldsymbol{A}$: $|\boldsymbol{A}|$

Determinant of product $|\boldsymbol{AB}| = |\boldsymbol{A}||\boldsymbol{B}|$

Removal of row i and column j from matrix $\boldsymbol{A}$: $\mathrm{De}(i,j,\boldsymbol{A})$

Minor of matrix $\boldsymbol{A}$: $|\mathrm{De}(i,j,\boldsymbol{A})|$

Cofactor of matrix $\boldsymbol{A}$ (signed minor): $(-1)^{(i+j)}|\mathrm{De}(i,j,\boldsymbol{A})|$

Adjoint (matrix of cofactors) of matrix $\boldsymbol{A}$: $\mathrm{Adj}(\boldsymbol{A})$

Inverse of $\boldsymbol{A}$: $\boldsymbol{A}^{-1} = \dfrac{Adj(\boldsymbol{A})}{|\boldsymbol{A}|}$

$\boldsymbol{A}^{-1}\boldsymbol{A} = \mathbf{I}$

$(\boldsymbol{AB})^{-1} = \boldsymbol{B}^{-1}\boldsymbol{A}^{-1}$

Unitary matrix $\boldsymbol{U}$: $\boldsymbol{U}\boldsymbol{U}^{\mathrm{H}} = \mathbf{I}$

also $\boldsymbol{U}^{\mathrm{T}} = \overline{\boldsymbol{U}}^{-1}$ (inverse of complex conjugate = transpose)

Hermitian matrix $\boldsymbol{A}$: $\boldsymbol{A}^{\mathrm{T}} = \overline{\boldsymbol{A}}$ (complex conjugate = transpose)

also $\boldsymbol{A} = \overline{\boldsymbol{A}}^{\mathrm{T}}$

Real Hermitian matrix or *symmetric matrix* $\boldsymbol{A}^{\mathrm{T}} = \boldsymbol{A}$ ($\boldsymbol{A} = \overline{\boldsymbol{A}}$ since A is real)

Skew symmetric matrix $\boldsymbol{A}^{\mathrm{T}} = -\boldsymbol{A}$ (therefore diagonal elements are zero)

Orthogonal matrix $\boldsymbol{A}^{-1} = \boldsymbol{A}^{\mathrm{T}}$

Involutary matrix $\boldsymbol{A}^{-1} = \boldsymbol{A}$

Normal matrix (must be square): $\boldsymbol{Q}^{\mathrm{H}}(s)\boldsymbol{Q}(s) = \boldsymbol{Q}(s)\boldsymbol{Q}^{\mathrm{H}}(s)$

Polynomial matrix: matrix of polynomials

Unimodular polynomial matrix: matrix of polynomials whose inverse is also a polynomial matrix

(Note - a *rational transfer function matrix* is expressible as a polynomial matrix and a common denominator polynomial)

A2.5 Rank

Rank of $m \times n$ matrix

- maximum value is $\min(m,n)$
- number of linearly independent pieces of information contained in the matrix
- rank r means that matrix contains at least one $r \times r$ matrix with non-zero determinant, and $|(r+1),(r+1)| = 0$

A2.6 Eigenvectors and Eigenvalues

For matrix $\boldsymbol{A}$,

$\lambda \boldsymbol{x} = \boldsymbol{A}\boldsymbol{x}$ where λ is an *eigenvalue* and $\boldsymbol{x}$ is an *eigenvector* (column).

$|\lambda \mathbf{I} - \boldsymbol{A}| = 0$

For the ith eigenvector $\boldsymbol{x}_i$ of n,

$[\lambda_i \mathbf{I} - \boldsymbol{A}]x_i = 0$

If matrix $\boldsymbol{P} = [\boldsymbol{x}_1 \quad \boldsymbol{x}_i \quad \boldsymbol{x}_n]$

then $\boldsymbol{P}^{-1}\boldsymbol{A}\boldsymbol{P} = \begin{bmatrix} \lambda_1 & 0 & 0 \\ 0 & \lambda_i & 0 \\ 0 & 0 & \lambda_n \end{bmatrix}$

A2.7 Determinants and Eigenvalues

The *determinant* of a matrix is the product of its eigenvalues.

i.e.

$|\boldsymbol{A}| = \Pi\lambda_i$

A *singular matrix* has at least one zero eigenvalue.

Proof:

Consider a 2×2 matrix A

$$\boldsymbol{A} = \begin{bmatrix} a_{11} & a_{12} \\ a_{21} & a_{22} \end{bmatrix}$$

$|\boldsymbol{A}| = (a_{11}a_{22} - a_{21}a_{12})$

Now find eigenvalues as roots of characteristic equation:

$$\left|\boldsymbol{A} - \lambda\mathbf{I}\right| = \begin{vmatrix} (a_{11} - \lambda) & a_{12} \\ a_{21} & (a_{22} - \lambda) \end{vmatrix} = (a_{11} - \lambda)(a_{22} - \lambda) - a_{12}a_{21}$$

$$\left|\boldsymbol{A} - \lambda\mathbf{I}\right| = \lambda^2 - (a_{11} + a_{22})\lambda + (a_{11}a_{22} - a_{12}a_{21})$$

Product of roots, that is product of eigenvalues, is $(a_{11}a_{22} - a_{12}a_{21})$

This is also the determinant.

For higher order, consider $|\boldsymbol{A} - \lambda\mathbf{I}|$ and expand to give the characteristic equation. The product of the roots is given by the term which does not include λ^i . This term may be arrived at by deriving $|\boldsymbol{A} - \lambda\mathbf{I}|$ and setting $\lambda = 0$, i.e. $|\boldsymbol{A}|$. Thus $|\boldsymbol{A}|$ is the product of the roots of the characteristic equation, i.e. the product of eigenvalues.

A2.8 Definiteness

For matrix *A*:

+ve definite ($\boldsymbol{A} > 0$) if $\boldsymbol{x}^{\mathrm{T}}\boldsymbol{A}\boldsymbol{x} > 0$ for $\boldsymbol{x} \neq \mathbf{0}$

+ve semi-definite ($\boldsymbol{A} \geq 0$) if $\boldsymbol{x}^{\mathrm{T}}\boldsymbol{A}\boldsymbol{x} \geq 0$ for $\boldsymbol{x} \neq \mathbf{0}$

–ve definite ($\boldsymbol{A} < 0$) if $\boldsymbol{x}^{\mathrm{T}}\boldsymbol{A}\boldsymbol{x} < 0$ for $\boldsymbol{x} \neq \mathbf{0}$

–ve semi-definite ($\boldsymbol{A} \leq 0$) if $\boldsymbol{x}^{\mathrm{T}}\boldsymbol{A}\boldsymbol{x} \leq 0$ for $\boldsymbol{x} \neq \mathbf{0}$

If eigenvectors are λ_i the following apply:

+ve definite $\lambda_i > 0$ for all i

+ve semi-definite $\lambda_i \geq 0$ at least one λ_i is zero (singular matrix)

–ve definite $\lambda_i < 0$ for all i

–ve semi-definite $\lambda_i \leq 0$ at least one λ_i is zero (singular matrix)

Scalar Quadratic Form f($\boldsymbol{x}$) where $\boldsymbol{x}$ is a non-zero vector, i.e. at least one element of $\boldsymbol{x}$ is non-zero. For all non-zero $\boldsymbol{x}$:

if f($\boldsymbol{x}$) > 0 f($\boldsymbol{x}$) is +ve definite

if f($\boldsymbol{x}$) ≥ 0 f($\boldsymbol{x}$) is +ve semi-definite

if f($\boldsymbol{x}$) < 0 f($\boldsymbol{x}$) is –ve definite

if f($\boldsymbol{x}$) ≤ 0 f($\boldsymbol{x}$) is –ve semi-definite

Other forms are indefinite.

Symmetric matrix $\boldsymbol{Q}$

(associated with $\boldsymbol{x}^{\mathrm{T}}\boldsymbol{Q}\boldsymbol{x}$)

Eigenvalues are $\lambda_i = \sigma_i + j\omega_i$

If $\sigma_i > 0$ $\boldsymbol{Q}$ is +ve definite

If $\sigma_i \geq 0$ $\boldsymbol{Q}$ is +ve semi-definite

If $\sigma_i < 0$ $\boldsymbol{Q}$ is –ve definite

If $\sigma_i \leq 0$ $\boldsymbol{Q}$ is –ve semi-definite

If det(i,$\boldsymbol{Q}$) is the determinant of the upper left-hand $i \times i$ submatrix, then if for all $i = 1 \rightarrow n$

where $\boldsymbol{Q}$ is $n \times n$:

If det(i,$\boldsymbol{Q}$) > 0 $\boldsymbol{Q}$ is +ve definite

If det(i,$\boldsymbol{Q}$) ≥ 0 $\boldsymbol{Q}$ is +ve semi-definite

If det(i, -$\boldsymbol{Q}$) > 0 $\boldsymbol{Q}$ is –ve definite

If det(i, -$\boldsymbol{Q}$) ≥ 0 $\boldsymbol{Q}$ is –ve semi-definite

Example of positive definite:

All determinants of matrix C are positive, as follows

$$|c_{11}| \quad \begin{vmatrix} c_{11} & c_{12} \\ c_{21} & c_{22} \end{vmatrix} \quad \begin{vmatrix} c_{11} & c_{12} & c_{13} \\ c_{21} & c_{22} & c_{23} \\ c_{31} & c_{32} & c_{33} \end{vmatrix} \ \ldots\ldots$$

A2.9 Quadratic Forms and Symmetry

Consider

f($\boldsymbol{x}$) = $\boldsymbol{x}^{\mathrm{T}}\boldsymbol{Q}\boldsymbol{x}$ where $\boldsymbol{Q}$ is square and symmetric and f($\boldsymbol{x}$) is scalar quadratic

Thus $\boldsymbol{Q}^{\mathrm{T}} = \boldsymbol{Q}$

$\boldsymbol{Q}_S = (\boldsymbol{Q} + \boldsymbol{Q}^{\mathrm{T}})/2$ is also symmetrical and $\boldsymbol{Q}_S{}^{\mathrm{T}} = \boldsymbol{Q}_S$

$\boldsymbol{Q}_{SK} = (\boldsymbol{Q} - \boldsymbol{Q}^{T})/2$ is skew symmetric ($\boldsymbol{Q}_{SK}{}^{T} = (\boldsymbol{Q}^{T} - \boldsymbol{Q})/2 = - \boldsymbol{Q}_{SK}$)

$\boldsymbol{Q} = \boldsymbol{Q}_{S} + \boldsymbol{Q}_{SK}$

$\boldsymbol{x}^{T}\boldsymbol{Q}_{SK}\boldsymbol{x} = 0$ (leading diagonal elements are all zero; above and below diagonal elements have equal size and opposite sign)

$\boldsymbol{x}^{T}\boldsymbol{Q}\boldsymbol{x} = \boldsymbol{x}^{T}(\boldsymbol{Q}_{S} + \boldsymbol{Q}_{SK})x = \boldsymbol{x}^{T}\boldsymbol{Q}_{S}\boldsymbol{x}$

Thus $\boldsymbol{Q}$ is always symmetric when f($\boldsymbol{x}$) is quadratic.

A2.10 Schur's Formula for Partial Determinants

Square matrix $\boldsymbol{G}$ is partitioned as follows

$$\boldsymbol{G} = \begin{bmatrix} \boldsymbol{G}_{11} & \boldsymbol{G}_{12} \\ \boldsymbol{G}_{21} & \boldsymbol{G}_{22} \end{bmatrix}$$

Then

$|\boldsymbol{G}| = |\boldsymbol{G}_{11}| * |(\boldsymbol{G}_{22} - \boldsymbol{G}_{21}\boldsymbol{G}_{11}{}^{-1}\boldsymbol{G}_{12})|$ if $|\boldsymbol{G}_{11}| \neq 0$

or

$|\boldsymbol{G}| = |\boldsymbol{G}_{22}| * |(\boldsymbol{G}_{11} - \boldsymbol{G}_{12}\boldsymbol{G}_{22}{}^{-1}\boldsymbol{G}_{21})|$ if $|\boldsymbol{G}_{22}| \neq 0$

example:

$|(\mathbf{I} - \boldsymbol{G}\boldsymbol{K})| = |\ \mathbf{I}\ | * |(\mathbf{I} - (-\boldsymbol{G}\mathbf{I}^{-1}\text{-}\boldsymbol{K}))|$

comparing terms:

$$\left[\mathbf{I} - \boldsymbol{G}\boldsymbol{K}\right] = \begin{bmatrix} \mathbf{I} & -\boldsymbol{K} \\ -\boldsymbol{G} & \mathbf{I} \end{bmatrix}$$

A2.11 Transfer Functions

$G(s) = \dfrac{num(s)}{den(s)}$ where *num*(*s*) and *den*(*s*) are polynomials in complex variable *s*

Rational	- ratio of polynomials
Real	- coefficients are real not complex
Proper	- degree of denominator ≥ degree of numerator
Strictly proper	- degree of denominator > degree of numerator
Stable	- poles are in LHP
Proper	- $G(j\infty)$ is finite
Strictly proper	- $G(j\infty) = 0$
Biproper	- G and G^{-1} are both proper

Singular value - positive square root of eigenvalue of $\boldsymbol{GG}^H$

Principal gain - singular value as a function of frequency ω.

A2.12 State Space Realisation

A2.12.1 State Space and Transfer Functions

Consider state space realisation ($\boldsymbol{A}$,$\boldsymbol{B}$,$\boldsymbol{C}$,$\boldsymbol{D}$):

$$\dot{\boldsymbol{x}} = \boldsymbol{A}\boldsymbol{x} + \boldsymbol{B}\boldsymbol{u}$$

$$\boldsymbol{y} = \boldsymbol{C}\boldsymbol{x} + \boldsymbol{D}\boldsymbol{u}$$

Taking Laplace transforms and re-arranging gives:

$$(s\mathbf{I} - \boldsymbol{A})\boldsymbol{x} = \boldsymbol{B}\boldsymbol{u}$$

$$\boldsymbol{x} = (s\mathbf{I} - \boldsymbol{A})^{-1}\boldsymbol{B}\boldsymbol{u}$$

$$\boldsymbol{G}(s) = \frac{\boldsymbol{y}}{\boldsymbol{u}} = \boldsymbol{C}(s\mathbf{I} - \boldsymbol{A})^{-1}\boldsymbol{B} + \boldsymbol{D}$$

If degree of denominator > degree of numerator, $\boldsymbol{D} = 0$

Therefore $\boldsymbol{D} = 0$ for strictly proper transfer function.

If $\boldsymbol{D} \neq 0$

$$\boldsymbol{G}(s) = \frac{\boldsymbol{C}adj(s\mathbf{I} - \boldsymbol{A})\boldsymbol{B} + \det(s\mathbf{I} - \boldsymbol{A})\boldsymbol{D}}{\det(s\mathbf{I} - \boldsymbol{A})}$$

i.e. both numerator and denominator are polynomials whose order is that of the characteristic equation.

As $s \to \infty$, $\boldsymbol{G}(s) \to \infty$

A2.12.2 Minimum Phase Transfer Function

All poles and zeros are in the LHP

The phase lag associated with a pole in the LHP increases with frequency; the phase lag associated with a zero in the RHP increases with frequency. Presence of a zero in RHP thus increases the phase lag.

A2.12.3 State Space Realisations - Canonical Forms

Strictly proper transfer function:

$$G(s) = \frac{b_1 s^{n-1} + \ldots + b_{n-1} s + b_n}{s^n + a_1 s^{n-1} + a_2 s^{n-2} + \ldots a_n}$$

Phase Variable Form

$$\boldsymbol{A} = \begin{bmatrix} 0 & 1 & 0 & 0 \\ 0 & 0 & 1 & 0 \\ 0 & 0 & 0 & 1 \\ -a_n & -a_{n-1} & .. & -a_1 \end{bmatrix}$$

$$\boldsymbol{B} = \begin{bmatrix} 0 \\ 0 \\ .. \\ 1 \end{bmatrix}$$

$$\boldsymbol{C} = \begin{bmatrix} b_n & b_{n-1} & .. & b_1 \end{bmatrix}$$

$$\boldsymbol{D} = \begin{bmatrix} 0 \end{bmatrix}$$

Dual Phase Variable Form

$$\boldsymbol{A} = \begin{bmatrix} -a_1 & 1 & 0 & 0 \\ .. & 0 & 1 & 0 \\ -a_{n-1} & 0 & 0 & 1 \\ -a_n & 0 & .. & 0 \end{bmatrix}$$

$$\boldsymbol{B} = \begin{bmatrix} b_1 \\ b_2 \\ b_{n-1} \\ b_n \end{bmatrix}$$

$$\boldsymbol{C} = \begin{bmatrix} 1 & 0 & 0 & 0 \end{bmatrix}$$

$$\boldsymbol{D} = \begin{bmatrix} 0 \end{bmatrix}$$

'*Dual'* - substitution enables move from one form to the other;

The ***A*** matrices are in companion form;

The characteristic equation may be derived by inspection from column 1 or row 1.

If the ***A*** matrix is diagonal, the state variables are *canonical*.

To diagonalise, choose canonical state vector ***z*** so that

$\boldsymbol{z} = \boldsymbol{P}^{-1}\boldsymbol{x}$;

$\overline{\boldsymbol{A}} = \boldsymbol{P}^{-1}\boldsymbol{A}\boldsymbol{P}$

$\boldsymbol{P}$ is a matrix of eigenvectors of $\boldsymbol{A}$; $\overline{\boldsymbol{A}}$ is a diagonal matrix of eigenvalues of $\boldsymbol{A}$.

$\dot{\boldsymbol{z}} = \boldsymbol{P}^{-1}\dot{\boldsymbol{x}} = \boldsymbol{P}^{-1}\boldsymbol{A}\boldsymbol{x} + \boldsymbol{P}^{-1}\boldsymbol{B}\boldsymbol{u}$

$\dot{\boldsymbol{z}} = \boldsymbol{P}^{-1}\boldsymbol{A}\boldsymbol{P}\boldsymbol{z} + \boldsymbol{P}^{-1}\boldsymbol{B}\boldsymbol{u}$

$\boldsymbol{y} = \boldsymbol{C}\boldsymbol{P}\boldsymbol{z} + \boldsymbol{D}\boldsymbol{u}$

A2.13 Bounds

Supremum : least upper bound

For supremum σ,

(i) $a \leq \sigma \quad \forall a \in A$

and

(ii) $\forall \sigma' < \sigma, \exists a \in A$ such that $a > \sigma'$

Then $\sigma = \sup A$

Infimum: greatest lower bound

For infimum τ

(i) $\tau \leq a \quad \forall a \in A$

and

(ii) $\forall \tau' > \tau, \exists a \in A$ such that $a < \tau'$

Then $\tau = \inf A$

A2.14 Vector Spaces

Dimension of a vector space is the number of vectors in its *Basis Set*.

If $\{\boldsymbol{u}_i , i=1,m\}$ is a set of vectors in a vector space, then the set $\{\boldsymbol{u}_i\}$ spans the space if for every vector $\boldsymbol{x}$ in the space there is at least one set of scalars a_i which permits $\boldsymbol{x}$ to be expressed as a linear combination of the vectors $\boldsymbol{u}_i$

$$\boldsymbol{x} = \sum_{i=1}^{m} a_i \boldsymbol{u}_i$$

A *set of basis vectors* (Basis Set) is a set consisting of the minimum number required to span the space.

A *linear vector space* $\mathcal{X}$ is a set of elements (or vectors) defined over a scalar number field, which satisfies:

1. for $\boldsymbol{x} \in \mathcal{X}$ and $\boldsymbol{y} \in \mathcal{X}$ then $\boldsymbol{v} = \boldsymbol{x}+\boldsymbol{y}$ also belongs to $\mathcal{X}$
2. addition is commutative i.e. $\boldsymbol{x} + \boldsymbol{y} = \boldsymbol{y}+ \boldsymbol{x}$
3. addition is associative i.e. $(\boldsymbol{x} + \boldsymbol{y}) + \boldsymbol{z} = \boldsymbol{x} + (\boldsymbol{y} + \boldsymbol{z})$
4. the space contains a zero vector which satisfies $\boldsymbol{x} + 0 = 0 + \boldsymbol{x} = \boldsymbol{x}$
5. for every $\boldsymbol{x} \in \mathcal{X}$ there is a unique $\boldsymbol{x} \in \mathcal{X}$ such that $\boldsymbol{x} + \boldsymbol{y} = 0$
6. for every $\boldsymbol{x}$ and for any scalar $a \in \mathcal{F}$ (field of numbers) the product $a\boldsymbol{x}$ gives another vector $\boldsymbol{y}$
7. for scalars $a \in \mathcal{F}$ and $b \in \mathcal{F}$, and for any vector $\boldsymbol{x}$ in the vector space, $a(b\boldsymbol{x}) = (ab)\boldsymbol{x}$
8. multiplication by scalars is distributive $(a + b)\boldsymbol{x} = a\boldsymbol{x} + b\boldsymbol{x}$; $a(\boldsymbol{x} + \boldsymbol{y}) = a\boldsymbol{x} + a\boldsymbol{y}$

Note that products are not defined.

Examples of vector spaces include

- ordered n-tupals of real numbers $[a_1\ a_2\ ...\ a_i\ ...a_n]^{\mathrm{T}}$ - if a_i is real, then space is $\mathcal{R}^n$; if a_i is complex, then space is C^n

- set of all $m \times n$ matrices. Matrix elements may be real or complex numbers, or rational polynomial functions with real or complex coefficients.

- set of all continuous or piecewise continuous time functions f(t) on interval $a \le t \le b$ or an ordered set of such functions

- set of polynomials with degree $\le n$

All of these sets must include a suitable null vector, e.g. an $m \times n$ null matrix

An *Inner Product Space* is one in which a unique scalar is assigned to every pair of vectors. The scalar valued function of $\boldsymbol{x}$ and $\boldsymbol{y}$ is called the inner product $\langle \boldsymbol{x},\boldsymbol{y} \rangle$ provided that

1. $\langle \boldsymbol{x},\boldsymbol{y} \rangle$ = complex conjugate $\langle \boldsymbol{y},\boldsymbol{x} \rangle$ (complex conjugate property)

2. $\langle \boldsymbol{x}, a\boldsymbol{y}_1 + b\boldsymbol{y}_2 \rangle = a\langle \boldsymbol{x}, \boldsymbol{y}_1 \rangle + b\langle \boldsymbol{x}, \boldsymbol{y}_2 \rangle$ (linear homogenous property)

3. $\langle \boldsymbol{x}, \boldsymbol{x} \rangle \geq 0 \ \forall \ \boldsymbol{x}$ and $\langle \boldsymbol{x}, \boldsymbol{x} \rangle = 0$ iff $\boldsymbol{x} = 0$

A *Norm* of $\boldsymbol{x}$ can be defined as $\|\boldsymbol{x}\| = \langle \boldsymbol{x}, \boldsymbol{x} \rangle^{1/2}$ and *metric* or distance between $\boldsymbol{x}$ and $\boldsymbol{y}$ as $\rho(\boldsymbol{x}, \boldsymbol{y}) = \|\boldsymbol{x} - \boldsymbol{y}\|$

$L_2[a,b]$ is the linear space of all square integrable functions of t, i.e. all functions $f(t)$ such that

$$\int_a^b f(\tau)^2 d\tau < \infty$$

If $\boldsymbol{x}, \boldsymbol{y} \in L_2[a,b]$ then

$\langle \boldsymbol{x}, \boldsymbol{y} \rangle = \int_a^b \boldsymbol{x}(\tau)\boldsymbol{y}(\tau) d\tau$ is a valid inner product.

A transfer function $\boldsymbol{G}(s)$ is said to be in the space H_∞ (where the H stands for Hardy space), if $\sup_{\mathrm{Re}(s) > 0} |\boldsymbol{G}(s)| < \infty$

Thus all poles of $\boldsymbol{G}(s)$ are in left hand plane and it is stable.

A2.15 Norms

Induced norm of matrix $\boldsymbol{G}$

$$\|\boldsymbol{G}\| = \sup_{\boldsymbol{x} \to \boldsymbol{0}} \frac{\|\boldsymbol{G}\boldsymbol{x}\|}{\|\boldsymbol{x}\|}$$

where $\|\boldsymbol{G}\boldsymbol{x}\|$ and $\|\boldsymbol{x}\|$ are any vector norms

Euclidean norm of vector

$$\|\boldsymbol{x}\| = \sqrt{\boldsymbol{x}^{\mathrm{H}}\boldsymbol{x}}$$

Hilbert or *Spectral* norm of $\boldsymbol{G}$ is induced by the Euclidean vector norm

$\|\boldsymbol{G}\|_{\mathrm{s}} = \bar{\sigma}$ where $(\bar{\sigma})^2$ is the maximum eigenvalue of $\boldsymbol{G}\boldsymbol{G}^{\mathrm{H}}$ or $\boldsymbol{G}^{\mathrm{H}}\boldsymbol{G}$

The H_∞-norm is defined as

$$\|\boldsymbol{G}(s)\|_\infty = \sup_{\mathrm{Re}(s) > 0} |\boldsymbol{G}(s)|$$

The *Hankel* norm $\|\Delta\|_H$ of a linear time invariant (LTI) system with transfer matrix Δ input $\boldsymbol{w}$, and output $\boldsymbol{v}$, is defined as the L_2 gain of the associated Hankel operator H_Δ, i.e. as the maximum of the "future output energy integral"

$$\sqrt{\int_0^\infty |\boldsymbol{v}(t)|^2 dt}$$

subject to the constraints

$\boldsymbol{w}(t) = 0$ for $t \geq 0$

and $\int_{-\infty}^{0} |\boldsymbol{w}(t)|^2 dt \leq 1$

A2.16 Singular Value Decomposition of Matrix *G*

If $\boldsymbol{\Sigma} = diag\{\sigma_1 \quad \sigma_2 \quad .. \quad \sigma_n\} = diag\{\bar{\sigma} \quad \sigma_2 \quad ... \quad \underline{\sigma}\}$ i.e. a diagonal matrix of singular values;

$$\boldsymbol{G} = \boldsymbol{Y}\boldsymbol{\Sigma}\boldsymbol{U}^H$$

$\boldsymbol{Y}\boldsymbol{Y}^H = \mathbf{I}$

$\boldsymbol{U}\boldsymbol{U}^H = \mathbf{I}$

i.e. unitary matrices.

The unitary matrices rotate and the diagonal matrix scales.

$\boldsymbol{G}^H = \left(\boldsymbol{\Sigma}\boldsymbol{U}^H\right)^H \boldsymbol{Y}^H = \boldsymbol{U}\boldsymbol{\Sigma}^H\boldsymbol{Y}^H = \boldsymbol{U}\boldsymbol{\Sigma}\boldsymbol{\Sigma}^H$ since $\boldsymbol{\Sigma}$ is real and diagonal, so that $\boldsymbol{\Sigma} = \boldsymbol{\Sigma}^H$

$\boldsymbol{G}\boldsymbol{G}^H = \boldsymbol{Y}\boldsymbol{\Sigma}\boldsymbol{\Sigma}^H\boldsymbol{U}\boldsymbol{\Sigma}\boldsymbol{\Sigma}^H = \boldsymbol{Y}\boldsymbol{\Sigma}^2\boldsymbol{Y}^H$

$\boldsymbol{Y}^H = \boldsymbol{Y}^{-1}$ for a unitary matrix.

Thus $\boldsymbol{Y}$ is a matrix of eigenvectors of $\boldsymbol{G}\boldsymbol{G}^H$ and $\boldsymbol{\Sigma}^2$ is a diagonal matrix of the eigenvalues of $\boldsymbol{G}\boldsymbol{G}^H$, i.e. σ_i^2, in accord with the definition of σ_i.

Similarly,

$\boldsymbol{G}^H\boldsymbol{G} = \boldsymbol{U}\boldsymbol{\Sigma}^2\boldsymbol{U}^H$

where $\boldsymbol{U}$ is a matrix of eigenvectors of $\boldsymbol{G}^H\boldsymbol{G}$.

$\boldsymbol{Y}$ and $\boldsymbol{U}$ are not unique.

Consider

$\boldsymbol{Y}' = \boldsymbol{Y}e^{j\theta}$,

$\boldsymbol{U}' = \boldsymbol{U}e^{j\theta}$

$\boldsymbol{U}'^{\mathrm{H}} = \boldsymbol{U}^{\mathrm{H}}e^{-j\theta}$

Thus

$\boldsymbol{G} = \boldsymbol{Y}'\boldsymbol{\Sigma}\boldsymbol{U}'^{\mathrm{H}} = \boldsymbol{Y}e^{j\theta}\boldsymbol{\Sigma}\boldsymbol{U}^{\mathrm{H}}e^{-j\theta} = \boldsymbol{Y}\boldsymbol{\Sigma}\boldsymbol{\Sigma}^{\mathrm{H}}$

If

$\boldsymbol{H} = \boldsymbol{U}\boldsymbol{\Sigma}^{-1}\boldsymbol{Y}^{\mathrm{H}}$

then

$$\begin{aligned}\boldsymbol{HGH} &= \left(\boldsymbol{U}\boldsymbol{\Sigma}^{-1}\boldsymbol{Y}^{\mathrm{H}}\right)\left(\boldsymbol{Y}\boldsymbol{\Sigma}\boldsymbol{\Sigma}^{\mathrm{H}}\right)\left(\boldsymbol{U}\boldsymbol{\Sigma}^{-1}\boldsymbol{Y}^{\mathrm{H}}\right)\\ &= \boldsymbol{U}\boldsymbol{\Sigma}^{-1}\boldsymbol{\Sigma}\boldsymbol{\Sigma}^{-1}\boldsymbol{Y}^{\mathrm{H}}\\ &= \boldsymbol{U}\boldsymbol{\Sigma}^{-1}\boldsymbol{Y}^{\mathrm{H}}\\ &= \boldsymbol{H}\end{aligned}$$

and

$$\begin{aligned}\boldsymbol{GHG} &= \left(\boldsymbol{Y}\boldsymbol{\Sigma}\boldsymbol{\Sigma}^{\mathrm{H}}\right)\left(\boldsymbol{U}\boldsymbol{\Sigma}^{-1}\boldsymbol{Y}^{\mathrm{H}}\right)\left(\boldsymbol{Y}\boldsymbol{\Sigma}\boldsymbol{\Sigma}^{\mathrm{H}}\right)\\ &= \boldsymbol{Y}\boldsymbol{\Sigma}\boldsymbol{\Sigma}^{-1}\boldsymbol{\Sigma}\boldsymbol{U}^{\mathrm{H}}\\ &= \boldsymbol{Y}\boldsymbol{\Sigma}\boldsymbol{\Sigma}^{\mathrm{H}}\\ &= \boldsymbol{G}\end{aligned}$$

Thus $\boldsymbol{H}$ is a *pseudoinverse* of $\boldsymbol{G}$.

A2.17 Controllability

Consider the discrete state space system:

$\boldsymbol{x}(k+1) = \boldsymbol{A}\boldsymbol{x}(k) + \boldsymbol{B}\boldsymbol{u}(k)$

Then

$x(1) = \boldsymbol{A}\boldsymbol{x}(0) + \boldsymbol{B}\boldsymbol{u}(0)$

$\boldsymbol{x}(2) = \boldsymbol{A}\boldsymbol{x}(1) + \boldsymbol{B}\boldsymbol{u}(1)$

$\boldsymbol{x}(2) = \boldsymbol{A}(\boldsymbol{A}\boldsymbol{x}(0) + \boldsymbol{B}\boldsymbol{u}(0)) + \boldsymbol{B}\boldsymbol{u}(1)$

$\boldsymbol{x}(2) = \boldsymbol{A}^2\boldsymbol{x}(0) + \boldsymbol{A}\boldsymbol{B}\boldsymbol{u}(0) + \boldsymbol{B}\boldsymbol{u}(1)$

$\boldsymbol{x}(3) = \boldsymbol{A}(\boldsymbol{A}^2\boldsymbol{x}(0) + \boldsymbol{A}\boldsymbol{B}\boldsymbol{u}(0) + \boldsymbol{B}\boldsymbol{u}(1)) + \boldsymbol{B}\boldsymbol{u}(2)$

$\boldsymbol{x}(3) = \boldsymbol{A}^3\boldsymbol{x}(0) + \boldsymbol{A}^2\boldsymbol{B}\boldsymbol{u}(0) + \boldsymbol{A}\boldsymbol{B}\boldsymbol{u}(1) + \boldsymbol{B}\boldsymbol{u}(2)$

Thus

$$\boldsymbol{x}(n) = \boldsymbol{A}^{n}\mathrm{x}(0) + \boldsymbol{A}^{n-1}\boldsymbol{B}\boldsymbol{u}(0) \ldots + \boldsymbol{A}^{n-i}\boldsymbol{B}\boldsymbol{u}(i\text{-}1) \ldots \boldsymbol{B}\boldsymbol{u}(n\text{-}1)$$

$$\boldsymbol{x}(n) = \boldsymbol{A}^{n}\boldsymbol{x}(0) + \begin{bmatrix}\boldsymbol{B} & \boldsymbol{AB} & \ldots & \boldsymbol{A}^{n-1}\mathrm{B}\end{bmatrix}\begin{bmatrix}\boldsymbol{u}(n-1)\\ \boldsymbol{u}(n-2)\\ \ldots.\\ \boldsymbol{u}(0)\end{bmatrix}$$

Rewrite as

$\boldsymbol{x}(n) - \boldsymbol{A}^{n}\boldsymbol{x}(0) = \boldsymbol{PU}$

Or

$\boldsymbol{PU} = \boldsymbol{C}$

For this equation to be soluble, $\boldsymbol{P}$ must be of full rank. The height of $\boldsymbol{P}$ is equal to the number of states. Thus rank of $\boldsymbol{P}$ must be equal to number of states.

A2.18 The Riccati Equation

Consider the dynamic system

$$\dot{\boldsymbol{x}} = \boldsymbol{A}\boldsymbol{x} + \boldsymbol{B}\boldsymbol{u} \qquad (1)$$

and the control law

$$\boldsymbol{u} = -\boldsymbol{G}\boldsymbol{x} \qquad (2)$$

The optimal control problem may be expressed as the desire to find the gain matrix $\boldsymbol{G}$ which minimises a cost function V which is defined as

$$V = \int_{t}^{T} [\boldsymbol{x}'(\tau)\boldsymbol{Q}(\tau)\boldsymbol{x}(\tau) + \boldsymbol{u}'(\tau)\boldsymbol{R}\boldsymbol{u}(\tau)]d\tau \qquad (3)$$

$\boldsymbol{Q}$ and $\boldsymbol{R}$ are symmetric matrices chosen by the designer to penalise states $\boldsymbol{x}$ or control effort $\boldsymbol{u}$.

T is the end time; t is present time; $(T\text{-}t)$ is remaining time. If T is set to ∞ then the integral runs from now into steady state. (See below.)

$\boldsymbol{x'Qx}$ penalises departure of state vector from the origin;

$\boldsymbol{u'Ru}$ penalises or limits the magnitude of control effort.

Consider now the closed loop:

$$\begin{aligned}\dot{\boldsymbol{x}} &= \boldsymbol{A}\boldsymbol{x} - \boldsymbol{B}\boldsymbol{G}\boldsymbol{x} \\ &= \boldsymbol{A}_{\boldsymbol{c}}\boldsymbol{x} \\ \boldsymbol{A}_{\boldsymbol{c}} &= \boldsymbol{A} - \boldsymbol{B}\boldsymbol{G}\end{aligned} \tag{4}$$

$\boldsymbol{A_c}$ is the closed loop dynamic matrix. If $\boldsymbol{A_c}$ is time invariant, then

$$\boldsymbol{x}(t) = e^{\boldsymbol{A}_c t}\boldsymbol{c} \tag{5}$$

is a solution where $\boldsymbol{c}$ is a constant vector which may be evaluated by reference to initial conditions.

If $\boldsymbol{A_c}$ is time invariant, then

$$\begin{aligned}\boldsymbol{x}(\tau) &= e^{\boldsymbol{A}_c \tau}\boldsymbol{c} \\ &= e^{\boldsymbol{A}_c(\tau - t)}\boldsymbol{x}(t)\end{aligned} \tag{6}$$

More generally, in a linear system which is unforced (homogenous), the current state at time τ depends only on the state at time t, according to a linear relationship

$$\boldsymbol{x}(\tau) = \boldsymbol{\Phi}_c(\tau, t)\boldsymbol{x}(t) \tag{7}$$

where $\boldsymbol{\Phi}_c(\tau, t)$ is the state transition matrix corresponding to $\boldsymbol{A_c}$**.**

Thus, transposing,

$$\boldsymbol{x}'(\tau) = \boldsymbol{x}'(t)\boldsymbol{\Phi}_c^{'}(\tau, t) \tag{8}$$

Also, transposing eq. (2),

$$\begin{aligned}\boldsymbol{u}(t) &= -\boldsymbol{G}\boldsymbol{x}(t) \\ \boldsymbol{u}'(t) &= -\boldsymbol{x}'(t)\boldsymbol{G}'\end{aligned} \tag{9}$$

By using eq. (8) and eq. (9) the expression for the cost function eq. (3)may now be re-written as

$$\begin{aligned}V(t) &= \int_t^T \left[\boldsymbol{x}'(t)\boldsymbol{\Phi}_c^{'}(\tau, t)\boldsymbol{Q}(\tau)\boldsymbol{\Phi}_c(\tau, t)\boldsymbol{x}(t) + \boldsymbol{x}'(t)\boldsymbol{\Phi}_c^{'}(\tau, t)\boldsymbol{G}'\boldsymbol{R}\boldsymbol{G}\boldsymbol{\Phi}_c(\tau, t)\boldsymbol{x}(t)\right] d\tau \\ &= \int_t^T \left[\boldsymbol{x}'(t)\boldsymbol{\Phi}_c^{'}(\tau, t)[\boldsymbol{Q} + \boldsymbol{G}'\boldsymbol{R}\boldsymbol{G}]\boldsymbol{\Phi}_c(\tau, t)\boldsymbol{x}(t)\right] d\tau\end{aligned} \tag{10}$$

Now define

$$\boldsymbol{M}(t, T) = \int_t^T \boldsymbol{\Phi}_c^{'}(\tau, t)[\boldsymbol{Q} + \boldsymbol{G}'\boldsymbol{R}\boldsymbol{G}]\boldsymbol{\Phi}_c(\tau, t) d\tau \tag{11}$$

$\boldsymbol{Q}$ and $\boldsymbol{R}$ are symmetric (by definition); thus $\boldsymbol{M}$ is symmetric.

$$V = \boldsymbol{x}'(t)\boldsymbol{M}(t,T)\boldsymbol{x}(t) \tag{12}$$

Thus to minimise V, it is necessary to find $\boldsymbol{G}$ which minimises $\boldsymbol{M}$.

By using eq. (7), eq. (8) and eq. (10) it is also convenient to write

$$V = \int_t^T \boldsymbol{x}'(\tau)\boldsymbol{L}(\tau)\boldsymbol{x}(\tau)d\tau \tag{13}$$

and, from eq. (11),

$$\boldsymbol{M}(t,T) = \int_t^T \boldsymbol{\Phi}_c'(\tau,t)\boldsymbol{L}(\tau)\boldsymbol{\Phi}_c(\tau,t)d\tau \tag{14}$$

where

$$\boldsymbol{L} = \boldsymbol{Q} + \boldsymbol{G}'\boldsymbol{R}\boldsymbol{G} \tag{15}$$

Noting that

$$\begin{aligned} \frac{dV}{dt} &= -\boldsymbol{x}'(\tau)\boldsymbol{L}(\tau)\boldsymbol{x}(\tau) \,\Big|_{\tau = t} \\ &= -\boldsymbol{x}'(t)\boldsymbol{L}(t)\boldsymbol{x}(t) \end{aligned} \tag{16}$$

because

$$\begin{aligned} V &= \left[\int \boldsymbol{x}'(\tau)\boldsymbol{L}(\tau)\boldsymbol{x}(\tau)d\tau\right]_{\tau = T} - \left[\int \boldsymbol{x}'(\tau)\boldsymbol{L}(\tau)\boldsymbol{x}(\tau)d\tau\right]_{\tau = t} \\ \frac{dV}{dt} &= 0 - \frac{d}{dt}\left[\int \boldsymbol{x}'(\tau)\boldsymbol{L}(\tau)\boldsymbol{x}(\tau)d\tau\right]_{\tau = t} \end{aligned} \tag{17}$$

Also, differentiating eq. (12),

$$\frac{dV}{dt} = \dot{\boldsymbol{x}}'(t)\boldsymbol{M}(t,T)\boldsymbol{x}(t) + \boldsymbol{x}'(t)\dot{\boldsymbol{M}}(t,T)\boldsymbol{x}(t) + \boldsymbol{x}'(t)\boldsymbol{M}(t,T)\dot{\boldsymbol{x}}(t) \tag{18}$$

where

$$\dot{\boldsymbol{M}}(t,T) = \frac{\partial \boldsymbol{M}(t,T)}{\partial t}$$

Using simplified notation from now on, and noting the relationships (from eq. (4)),

$$\begin{aligned} \dot{\boldsymbol{x}} &= \boldsymbol{A}_c \boldsymbol{x} \\ \dot{\boldsymbol{x}}' &= \boldsymbol{x}' \boldsymbol{A}_c' \end{aligned} \tag{19}$$

the time derivatives of the state vector may be substituted in eq. (18) to give:

$$\frac{dV}{dt} = \boldsymbol{x}' [\boldsymbol{A}_c' \boldsymbol{M} + \dot{\boldsymbol{M}} + \boldsymbol{M}\boldsymbol{A}_c] \boldsymbol{x} \tag{20}$$

Thus, by equating the relationships (16) and (18) for $\frac{dV}{dt}$, re-arranging and substituting using eq. (4) and eq. (15),

$$\begin{aligned} -\boldsymbol{L} &= \boldsymbol{A}_c' \boldsymbol{M} + \dot{\boldsymbol{M}} + \boldsymbol{M}\boldsymbol{A}_c \\ -\dot{\boldsymbol{M}} &= \boldsymbol{M}\boldsymbol{A}_c + \boldsymbol{A}_c' \boldsymbol{M} + \boldsymbol{L} \\ -\dot{\boldsymbol{M}} &= \boldsymbol{M}(\boldsymbol{A} - \boldsymbol{B}\boldsymbol{G}) + (\boldsymbol{A}' - \boldsymbol{G}'\boldsymbol{B}')\boldsymbol{M} + \boldsymbol{Q} + \boldsymbol{G}'\boldsymbol{R}\boldsymbol{G} \end{aligned} \tag{21}$$

To solve the optimisation problem, V must be made as small as possible. Thus $\boldsymbol{M}$ must be as small as possible. Finding $\boldsymbol{G}$ which makes $\boldsymbol{M}$ as small as possible solves the optimal control problem. The sense in which $\boldsymbol{M}$ is to be made small is defined by its quadratic form $\boldsymbol{x}'\boldsymbol{M}\boldsymbol{x}$.

Defining $\hat{V}$ as the minimum value of V enables the minimum value of $\boldsymbol{M}$, $\hat{\boldsymbol{M}}$, to be defined through

$$\begin{aligned} \hat{V} &= \boldsymbol{x}' \hat{\boldsymbol{M}} \boldsymbol{x} \\ \boldsymbol{x}' \hat{\boldsymbol{M}} \boldsymbol{x} &< \boldsymbol{x}' \boldsymbol{M} \boldsymbol{x} \quad \forall \quad \boldsymbol{M} \neq \hat{\boldsymbol{M}} \end{aligned} \tag{22}$$

These relations must be true for any initial state $\boldsymbol{x}(t)$. $\hat{\boldsymbol{G}}$ corresponds to $\hat{\boldsymbol{M}}$.

Redefine $\boldsymbol{M}$ and $\boldsymbol{G}$ as follows:

$$\begin{aligned} \boldsymbol{M} &= \hat{\boldsymbol{M}} + \boldsymbol{N} \\ \boldsymbol{G} &= \hat{\boldsymbol{G}} + \boldsymbol{Z} \end{aligned} \tag{23}$$

Substituting in eq. (21) for $\boldsymbol{M}$ and $\boldsymbol{G}$ gives

$$-(\dot{\hat{\boldsymbol{M}}} + \dot{\boldsymbol{N}}) = (\hat{\boldsymbol{M}} + \boldsymbol{N})[\boldsymbol{A} - \boldsymbol{B}(\hat{\boldsymbol{G}} + \boldsymbol{Z})] + [\boldsymbol{A}' - (\hat{\boldsymbol{G}}' + \boldsymbol{Z}')\boldsymbol{B}']\boldsymbol{M} + \boldsymbol{Q} + (\hat{\boldsymbol{G}}' + \boldsymbol{Z}')\boldsymbol{R}(\hat{\boldsymbol{G}} + \boldsymbol{Z}) \tag{24}$$

Also, from eq. (21),

$$-\dot{\hat{\boldsymbol{M}}} = \hat{\boldsymbol{M}}(\boldsymbol{A}-\boldsymbol{B}\hat{\boldsymbol{G}}) + (\boldsymbol{A}'-\hat{\boldsymbol{G}}'\boldsymbol{B}')\hat{\boldsymbol{M}} + \boldsymbol{Q} + \hat{\boldsymbol{G}}'\boldsymbol{R}\hat{\boldsymbol{G}} \tag{25}$$

Eliminating $\dot{\hat{\boldsymbol{M}}}$ by subtraction of eq. (25) from eq. (24) yields

$$-\dot{\boldsymbol{N}} = \boldsymbol{N}\boldsymbol{A}_c + \boldsymbol{A}_c'\boldsymbol{N} + (\hat{\boldsymbol{G}}'\boldsymbol{R} - \hat{\boldsymbol{M}}\boldsymbol{B})\boldsymbol{Z} + \boldsymbol{Z}'(\boldsymbol{R}\hat{\boldsymbol{G}} - \boldsymbol{B}'\hat{\boldsymbol{M}}) + \boldsymbol{Z}'\boldsymbol{R}\boldsymbol{Z} \tag{26}$$

where

$$\boldsymbol{A}_c = \boldsymbol{A} - \boldsymbol{B}(\hat{\boldsymbol{G}} + \boldsymbol{Z})$$

Thus, by analogy to the definition of $\boldsymbol{M}(t,T)$ in eq. (11),

$$\boldsymbol{N}(t,T) = \int_t^T \boldsymbol{\Phi}_c'(\tau,t)[(\hat{\boldsymbol{G}}'\boldsymbol{R} - \hat{\boldsymbol{M}}\boldsymbol{B})\boldsymbol{Z} + \boldsymbol{Z}'(\boldsymbol{R}\hat{\boldsymbol{G}} - \boldsymbol{B}'\hat{\boldsymbol{M}}) + \boldsymbol{Z}'\boldsymbol{R}\boldsymbol{Z}]\boldsymbol{\Phi}_c(\tau,t)d\tau \tag{27}$$

Now from eq. (23)and eq. (24)

$$\begin{aligned} \hat{V} &= \boldsymbol{x}'\hat{\boldsymbol{M}}\boldsymbol{x} \\ \boldsymbol{x}'\hat{\boldsymbol{M}}\boldsymbol{x} &\le \boldsymbol{x}'(\hat{\boldsymbol{M}} + \boldsymbol{N})\boldsymbol{x} \\ \boldsymbol{x}'\hat{\boldsymbol{M}}\boldsymbol{x} &\le \boldsymbol{x}'\hat{\boldsymbol{M}}\boldsymbol{x} + \boldsymbol{x}'\boldsymbol{N}\boldsymbol{x} \end{aligned} \tag{28}$$

This requires that $\boldsymbol{x}'\boldsymbol{N}\boldsymbol{x}$ is positive or zero. Thus $\boldsymbol{N}(t,T)$ is positive definite or positive semi-definite.

By reference to the integral expression for $\boldsymbol{N}(t,T)$ in eq. (27) above, it is clear that for 'small' $\boldsymbol{Z}$ (when the quadratic term is dominated by the linear terms) the optimal value of $\boldsymbol{G}$ is given by

$$\begin{aligned} \boldsymbol{R}\hat{\boldsymbol{G}} &= \boldsymbol{B}'\hat{\boldsymbol{M}} \\ \hat{\boldsymbol{G}} &= \boldsymbol{R}^{-1}\boldsymbol{B}'\hat{\boldsymbol{M}} \end{aligned} \tag{29}$$

or, equivalently, since $\boldsymbol{R}$ and $\boldsymbol{M}$ are symmetrical

$$\begin{aligned} \hat{\boldsymbol{G}}'\boldsymbol{R} &= \hat{\boldsymbol{M}}\boldsymbol{B} \\ \hat{\boldsymbol{G}}' &= \hat{\boldsymbol{M}}\boldsymbol{B}\boldsymbol{R}^{-1} \\ \hat{\boldsymbol{G}} &= (\hat{\boldsymbol{M}}\boldsymbol{B}\boldsymbol{R}^{-1})' \\ &= (\boldsymbol{B}\boldsymbol{R}^{-1})'\hat{\boldsymbol{M}}' \\ &= (\boldsymbol{R}^{-1})'\boldsymbol{B}'\hat{\boldsymbol{M}}' \\ &= \boldsymbol{R}^{-1}\boldsymbol{B}'\hat{\boldsymbol{M}} \end{aligned} \tag{30}$$

To find $\hat{\boldsymbol{M}}$, substitute for $\hat{\boldsymbol{G}}$ in eq. (25) to give

$$-\dot{\hat{\boldsymbol{M}}} = \hat{\boldsymbol{M}}\boldsymbol{A} + \boldsymbol{A}'\hat{\boldsymbol{M}} - \hat{\boldsymbol{M}}\boldsymbol{B}\boldsymbol{R}^{-1}\boldsymbol{B}'\hat{\boldsymbol{M}} + \boldsymbol{Q} \tag{31}$$

This latter expression has become known as 'the Riccati equation'.

Now consider the 'steady state'. It is necessary to find the control gain $\overline{\boldsymbol{G}}$ which minimises the cost function

$$V_\infty = \int_t^\infty [\boldsymbol{x}'(\tau)\boldsymbol{Q}(\tau)\boldsymbol{x}(\tau) + \boldsymbol{u}'(\tau)\boldsymbol{R}\boldsymbol{u}(\tau)]d\tau \tag{32}$$

By examining the relationship between V and $\boldsymbol{M}$ in eq. (12), it is clear that if V_∞ is finite, then $\boldsymbol{M}(t,\infty)$ is also finite, i.e. as t increases $\boldsymbol{M}$ converges to a constant value $\overline{\boldsymbol{M}}$. Thus

$$\begin{aligned} V_\infty &= \boldsymbol{x}'\overline{\boldsymbol{M}}\boldsymbol{x} \\ \dot{\overline{\boldsymbol{M}}} &= \boldsymbol{0} \end{aligned} \tag{33}$$

From eq. (31), $\overline{\boldsymbol{M}}$ is the solution of

$$\boldsymbol{0} = \overline{\boldsymbol{M}}\boldsymbol{A} + \boldsymbol{A}'\overline{\boldsymbol{M}} - \overline{\boldsymbol{M}}\boldsymbol{B}\boldsymbol{R}^{-1}\boldsymbol{B}'\overline{\boldsymbol{M}} + \boldsymbol{Q} \tag{34}$$

This is known as 'the algebraic Riccati equation' (ARE).

The optimal control gain is then, from eq. (30),

$$\overline{\boldsymbol{G}} = \boldsymbol{R}^{-1}\boldsymbol{B}'\overline{\boldsymbol{M}} \tag{35}$$

"For most design applications the following facts about the solution of the ARE will suffice:

If the system is asymptotically stable, or
If the system defined by the matrices ($\boldsymbol{A}$,$\boldsymbol{B}$) is controllable, and the system defined by ($\boldsymbol{A}$,$\boldsymbol{C}$) where $\boldsymbol{C}'\boldsymbol{C} = \boldsymbol{Q}$ is observable
Then the ARE has a unique, positive definite solution $\overline{\boldsymbol{M}}$ which minimises V_∞ when the control law

$$\boldsymbol{u} = -\boldsymbol{B}\boldsymbol{R}^{-1}\boldsymbol{B}'\overline{\boldsymbol{M}}$$

is used." (Friedland, 1987).

APPENDIX 3 Sampling Rate Selection – a Discussion of Available Advice

"The selection of sampling interval is one of the most important problems that faces the control engineer, and probably the most difficult one. A unique solution cannot be offered even theoretically and in practice one has to use a trial-and-error procedure before a suitable rate is selected in any particular case." (Zikic, 1989, p.289).

Forsythe and Goodall (1991) comment that the chosen route in which the controller is designed in the *s*-domain and transformed into the *z*-domain can be expected to give a satisfactory result when the sampling rate is 'high', i.e. the algorithmic error introduced by the emulation method reduces with increasing sampling rate (p.96); too low a sampling rate can result in stability problems. They also identify as a 'rule of thumb' the choice of a sampling frequency of ten times the system bandwidth (p.95).

A number of other 'rules of thumb' are contained in the literature. Some of these are examined briefly here.

The following 'rules of thumb' for the determination of sampling frequency ω_s or sampling interval T are listed by Edge (1997):

- $\omega_s > 10\omega_b$ where ω_b is bandwidth of closed loop system (bandwidth – lowest frequency at which the gain falls to 3 dB below its DC value);
- $\omega_s > 10\omega_n$ where ω_n is natural frequency of closed loop system;
- $T < 0.1T_s$ where T_s is the settling time of the closed loop system (only appropriate if the system is well damped);

- T < 0.1*(dominant time constant of the open-loop system). This may be inappropriate if the controller has been designed in order to produce a faster closed loop system.

The combination of the processes of sampling and reconstruction of the output signal from the digital controller using a zero order hold introduces a lag. Astrom and Wittenmark (1990) show how the zero order hold circuit can be approximated to by a time delay of half a sampling interval (p.219). The Laplace transform of a zero order hold is given by

$$G(s) = \frac{1 - e^{-Ts}}{s} \tag{1}$$

This may be expanded to

$$G(s) = \frac{1 - (1 + (-Ts) + \frac{(-Ts)^2}{2} + ...}{s} \tag{2}$$

$$= \frac{Ts - \frac{(Ts)^2}{2} + ...}{s} \tag{3}$$

$$= T(1 - \frac{Ts}{2} + ...) \tag{4}$$

They point out that the first two terms of eq. (4) correspond to the series expansion of $Te^{\frac{-sT}{2}}$ for small T. The phase lag introduced by such a pure time delay is $\tan^{-1}\left(\frac{\omega T}{2}\right)$. Their 'rule of thumb' is that an acceptable reduction in the phase margin is 5^o to 15^o. Thus at the gain crossover frequency ω_c for the open-loop:

$$\frac{\omega_c T}{2} \approx \tan 5^o \rightarrow \tan 15^o \tag{5}$$

$$\omega_c T \approx 0.15 \rightarrow 0.5 \tag{6}$$

This 'rule of thumb' therefore suggests a sampling frequency of ten to 40 times the gain crossover frequency of the open-loop including the compensator. This result may also be arrived at by noting that the expansion of the Laplace transform for the

zero order hold also approximates to the expansion of the transform for a first order lag with time constant equal to half the sampling period; the relationship between the phase lag (but not the gain) and frequency for a first order lag is similar to that for a pure time delay.

Houpis and Lamont (1985) derive the Padé approximation for the zero order hold (p.249); they show that

$$e^{x} \approx \frac{1+x/2}{1-x/2} \tag{7}$$

Thus, for the zero order hold

$$G(s) = \frac{1-e^{-Ts}}{s} \tag{8}$$

$$\approx \frac{2T}{Ts+2} \tag{9}$$

Once again, the latter transfer function eq. (9) introduces a phase shift of $\tan^{-1}\left(\frac{\omega T}{2}\right)$.

In his 'hints on sampling rate selection', Zikic (1989) includes references to the relevance of the Nyquist rate and noise rejection in the choice of sampling rate (p.288 *et seq.*). He suggests, without explanation, that it is normal to sample at 'two to four times the system rise time value', meaning that the sampling interval should lie in the range 0.25 to 0.5 of the rise time. This can be explored further for a second order system as follows.

Defining the rise time T_{r1} as the time for the output to move from 10% to 90% of the steady state output when the input is a step, one may write (Dorf, 1995, p.225)), as an approximation,

$$T_{r1} = \frac{2.16\xi + 0.60}{\omega_n} \tag{10}$$

For an under-damped system (e.g. $\xi = 0.5$) and sampling interval 0.25 of rise time,

$$\omega_s \approx 15\omega_n \tag{11}$$

Forsythe and Goodall (1991) point out that there is a complex interaction between sampling interval, controller algorithm and structure, processor word-length, and number of bits in the analogue to digital converter (p.88 *et seq.*). Their analysis shows clear benefits for controllers in which the algorithm is realised in 'canonical' rather than 'direct' form, and for the use of the δ rather than z form for emulation (p.102).

Older texts, such as Franklin and Powell (1981), place emphasis on sampling as slowly as possible to minimise the demands made on the processor (p.275 *et seq.*). The availability of modestly priced high-speed processors has now largely eliminated this as a consideration.

Vibet (1987) has shown, by reference to the work of Madwed (1953), how a suitable sampling interval may be derived from the characteristic equation of the closed loop transfer function. Madwed's method (the number series transformation method) for the solution of linear and nonlinear integro-differential equations shows that if the characteristic equation of a differential equation linearised around a working point is written as

$$a_n\sigma^{\mathrm{n}} + a_{n-1}\sigma^{\mathrm{n}-1} + \ldots + a_1\sigma + 1 = 0 \qquad (12)$$

then the number series method becomes as accurate as the analytic method if the sampling period *T* is taken as

$$T \leq \tfrac{1}{5} a_n^{\frac{1}{n}} \qquad (13)$$

It is informative to consider how this rule relates to the various 'rules of thumb' when applied to a second order system. The transfer function of a second order system may be written as

$$G(s) = \frac{\omega_n^2}{s^2 + 2\xi\omega_n s + \omega_n^2} \qquad (14)$$

From this it is clear, by the rule of eq. (13), that

$$T \leq \tfrac{1}{5} \frac{1}{\omega_n} \qquad (15)$$

But

$$T = \frac{2\pi}{\omega_s} \qquad (16)$$

Thus

$$\omega_s \geq 10\pi\,\omega_n \tag{17}$$

Consider also the bandwidth of the transfer function in eq. (14) . Its frequency response is given by

$$G(j\omega) = \frac{\omega_n^2}{-\omega^2 + 2\xi\omega_n\, j\omega + \omega_n^2} \tag{18}$$

Re-writing using the ratio of the frequency to the natural frequency $r = \frac{\omega}{\omega_n}$ yields:

$$G(j\omega) = \frac{1}{2\xi\ jr + (1 - r^2)} \tag{19}$$

Taking modulus:

$$\left|G(j\omega)\right| = \frac{1}{\sqrt{4\xi^2 r^2 + (1 - r^2)^2}} \tag{20}$$

At the bandwidth frequency, $\omega = \omega_b$ and the gain is 0.5 since the D.C. gain is 1. For the under-damped case $\xi = 0.5$, *r* may be evaluated as 1.53; for the critically damped case $\xi = 0.7071$, *r* may be evaluated as 1.732.

Thus

$$\omega_s \geq 20\,\omega_b \text{ or } \omega_s \geq 18\,\omega_b \tag{21}$$

respectively.

Franklin and Powell (1981) discuss sampling rate in the context of tracking effectiveness, disturbance rejection and sensitivity to parameter variations (p.275 *et seq.*). For effective tracking, they point out that the sampling rate must be at least double the closed loop bandwidth of the system to satisfy the sampling theorem. However, they reason that for good tracking a sampling rate of four to 20 times the closed loop bandwidth is appropriate; a ratio of 10 to 40 is shown to be appropriate for disturbance rejection. This ratio depends on the noise spectrum of the disturbance. These ideas are developed further in Franklin *et al*. (1991) (p.618 *et seq.*).

An examination of the state space representation of a discrete time system provides a pointer to the effect of too short a sampling interval.

A discrete time state space system may be represented by the equation

$$\boldsymbol{x}(kT+1) = \boldsymbol{A}_1\boldsymbol{x}(kT) + \boldsymbol{B}_1\boldsymbol{u}(kT) \tag{22}$$

By reference to the continuous state space system

$$\dot{\boldsymbol{x}}(t) = \boldsymbol{A}\boldsymbol{x}(t) + \boldsymbol{B}\boldsymbol{u}(t) \tag{23}$$

it may be shown that (e.g. Schwarzenbach and Gill, 1992, p.83)

$$\boldsymbol{A}_1 = e^{\boldsymbol{A}T} \tag{24}$$

$$= \mathbf{I} + \boldsymbol{A}T + \frac{1}{2!}(\boldsymbol{A}T)^2 + \ldots \tag{25}$$

$$\boldsymbol{B}_1 = T\left[\mathbf{I} + \frac{1}{2!}\boldsymbol{A}T + \frac{1}{3!}(\boldsymbol{A}T)^2 + \ldots\right]\boldsymbol{B} \tag{26}$$

Clearly, if the sampling interval T is 'too small' then the product $\boldsymbol{A}T$ becomes small, and the dynamic information that it contains on the system it represents may be lost in rounding and truncation in arithmetic processors.

Zikic (1989) also draws attention to the possibility that the controllability and/or observability matrices may lose rank for certain values of the sampling interval, implying loss of controllability/observability (p.291).

Kuo (1992) provides a thorough analysis and examples to show the effect of sampling interval on the matrix coefficients. Kuo (p.186) defines the state transition matrix $\boldsymbol{\varphi}(t)$ as a matrix which satisfies the homogeneous state equation

$$\frac{d\boldsymbol{x}(t)}{dt} = \boldsymbol{A}\boldsymbol{x}(t) \tag{27}$$

so

$$\frac{d\boldsymbol{\varphi}(t)}{dt} = \boldsymbol{A}\boldsymbol{\varphi}(t) \tag{28}$$

Alternatively,

$$\boldsymbol{x}(t) = \boldsymbol{\varphi}(t)\boldsymbol{x}(0) \tag{29}$$

(verifiable by substitution.)

Using Laplace transforms, it is straightforward to show that

$$\boldsymbol{\varphi}(t) = \ell^{-1}[(s\mathbf{I} - \boldsymbol{A})^{-1}] \tag{30}$$

thus

$$\varphi(t) = e^{At} \tag{31}$$

Kuo (1992) shows that if

$$\varphi(iT) = \varphi(jT) \quad (i \neq j) \tag{32}$$

then the system is neither controllable nor observable. The principle may be investigated theoretically by considering the case where elements of the state transition matrix are trigonometric functions of the sampling interval *T*. They can thus take on the same values for an infinite number of values of the sampling interval.

APPENDIX 4 Introduction to Fuzzy Logic

This section begins with an introduction to classical sets (or 'crisp' sets) and to the symbolism used. Crisp sets are so named because whether or not an object or element belongs to a set is crisply defined - it either does or does not belong. (See, for example, Stoll (1961).)

A4.1 Classical Sets

Element

Sets contain *elements*.

x is *an element* of set A or *belongs to* set A

$$x \in A$$

Elements of set A

A = {list of elements in set}

$A = \{x_1, x_2, ...x_i, ...x_n\}$

Set A consists of elements x which have a property Q

$A = \{x \mid x \text{ is } Q\}$

Set A consists of elements x which satisfy a formula $P(x)$

$A = \{x \mid P(x)\}$

Equal sets

Sets A and B are equal if and only if (i.e. iff) they contain the same elements

$$A = B$$

Subsets

B is *a subset* of A if all elements contained in B are also contained in A

$$B \subseteq A$$

B is *included* in A

B is *a proper subset* of *A* if all elements contained in *B* are also contained in *A* and set *A* contains *B* and more

$$B \subset A$$

B is *properly included* in *A*

Union

Set *C* is *union* of sets *A* and *B*

$$C = A \cup B$$

$$C = \{c \mid c \in A \text{ or } c \in B\}$$

(i.e. the set *C* is sets *A* and *B* 'added together')

Intersection

Set D is *intersection* of sets A and B

$$D = A \cap B$$

$$D = \{d \mid d \in A \text{ and } d \in B\}$$

(i.e. the set *D* is the 'overlap' of sets *A* and *B*)

Empty set

An *empty set* contains no elements

Empty set - O

Universal set

The *universal set* contains all elements relevant to the current problem.

Universal set U

Thus

$$O \subseteq A \subseteq U$$

Complement

The *complement* of set *A* contains all elements not in set *A*

$$\overline{A}$$

Thus

$$A \cap \overline{A} = O;$$

$$A \cup \overline{A} = U$$

A4.2 Fuzzy Sets

A4.2.1 Elements

In fuzzy set theory, individual *elements* (singletons) *x* are considered to exist in a *universe of discourse* (also known as *universe of information*) *X*.

Combinations of *x* make up sets *A* on the universe.

A4.2.2 Membership

For *crisp sets A*, an element *x* is either a member or not. *Membership* is indicated by the '*indicator function*' (Ross, 1995) or '*characteristic function*' (Tsoukalas and Uhrig, 1997):

$$\chi_A(x) \equiv \begin{cases} 1, x \in A \\ 0, x \notin A \end{cases}$$

or

$$\chi_A(x) : X \to \{0,1\}$$

'There exists a characteristic function $\chi_A(x)$ mapping every element of the universe of discourse *X* to the **set** $\{0,1\}$.'

Thus the characteristic function takes the value 0 or 1.

For *fuzzy sets*, membership is indicated by the '*membership function*':

$$\mu_A(x) : X \to [0,1]$$

'The membership function $\mu_A(x)$ maps every element of the universe of discourse X to the **interval** $[0,1]$.'

Fuzzy set A may be written as a collection of ordered pairs:

$$A = \{(x, \mu_A(x))\}, x \in X$$

Each pair $(x, \mu_A(x))$ is called a singleton. (For a crisp set, the singleton consists of x alone.)

The singleton may also be written $\mu_A(x)/x$. Note that '/' here is a 'marker' and does not indicate division.

A4.2.3 Support Set

The *support set* of fuzzy set *A* is the set of its elements which have non-zero membership.

A is the union of all the singletons:

$$A = \sum_{x_i \in X} \mu_A(x_i) / x_i$$

for a discrete universe of discourse.

$$A = \int_X \mu_A(x) / x$$

for a continuous universe of discourse.

A4.2.4 Fuzzification

$$F(A;K) = \int_X \mu_A(x).\mu_{K(x)}(x) / x$$

$F(A;K)$ is a fuzzy set which results from the fuzzification of crisp set *A* in accordance with the fuzzy kernel *K*(*x*), or from changing the fuzziness of a fuzzy set *A* in accordance with the fuzzy kernel *K*(*x*). *K*(*x*) is the fuzzy set which results from the application of fuzzyfier *F* to singleton *x*.

A4.2.5 Ordered Pairs

Given two objects *x* and *y*, there exists another object called the '*ordered pair*' of *x* and *y*, written <*x*,*y*>. An ordered sequence of *r* objects is called an 'ordered *r*-tuple'.

A4.2.6 Cartesian Product

The *Cartesian product* of sets *X* and *Y* is the set of all ordered pairs <*x*,*y*>.

$$X \times Y = \{< x, y > | \, x \in X, and, y \in Y\}$$

Its characteristic function may be written

$$\chi_{X \times Y} < x, y > = \begin{cases} 1, < x, y > \in X \times Y \\ 0, < x, y > \notin X \times Y \end{cases}$$

The Cartesian product $X \times Y$ (or product space) is itself a 'universe of discourse' for ordered pairs <*x*,*y*> where *X* and *Y* are themselves universes of discourse.

A4.3 Relations

A4.3.1 Crisp Relations

A binary *relation* is concerned with the existence or otherwise of some sort of 'bond' between pairs of 'objects' considered in a definite order.

Example:

"is greater than"

Higher order relations also exist, e.g. ternary relations are concerned with triplets of objects.

If an ordered pair <*x*,*y*> is in a relation *R* ('satisfies' *R*) then

$$< x, y > \in R$$

This may also be written

$$xRy$$

This is analogous to '$x>y$' if *R* is the relation "is greater than".

A relation *R* may be considered as a subset of $X \times Y$ whose members are only those ordered pairs which satisfy the relationship.

Thus

$$\chi_R < x, y >= \begin{cases} 1, < x, y > \in R \\ 0, < x, y > \notin R \end{cases}$$

For example

X={1,3,5}

and

Y={2,4,6}

$$X \times Y = \{<1,2>, <1,4>, <1,6>, <3,2>, <3,4>, <3,6>, <5,2>, <5,4>, <5,6>\}$$

For the relation 'is greater than'

$$R = \{<3,2>, <5,2>, <5,4>\}$$

It is possible to show this relation in the form of a 'relation matrix'

$$\begin{bmatrix} 0 & 0 & 0 \\ 1 & 0 & 0 \\ 1 & 1 & 0 \end{bmatrix}$$

This may be understood by reference to

$$\begin{matrix} & \begin{bmatrix} 2 & 4 & 6 \end{bmatrix} \\ \begin{bmatrix} 1 \\ 3 \\ 5 \end{bmatrix} & \begin{bmatrix} 0 & 0 & 0 \\ 1 & 0 & 0 \\ 1 & 1 & 0 \end{bmatrix} \end{matrix}$$

A4.3.2 Fuzzy Relations

The ideas of crisp relations can be extended to enable fuzzy relations to be defined. A binary fuzzy relation *R* on a discrete Cartesian product $X \times Y$ may be expressed as a list of all the pairs (*x*,*y*) in its relation together with the grade of membership $\mu_R(x, y)$ each has in the relation:

$$R = \{((x, y), \mu_R(x, y))\}$$

or alternatively

$$R = \sum_{(x_i, y_j) \in X \times Y} \mu_R(x_i, y_j) / (x_i, y_j)$$

For continuous universes of discourses, leading to continuous Cartesian products,

$$R = \int_{X \times Y} \mu_R(x, y) / (x, y)$$

The relation may also be expressed as a relation matrix or membership matrix for a discrete Cartesian product $X \times Y$

$$\begin{bmatrix} \mu_R(x_1, y_1) & \mu_R(x_1, y_2) & .... & .... \\ \mu_R(x_2, y_1) & \mu_R(x_2, y_2) & .... & .... \\ \mu_R(x_3, y_1) & .... & .... & .... \\ .... & .... & .... & .... \end{bmatrix}$$

A4.3.3 Composition

If there is a fuzzy relation R_1 in a discrete product space $X \times Y$ and another R_2 in the discrete product space $Y \times Z$ then a new relation R_3 in the product space $X \times Z$ is known as the composition of R_1 and R_2

$$R_3 \equiv R_1 \circ R_2$$

For each (x,z) pair in the new relation R_3 the grade of membership is

$$\mu_{R_3}(x,z) = \vee_{y \in Y}\left[\mu_{R_1}(x,y) \wedge \mu_{R_2}(y,z)\right]$$

Here, $\vee$ is the maximum operator and $\wedge$ is the minimum operator.

This is the 'max-min' composition rule. The grade of membership for each (x,z) in the relation R_3 is found as the maximum over all y of the minima of the membership grades of R_1 and R_2. Clearly, and by analogy to matrix multiplication, the number of columns in fuzzy relation R_1 must match the number of rows in fuzzy relation R_2; the number of columns in fuzzy relation R_3 is the same as the number of columns in fuzzy relation R_2 and the number of rows in fuzzy relation R_3 is the same as the number of rows in fuzzy relation R_1.

A4.3.4 Propositions

A proposition is a linguistic statement which may be true or false, or, in fuzzy logic, to which a degree of truth may be assigned.

Consider the following

Proposition *A* : creature *x* is a bird;

Proposition *B* : creature *x* can fly.

Veracity (binary truth value) of a Proposition *P* is *T*(*P*).

A4.3.5 Compound Propositions

Simple propositions may be compounded using connectives to produce compound propositions. These have their own 'veracity' which may be determined by truth tables as indicated below:

1. Creature *x* is a bird **and** creature x can fly.

creature x	*T*(*A*)	*T*(*B*)	*T*(*A* and *B*)
cat	0	0	0
bee	0	1	0
eagle	1	1	1
chicken	1	0	0

2. Creature *x* is a bird **or** creature *x* can fly.

creature *x*	*T*(*A*)	*T*(*B*)	*T*(*A* or *B*)
cat	0	0	0

bee	0	1	1
eagle	1	1	1
chicken	1	0	1

3. **If** creature *x* is a bird **then** creature *x* can fly.

creature x	*T*(*A*)	*T*(*B*)	*T*(If *A* then *B*)
cat	0	0	1
bee	0	1	1
eagle	1	1	1
chicken	1	0	0

The last example 3. is an example of a conditional compound proposition of the form **if** *antecedent* **then** *consequent*.

> "... in this case normal English usage is not helpful in constructing a truth table, and the table that we use is a common source of intuitive difficulty. The difficulty arises with the truth value *T* assigned to (If *A* then *B*) in the cases where *A* is false. Consideration of examples of conditional statements in which the antecedent is false might perhaps lead one to the conclusion that such statements do not have a truth value at all. One might also gain the impression that such statements are not useful or meaningful...The significance of a conditional statement (If *A* then *B*) is that its truth enables the truth of *B* to be inferred from the truth of *A*, and nothing in particular to be inferred from the falsity of *A*." (Hamilton,1978.)

If C is the set of all birds and D is the set of all flying creatures,

$$A : x \in C$$

$$\overline{A} : x \notin C$$

$$B : x \in D$$

$$\overline{B} : x \notin D$$

So

$T(A) = 1$ means $x \in C$

$T(A) = 0$ means $x \notin C$

$T(B) = 1$ means $x \in D$

$T(B) = 0$ means $x \notin D$

From the table above,

T(If A then B) =1 if $T(A) = 0$ or if $T(B) = 1$

and thus

T(If A then B) =1 if $x \notin C$ or $x \in D$

that is if

$$x \in (\overline{C} \cup D)$$

But

$$\overline{A} : x \in \overline{C}$$

so

$$x \in (\overline{C} \cup D)$$

means

$\overline{A}$ or B

which may be written

$$\overline{A} \vee B$$

A4.3.6 Implications

The compound proposition

If A then B

is known as an *implication.*

The implication is commonly written

$$A \rightarrow B$$

Finally

$$T(A \rightarrow B) = T(\overline{A} \vee B)$$

A4.4 Linguistic Rules

An example of a linguistic rule is

IF A THEN B

What does this mean?

Consider an event x, drawn from a Universe X. Assume that the rule is satisfied, that is, it is true. Consider also the consequence of x, which is y, contained in a Universe Y.

(1) Then if x is contained in set A, which is defined in X, the resulting y is contained

in *B*, defined in *Y*.

(2) If *x* is *not* contained in set *A*, then *any* consequence *y* is consistent with the rule being satisfied, for the rule makes no statement about this eventuality.

The rule does not indicate how a *y* which is not in *B* might result. If *x* is in *A* and the resulting y is outside *B*, the rule will have been broken.

Now consider the Cartesian space $X \times Y$. The region in it defined in (1) above is $A \times B$.The region in it defined by (2) contains the entire *Y* and that part of *X* which is outside *A*, i.e. $\overline{A}$ .This region is thus $\overline{A} \times Y$. The rule may be expressed as a relation in the Cartesian space $X \times Y$ which is the union of the two components $A \times B$ and $\overline{\mathrm{A}} \times \mathrm{Y}$. The rule IF *A* THEN *B* may thus be represented by the relation

$$(A \times B) \bigcup (\overline{A} \times Y)$$

Now consider

IF *A* THEN *B* ELSE *C*

This rule may be rewritten linguistically as

IF *A* THEN *B* OR IF $\overline{A}$ THEN *C*

in which *B* and *C* are both sets defined in *Y*. Clearly, for the rule to hold, the *y* which results from any x must lie either in *B* or in *C*.

As above,

(1) If *x* is contained in set *A*, which is defined in *X*, the resulting *y* is contained in *B*, defined in *Y*.

(2) Then if *x* is *not* contained in set *A*, i.e. *x* is in $\overline{A}$, the resulting *y* is contained in *C*, also defined in *Y*.

Now consider the Cartesian space $X \times Y$. The region in it defined in (1) above is $A \times B$. The region in it defined in (2) above is $\overline{A} \times C$. The rule may be expressed as a relation in the Cartesian space $X \times Y$ which is the union of the two components $A \times B$ and $\overline{A} \times C$. The rule IF A THEN B ELSE C may thus be represented by the relation

$$(A \times B) \bigcup (\overline{A} \times C)$$

These relations may also be expressed in terms of characteristic functions:

IF *A* THEN *B*

$$(A \times B) \bigcup (\overline{A} \times Y)$$

Consider first $(A \times B)$

$$\chi_{X \times Y} < x, y >= \begin{cases} 1, < x, y > \in A \times B \\ 0, < x, y > \notin A \times B \end{cases}$$

Clearly, the ordered pair <*x*,*y*> is a member of $A \times B$ if both *x* is a member of A and *y* is member of *B*, that is if $\chi_A(x) = 1$ and $\chi_B(y) = 1$

So

$$\chi_{A \times B} < x, y >= \chi_A(x) \wedge \chi_B(y)$$

Similarly, <*x*,*y*> is a member of $(\overline{A} \times Y)$ if both *x* is a member of $\overline{A}$ and *y* is member of *Y*.

$$\chi_{\overline{A} \times Y} < x, y >= \chi_{\overline{A}}(x) \wedge \chi_Y(y)$$

But $\chi_{\overline{A}}(x) = 1 - \chi_A(x)$

and $\chi_Y(y) = 1$

since Y is the universe which contains y.

So

$$\chi_{\overline{A} \times Y} < x, y >= (1 - \chi_A(x)) \wedge 1$$

$$= (1 - \chi_A(x))$$

The 'union' in the relation is represented by a 'maximum' operator to create the characteristic function for the entire relation:

$$\chi_R < x, y >= (\chi_A(x) \wedge \chi_B(y)) \vee (1 - \chi_A(x))$$

IF A THEN B ELSE C

$$(A \times B) \bigcup (\overline{A} \times C)$$

Consider first $(A \times B)$

Then, as above,

$$\chi_{A \times B} < x, y >= \chi_A(x) \wedge \chi_B(y)$$

Similarly, <*x*,*y* > is a member of $(\overline{A} \times C)$ if both *x* is a member of $\overline{A}$ and *y* is member of *C*.

$$\chi_{\bar{A}\times C} < x, y >= \chi_{\bar{A}}(x) \wedge \chi_C(y)$$

But

$$\chi_{\bar{A}}(x) = 1 - \chi_A(x)$$

So

$$\chi_{\bar{A}\times C} < x, y >= (1 - \chi_A(x)) \wedge \chi_C(y)$$

The 'union' in the relation is represented by a 'maximum' operator to create the characteristic function for the entire relation:

$$\chi_R < x, y >= (\chi_A(x) \wedge \chi_B(y)) \vee ((1 - \chi_A(x)) \wedge \chi_C(y))$$

A4.5 Implications with Multiple Antecedents

In a control problem, the linguistic rules often have multiple antecedents. For example, if the 'error' in a system is defined as the difference between the required and actual outputs, a linguistic rule might be:

IF ERROR IS LARGE AND RATE OF INCREASE OF ERROR IS LARGE, THEN CONTROLLER OUTPUT IS MAXIMUM

By analogy with the preceding section, such a rule may be written in the form

IF A_1 AND A_2 THEN B

What does this mean?

Consider an event x_1, drawn from a Universe X_1 and an event x_2, drawn from a Universe X_2. Assume that the rule is satisfied, that is, it is true. Consider also the consequence of x_1 and x_2, which is y, contained in a Universe Y.

(1) Then if x_1 is contained in set A_1, which is defined in X_1, and x_2 is contained in set A_2, which is defined in X_2 the resulting y is contained in B, defined in Y.

(2) If x_1 is *not* contained in set A_1, or x_2 is *not* contained in set A_2 then *any* consequence y is consistent with the rule being satisfied, for the rule makes no statement about this eventuality.

The rule does not indicate how a y which is not in B might result. If x_1 is contained in set A_1 and x_2 is contained in set A_2 and the resulting y is outside B, the rule will have been broken.

Now consider the Cartesian space $X_1 \times X_2 \times Y$. The region in it defined in (1) above is $A_1 \times A_2 \times B$. (See Figure A4.1 below.)

The region in the space defined by (2) contains the entire Y and that part of $X_1 \times X_2$ which is outside $A_1 \times A_2$, i.e. $\overline{A_1 \times A_2}$.

But

$$\overline{A_1 \times A_2} = (\overline{A_1} \times X_2) \cup (\overline{A_2} \times X_1)$$

The region defined by (2) is thus.

$$(\overline{A_1} \times X_2 \times Y) \cup (\overline{A_2} \times X_1 \times Y)$$

The rule may be expressed as a relation in the Cartesian space $X_1 \times X_2 \times Y$ which is the union of the two components $A_1 \times A_2 \times B$ and $(\overline{A_1} \times X_2 \times Y) \cup (\overline{A_2} \times X_1 \times Y)$.

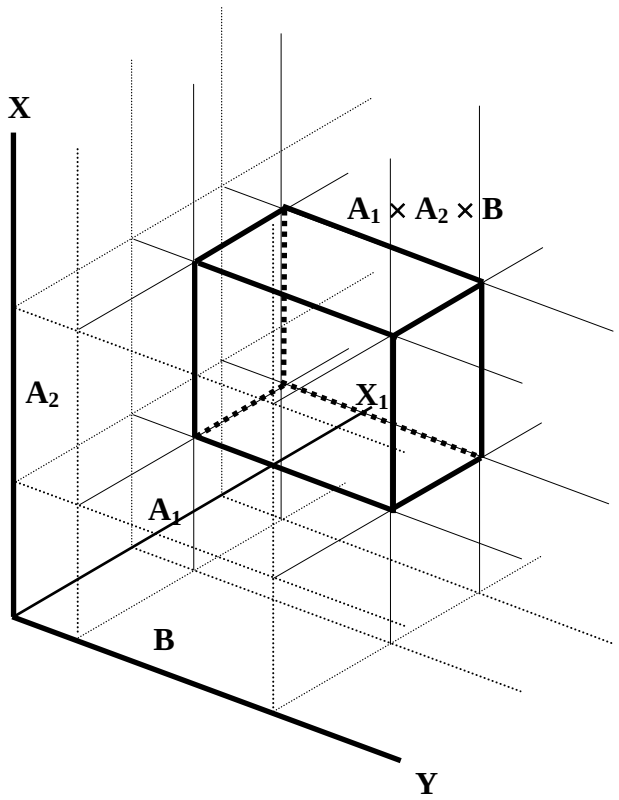

Figure A4.1 Cartesian Space

The rule IF A_1 AND A_2 THEN B may thus be represented by the relation

$$(A_1 \times A_2 \times B) \cup (\overline{A_1} \times X_2 \times Y) \cup (\overline{A_2} \times X_1 \times Y)$$

This may be visualised as a solid in three dimensional space. The projection of this solid on to the X_1 Y plane is a two dimensional space which represents

$(A_1 \times B) \cup (\overline{A_1} \times Y)$. This has already been shown to be the relation which represents the linguistic rule IF A_1 THEN *B*. The foregoing suggests how relations for multiple antecedents may be developed.

An alternative approach to developing a relation for the rule IF A_1 AND A_2 THEN B is as follows:

Consider again IF A THEN B

Now define

$$A = A_1 \times A_2$$

(An interpretation of this is that '*x* is in *A*' means that 'x_1 is in A_1 and x_2 is in A_2')

Then

$$\overline{A} = \overline{A_1 \times A_2}$$

But

$$\overline{A_1 \times A_2} = (\overline{A_1} \times X_2) \cup (\overline{A_2} \times X_1)$$

So now

$$(A \times B) \cup (\overline{A} \times Y) = (A_1 \times A_2 \times B) \cup (\overline{A_1 \times A_2} \times Y)$$

Thus the relation for the multiple antecedent rule may be written

$$(A_1 \times A_2 \times B) \cup (\overline{A_1} \times X_2 \times Y) \cup (\overline{A_2} \times X_1 \times Y)$$

as before.

This relation may be expressed in terms of characteristic functions as follows:

The Cartesian product is interpreted as the conjunction 'and', or minimum $\wedge$; the union $\cup$ is interpreted as the disjunction 'or' or maximum $\vee$.

The relation may thus be written

$$\chi_R < x_1, x_2, y > = (\chi_{A_1}(x_1) \wedge \chi_{A_2}(x_2) \wedge \chi_B(y)) \vee ((1 - \chi_{A_1}(x_1)) \wedge 1 \wedge 1) \vee ((1 - \chi_{A_2}(x_2)) \wedge 1 \wedge 1)$$

which simplifies to

$$\chi_R < x_1, x_2, y > = (\chi_{A_1}(x_1) \wedge \chi_{A_2}(x_2) \wedge \chi_B(y)) \vee (1 - \chi_{A_1}(x_1) \vee (1 - \chi_{A_2}(x_2))$$

The foregoing has been presented for crisp sets using the characteristic function χ, which can take the value 0 or 1. For fuzzy rules, similar expressions may be derived in terms of the membership function μ.

For the fuzzy rule

IF A THEN B

where *A* and *B* are now fuzzy, the implication relation in terms of membership functions is

$$\mu_R(x,y) = (\mu_A(x) \wedge \mu_B(y)) \vee (1 - \mu_A(x))$$

This is attributed to Zadeh (Zadeh max min implication operator (Zadeh, 1988)).

Other forms of the implication operator have been used (Lee (1990), Ross (1995), Tsoukalas and Uhrig (1997), etc.), such as

Mamdani minimum

$$\mu_R(x,y) = \mu_A(x) \wedge \mu_B(y)$$

which generates membership functions identical to those produced by Zadeh max min implication operator when $\mu_A(x) \geq 0.5$ and $\mu_B(y) \geq 0.5$

Larsen product

$$\mu_R(x,y) = \mu_A(x).\mu_B(y)$$

which eliminates the discontinuities produced by the Mamdani minimum operator.

The application of the fuzzy rule

IF *A* THEN *B*

to the situation where the input is a single crisp value *x*, producing a fuzzy output B' is next examined.

In general, for a fuzzy input A', the fuzzy output B' may be found using composition:

$$B' = A' \circ R$$

where *R* is the implication relation.

Using the max-min composition rule, then for each *y* in the discrete output universe of discourse *Y*,

$$\mu_{B'}(y) = \vee_{x \in X} \left[\mu_{A'}(x) \wedge \mu_R(x,y) \right]$$

For the relation, using Mamdani minimum

$$\mu_R(x,y) = \mu_A(x) \wedge \mu_B(y)$$

Thus

$$\mu_{B'}(y) = \vee_{x \in X} \left[\mu_{A'}(x) \wedge \mu_A(x) \wedge \mu_B(y) \right]$$

However, as *x* is discrete, there is only one non zero value of $\mu_{A'}(x)$ and thus

$$\mu_{B'}(y) = \left[\mu_{A'}(x) \wedge \mu_A(x) \wedge \mu_B(y) \right]$$
$$\mu_{A'}(x) = 1$$

thus the membership functions for B' are computed from

$$\mu_{B'}(y) = \left[\mu_A(x) \wedge \mu_B(y)\right]$$

If the max-product composition rule is used, then for each *y* in the discrete output universe of discourse *Y*,

$$\mu_{B'}(y) = \vee_{x \in X}\left[\mu_{A'}(x).\mu_R(x,y)\right]$$

and using the Larsen product for the implication

$$\mu_R(x,y) = \mu_A(x).\mu_B(y)$$

Thus now

$$\mu_{B'}(y) = \vee_{x \in X}\left[\mu_{A'}(x).\mu_A(x).\mu_B(y)\right]$$

Again, as *x* is discrete, there is only one non zero value of $\mu_{A'}(x)$ and thus

$$\mu_{B'}(y) = \left[\mu_{A'}(x).\mu_A(x).\mu_B(y)\right]$$

$$\mu_{A'}(x) = 1$$

and so the membership functions for B' are computed from

$$\mu_{B'}(y) = \left[\mu_A(x).\mu_B(y)\right]$$

Now consider a rule that has multiple antecedents and a single consequent. If the antecedents are expressed in terms of fuzzy sets A_1 in universe of discourse X_1, A_2 in universe of discourse X_2, A_i in universe of discourse X_i, etc. then the membership function of B' can be computed by either of the two preceding formulae, replacing *x* by $\{x_1, x_2, ...x_i,.....\}$ and *A* by $A_1 \times A_2 \times ...A_i \times .....$

The computation of the membership functions for B' requires a decision on how the membership of the product space is to be treated.

The use of the max-min composition rule and the Mamdani minimum for implication point to the following expression:

$$\mu_{B'}(y) = \left[\mu_{A_1}(x_1) \wedge \mu_{A_2}(x_2) \wedge ...\mu_{Ai}(x_i) \wedge .... \wedge \mu_B(y)\right]$$

whereas use of the max product composition rule and the Larsen product for implication point to the following expression

$$\mu_{B'}(y) = \left[\mu_{A_1}(x_1).\mu_{A_2}(x_2)....\mu_{Ai}(x_i).....\mu_B(y)\right]$$

Alternatively, the preceding expressions may be derived by considering the derivation of the membership functions for the implication relation with multiple antecedents:

Using Mamdani minimum

$$\mu_R(x_1, x_2, ...x_i..., y) = \mu_{A_1}(x_1) \wedge \mu_{A_2}(x_2)... \wedge \mu_{A_i}(x_i)... \wedge \mu_B(y)$$

Using Larsen product

$$\mu_R(x_1, x_2, ...x_i..., y) = \mu_{A_1}(x_1).\mu_{A_2}(x_2)....\mu_{A_i}(x_i)....\mu_B(y)$$

Whichever method is used to calculate the membership function for B', its support set is included within the support set of B because for any y outside the support set for B $\mu_B(y)$ is zero. The use of minimum or product operators will then result in $\mu_{B'}(y)$ being zero.

Where there is more than one rule, it is necessary to aggregate the effects of each. Linguistically, a series of rules may be linked with the connective ELSE as follows in the case where there are two antecedents in each implication:

IF A_{11} AND A_{21} THEN B_1 ELSE
IF A_{12} AND A_{22} THEN B_2 ELSE
IF A_{1i} AND A_{2i} THEN B_i ELSE
IF A_{1n} AND A_{2n} THEN B_n

where there are n rules. Such a list of rules can be termed an algorithm.

For crisp inputs x_1 and x_2 a fuzzy output set B_{TOT} results. This is the aggregation of the B_i' having membership function $\mu_{B_i'}(y)$ which is computed for rule i. Intuitively, if the method of computation of the membership function for any rule i in the algorithm could result in a null set for B_i', it would be inappropriate to represent the connective ELSE by the AND or minimum $\wedge$ operator, as a null output set B_{TOT} would then result. Thus, where Mamdani minimum or Larsen product methods are used as above the connective ELSE should be represented by the OR or maximum operator $\vee$. The membership function $\mu_{B_{TOT}}(y)$ of the fuzzy output set B_{TOT} is thus computed using this operator:

$$\mu_{B_{TOT}}(y) = \mu_{B_1}(y) \vee \mu_{B_2}(y) \vee ....\mu_{B_i}(y) \vee ....\mu_{B_n}(y)$$

To establish a crisp output a single value y must be derived from the fuzzy output set B_{TOT} by a defuzzification process.

A4.6 Quantisation

In the literature, there are often references to a 'quantisation' process in which a discrete input *x* (or x_i where there are multiple inputs to the controller) is replaced by an appropriate rounded value taken from a vector of values. The quantised values may be used with a look up table to derive output membership functions. The requirement to calculate these is thus obviated. Emphasis is placed in older papers (e.g. Lee (1990) and Rutherford and Bloore (1976)) on the use of look up tables as a means of reducing computational demands.

A4.7 Defuzzification

The membership function $\mu_{B_{TOT}}(y)$ for the fuzzy output has been derived in the previous section. Defuzzification is the process whereby a crisp output value is derived. Of the various alternative methods, the most commonly applied in the literature are the 'maximum membership' and 'centre of gravity' methods. (See, for example, Pedrycz (1998).)

A4.7.1 Maximum Membership

The crisp output y is that value at which $\mu_{B_{TOT}}(y)$ has its maximum value. If there are more than one equal maxima, then the mean of the values of *y* corresponding to the maxima is taken. If the maximum is a plateau, then *y* is taken as the mean of the values corresponding to the extremities of the plateau. If $\mu_{B_{TOT}}(y)$ has several maxima, the method may be inappropriate.

A4.7.2 Centre of Gravity

The crisp output y is the centroid of the fuzzy set. This may be expressed as

y = (first moment of area of fuzzy set)/(area of fuzzy set)

$$y = \frac{\int \mu_{B_{TOT}}(y).y.dy}{\int \mu_{B_{TOT}}(y).dy}$$

To compute this requires that the 'overlaps' of the contributions of each rule are identified. This complicates the process, so that in practice a weighted average method is used, although it is often imprecisely termed 'centre of gravity'

$$y = \frac{\sum_i \int \mu_{B_i}(y).y.dy}{\sum_i \int \mu_{B_i}(y).dy}$$

The weighted average (or centre of gravity) method gives a smoother variation of output with input(s) than does the maximum membership method. The latter can generate discontinuities in the output which would be undesirable in a control application.

A4.8 Non-linear Mapping

Fuzzy algorithms are said to provide a non-linear mapping from an input space to an output space. This can be demonstrated as follows.

Consider the following algorithm:

IF A_1 THEN B_1 ELSE

IF A_2 THEN B_2

Let the discrete input be x. Compute the discrete (defuzzified) output y as follows. Let the maximum value of the membership function for B_1 occur at $y = Y_1$ and let the maximum value of the membership function for B_2 occur at $y = Y_2$. For convenience, let these membership functions be symmetrical about their maxima, and let these maxima be unity. The areas under these membership functions are respectively b_1 and b_2.

Using product rules for inference and composition results in a fuzzy output which is the union of the membership function for B_1 scaled by $\mu_{A_1}(x)$ and the membership function for B_2 scaled by $\mu_{A_2}(x)$. By using the weighted average (or centre of gravity) method for defuzzification, the discrete output y is computed as follows:

$$y = \frac{Y_1 b_1 \mu_{A_1}(x) + Y_2 b_2 \mu_{A_2}(x)}{b_1 \mu_{A_1}(x) + b_2 \mu_{A_2}(x)}$$

Thus even if $\mu_{A_1}(x)$ and $\mu_{A_2}(x)$ are linear functions, *y* is not a linear function of *x*. The equation therefore represents a non-linear mapping from *x* to *y*. It is the control characteristic for the fuzzy algorithm. If at least one of the rules in the fuzzy algorithm has two antecedents, with inputs x_1 and x_2, a similar analysis will show that the fuzzy algorithm may be represented by a control characteristic which is a surface in three dimensions.

APPENDIX 5. Principles of Fuzzy Logic Controllers

A5.1 The Human Operator as a Fuzzy Logic Controller

An operator, required to control a single input single output system, will take a control action based on intuition and experience in response to his/her perception of the difference between the actual output of the system and what he/she wants it to be. His/her actions will consciously or unconsciously be based on 'rules' such as 'if difference is a large excess then input must be made small'. Depending on his/her 'feel' for the dynamics, he/she may use a more complex set of rules which take account of the way in which the difference is changing. A rule might then be 'if difference is a large excess but is reducing then input must be made small to medium'. Such a rule points towards the development of a two degree of freedom 'PD' (proportional plus derivative) fuzzy controller.

A5.2 A Two Degree of Freedom Fuzzy Logic Controller

In this section, the structure of a simple fuzzy logic controller is briefly described. Fuzzy logic terms are explained in Appendix 4.

A5.2.1 Structure

The structure of a two degree of freedom PD error driven fuzzy controller for a single input single output system is shown in its most general form in Figure A5.1.

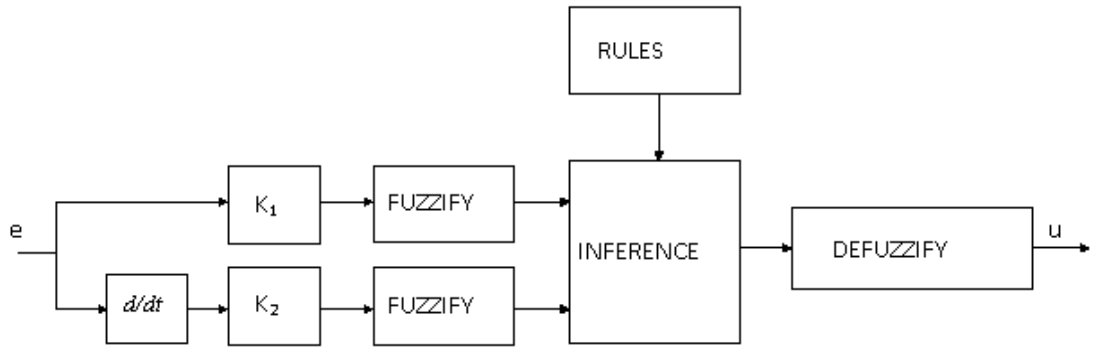

Figure A5.1 Block diagram of fuzzy controller

A5.2.2 Operation

In Figure A5.1 the input to the controller is *e* and the output is the control effort *u*. A rate of change of error is derived. The error and rate of change of error are scaled by gains K_1 and K_2 respectively. The scaled values are then fuzzified.

At the heart of the controller is a 'fuzzy rule based expert system' model. In this, the required controller outputs are derived from conditional relationships between the inputs and the output (rules). Here, there are two inputs and a single output, so that the rules are of the form:

'If input(1) is value(1) and input(2) is value(2) then output is value(3)'.

Value(1), value(2) and value(3) are verbal descriptions of the parameters. The rules are contained in a rules table. A series of linguistic rules in this form is described as being in 'canonical form' (Jamshidi *et al.*,1993, p.72).

Application of the rules results in the generation of a fuzzy output, which must be 'defuzzified' to generate a control signal. The rules table is constructed on the basis of expert human knowledge or intuition. The Self Organising Fuzzy Logic Controller differs from a 'simple' Fuzzy Logic Controller in that the contents of the table of rules are dynamically adjusted to meet a performance criterion; indeed, an initial table may not be required - the control algorithm develops and maintains its own. Self Organising Fuzzy Logic Controllers are discussed in Section A5.3.

A5.2.3 Representation of Rules

The controller has been designed around a two dimensional table of rules (contained in the 'RULES' block in the figure). Thus two fuzzy input parameters are used to generate by inference a single fuzzy output parameter. The rules table summarises a series of rules of the form

IF (INPUT1 IS A_1) AND (INPUT2 IS A_2) THEN (OUTPUT IS U)

where A_1, A_2 and U are respectively the names of fuzzy sets ('fuzzy labels') in the universes of discourse for INPUT1, INPUT2 and OUTPUT. The fuzzy labels for INPUT1 may be the column names in the table of rules and those for INPUT2 the row names. For any combination of INPUT1 and INPUT2 the appropriate fuzzy label for OUTPUT may be read from the table; each cell of the table corresponds to a rule.

The following fuzzy labels have been used here for the inputs:

NB - Negative Big
NM - Negative Medium
NS - Negative Small
ZE - Zero
PS - Positive Small
PM - Positive Medium
PB - Positive Big

Similar labels using lower case are used for the output.

An example of a two dimensional table of rules relating a single output to two inputs, an 'error' and a 'rate of change of error' ('rate') is shown in Table A5.1 .

Table A5.1 Rules table

			E	R	R	O	R	
		NB	NM	NS	ZE	PS	PM	PB
	NB	*nb*	*nb*	*nb*	*nb*	*nm*	*ns*	*ze*
R	NM	*nb*	*nm*	*nm*	*nm*	*ns*	*ze*	*ps*
A	NS	*nb*	*nm*	*ns*	*ns*	*ze*	*ps*	*pm*
T	ZE	*nb*	*nm*	*ns*	*ze*	*ps*	*pm*	*pb*
E	PS	*nm*	*ns*	*ze*	*ps*	*ps*	*pm*	*pb*
	PM	*ns*	*ze*	*ps*	*pm*	*pm*	*pm*	*pb*
	PB	*ze*	*ps*	*pm*	*pb*	*pb*	*pb*	*pb*

This table contains 49 rules, for example:

IF (RATE IS NM) AND (ERROR IS PB) THEN (OUTPUT IS *ps*)

A5.2.4 Justification of the Rules Table

Table A5.1 is an example which may be said to represent intuitively the control actions needed for any single input single output dynamic system. It is important to note that a sign convention is implied in it - a positive error is one in which the demand made on the system exceeds its output.

Thus, if the reference (demand) is *r*, the output is *y*, and the error is *e*,

$$e = r - y \qquad (1)$$

A positive error results when the output is less than it is required to be, and thus requires a positive control effort.

Differentiating with respect to time,

$$\dot{e} = \dot{r} - \dot{y} \qquad (2)$$

Considering regulator action, where r is constant and thus $\dot{r}$ is zero, it is easy to see that a positive rate of change of error results from a negative rate of change of output. Falling output in this situation requires positive control effort.

The preceding short analysis demonstrates the consistency of the rules in Table A5.1 with the sign convention.

A5.2.5 Codifying the Rules Table

For convenience in formulating computer code, the fuzzy labels have been codified as follows:

NB - 1

NM - 2

NS - 3

ZE - 4

PS - 5

PM - 6

PB - 7

Table A5.1 may then be presented in codified form as follows:

Table A5.2 Rules table – codified

			E	R	R	O	R	
		1	2	3	4	5	6	7
	1	**1**	**1**	**1**	**1**	**2**	**3**	**4**
R	2	**1**	**2**	**2**	**2**	**3**	**4**	**5**
A	3	**1**	**2**	**3**	**3**	**4**	**5**	**6**
T	4	**1**	**2**	**3**	**4**	**5**	**6**	**7**
E	5	**2**	**3**	**4**	**5**	**5**	**6**	**7**
	6	**3**	**4**	**5**	**6**	**6**	**6**	**7**
	7	**4**	**5**	**6**	**7**	**7**	**7**	**7**

Table A5.2 is known as a fuzzy associative memory (FAM) table.

A5.2.6 Fuzzification and Defuzzification

To enable the FAM table to be used in a controller (Figure A5.1), the two inputs must be fuzzified; a fuzzy output is generated using an inferencing algorithm; and a crisp output derived from the fuzzy output using a defuzzification algorithm. Fuzzification and defuzzification require the definition of universes of discourse for, respectively, the input and the output.

In the literature, a discrete universe of discourse is defined for each of the input parameters. This approach was adopted in the initial work (Njabeleke, 1998, Njabeleke *et al.*, 1998, Pannett *et al.,* 1999). The membership function for each of the fuzzy sets for each input parameter is defined in terms of the membership in the fuzzy set of the singletons contained in its support set. The support set is itself drawn

from the universe of discourse. The reason that this approach is adopted in the literature is apparently because it facilitates the use of look-up tables in the subsequent computation (see, for example, Lee (1990), Rutherford and Bloore (1976)). When processors operated at lower speeds than those of processors now readily available, this was an important consideration when designing real time controllers.

In the present work, the use of continuous universes of discourse has also been explored.

A5.2.7 Membership Functions

Universes of discourses, discrete or continuous, are defined for each of the input parameters. The membership function for each of the fuzzy sets for each input parameter is defined in terms of its geometry. Triangular membership functions have been used in this work. They are defined by the minimum and maximum values of the support set, and by the value at which membership is unity. The membership in each of the input fuzzy sets of each crisp input is computed directly from this information.

The number of input fuzzy sets for which a given crisp input has non-zero membership will depend on the degree to which the sets and thus their membership functions overlap. If no more than two membership functions overlap, then a crisp input can have non-zero membership of no more than two input fuzzy sets.

The output fuzzy sets are defined in a similar manner to the input fuzzy sets.

A5.2.8 Use of the FAM Table to Generate an Output

The rules in the FAM table which ‘fire’ for any combination of crisp inputs are identified by the cells which correspond to the input fuzzy sets in which the crisp inputs have non-zero membership. For each of these firing rules, an inferencing rule is applied to combine the memberships of the two inputs. The results of these combining operations, together with the fuzzy outputs of the rules which ‘fire’,

define the form of an overall fuzzy output. From this is computed by a defuzzification method a crisp output; this is the source of the control signal to the plant.

A5.3 Self Organising Fuzzy Logic Control (SOFLC)

A5.3.1 Motivation for SOFLC

A basic error driven fuzzy controller has performance shortfalls because it is unable to take account of the changes in characteristics of the system. The results of simulation studies of an error driven fuzzy logic controller as applied to the candidate system have been reported (Njabeleke, 1998). The merits of extending the dimensions of the rule base to recognise the effects of changes in system characteristics with speed and supply pressure were considered briefly. However, added complexity would then result: an additional transducer for supply pressure would be required and an extra dimension would be added to the rules table. Also, the design would become less intuitive. The development of a 'self organising' fuzzy logic controller (SOFLC) was pursued instead. In a SOFLC the rule base is adapted dynamically as the system characteristics alter with set point, etc. A relatively simple (and therefore undemanding in terms of computation speed) adaptation algorithm has been devised and applied.

A5.3.2 Principles of SOFLC

The SOFLC has been designed in accordance with principles initially published by Procyk and Mamdani (1979). They identified two tasks which the SOFLC must perform simultaneously - it must observe the environment while issuing the appropriate control actions and it must use the results of these control actions to improve them further.

The SOFLC extends the standard fuzzy logic controller by incorporating performance feedback in the basic fuzzy logic controller.

The basic functions of the SOFLC can be summarised as follows:

- to issue appropriate control action;
- to evaluate the performance;
- to modify the rule-base based on this evaluation.

The control action is computed in accordance with the current rules as contained in the FAM. This was considered further above.

To evaluate performance, following the method of Procyk and Mamdani (1979), a performance measure calculated from the error and rate of change of error is used. A two-dimensional performance table, which summarises a series of linguistic statements about performance, is used in accordance with the principles of fuzzy logic to infer the value of a performance measure.

The performance table used is shown in Table A5.3.

Table A5.3 Performance table

			E	R	R	O	R	
		NB	NM	NS	ZE	PS	PM	PB
	NB	*nb*	*nb*	*nb*	*nb*	*nm*	*ns*	*ze*
R	NM	*nb*	*nm*	*nm*	*nm*	*ns*	*ze*	*ps*
A	NS	*nb*	*nm*	*ns*	*ns*	*ze*	*ps*	*pm*
T	ZE	*nb*	*nm*	*ns*	*ze*	*ps*	*pm*	*pb*
E	PS	*nm*	*ns*	*ze*	*ps*	*ps*	*pm*	*pb*
	PM	*ns*	*ze*	*ps*	*pm*	*pm*	*pm*	*pb*
	PB	*ze*	*ps*	*pm*	*pb*	*pb*	*pb*	*pb*

An example of the interpretation of the table is that if error and rate are both PB ('positive big') then the performance is also 'positive big'. Since the system is monotonic (an increase in output always results from an increase in input), in this example the linguistic performance measure indicates that to improve performance the input to the system must be increased. Procyk and Mamdani (1979) describe how the performance measure may be interpreted as the change in system output which is required if performance is to be improved. They show how the inverse of an incremental model of the system may be used to derive the required change to the system input (reward); to achieve a change to the system input (which is of course the controller output) requires an adjustment to the rules table within the controller. They also show that for a single input single output system the incremental model of the system, and thus its inverse also, may be treated as a unit gain. Their analysis is summarised in Figure A5.2 which is taken from their paper.

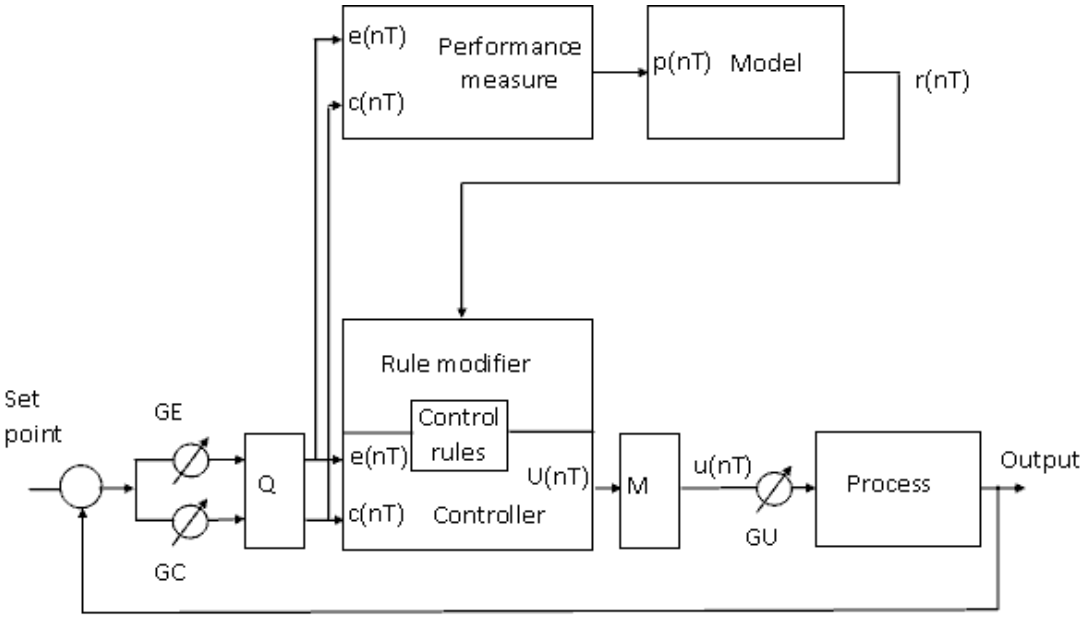

Q - Quantisation process; M - Derivation of deterministic control action.
GE, GC, GU - gains for error, error rate and control action; T - sample interval
e(nT), c(nT) - quantised and scaled discrete time error and error rate.
p(nT), r(nT) - performance measure and reward.
U(nT) - fuzzy control action; u(nT) - deterministic control action.

Figure A5.2 Self Organising Fuzzy Logic Controller (taken from Procyk and Mamdani (1979))

It is necessary to recognise that lags and delays in the process result in its output being dependent on control actions taken in the past. 'High order processes with large time lags and delays will require control actions further back from the present to be rewarded in order to overcome these delays. Low order processes with short lags will require more recent control actions to be rewarded. This distribution of reward depends on the type of process being controlled and the sampling rate. Consequently, it is set by the user according to his judgement about the process he wants controlled. It is worth noting here that this in itself also implies a model of the dynamics of the process, this time by virtue of the time lags' (*ibid*.).

A5.3.3 Development of SOFLC

The approach of Linkens and Abbod (1991) to the development of a SOFLC is summarised in Figure A5.3 which is taken from their paper.

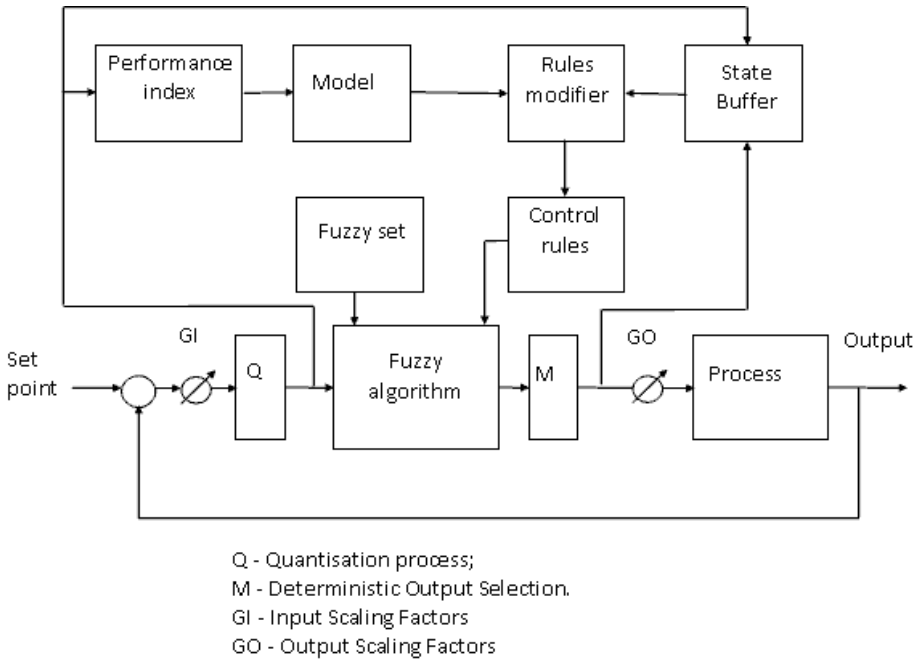

Figure A5.3 Self Organising Fuzzy Logic Controller (from Linkens and Abbod (1991))

The ‘state buffer’ is a first in, first out register which records the values of the error, error rate and controller output. The output of the register lags the input to it by a time equal to the reward delay.

In work reported by Njabeleke (1998), and further studies reported in Njabeleke *et al.* (1998) and Pannett *et al.* (1999), all of which were based on simulation, controllers for the candidate fluid power system were designed according to the principles of Linkens and Abbod (1991). They describe a controller in which the input, which may be multi-dimensional, is scaled to bring it into an appropriate range, then quantised. It is then fuzzified: for each of its input channels, its membership in each of the input fuzzy sets is established. The fuzzified input is used with a fuzzy algorithm, the current control rules and a defuzzification process to derive a controller output.

Superimposed on these processes is the rules modification process.

A5.4 Design of SOFLC

A5.4.1 Overview

Initial work on the design of a SOFLC centred on simulation. For this, the starting point of the controller design was the control structure of Linkens and Abbod, discussed above. The controller is shown in block form in Figure A5.4.

In this, the blocks labelled ‘fuzzify’ include a quantisation process. The controller used in the initial studies is essentially a PD (proportional plus derivative) controller working in continuous time. Gains K_1 and K_2 are included to scale respectively the error and error rate. A discrete universe of discourse is defined for each of the scaled error and error rate crisp inputs. These inputs are quantised, i.e. reset to the nearest member of the appropriate universe of discourse. Each of the two quantised inputs is fuzzified. Thus, the fit of each input to each of the fuzzy sets which correspond to the linguistic terms used is computed. The result for each input is a vector whose length is equal to the number of linguistic terms (or fuzzy sets) used to describe that input and whose members are the fits. These are the fuzzified inputs.

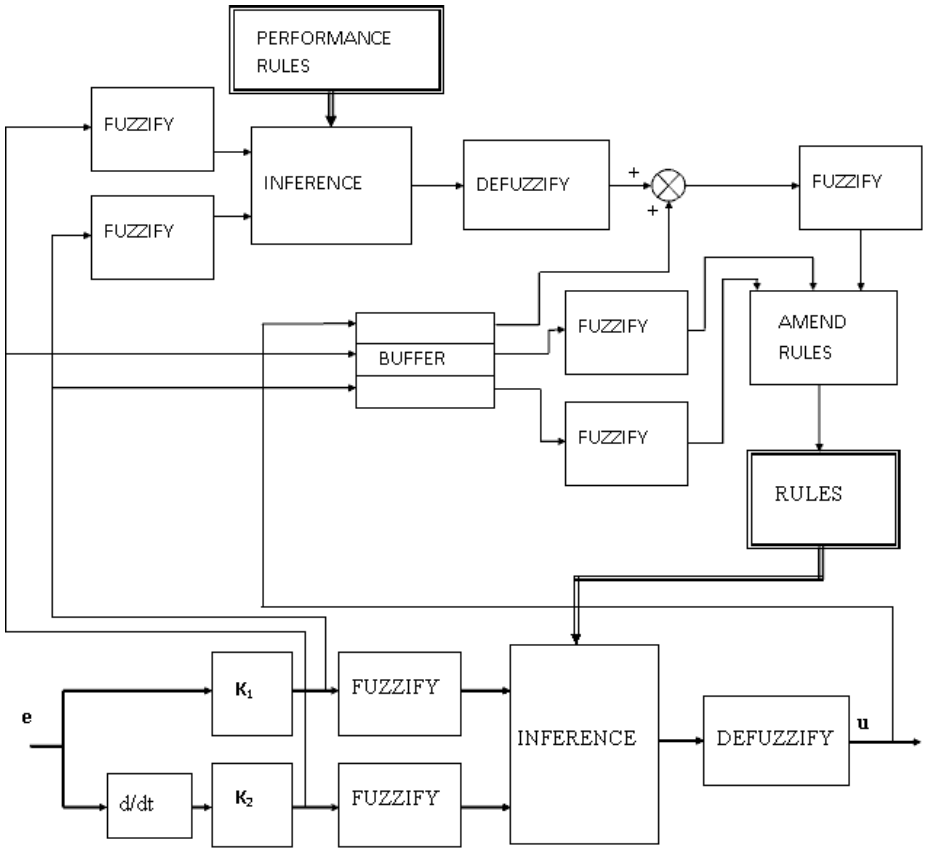

Figure A5.4 SOFLC structure – detail

A5.4.2 Operation of SOFLC

There are two levels of operation:

The first is the 'standard' fuzzy logic controller. Using the current rules, a fuzzy inference is made from the fuzzified inputs and the resulting output is defuzzified into a crisp value which becomes, after scaling, the controller output. For each rule in the rule table (FAM), the fits of the two inputs are aggregated to establish the degree to which the rule 'fires' ('degree of fulfilment' (Tsoukalas and Uhrig, 1997)). The aggregation process used is 'arithmetic product' (*op. cit.*) (see Appendix 4). To obtain a 'crisp' output, it is necessary to amalgamate the effects of the rules which have fired and to defuzzify the result. Using the 'centre of gravity method' (Appendix 4), the fuzzy output is computed in terms of the area and first moment of area about the membership axis of its membership function. For each rule which has

fired the contribution to the total moment and total area is computed as the product of the degree of fulfilment with its moment and area respectively. The algebraic sums of the moments and areas are found, and the ratio of these sums gives the crisp output (within its universe of discourse). This process is repeated for each input sample. A look-up rules table is not used.

On this 'standard' fuzzy logic controller is superimposed the self-organising mechanism. In essence, this consists of a performance index, a 'model' of the process, a rule modifier and a state buffer. The current states and output of the plant are determined in part by controller output in the past. Therefore the rule modification process uses delayed values of error, rate of change of error and output. These are read from the buffer. Only one rule in the FAM table, that which is considered to have most contributed to producing the controller output which resulted in the current performance, is modified. This is in contrast with algorithms which use a look-up rules table.

A5.4.3 Rule Modification

The rationale of the rule modification algorithm is as follows:

> Use fuzzy values of current error and current error rate with the performance rules to calculate a 'performance output adjustment'. This is the change in output which would have resulted in improved performance;
>
> Find the 'adjusted delayed controller output' which would have resulted in the improved performance by adding the performance output adjustment to the 'delayed controller output' (read from the buffer);
>
> Fuzzify the 'adjusted delayed controller output';
>
> Fuzzify the 'delayed error' and 'delayed rate of change of error' (read from the buffer). For improved performance, these should have resulted in the 'adjusted delayed controller output' rather than the controller output which actually obtained;

Find the highest memberships for ‘delayed error’ and ‘delayed rate of change of error’;

Use these as cell co-ordinates in the rule table to determine which rule in the FAM table to modify;

Find the fuzzy output set having the highest membership for ‘adjusted delayed controller output’;

Use this fuzzy output set in the new rule;

Update the corresponding cell in the FAM table.

APPENDIX 6 Control Surfaces

This Appendix contains complete sets of control surfaces pertaining to the SOFLC simulations and rig tests which are summarised in Chapter 7. They are listed below:

Control surfaces for simulation 2	Section 7.4.2:	Figure A6.1
Control surfaces for revised SOFLC (simulation)	Section 7.5.2:	Figure A6.2
Control surfaces for rig test 1	Section 7.5.4.1:	Figure A6.3
Control surfaces for rig test 2	Section 7.5.4.2:	Figure A6.4
Control surfaces for rig test 3	Section 7.5.4.3:	Figure A6.5

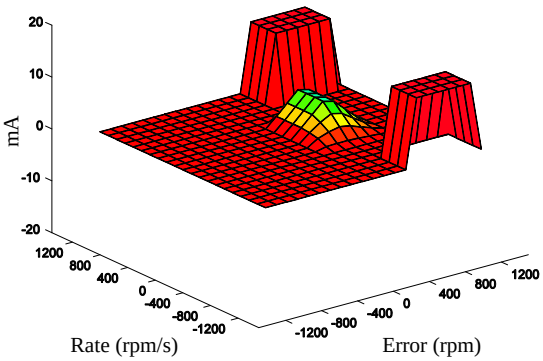

(a) Time = 0.4 s

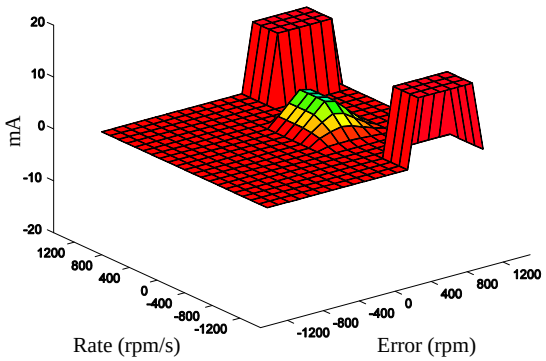

(b) Time = 0.8 s

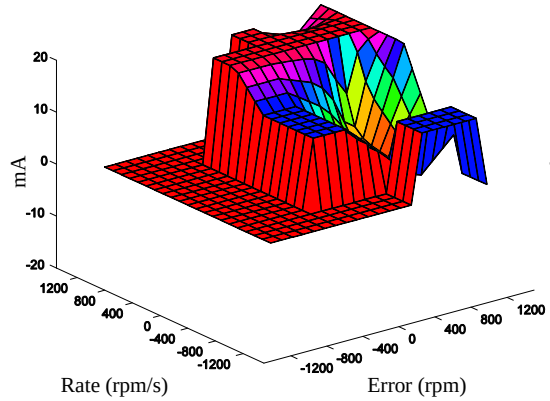

(c) Time = 1.2

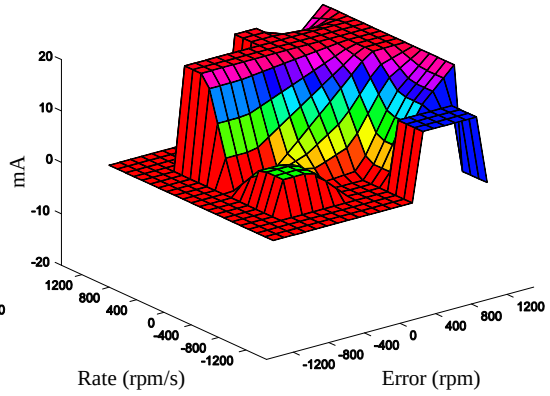

(d) Time = 1.6

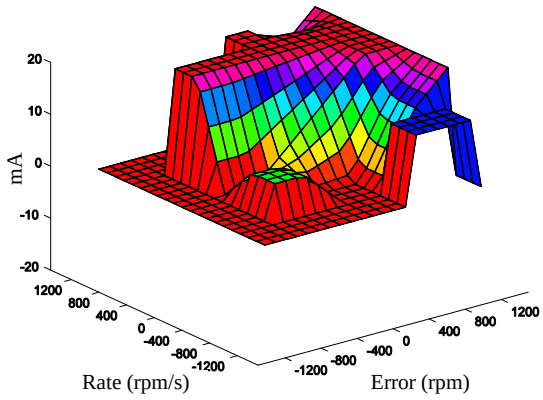

(e) Time = 2.0

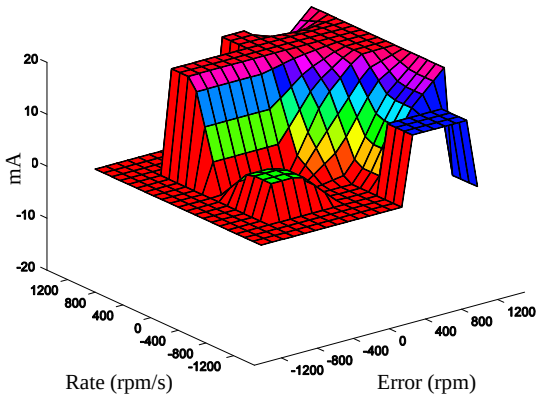

(f) Time = 2.4

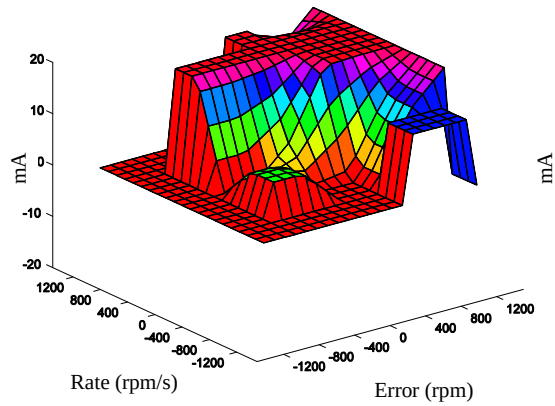

(g) Time = 2.8 s

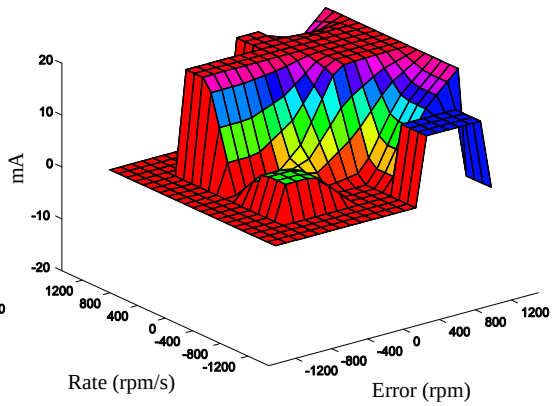

(h) Time = 3.2 s

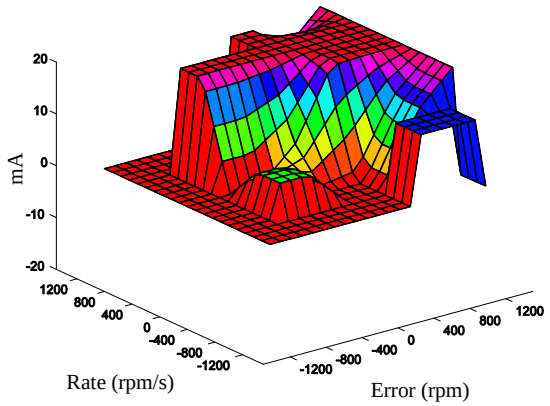

(i) Time = 3.6 s

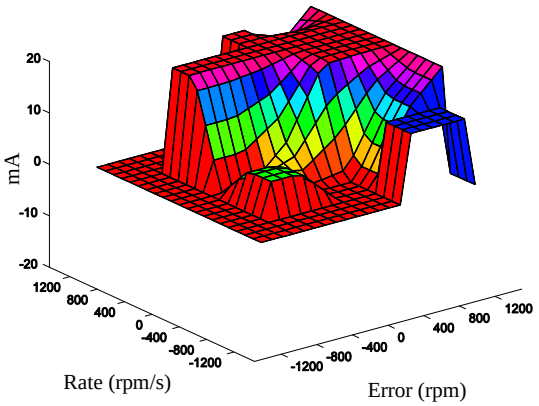

(j) Time = 4.0 s

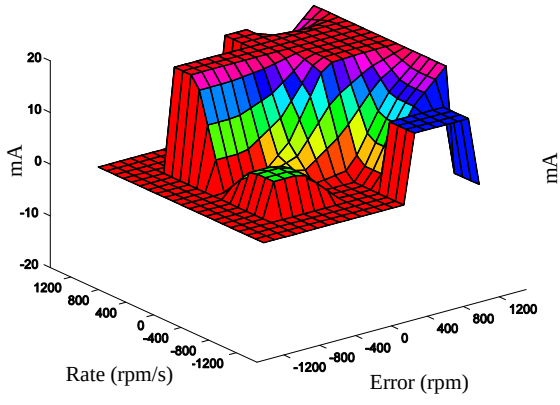

(k) Time = 4.4 s

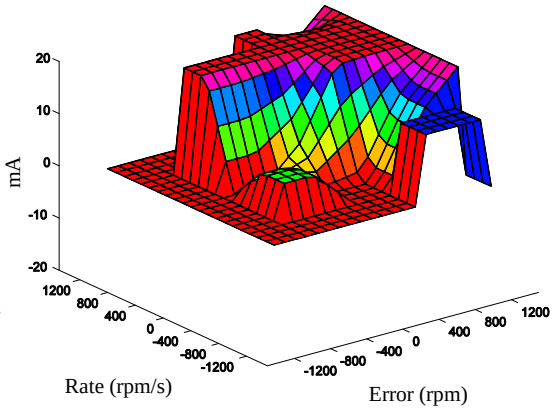

(l) Time = 4.8 s

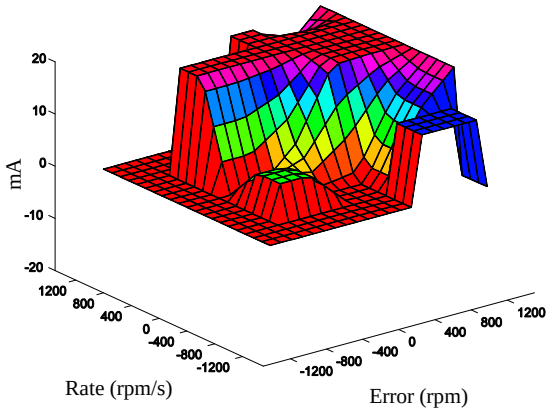

(m) Time = 5.2 s

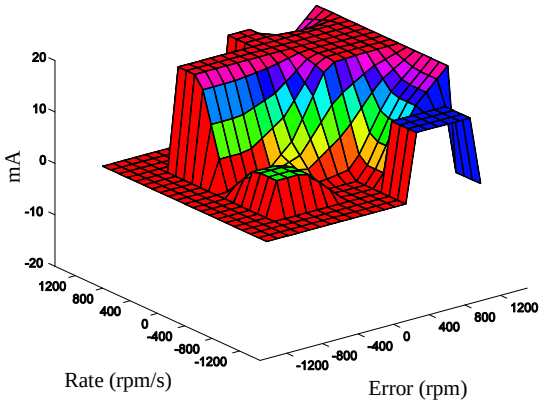

(n) Time = 5.6 s

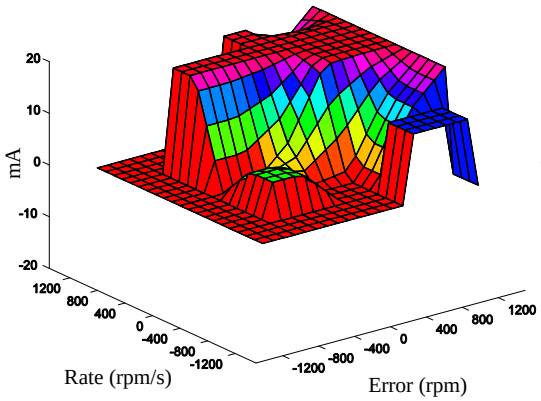

(o) Time = 6.0 s

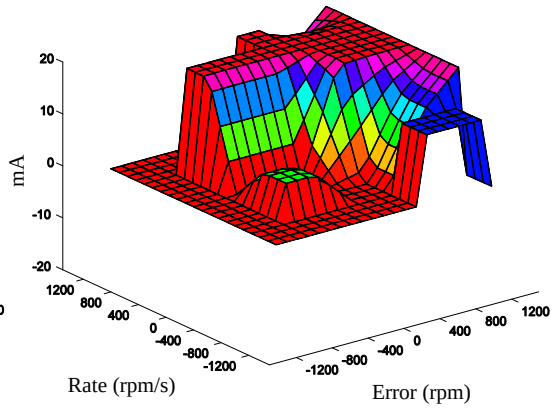

(p) Time = 6.4 s

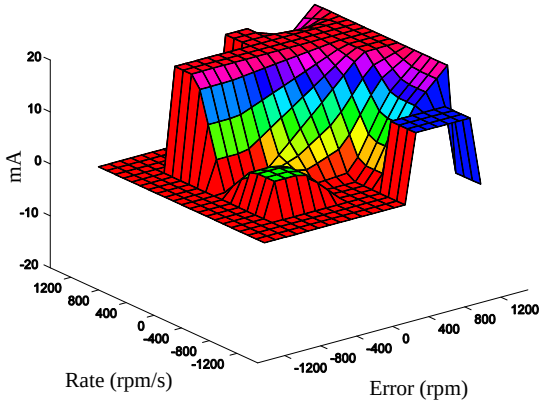

(q) Time = 6.8 s

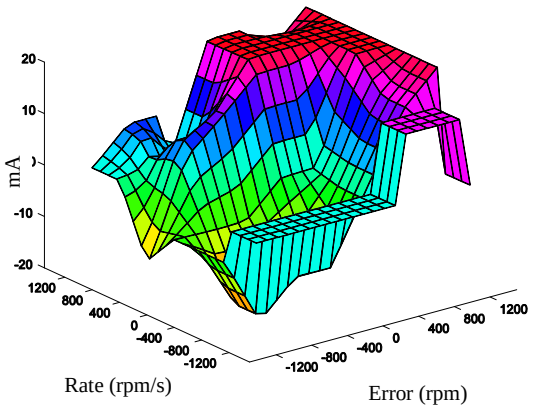

(r) Time = 7.2 s

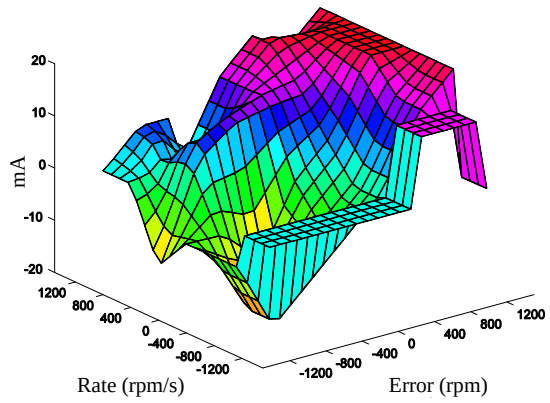

(s) Time = 7.6 s

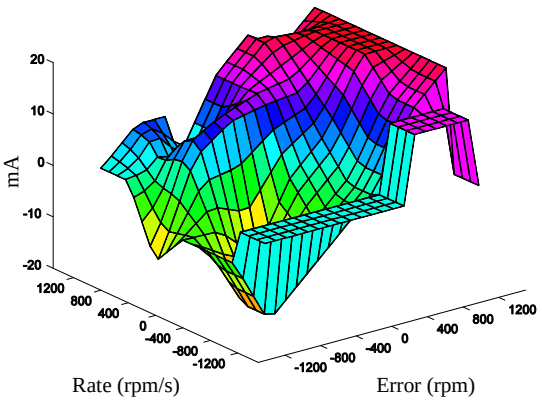

(t) Time = 8.0 s

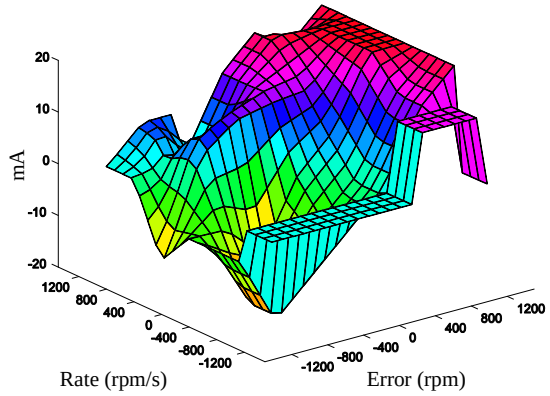

(u) Time = 8.4 s

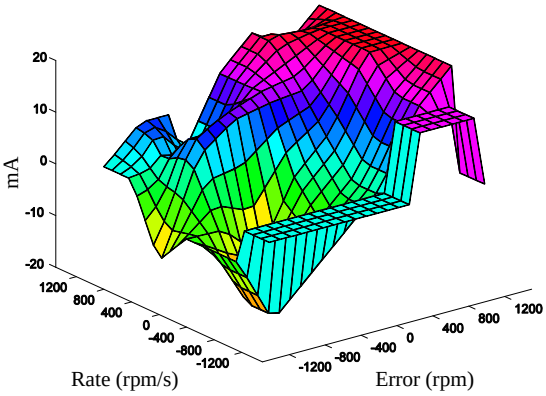

(v) Time = 8.8 s

Figure A6.1 Control surfaces for simulation 2

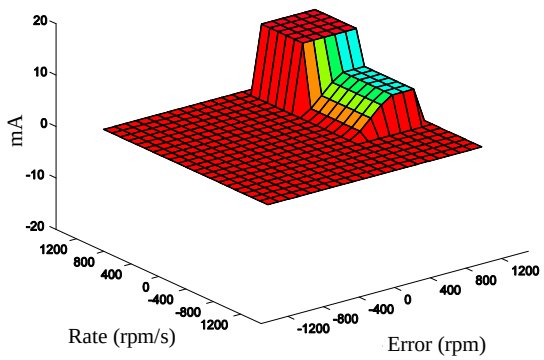

(a) Time = 0.4 s

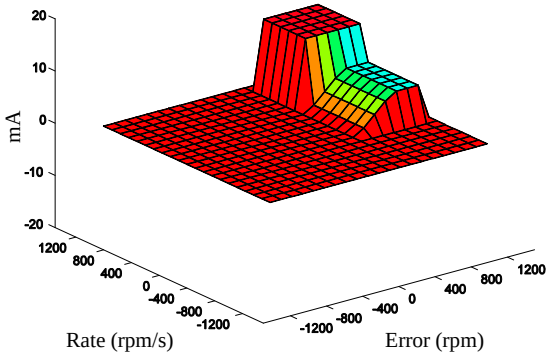

(b) Time = 0.8 s

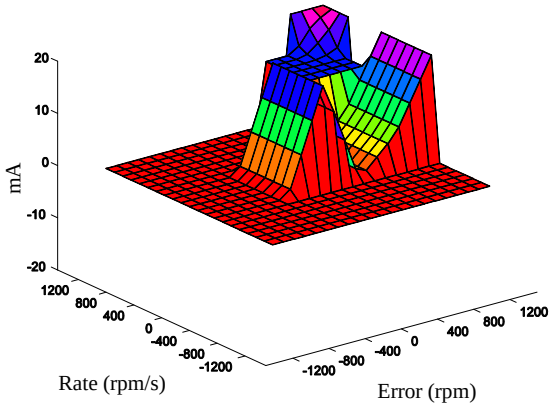

(c) Time = 1.2 s

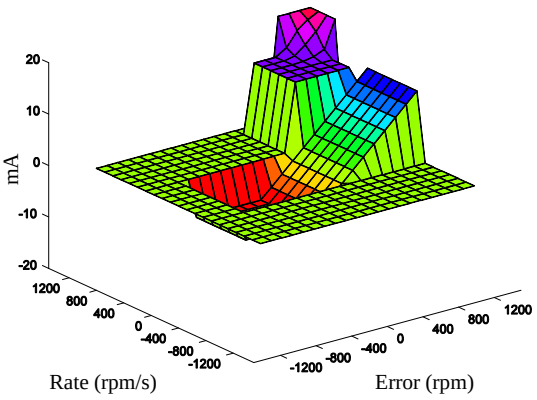

(d) Time = 1.6 s

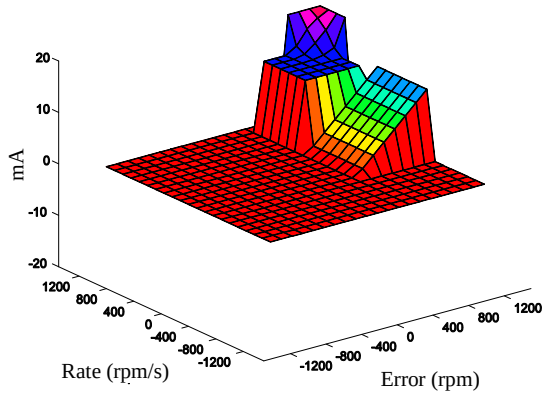

(e) Time = 2.0 s

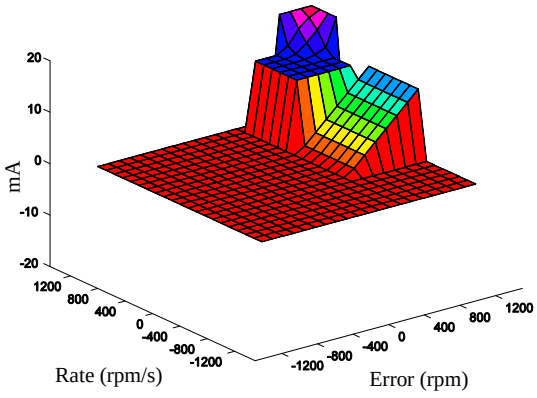

(f) Time = 2.4 s

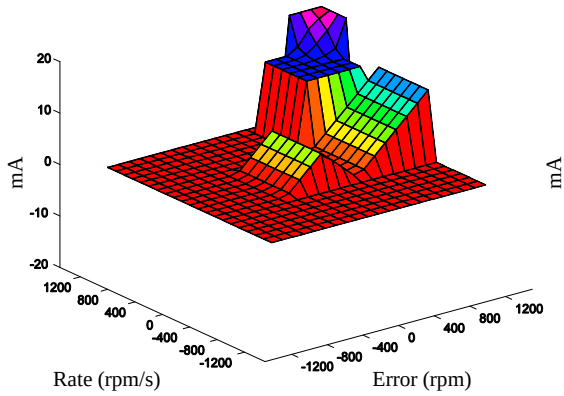

(g) Time = 2.8 s

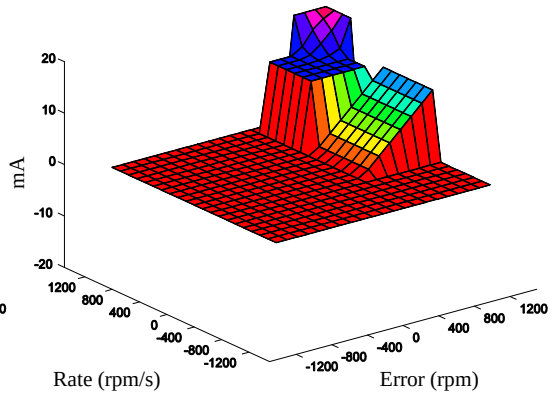

(h) Time = 3.2 s

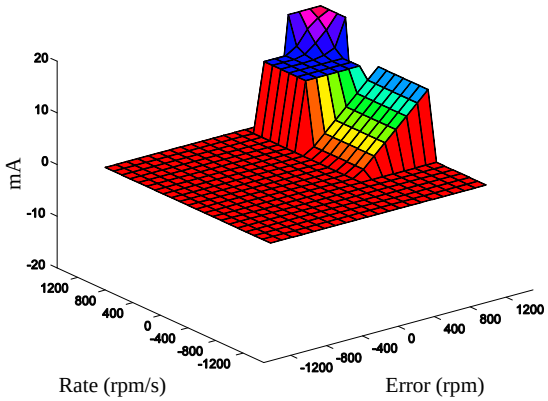

(i) Time = 3.6 s

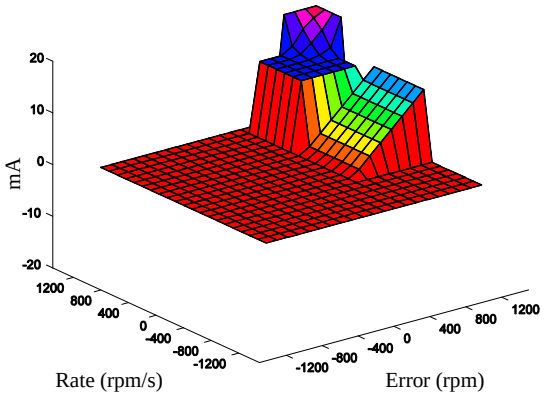

(j) Time = 4.0 s

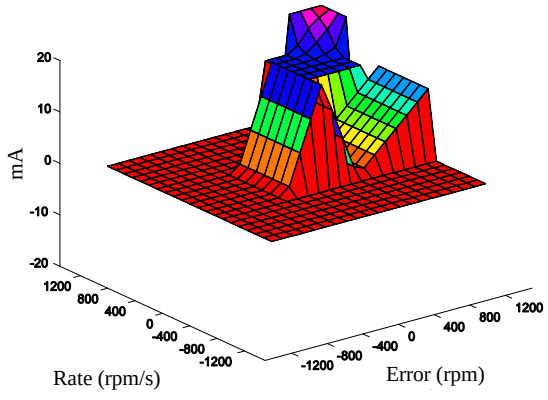

(k) Time = 4.4 s

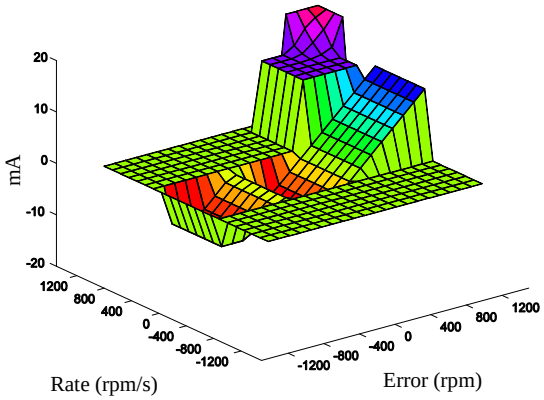

(l) Time = 4.8 s

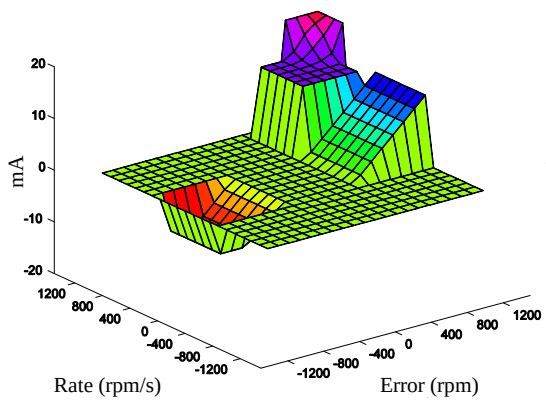

(m) Time = 5.2 s

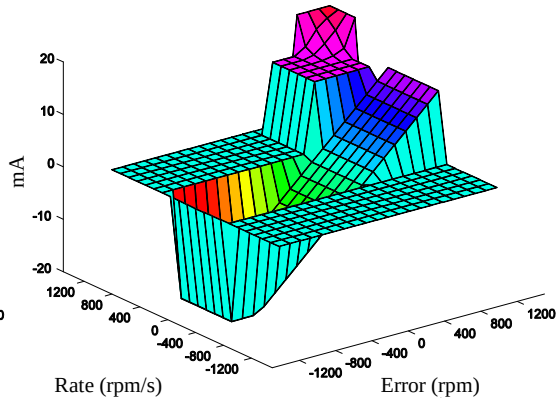

(n) Time = 5.6 s

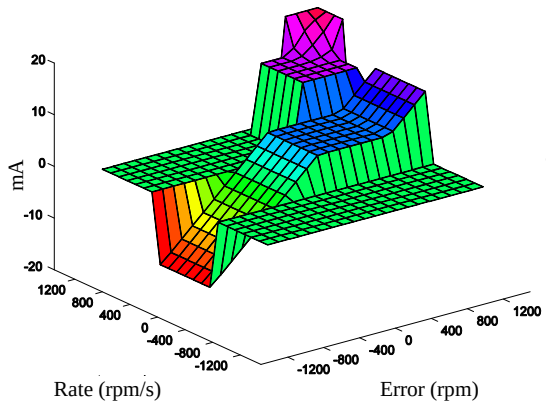

(o) Time = 6.0 s

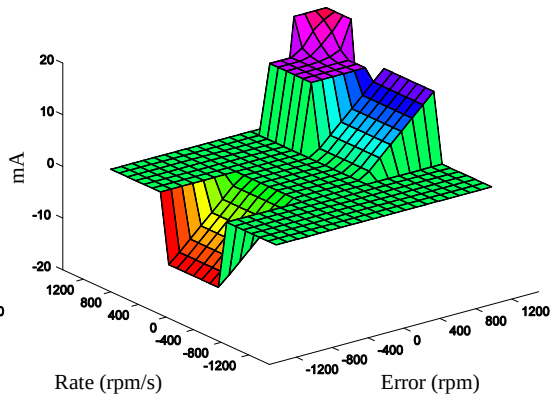

(p) Time = 6.4 s

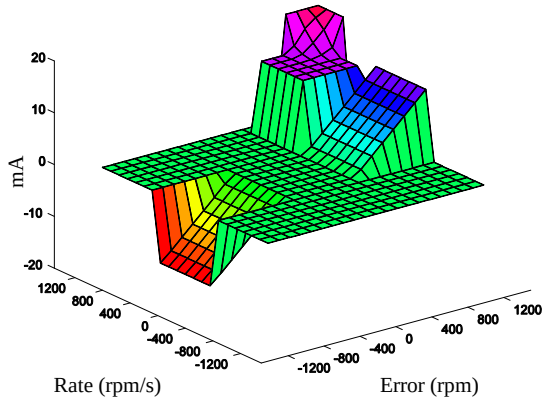

(q) Time = 6.8 s

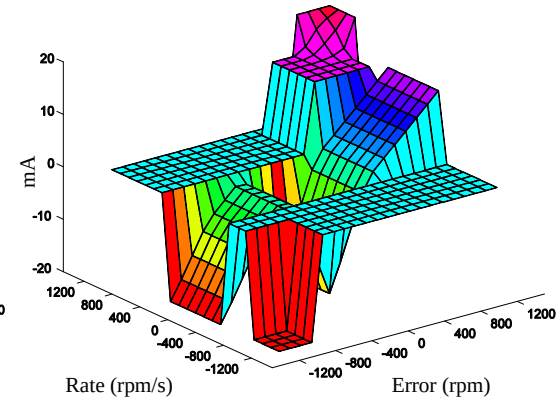

(r) Time = 7.2 s

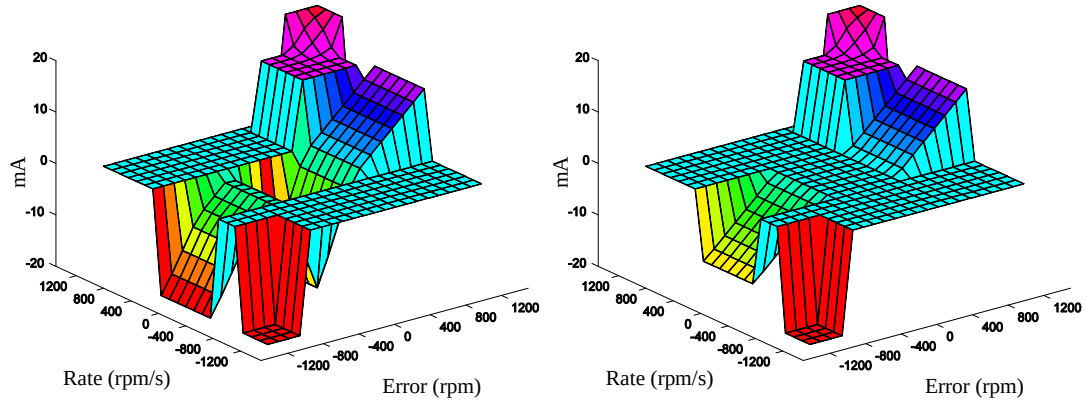

(s) Time = 7.6 s **(t) Time = 8.0 s**

Figure A6.2 Control surface evolution – revised SOFLC (simulation)

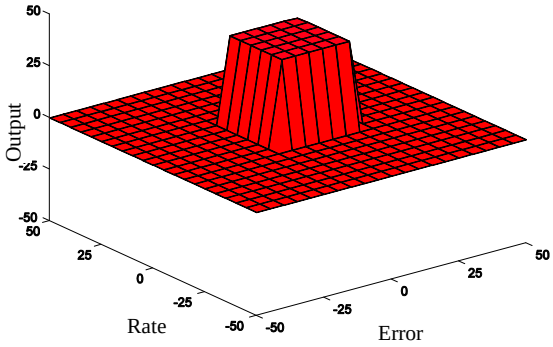

(a) Time = 0^+s

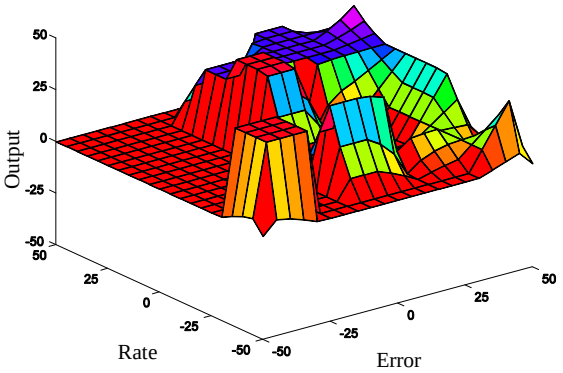

(b) Time = 1.0 s

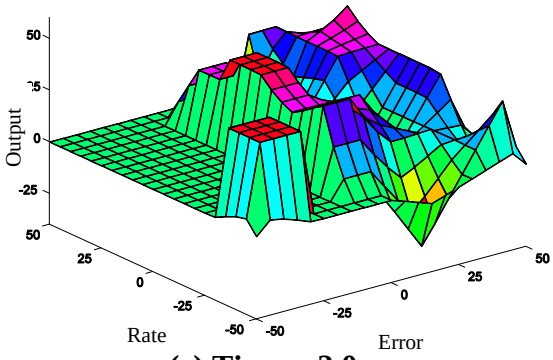

(c) Time = 2.0 s

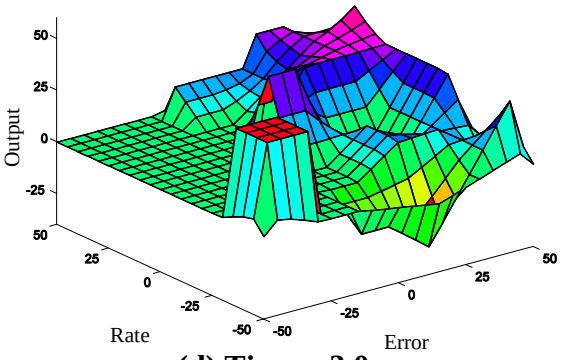

(d) Time = 3.0 s

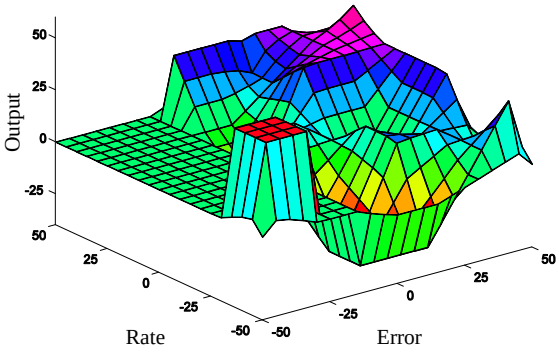

(e) Time = 4.0 s

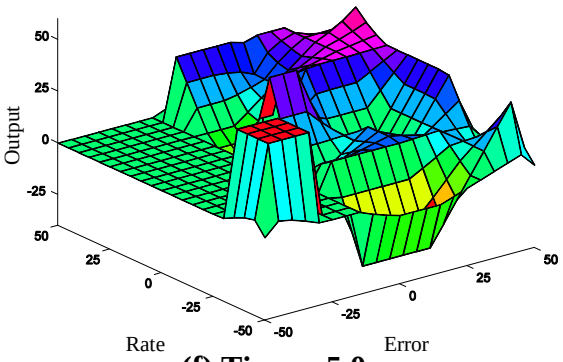

(f) Time = 5.0 s

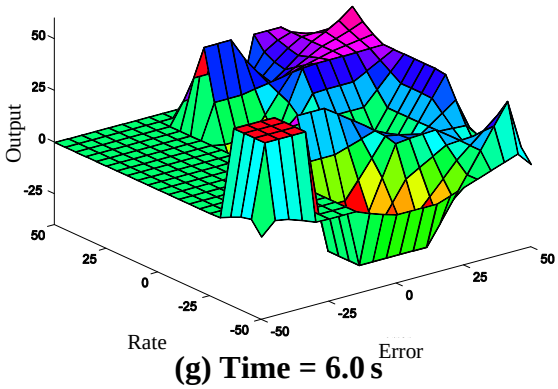

(g) Time = 6.0 s

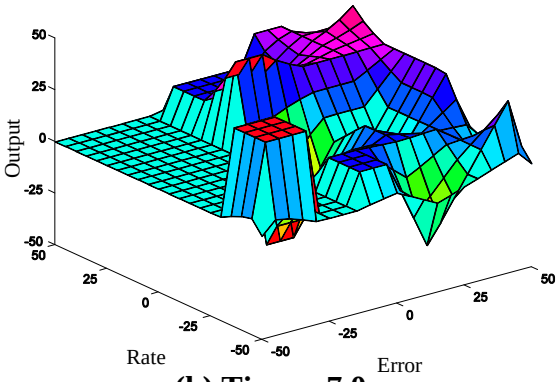

(h) Time = 7.0 s

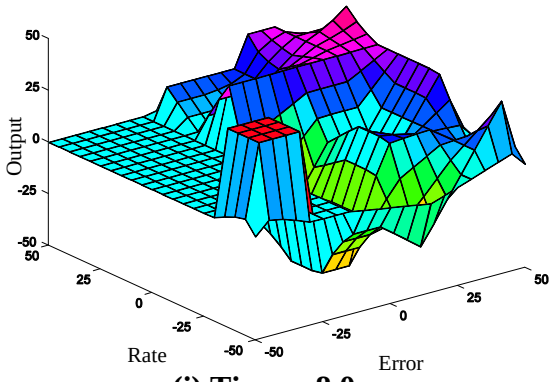

(i) Time = 8.0 s

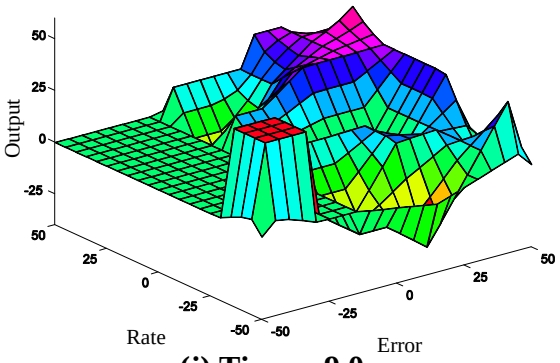

(j) Time = 9.0 s

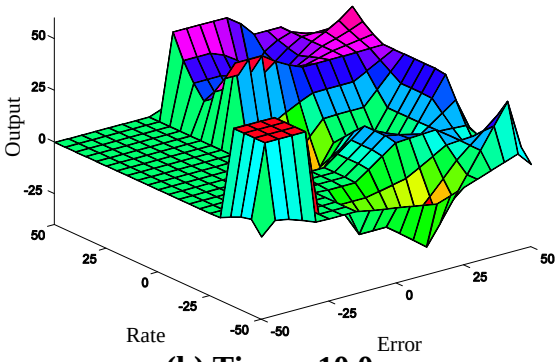

(k) Time = 10.0 s

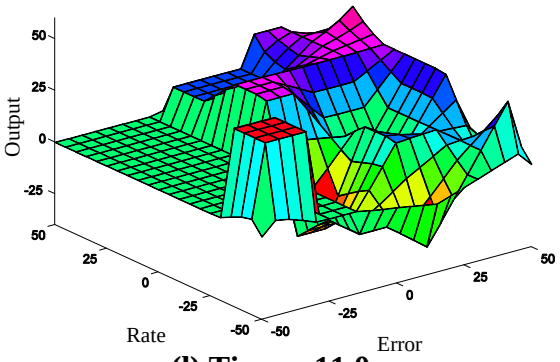

(l) Time = 11.0 s

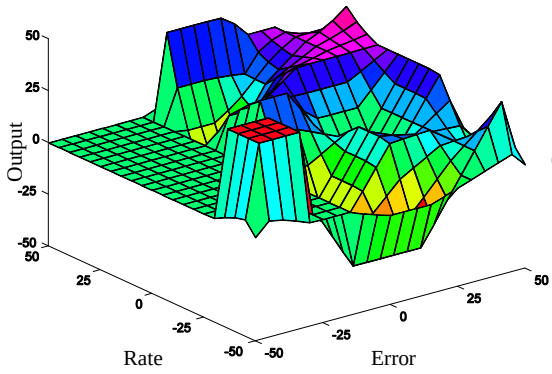

(m) Time = 12.0 s

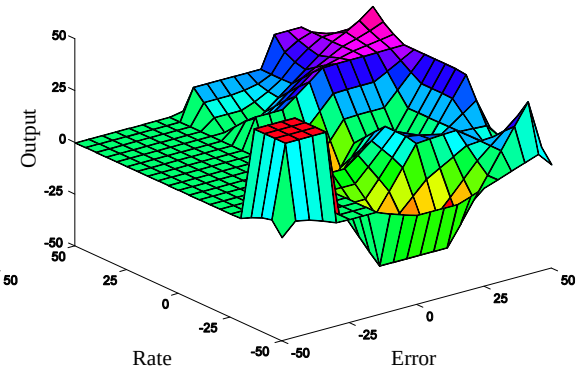

(n) Time = 13.0 s

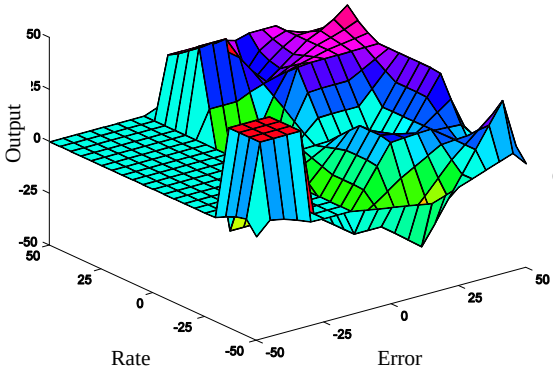

(o) Time = 14.0 s

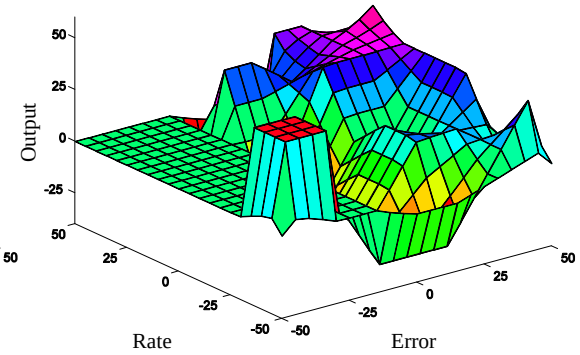

(p) Time = 15.0 s

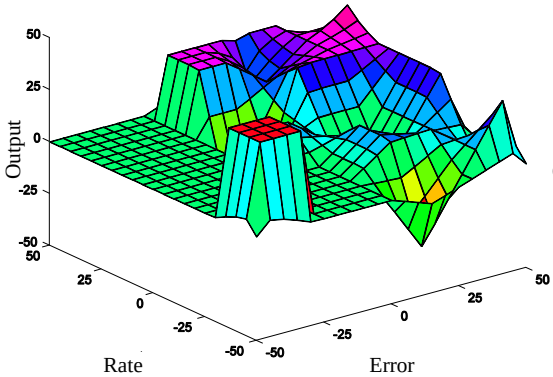

(q) Time = 16.0 s

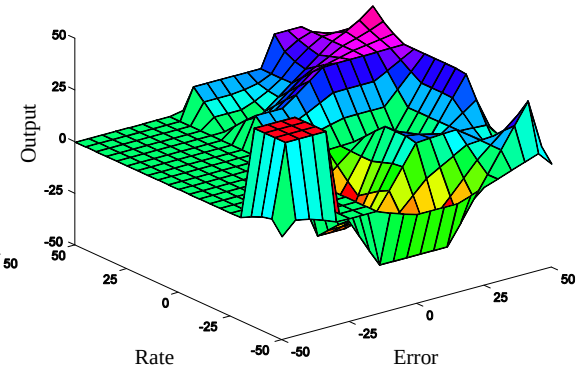

(r) Time = 17.0 s

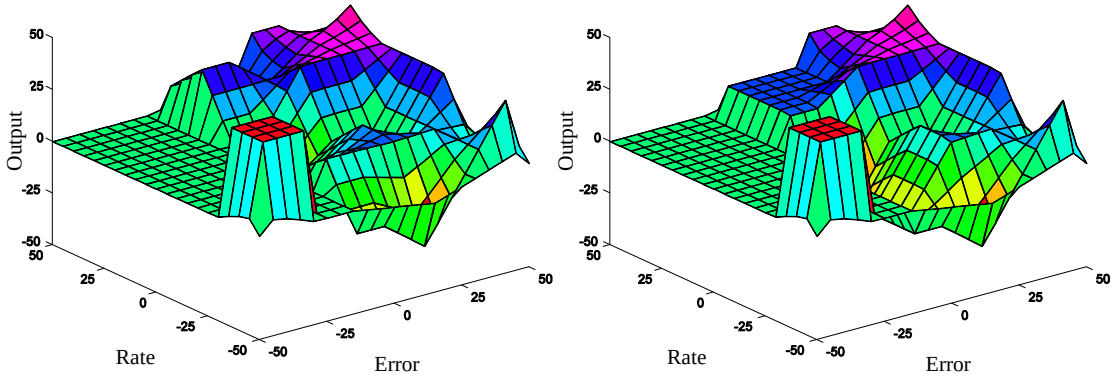

(s) Time = 18.0 s **(t) Time = 19.0 s**

Figure A6.3 Control surfaces for rig test 1

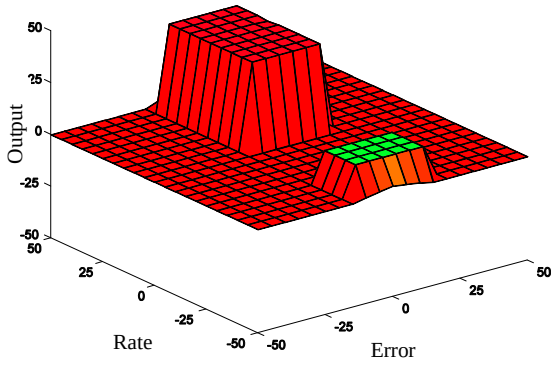

(a) Time = 0^+s

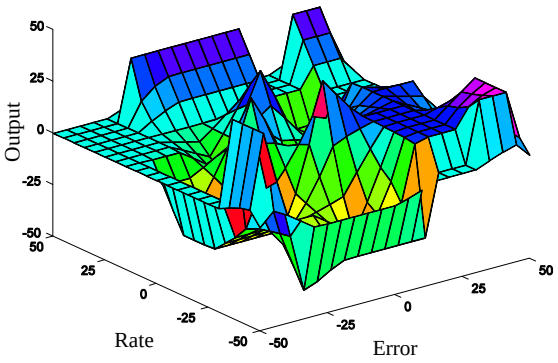

(b) Time = 1.0 s

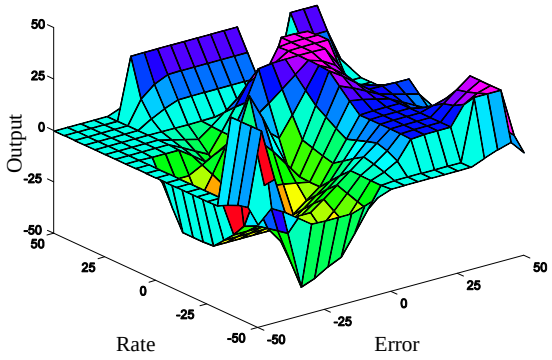

(c) Time = 2.0 s

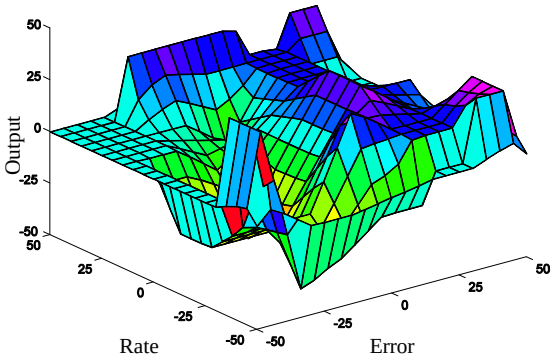

(d) Time = 3.0 s

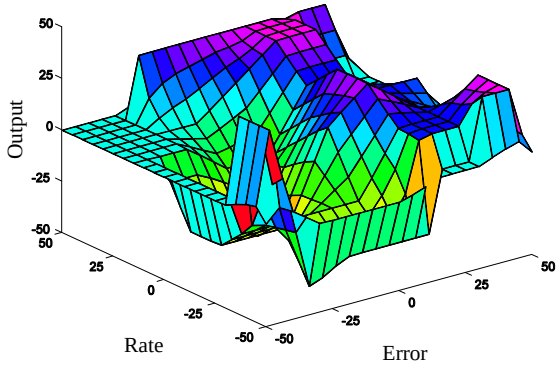

(e) Time = 4.0 s

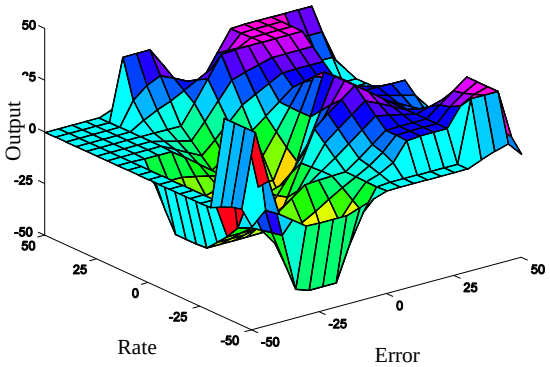

(f) Time = 5.0 s

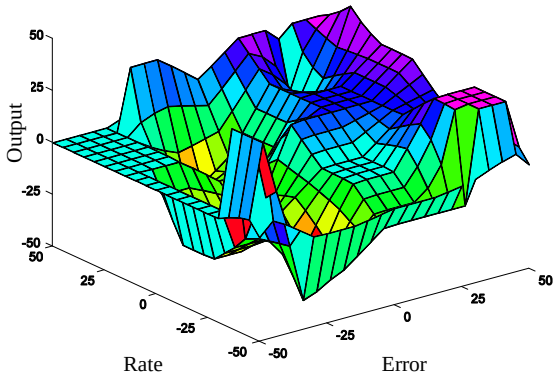

(g) Time = 6.0 s

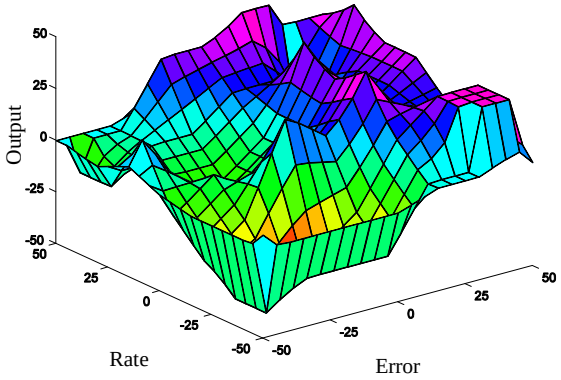

(h) Time = 7.0 s

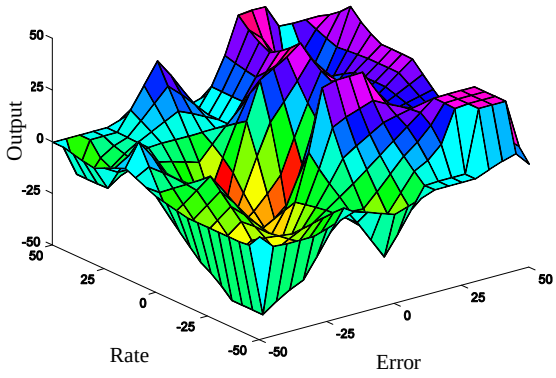

(i) Time = 8.0 s.

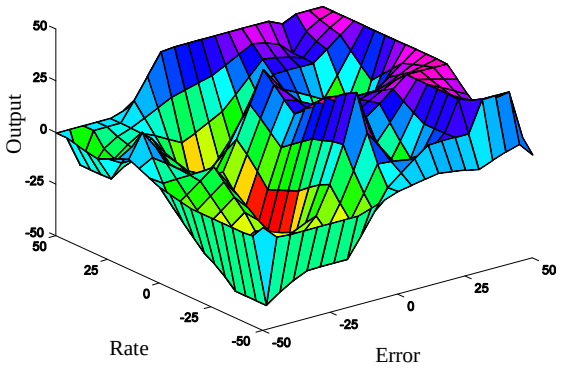

(j) Time = 9.0 s

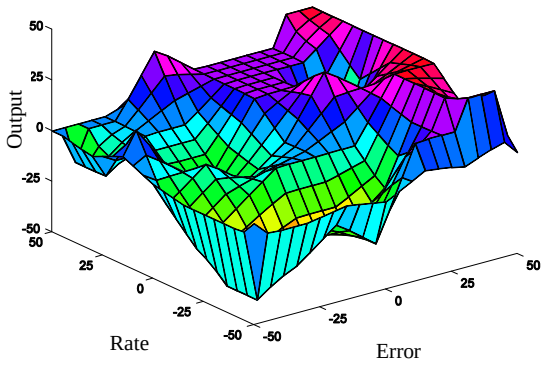

(k) Time = 10.0 s

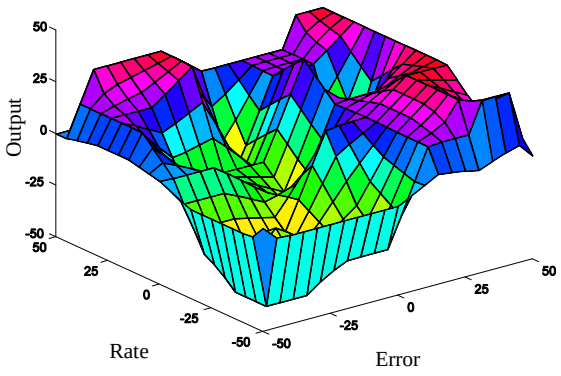

(l) Time = 11.0 s

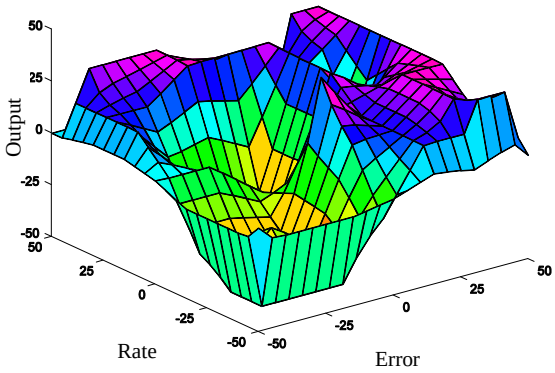

(m) Time = 12.0 s

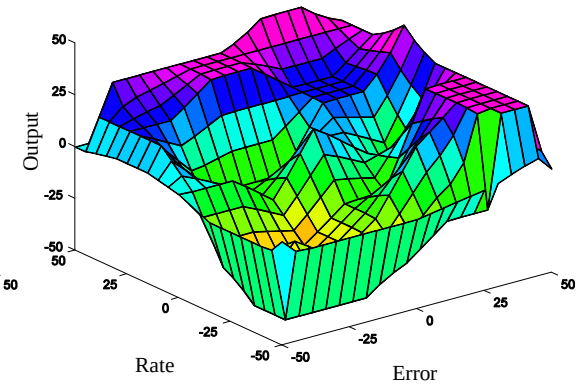

(n) Time = 13.0 s

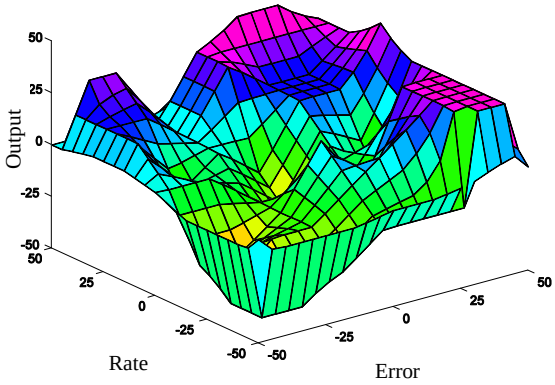

(o) Time = 14.0 s

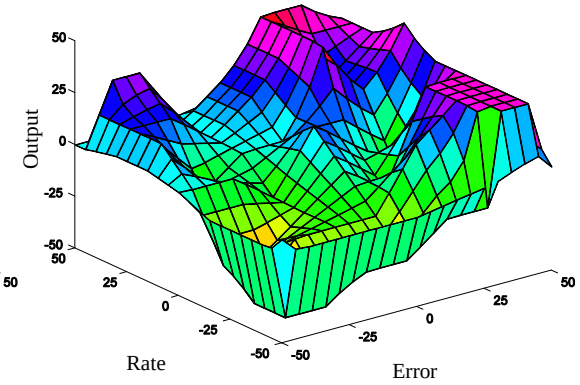

(p) Time = 15.0 s

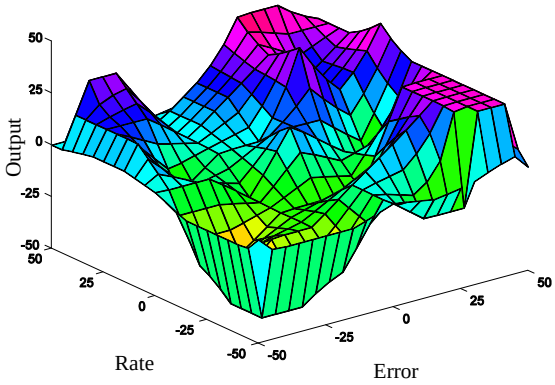

(q) Time = 16.0 s

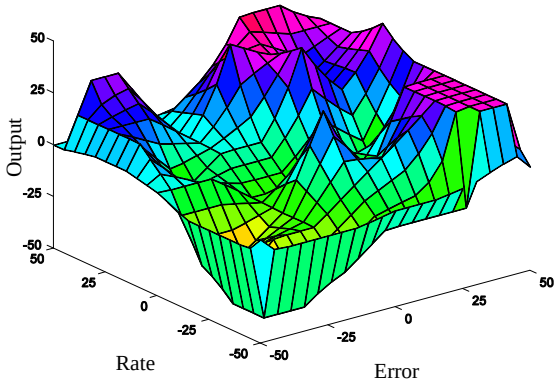

(r) Time = 17.0 s

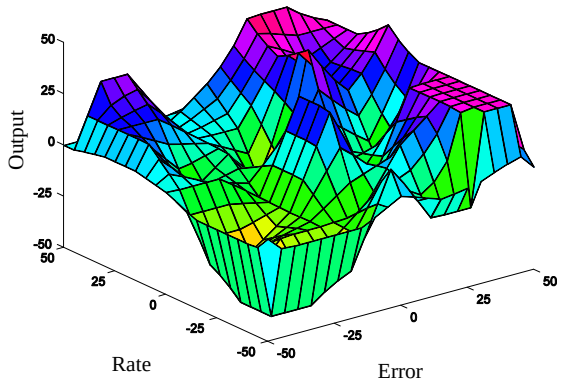

(s) Time = 18.0 s

FigureA 6.4 Control surfaces for rig test 2

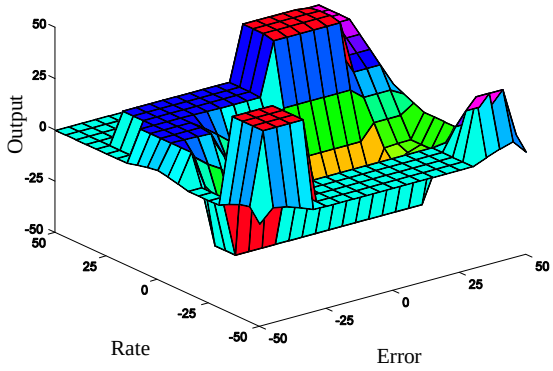

(a) Time = 1.0 s

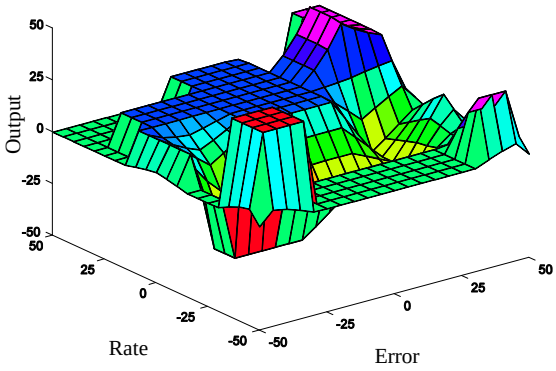

(b) Time = 2.0 s

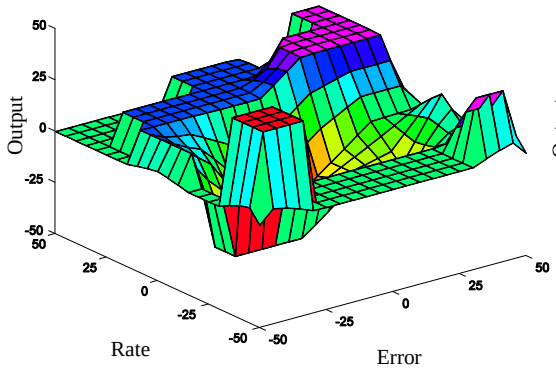

(c) Time = 3.0 s

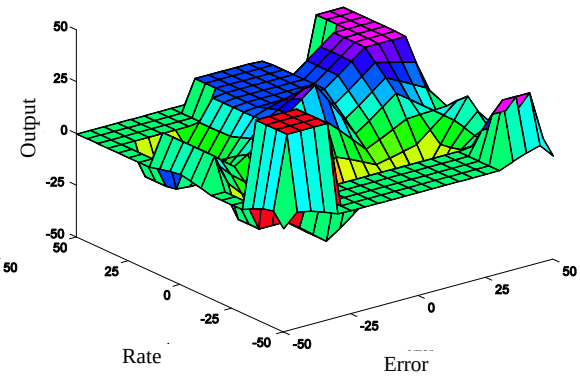

(d) Time = 4.0 s

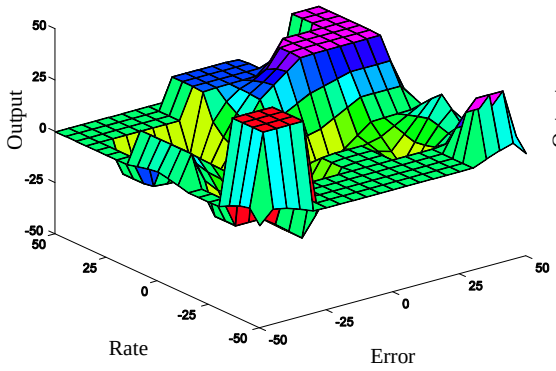

(e) Time = 5.0 s.

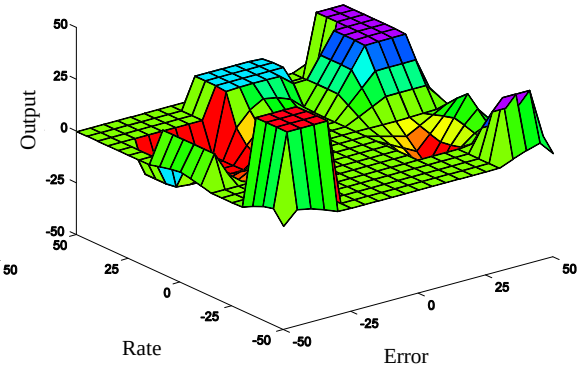

(f) Time = 6.0 s

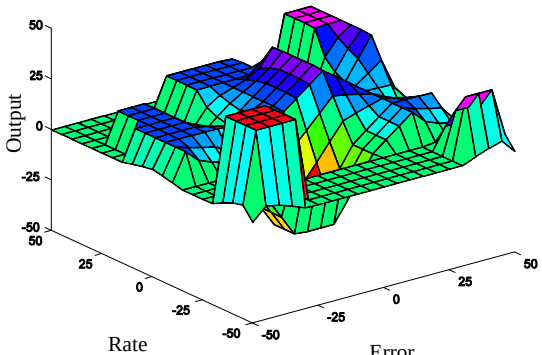

(g) Time = 7.0 s

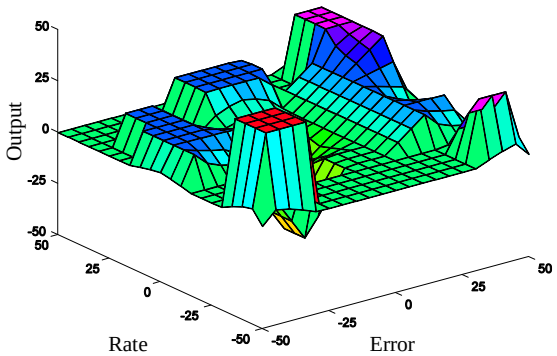

(h) Time = 8.0 s

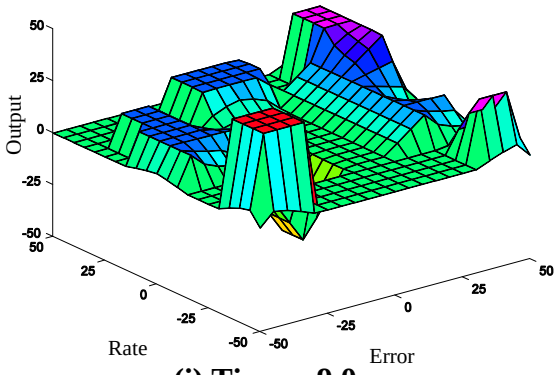

(i) Time = 9.0 s

Figure A6.5 Control surfaces for rig test 3